

## ABSTRACT

Title of Document: DEVELOPMENT OF A FATIGUE LIFE  
ASSESSMENT MODEL FOR PAIRING  
FATIGUE-DAMAGE PROGNOSSES WITH  
BRIDGE MANAGEMENT SYSTEMS

Timothy K. Saad, Doctor of Philosophy, 2015

Directed By: Research Professor Chung C. Fu  
Civil and Environmental Engineering

Fatigue damage is one of the primary safety concerns for steel bridges reaching the end of their design life. Currently, federal requirements mandate regular inspection of steel bridges for fatigue cracks with evaluative reporting to bridge management systems. The quality of the inspection is subjective and time delayed due to inspection cycles, which are scheduled for every two years. However, structural health monitoring (SHM) data collected between inspection-intervals can provide supplementary information on structural condition that ameliorates some drawbacks of current inspection methods. Through the use of SHM and finite element models, fatigue performance assessments can be utilized throughout the service life of fatigue sensitive bridge elements for mitigating fatigue damage and preventing sudden fatigue failure. These assessments will additionally be useful to

inspectors when reporting bridge condition evaluations to bridge management systems.

The main goal of this study is to develop a fatigue life assessment method used for determining the remaining useful life of steel bridges and to map these results to existing bridge management systems. In order to achieve this goal, the current practices and methodologies associated with fatigue life of bridge elements and the use of bridge management systems are investigated.

For analyses of fatigue damage, the fatigue life is split into two different periods of analyses: a crack initiation period and crack growth period. In order to quantify the effects of fatigue damage, each period of the fatigue life is associated with a unique assessment method, an empirical correlation assessment and a fracture mechanics assessment. Structural health monitoring techniques are employed to monitor the behavior of the bridge components and bridge elements. These two assessment methods are combined to form a damage accumulation model to estimate the fatigue life. The proposed damage accumulation model uses the acquired data from structural health monitoring alongside finite element modeling to derive a damage prognosis of bridge elements. The damage prognosis attempts to forecast the structure's performance by measuring the cumulative fatigue damage, estimating future loads, and ultimately determining the remaining useful life of the bridge element. A technique for mapping the results of the damage prognosis into condition state classifications is proposed.

The suitability and applicability of the proposed damage accumulation model is illustrated on an existing highway bridge. This bridge was selected as a good

candidate for fatigue monitoring due to the average daily truck traffic and the identification of existing and active fatigue cracks. The application of the damage accumulation model is demonstrated and a damage prognosis is derived. Finally, the damage accumulation results are integrated with current condition state classifications used in bridge management systems.

DEVELOPMENT OF A FATIGUE LIFE ASSESSMENT MODEL FOR PAIRING  
FATIGUE-DAMAGE PROGNoses WITH BRIDGE MANAGEMENT SYSTEMS

By

Timothy K. Saad

Dissertation submitted to the Faculty of the Graduate School of the  
University of Maryland, College Park, in partial fulfillment  
of the requirements of the degree of  
Doctor of Philosophy  
2015

Advisory Committee:  
Research Professor Chung C. Fu, Chair/Advisor  
Professor Amde M. Amde  
Professor Sherif Aggour  
Professor Yunfeng Zhang  
Professor Sung W. Lee

© Copyright by  
Timothy K. Saad  
2015

## Acknowledgements

The research work in this dissertation was partially supported by the Office of the Assistant Secretary for Research and Technology (Grant No. RITARS11HUMD; Program Director: Caesar Singh). Financial support provided by Dr. Chung C. Fu and the Bridge Engineering Software and Technology (BEST) Center, University of Maryland, is gratefully acknowledged.

I am very grateful to my graduate advisor, Dr. Chung C. Fu, for his 5+ years of advice and guidance during my studies. His support was essential for the success of this work and I have truly enjoyed my time working for him. My gratitude also extends to my committee members: Dr. Amde M. Amde, Dr. M. Sherif Aggour, Dr. Yunfeng Zhang and Dr. Sung W. Lee for their valuable time reading my work.

I would like to thank Maryland State Highway Administration for their assistance and arrangement in the field tests. I would also like to thank Dr. Y. Edward Zhou from AECOM (formerly URS Corporation) for his assistance and insight on fatigue related topics.

A special thanks to my friend and colleague, Noah C. Blum. I am very appreciative of the time he spent to share valuable skill sets, and am also appreciative for his feedback and input with other miscellaneous analyses on this dissertation. Also, special thanks to my friend Michelle Shevin, who has spent multiple hours of the course of my graduate program reviewing my writings for journal submissions, proposals, and conference papers. And thank you to the rest of my colleagues, particularly, Changjiang Zhou and Gengwen Zhao who have been helpful and willing to provide their expertise on relevant research topics. Lastly and most importantly, I would like to thank all my parents for

their encouragement, which has allowed me to realize my own potential. I sincerely appreciate their guidance and support throughout my entire academic career.

# Table of Contents

Acknowledgements.....	ii
Table of Contents.....	iv
List of Tables.....	vii
List of Figures.....	viii
Chapter One : Introduction and Overview.....	1
1.1 Problem Statement.....	1
1.2 Research Objective.....	3
1.3 Organization of Dissertation.....	4
Chapter Two : Literature Review.....	6
2.1 National Bridge Inspection Program.....	8
2.1.1 National Bridge Inventory.....	10
2.1.1.1 NBI Condition Ratings.....	11
2.2 Fatigue Failure Mechanics.....	24
2.2.1 Fatigue Life.....	25
2.2.2 Fatigue Life Prediction.....	27
2.2.2.1 Stress-Based Method.....	28
2.2.2.2 Fracture Mechanics.....	29
2.3 Role of Structural Health Monitoring in Failure Mechanics.....	31
2.4 SHM Paired with Condition Assessments.....	31
Chapter Three : Theoretical Development of Fatigue Crack Initiation Period.....	33
3.1 Crack Initiation.....	34
3.1.1 Defects in Fabricated Steel Structures.....	36
3.2 Load-Induced Fatigue from Variable-Amplitude Loading.....	41
3.2.1 Strain Gage Analysis.....	42
3.2.2 Strain Data Acquisition.....	43
3.2.3 Stress-Strain Relationships.....	46
3.2.4 Rainflow Cycle Counting.....	50
3.2.5 Stress Range Histograms.....	54
3.2.6 Extrapolation of Load Histories.....	56
3.2.6.1 Statistical Extreme Value Theory.....	58
3.2.6.2 Analytical procedure for extrapolation.....	60

3.3 Crack-Initiation Life Prediction .....	64
3.3.1 Linear Cumulative Damage Rule.....	65
3.3.1.1 Shortcomings of the Miner Rule.....	66
3.3.1.2 Nonlinear Damage Accumulation.....	69
3.3.1.3 Linear vs. Nonlinear Damage Accumulation.....	72
3.3.2 Application of S-N Curve .....	72
3.3.2.1 Fatigue Prone Details.....	76
3.3.2.2 Effective Stress Range .....	80
3.3.2.3 Truncation Stress Range for Fatigue Details .....	82
3.4 Remaining Useful Life – Crack Initiation Period .....	83
3.5 Uncertainties in Crack-Initiation Life Modeling.....	84
3.6 Summary .....	87
Chapter Four : Theoretical Development of Fatigue Crack Growth Period .....	88
4.1 Crack Types .....	89
4.1.1 Crack Detection.....	91
4.1.2 Cracks on Welded Structures.....	93
4.2 Linear Elastic Fracture Mechanics.....	95
4.2.1 Stress Intensity Factors .....	96
4.2.2 Stress Intensity Factor and Similarity Factor.....	96
4.2.3 Crack Growth Behavior .....	98
4.3 Fracture Toughness .....	101
4.3.1 Charpy V-Notch Test.....	102
4.3.2 Computations of Stress Intensity Factors.....	104
4.3.3 Modeling Stress Intensification Factors.....	104
4.3.3.1 Displacement extrapolation method .....	105
4.4 Validating FEM Models with a simple LEFM model .....	106
4.4.1 Stress Intensity Factor with 2D Geometry in ANSYS.....	107
4.4.2 Stress Intensity Factor with 3D Geometry in ANSYS.....	112
4.5 Crack Growth Models and AE sensors .....	116
4.7 Crack Propagation Period Cumulative Damage .....	120
4.8 Remaining Useful Life – Crack Propagation Period.....	122
Chapter Five : System Failure due to Fatigue.....	124
5.1 Geometry of the Bridge.....	124
5.2 Bridge Configuration .....	126
5.2.1 Redundancy of Bridges .....	126
5.2.1.1 Fracture-critical structures .....	127

5.2.1.2 Determination of fracture-critical members.....	128
5.2.1.3 Fracture-critical members in failure mechanics.....	129
5.2.1.4 Evaluating Fracture-critical Members and Fatigue Prone Details.....	130
5.2.2 Distortion-Induced Fatigue .....	131
5.3 Damage Prognosis of Fatigue Life.....	133
5.4 Integration of Damage Prognosis with Condition States .....	135
5.4.1 Calculation of Total Damage from Stress Cycles and Fracture.....	138
5.5 Integration of Damage Prognosis into Federal Condition Ratings .....	140
Chapter Six : Validation of Fatigue-Damage Accumulation Model by Field Test and Data Processing .....	142
6.1 Structural Health Monitoring .....	145
6.2 Data Acquisition Selection.....	146
6.2.1 Preliminary Monitoring.....	147
6.3 Long-Term Monitoring and Data Processing .....	149
6.3.1 Data Detrending .....	151
6.4 Fatigue Analysis.....	153
6.4.1 Rainflow Counting.....	153
6.4.2 Extrapolation Results .....	154
6.4.3 Effective Stress Range .....	160
6.4.4 Remaining Useful Life for Crack Initiation.....	162
6.5 Fracture Analysis .....	165
6.5.1 Finite Element Modeling .....	165
6.5.1.1 Stress Intensity Factor.....	171
6.5.2 Damage Tolerance and Fracture Toughness .....	172
6.5.3 Crack Growth Rate.....	174
6.5.1 Remaining Useful Life for Crack Propagation .....	175
6.6 Total Cumulative Damage .....	179
Chapter Seven : Conclusions and Future Research .....	181
7.1 Conclusions .....	181
7.3 Recommendation of Future Research .....	184
7.3.1 Condition Ratings Modifications .....	185
7.3.2 Future Role of Technology in Bridge Management Systems .....	186
References.....	187

## List of Tables

Table 2.1 Items considered in NBI component condition ratings .....	12
Table 2.2 General component condition ratings guidelines from FHWA's <i>Coding Guide</i> ....	13
Table 2.3 Smart Flags found in Pontis bridge management systems .....	20
Table 2.4 Pontis System condition state definitions for steel fatigue.....	20
Table 2.5 Condition state definitions for CoRe section loss .....	21
Table 2.6 Bridge element condition state definitions.....	23
Table 2.7 Actions associated with bridge element condition states .....	24
Table 3.1 Sample of details that are considered fatigue prone.....	78
Table 3.2 Allowable Fatigue Stress Range for CAFL.....	79
Table 3.3 Constant A and CAFL of AASHTO Fatigue Categories .....	80
Table 4.1 Compilation of non-destructive testing methods and the detectable crack size .....	92
Table 4.2 Coordinates and displacements of nodes on crack face .....	110
Table 4.3 Motion of one crack face with respect to another, $\Delta v$ .....	111
Table 4.4 Local coordinates and final factor, $\Delta v/r$ .....	111
Table 5.1 Redundancy classifications .....	126
Table 5.2 AASHTO CVN impact energy requirements for fracture-critical members.....	130
Table 5.3 AASHTO CVN impact energy requirements for nonfracture-critical members...	130
Table 5.4 Fatigue condition states translated into national bridge element.....	136
Table 5.5 Actions associated with bridge element condition states .....	138
Table 5.6 Mapping of damage calculations into condition states.....	139
Table 5.7 Actions associated with NBI condition ratings .....	141
Table 6.1 Selected detail categories for load-induced fatigue.....	160
Table 6.2 Mapping of damage calculations into condition states.....	179
Table 6.3 Fatigue condition states translated into national bridge element.....	180

## List of Figures

Figure 2.1 Relationships of aspects in the National Bridge Inspection Program .....	10
Figure 2.2 Categorization of bridge elements .....	16
Figure 2.3 National bridge elements corresponding with bridge component.....	17
Figure 2.4 Bridge management elements corresponding with bridge component .....	18
Figure 2.5 Mapping of bridge management elements into National Bridge Elements .....	22
Figure 2.6 Illustration of fatigue life concepts .....	26
Figure 2.7 Schematic plot of damage parameter versus fatigue life curve.....	28
Figure 3.1 Illustration of fatigue-crack-initiation life.....	33
Figure 3.2 Development of cyclic slip bands and a microcrack.....	34
Figure 3.3 Surface crack penetrating grain boundaries .....	35
Figure 3.4 Elliptical crack front as crack passes through multiple grains .....	36
Figure 3.5 Nomenclature of fillet welds.....	37
Figure 3.6 Illustration and terms of possible weld defects.....	39
Figure 3.7 Fatigue crack forming from internal porosity in web-flange connection.....	40
Figure 3.8 Fatigue crack enlarged to three –ended crack from internal porosity .....	40
Figure 3.9 Fracture surface of cross section .....	41
Figure 3.10 Circuit of Wheatstone Bridge .....	43
Figure 3.11 Illustration of stress range and associated variables for CAFL.....	45
Figure 3.12 Illustration of stress range and associated variables within VAFL .....	45
Figure 3.13 Engineering stress-strain curve .....	46
Figure 3.14 Loading and unloading on a stress strain specimen.....	48
Figure 3.15 Tension and compression loading on specimen.....	49
Figure 3.16 Complete stress-strain hysteresis .....	49
Figure 3.17 Sample of variable amplitude strain data .....	50
Figure 3.18 Sample of variable amplitude stress data .....	50
Figure 3.19 Hysteresis loop to stress data .....	51
Figure 3.20 Rainflow cycle counting on the load history.....	52
Figure 3.21 Illustration of rainflow counting on stress cycle (Schijve, 2009) .....	53
Figure 3.22 Successive rainflow counts .....	54
Figure 3.23 Histogram that reflects the frequency of measured stress ranges .....	55
Figure 3.24 Kernel density fit to histogram.....	56

Figure 3.25 Allocation of stress ranges into specific intervals .....	62
Figure 3.26 Traffic load distribution as histogram .....	63
Figure 3.27 Exponential distribution fit to histogram .....	64
Figure 3.28 Variable amplitude loading with two blocks of load cycles .....	65
Figure 3.29 Sequence in loadings, each with two different size load blocks .....	68
Figure 3.30 Illustration of linear damage accumulation.....	70
Figure 3.31 Illustration of non-linear damage accumulation .....	70
Figure 3.32 Non-linear damage curve from HiLo VA sequence .....	71
Figure 3.33 Non-linear damage curve approximated by double linear functions .....	71
Figure 3.34 Schematic constant amplitude S-N curve of a steel component .....	73
Figure 3.35 CA S-N curve for a steel component subjected to VA loads.....	75
Figure 3.36 AASHTO fatigue strength S-N curves.....	79
Figure 3.37 Rayleigh-type stress range histogram .....	81
Figure 3.38 Effective stress range fits into S-N curves .....	83
Figure 3.39 Approach to fatigue crack-initiation life analysis .....	87
Figure 4.1 Illustration of fatigue-crack-propagation life .....	88
Figure 4.2 Different types of cracking starting from a hole .....	89
Figure 4.3 Three modes of loading used in fracture mechanics .....	90
Figure 4.4 Transverse gusset on a plate - types of crack in a weld .....	93
Figure 4.5 Initiation of root crack.....	94
Figure 4.6 Simultaneous propagation of cracks from toe and root of weld .....	95
Figure 4.7 Variation of stress intensity factor related to the variation in stress cycle .....	97
Figure 4.8 Example of similarity principle.....	98
Figure 4.9 Schematic of crack growth curve showing crack growth regions.....	99
Figure 4.10 Crack growth curve fits into fatigue life curve .....	101
Figure 4.11 CVN transition curve relating temperature with fracture toughness .....	103
Figure 4.12 Stress field at the crack tip .....	107
Figure 4.13 Elements and nodes of 2D full crack model .....	109
Figure 4.14 Deformed and undeformed shape of crack tip .....	110
Figure 4.15 Relationship between crack face displacements and stress intensity factor.....	111
Figure 4.16 SIF results of the FEM analysis on full crack model with 2D geometry .....	112
Figure 4.17 Elements of 3D full crack model .....	113
Figure 4.18 Crack zone for mode I loading.....	114

Figure 4.19 Elastic strain in the Y-direction at the crack tip .....	115
Figure 4.20 SIF results of the FEM analysis on full crack model with 3D geometry .....	116
Figure 4.21 AE signal with labeled parameters.....	118
Figure 4.22 Propagation-life curve with final crack sizes .....	122
Figure 5.1 Plan view of bridge with skewed supports.....	125
Figure 5.2 Distortion induced fatigue at floor beam-to-girder connection.....	132
Figure 5.3 Fatigue damage prognosis with structural health monitoring .....	134
Figure 5.4 CoRe fatigue elements mapped into national bridge elements .....	135
Figure 5.5 BME condition states integrated into fatigue life curve.....	137
Figure 6.1 Maryland bridge carrying I-270 over Middlebrook Road.....	142
Figure 6.2 I-270 Bridge framing plan and cross section .....	143
Figure 6.3 K-type cross brace on Middlebrook Bridge .....	144
Figure 6.4 Magnified plan view of cross frame and angle of attachment .....	145
Figure 6.5 Location of sensors for preliminary testing .....	147
Figure 6.6 Stress data on web stiffeners to illustrate compression and tension .....	148
Figure 6.7 Connection plate with known crack Girder 15 .....	149
Figure 6.8 Placement of strain gauge on high tension web stiffener.....	150
Figure 6.9 Illustration of variable amplitude loading .....	151
Figure 6.10 Illustration of drift that occurred in acquired data .....	152
Figure 6.11 Detrending on a segment of strain data.....	153
Figure 6.12 Rainflow cycle counting implemented on variable amplitude stress .....	154
Figure 6.13 Days of captured data (blue) and extrapolated data (red) .....	155
Figure 6.14 Relationship between the truncation stress and the effective stress range.....	161
Figure 6.15 Number of cycles to failure based on effective stress range .....	162
Figure 6.16 AASHTO S-N curve with point of 1-year damage plotted.....	163
Figure 6.17 Years to failure based on effective stress range .....	164
Figure 6.18 AASHTO S-N curve with cumulative points plotted until failure.....	164
Figure 6.19 Global model of Middlebrook Bridge.....	165
Figure 6.20 K-brace, connection plate and girder on global model .....	166
Figure 6.21 Location of local model within the global model .....	167
Figure 6.22 Three Dimensional local finite element model meshed into elements.....	168
Figure 6.23 Finite element local model with applied displacements and forces .....	169
Figure 6.24 Radial elements at the crack tip .....	170

Figure 6.25 Stress contour (Y-Component) of connection between stiffener and flange .....	171
Figure 6.26 Stress contour (Y-Component) of crack between stiffener and flange .....	171
Figure 6.27 SIF for two-dimensional crack modeled at toe of weld .....	172
Figure 6.28 Change in critical crack size based on effective stress range.....	173
Figure 6.29 Paris Law for fatigue crack growth rates .....	174
Figure 6.30 Paris Law for fatigue crack growth rates, log-log.....	175
Figure 6.31 Variation in crack size changes with the effective stress range .....	176
Figure 6.32 Relationship of crack size to critical crack size .....	177
Figure 6.33 Number of Years to failure based on the crack growth rate .....	178

## **Chapter One: Introduction and Overview**

### **1.1 Problem Statement**

As a large number of aging bridges are approaching the end of their design life and are continuously requiring more maintenance, there is increasing demand to assure their long term health. These aging bridges are increasingly experiencing damages and approaching failure when confronted with high traffic volume and weight, deteriorating components, as well as a large number of stress cycles. In 2013, the American Society for Civil Engineers (ASCE) released an updated Infrastructure Report Card that found nearly 25% of the nation's bridges to be either structurally deficient or functionally obsolete. A bridge is considered structurally deficient when it is in need of significant maintenance, rehabilitation or replacement due to deteriorated physical conditions and is considered functionally obsolete when it does not meet current standards, such as vertical clearances or lane widths. To make these condition assessments, the Federal Highway Administration uses information from inspection reports that are hosted by state and federal bridge management systems (BMS). Bridge management systems are heavily dependent on field inspectors, who are to collect information on bridge elements and bridge components, evaluate their condition, and enter this data into the BMS database. Among the various tasks of bridge management, field inspection is the most essential in evaluating the current condition of a bridge, which is continuously subjected to damaging loads from traffic.

Structurally deficient and functionally obsolete bridges are still open to daily traffic and continue to experience increasing traffic volumes. These effects of these loadings are most pertinent on steel bridges which are vulnerable to fatigue-induced damage: the

process of material degradation caused by repeated loads. Fatigue damage occurs over a long period of time and is the primary failure mechanism in steel bridges reaching their original design life (FHWA, 2011). Fatigue damage is largely dependent on the size of the traffic loadings, the frequency of the loads, and structural detailing in critical regions of a component or structure (Haldipur, et al., 2010). The process of metal fatigue begins with tiny material imperfections, or defects, that are amplified and enlarged into cracks from the dynamic loadings on bridges. These defects usually initiate at the fatigue prone areas of the bridge: the bridge connections, attachments, and details, such as welds connecting connection plates to steel girders. The defects begin to grow under repetitive loads until an unacceptable crack size is reached and eventually cause structural failure. Fatigue failure is particularly dangerous because it can sometimes occur without any obvious prior warnings (FHWA, 2011). The implementation of sensing instrumentation on a structure can be used in order to provide information on structural damage and structural performance. This is more often characterized as structural health monitoring.

Structural health monitoring (SHM) systems installed on aging bridges can increase their safety and reliability by replacing scheduled maintenance with condition-based maintenance based on the feedback from the SHM system (Rabiei, 2011). When SHM is performed in coordination with existing offline non-destructive inspection practices, the structural health monitoring data collected in between current inspection intervals can provide supplementary information of the structures condition that potentially alleviates some drawbacks associated with conventional offline inspection practices. For instance, while current federal requirements mandate bridges to be inspected regularly for fatigue cracks, these inspections are termed routine inspections, and are typically carried out by

the bridge owners every two years (NBIS, 2011). Further, these inspections may lack accuracy since they rely heavily on visual inspection, which are subjective to the inspector's experience and physically inherent limitations.

It has become evident that sound infrastructure management decisions can be supplemented through damage accumulation models developed from accurate condition data in the field (Hu, et al., 2005). Damage accumulation models can be used for the damage prognosis of bridge elements. Reporting the damage prognosis into bridge management systems is also a significant contribution to a strong bridge inspection program. The success of any bridge inspection program is dependent on its reporting system (FHWA, 2012).

## **1.2 Research Objective**

The primary goal of this research is to quantify fatigue damage that is currently overlooked by inspection methods and to develop a damage accumulation model used for the damage prognosis of existing highway bridge elements. The resulting damage prognosis is then tied to bridge management systems, which are used to effectively manage the information related to bridge conditions, by integrating the damage prognoses with bridge management condition states. The following specific objects are defined to accomplish the main goal:

- (1) To outline the factors that characterize a structure's fatigue life and to formulate a procedure for fatigue life assessment; an empirical correlation approach and fracture mechanics approach are combined for the formulation.

- (2) To provide a thorough review of bridge management systems; condition ratings used at the state and federal level must be clearly established in order to properly map the fatigue damage into relevant ratings.
- (3) To implement a structural health monitoring system on a particular element of an existing highway bridge. The SHM system will monitor and collect data that is representative of the bridge's response to every-day traffic loadings. The acquired data is then used in the damage accumulation model which can predict the remaining useful life (RUL) at the structural component level.
- (4) To develop and experimentally verify a fatigue damage accumulation model that uses the acquired data from structural health monitoring alongside finite element modeling of an existing highway bridge with an active crack. The damage accumulation model is used to derive the damage prognosis of the bridge element.
- (5) To devise a translator-tool that will integrate the damage prognosis into the condition ratings used by state and federal bridge management systems.

### **1.3 Organization of Dissertation**

This dissertation consists of seven chapters, including the introduction to this research in Chapter One and the conclusions summarized in Chapter Seven. The remaining chapters are organized as follows,

- Chapter 2 offers an extensive review of current bridge management systems, on both the federal and state levels along their corresponding methods for bridge condition ratings. Further, an overview of fatigue life concepts and definitions of failure mechanics is provided in this chapter.
- Chapter 3 provides background of the fatigue-crack initiation period. The analyses for acquisition and processing of data from fatigue loads; along

with the extrapolation of load histories is described. Further, the analysis for damage prognosis for the crack initiation period is discussed in detail.

- Chapter 4 provides background of the fatigue-crack propagation period. A review of crack growth behavior is provided. The use of linear elastic fracture mechanics and finite element models to evaluate and analyze crack growth is justified. A description on how fatigue crack growth can be paired with acoustic emission sensors is also provided. The chapter concludes with a damage prognosis that is compared with the fracture toughness of the material.
- Chapter 5 proposes how the fatigue life prediction model can be integrated with current condition ratings. This integration depends on many features, including the type of the structural detail, the condition of the structural detail, and the redundancy of the detail or the structure itself. Review of these features is provided. The features are mapped into a flow diagram that illustrates how a quantitative fatigue damage prognosis is derived and how it fits into the bridge management condition states.
- Chapter 6 provides a case study that demonstrates the configuration of the SHM system on an existing steel I-girder bridge in Maryland. This chapter shows the acquired sensor data, the results from data processing techniques, and how the SHM data was used to quantify fatigue damage assessments using the theories put forward in Chapter 3. Further, a local finite element model is developed and used to find information about the fatigue crack growth using the theories put forward in Chapter 4. Ultimately, the damage accumulation approach is used to derive the damage prognosis. These quantitative assessments are then tied to condition states, as put forth in Chapter 5.

## **Chapter Two: Literature Review**

The first signs of the fatigue failure became evident in the 19<sup>th</sup> century on structures experiencing fracture, e.g. steam engines, locomotives, and pumps. This unknown fracture phenomenon was initially studied by August Wöhler who recognized that a single load application, far below the static strength of a structure, did not do any damage and that repeated load cycles of the same magnitude could cause failure. Wöhler's research also revealed that fatigue occurs by crack growth from surface defects until the material/structure can no longer support the applied loads (Schijve, 2009). While fatigue as a technical problem was investigated in the 19<sup>th</sup> century, the most substantial research contributing to fatigue occurred in the second half of the 20<sup>th</sup> century.

The first signs of fatigue cracks on bridges were discovered in the 1960's. Although localized fatigue failures have been widespread, only a few bridges in the United States have collapsed as a result of fatigue damage (FHWA, 2012).

The first bridge collapse due to fatigue failure was the Silver Bridge, an eyebar-chain link suspension bridge with a 700'-span across the Ohio River, connecting Point Pleasant, West Virginia and Gallipolis, Ohio. The Silver Bridge collapsed on December 15, 1967 during rush-hour traffic and resulted in the death of 46 people. While chain link suspension bridges are usually built with eyebar links combed together to form a highly redundant structure, the Silver Bridge was built as a low-redundant bridge with high-strength steel eyebar links and composed of only two bars each. At the time of its collapse and almost forty years after its construction in 1928, the weight of the average automobile doubled and the large truck weight limit tripled, causing the bridge to carry much heavier loads than it had been initially designed for. The increase of traffic loads

caused the eyebar links to experience higher stress concentrations and ultimately develop stress corrosion cracking: the growth of cracks through the simultaneous action of a tensile stress and corrosive environment. The induced stress corrosion to the bridge triggered an existing microscopic crack (formed during casting) to propagate to approximately 0.1 inch (FHWA, 2012). With only two bars, once the first eyebar broke, other members of the bridge experienced higher stress, and the remaining steel buckled resulting in total failure of the bridge. It was the collapse of the Silver Bridge in 1967 that resulted in the development of the bridge inspection and reporting programs that remain in place today (Chen, et al., 2005 pp. 36-9).

The second bridge collapse due to fatigue failure occurred on June 28, 1983, when the Mianus River Bridge, a two girder span bridge, in Greenwich, Connecticut fell into the Mianus River. The collapse of the bridge was caused by a two pin and hangar assembly that held the bridge deck in place. The bridge first experienced problems when one of the pin bearings rusted over and exerted force on a hangar beyond its design limits and then off of the pin. The bridge load was shifted to the only other pin joint, causing higher stress levels which developed into a fatigue crack at the corner of the pin. On the night of collapse, the vulnerable bridge section fell under the load of two heavy trucks and a car, causing the remaining expansion joint to fail and the non-redundant bridge to crash into the river below.

The Silver Bridge and the Mianus River Bridge are both examples of fatigue cracking to the point of failure of fracture-critical members. In order for a bridge member to be classified as fracture-critical, the failure of one member will result in partial or total collapse of the bridge. At the time of failure, both the Silver Bridge and

Mianus River Bridge were lacking redundancy: a structural condition where there are more elements of support than necessary for stability. In cases of structural redundancy, the additional members have the capacity to carry the additional load and avoid the collapse of the structure (FHWA, 2012).

## **2.1 National Bridge Inspection Program**

The collapse of the Silver Bridge in 1967 aroused national interest in the safety inspection and maintenance of bridges. As a result, Congress issued the Federal-Aid Highway Act of 1968, which confronted the need of periodic and consistent bridge inspections. Upon the creation of Federal-Aid Highway Act of 1968, all bridges constructed with federal funds, or bridges that carried a federally funded road, were lawfully required to be inspected. To fulfill these requirements, a National Bridge Inspection Program (NBIP) was established in 1971 to ensure the safety of the nation's bridges through regular inspection and maintenance. Additionally, the Federal-Aid Highway Act of 1968 continues to serve as the foundation for the stream of legislation funding highway bridge replacement and rehabilitation in federal programs over the last 45 years (Chamberlin, 1999).

The NBIP provided a platform to develop a national policy of bridge inspection standards, which became known as the National Bridge Inspection Standards. The National Bridge Inspection Standards (NBIS) are federal regulations establishing requirements for:

- Inspection and rating procedures
- Inspection frequency
- Inspector qualifications
- Inspection reports formats

- Maintenance of state bridge inventory

Three manuals are currently used to guide state agencies with definitive guidelines for compliance with the NBIS. The first manual, *Bridge Inspectors Reference Manual (BIRM) 2012*, provides comprehensive information on programs, procedures, and techniques for inspecting and evaluating a variety of in-service highway bridges. The second manual, *Manual for Bridge Evaluation (AASHTO Manual 2010 with 2011, 2013 and 2014 Interim Revisions)* serves as a standard to provide uniformity in the procedures and policies for determining the physical condition, maintenance needs and load capacity of highway bridges. The third manual, *FHWA Recording and Coding Guide for the Structure Inventory and Appraisal of the Nation's Bridges (Coding Guide 1995)* provides detail and guidance in evaluating and coding specific bridge data. This manual is the basis behind the component condition rating method that makes up the National Bridge Inventory. Relationships between the National Bridge Inspection Program (NBIP), the National Bridge Inspection Standards (NBIS), and the National Bridge Inventory (NBI) are shown in Figure 2.1.

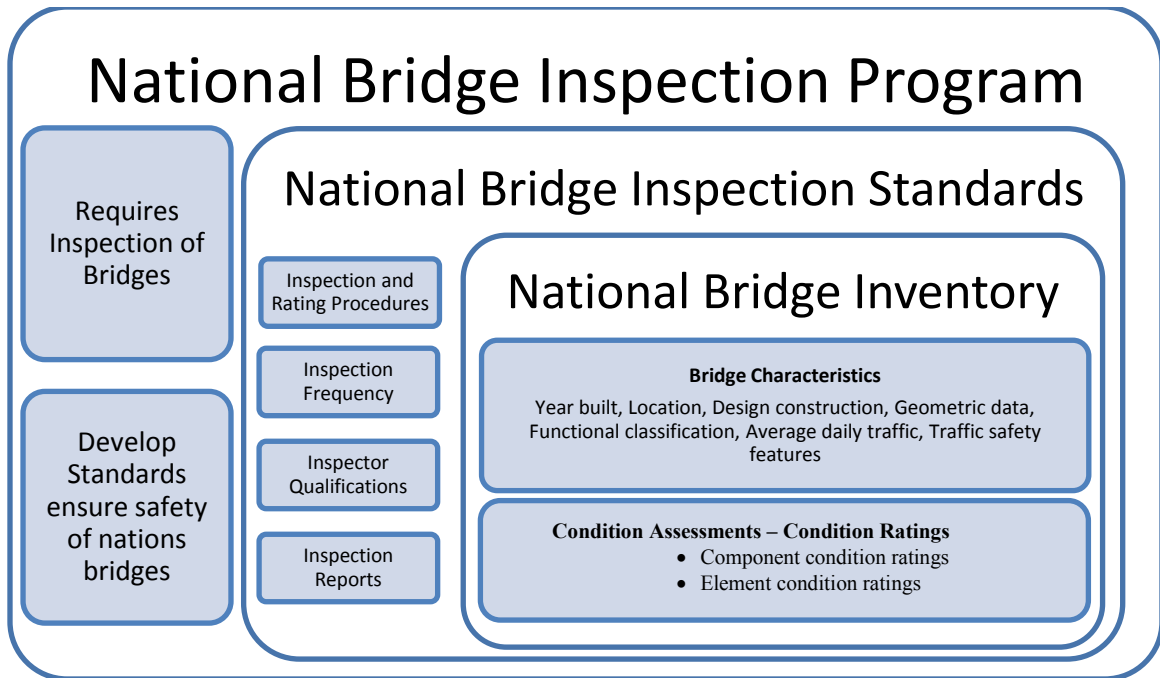


**Figure 2.1 Relationships of aspects in the National Bridge Inspection Program**

### 2.1.1 National Bridge Inventory

The success of any bridge inspection program is dependent on its bridge management system, which heavily relies on accurate and consistent bridge inspection data. Bridge management systems are used by transportation departments to effectively manage the information of bridges, including the regular inspection and maintenance activities. Bridge management systems consist of inventory database information of the bridge (e.g. previous repairs or replacement of components) and field evaluation assessments (e.g. assessment of condition and strength). Among the various tasks of bridge management, field inspection is the most essential in evaluating the current condition of a bridge. Thus, current bridge management systems are heavily dependent on field inspectors to collect information on all the individual elements of a bridge, to evaluate their condition, and to enter this data in to a BMS database.

In order to meet the demands of constructing a nationwide bridge management system, a National Bridge Inventory (NBI) was developed as part of the NBIP in order to establishing maintenance priorities and replacement priorities. The NBI unifies the nation's bridges into an aggregated database containing detailed technical and engineering information of the bridge (Ryan P.E., et al., 2012). This information is based on the most up-to-date condition of the bridge that has been evaluated by accredited inspectors. The NBI contains information on a bridge's characteristics, the existing in-place condition of the bridge, the bridges capacity, the estimated maintenance costs, and the current condition compared with current standards. Federal rating guidelines have been developed in order to provide continuity for the inspection of superstructures. The two major rating guideline systems currently in use are the *FHWA's Recording and Coding Guide for the Structural Inventory and Appraisal of the Nation's Bridges* used for the National Bridge Inventory component rating method and the element level condition state assessment method using the *AASHTO Guide Manual for Bridge Element Inspection* (FHWA, 2012). However, these element level condition assessments are integrated into the NBI ratings with instruction from the AASHTO Guide Manual.

#### ***2.1.1.1 NBI Condition Ratings***

Condition ratings are used to describe the existing, in-place bridge as compared to the as-built condition. These ratings are based on on-site inspections of each bridge structure/substructure and highly consider the structures age and the environmental conditions the structure has been subjected to. In the National Bridge Inventory, condition ratings are applied to the major parts of the bridge, i.e. the deck, the superstructure, and the substructure. These items are summarized in Table 2.1 below.

**Table 2.1 Items considered in NBI component condition ratings**

<b>Component</b>	<b>Description</b>
Deck	The bridge deck is the supporting surface of the bridge. It may or may not be covered with a wear surface such as asphalt. The bridge deck is often steel-reinforced concrete and is supported by the Superstructure (Svirsky, 2014). The condition rating describes the overall condition rating of the deck. This condition of the surface/protective systems, joints, expansion devices, curbs, sidewalks, parapets, fascia's, bridge rail and scuppers is not included in the rating, but the condition will be noted in the inspection form. Decks that are integral with the superstructure will be rated as a deck only and not influence the superstructure rating.
Superstructure	The superstructure includes all the structural members that support the bridge deck. These may include steel beams, a concrete frame or culvert, steel cables and a floorbeam system as used in a suspension bridge, or a steel truss (Svirsky, 2014). The condition rating describes the physical condition of all the structural members. The condition of the bearings, joints, paint system, etc. will not be included in the rating except for extreme situations, but the condition will be noted in the inspection form. Superstructures that are integral with the deck will be rated as a superstructure only and not influence the deck rating.
Substructure	The substructure is essentially the bridge's foundation supporting the superstructure (Svirsky, 2014). The condition rating describes the physical condition of the substructure; which may be piers, abutments, piles, fenders, footings or other components.

Depending on the amount of deterioration, the bridge components are categorized into ten condition ratings which were developed by the National Bridge Inspection Standards. Using NBI component condition rating guidelines, component condition rating codes range from 0 to 9, where 9 is the best possible rating. Table 2.2 outlines these Structure Inventory and Appraisal (SI&A) component condition ratings. The one-digit structure codes are reported by bridge inspectors and state DOTs to the NBI on a Federal SI&A forms. These forms are not inspection forms, but just summarize the

bridge data required by the FHWA to meet the requirements of the National Bridge Program.

**Table 2.2 General component condition ratings guidelines from FHWA’s *Coding Guide***

<b>Rating</b>	<b>Condition Description</b>
9	Excellent condition
8	Very good condition – no problems noted
7	Good condition – some minor problems
6	Satisfactory condition – structural elements show some minor deterioration
5	Fair condition – all primary structural elements are sound, but may have minor section loss, racking, spalling or scour
4	Poor condition – advanced section loss, deterioration, spalling or scour
3	Serious condition – loss of section, deterioration, spalling or scour have seriously affected primary structural components. Local failures are possible. Fatigue cracks in steel or shear cracks in concrete may be present.
2	Critical condition – advanced deterioration of primary structural elements. Fatigue cracks in steel or shear cracks in concrete may be present or scour may have removed substructure support. Unless closely monitored, it may be necessary to close the bridge until corrective action is taken.
1	“Imminent” failure condition – major deterioration or section loss present in critical structural components or obvious vertical or horizontal movement affecting structure stability. Bridge is closed to traffic but corrective action may put back in light service.
0	Failed condition – out of service – beyond corrective action

While the range of the ratings is from 0 to 9, a couple of these ratings hold more significance over the others. For instance, from ratings 5-9, the structure is not in need of any immediate repair, and in the worst case scenario (a rating of 5), the components are just selected to receive careful attention in the next inspection. However, when a primary component of a structure has a rating of 4 or lower, then the structure is then considered to be *structurally deficient* (FHWA, 2010). A rating description of structurally deficient

is used to classify a bridge whose structural elements are composed of deteriorated physical conditions and consequently the load capacity is reduced. A structurally deficient classification does not imply the bridge is unsafe. In most cases, when an inspection reports a bridge as structurally deficient then the bridge is posted for reduced loads and scheduled for repairs. In other cases, the bridge may be temporarily closed until repairs can be completed (ODOT, 2013). A bridge can also receive a *functionally obsolete* classification. A rating description of functionally obsolete is reserved for bridges that do not meet current standards, primarily geometric standards. For instance, a functionally obsolete bridge may not have adequate lane widths, shoulder widths, vertical clearances, or design loads to serve traffic demands. This term is also used to describe bridges that are occasionally flooded (ODOT, 2013). A functionally obsolete bridge is not bounded by any particular rating.

Component condition ratings are determined from condition descriptions, which are broad in nature; covering a large variety of bridge elements and materials types. The inspector is responsible for accurately mapping the structural deficiencies and condition descriptions into the appropriate condition ratings. The following list illustrates several common deficiency terms found in condition descriptions and their associated material types (FHWA, 2012):

- Section loss usually applies to steel members or reinforcing steel
- Fatigue crack applies to steel members
- Cracking/spalling usually are used to describe concrete
- Shear crack usually applies to concrete but may apply to timber as well
- Checks/splits applies to timber members
- Scour can apply to substructure

Guidelines set forth in the *Coding Guide* helpfully clarify how each component evaluation and structural deficiency affects the condition rating it receives. The following method for determining the proper condition rating has been found to help inspectors derive to a suitable rating (FHWA, 2012):

- Identify phrases that describe the component
- Read through the rating scale until encountering phrases that describe conditions that are more severe than what actually exists
- Be sure to read down the ratings list far enough
- Correct rating number then is one number higher

Proper assignment of the condition ratings is best achieved when bridge components are broken down into individual elements and then evaluated. Bridge elements are the individual members that are connected together to construct the bridge components. Bridge elements include components of bridges such as stringers, cables, girders, columns, piles, piers and other systems that are typically managed by agencies utilizing state bridge management systems (AASHTO, 2010). Bridge elements are categorized at different levels, i.e. National Bridge Elements and Bridge Management Elements, as seen in Figure 2.2. The National Bridge Elements (NBE) represent the primary structural elements of bridges that are a national concern for safety, while Bridge Management Elements (BME) include other bridge elements that state agencies have chosen to pay particular attention to.

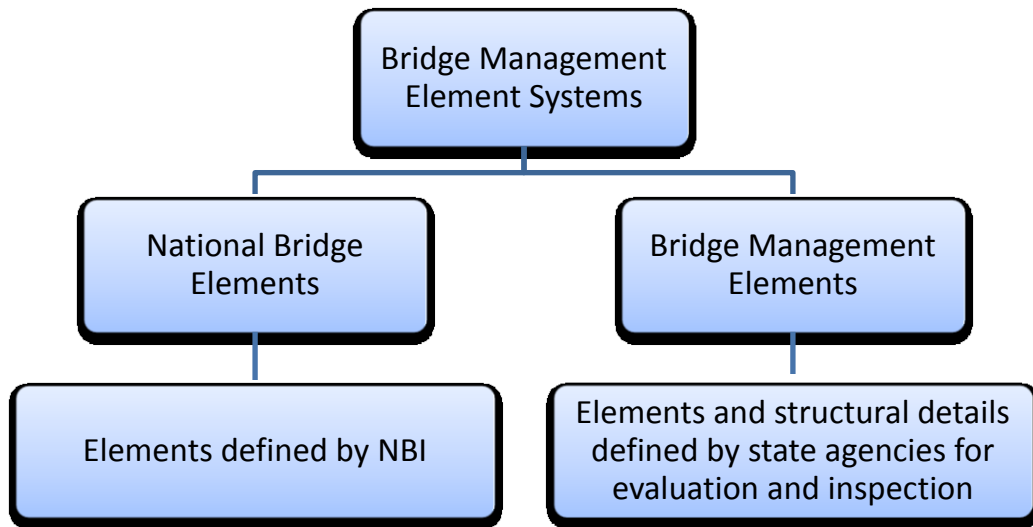


**Figure 2.2 Categorization of bridge elements**

Figure 2.3 displays the breakdown of various NBEs that correspond with the bridge components and material types. Since the NBI only considers ratings of bridge components, the national bridge element condition assessments should be translated into the component format used in the NBI. Processes to convert from NBE condition ratings to the component condition ratings are found in AASHTO's *Bridge Element Inspection Manual 2010*.

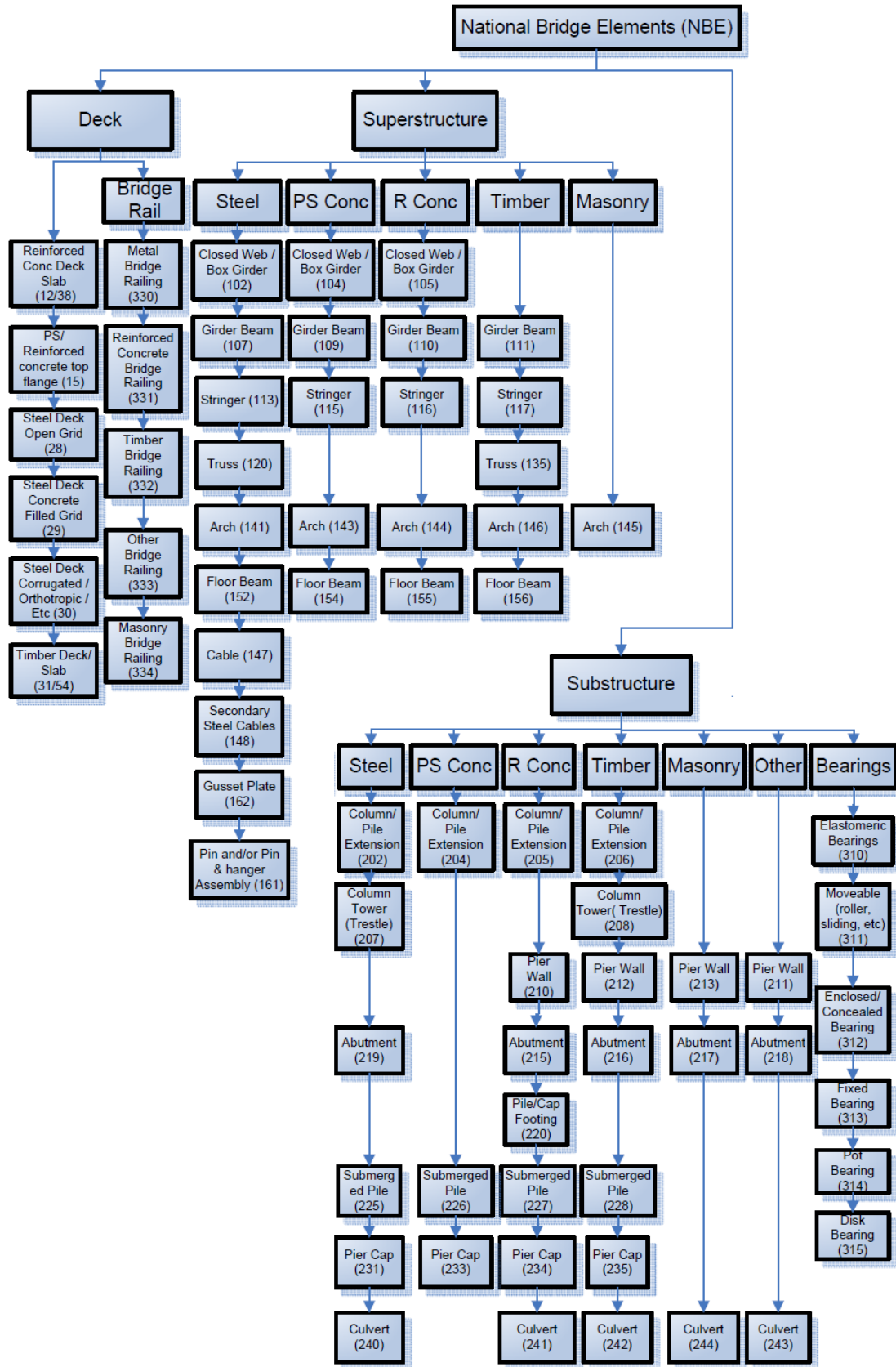


Figure 2.3 National bridge elements corresponding with bridge component (AASHTO, 2010)

While the NBE rating system offers a more detailed description of bridge damage by considering bridge elements, it is still largely generic in order to maintain compatibility of condition assessments between agencies and states. Diaphragms, cross bracing, and connection plates are not considered in the breakdown of national bridge elements (AASHTO, 2010). However these items are often assessed on a smaller scale by state agencies using their own BME system, broken down in Figure 2.4.

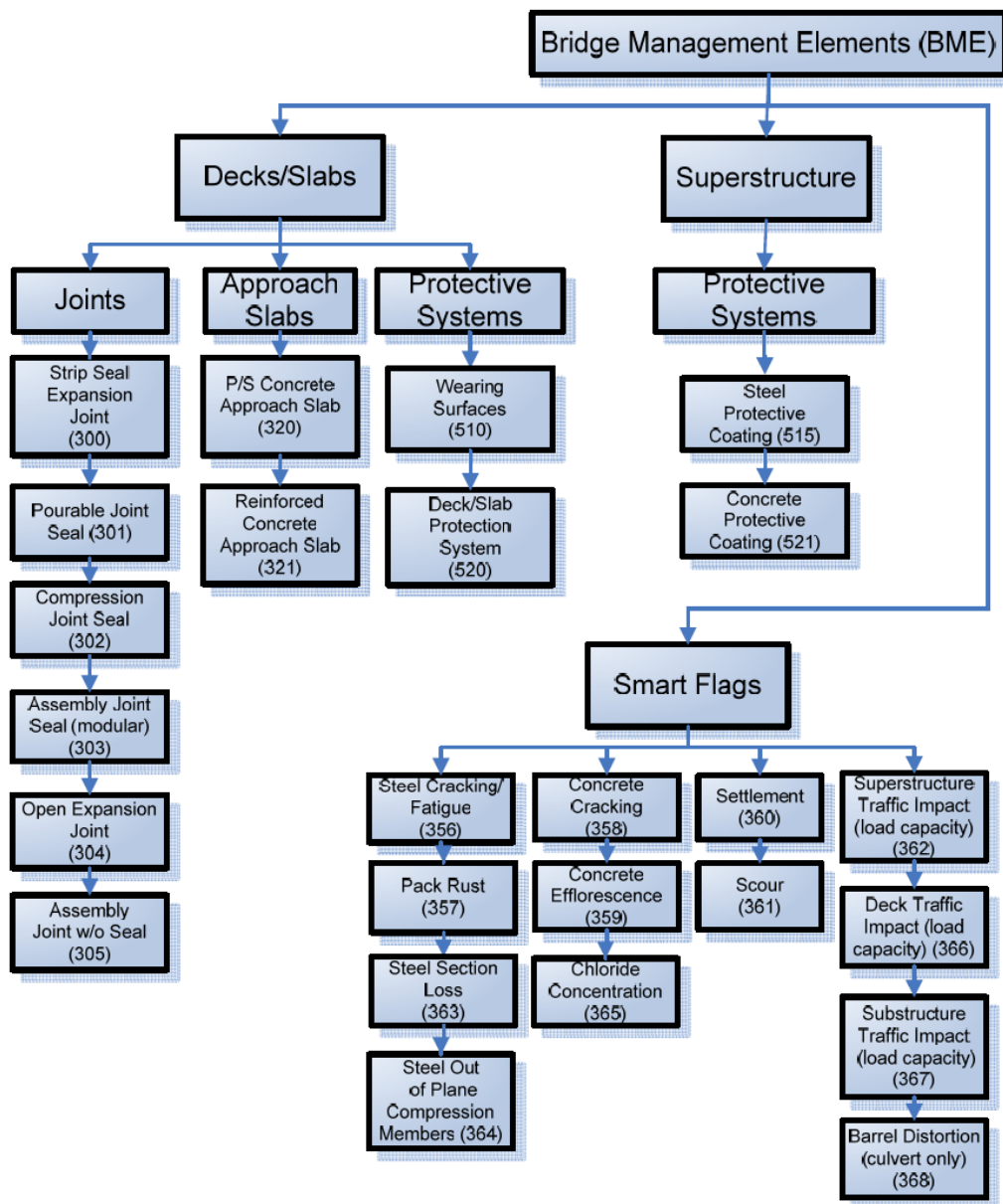


Figure 2.4 Bridge management elements corresponding with bridge component (AASHTO, 2010)

AASHTO's *Bridge Element Inspection Manual 2012* compiles information of all Bridge Management Elements and their sub-sets, known as Commonly Recognized Elements (CoRe) for Bridge Inspection. The purpose of adopting CoRe elements for bridge inspection was to standardize element-level condition data collection in the United States. The AASHTO manual defines each bridge element, provides definitions of the elements condition state, and provides a table of feasible actions for the condition state. In cases where the agency defined BME is also a NBE, the agency developed element condition states must have capability to be aggregated back with NBE for submission with the NBI.

Currently, many states use the *Pontis* system to assist inspectors with the on-site evaluations of bridge. *Pontis* is a bridge management software tool, which was developed under a FHWA contract with Cambridge Systematics and Optima, Inc. and California DOT, and then later sponsored by the FHWA for cross development amongst state DOTs (FHWA, 2013). The system is currently owned by AASHTO, who has licensed *Pontis* to over 45 state DOTs, including the Maryland State Highway Administration. There is no federal requirement for states to use the *Pontis* system, however, many states use the system because it can be more specific to categorize and describe the types of defects in the bridge elements. Bridges are presented by the CoRe elements in *Pontis*, and percentage condition states for bridge elements are inspected and stored in the database. The *AASHTO Bridge Element Inspection Manual 2010*, provides detailed information on how to map defects from the *Pontis* system into the correct condition states for National Bridge Elements.

The *Pontis* system stores more detailed information of the elemental defects than is required from the National Bridge Inventory. The system provides quantitative data about the physical condition and performance of bridge elements. For instance, Smart Flags (Defect Flags) are used by some agencies to identify the predominant defect for that condition state. These flags describe the level of deterioration on the structural element. They are prescribed their own condition states, which are later mapped into the Bridge Management Element component condition ratings. In cases where the Bridge Management Element is also a pre-defined National Bridge Element, then the defect flag condition state is also considered in the NBI. These smart flags are listed as:

**Table 2.3 Smart Flags found in Pontis bridge management systems**

Steel Cracking/Fatigue	Settlement	Steel Out-of-plane Compression Members
Pack Rust	Scour	Deck Traffic Impact
Concrete Cracking	Superstructure Traffic Impact	Substructure Traffic Impact
Concrete Efflorescence	Steel Section Loss	Barrel Distortion

The smart flags of particular interest in this paper are Steel Cracking/Fatigue. This flag is only used for elements that are already showing fatigue damage and is not applicable to bridges where fatigue damage is not present. Table 2.4 lists the three condition states associated with the Steel Cracking/Fatigue defect flag and their corresponding descriptions.

**Table 2.4 Pontis System condition state definitions for steel fatigue**

<b>Condition State 1</b>	Fatigue Damage	Fatigue damage exists, but has been repaired or arrested. The element may still be fatigue prone.
<b>Condition State 2</b>	Analysis warranted	Fatigue damage exists which is not arrested (normally, this condition state would be used the first time the element is identified and at any other time when additional fatigue damage occurs).
<b>Condition State 3</b>	Severe Fatigue Damage	Fatigue damage exists which warrants [structural] analysis of the element to ascertain the serviceability of the element or bridge.

Additionally, the Steel Section Loss flag is often used alongside the Steel Cracking/Fatigue flag in order to identify the severity of section loss in steel members. Section loss occurs when a structural member experiences corrosion due to high chloride content or carbonation. The corrosion causes a section loss in an area of the members design section, which causes the physical properties of the member to change. Ultimately the structural integrity becomes compromised and resulting in reduced capabilities of the structure to perform its original function. Table 2.5 lists the four condition states associated with the Section Loss defect flag and their corresponding descriptions.

**Table 2.5 Condition state definitions for CoRe section loss (DeIDOT, 2008) (VDOT, 2007)**

<b>Condition State 1</b>	Corrosion has been arrested	Section loss has been repaired or cleaned and coated over. No effect on the strength and/or serviceability of the bridge.
<b>Condition State 2</b>	Corrosion has not been arrested	Section loss exhibits active corrosion. No effect on strength and/or serviceability of the bridge. Structural analysis is not yet warranted.
<b>Condition State 3</b>	Analysis Warranted	Measurable section loss exists that warrants analysis to determine the serviceability of the element or bridge. Check to ensure there is no reduction in posted capacity.
<b>Condition State 4</b>	Load Capacity or serviceability affected	Section loss has affected the load carrying capacity or the ability of the bridge to function as intended. Code this condition state after structural analysis.

For agency defined sub-sets of National Bridge Elements, the agency must be able to combine the BMEs back into NBE form, in order to maintain compatibility for submission with the NBI. The following diagram shows how the smart flags and elemental condition ratings are mapped into the National Bridge Elements.

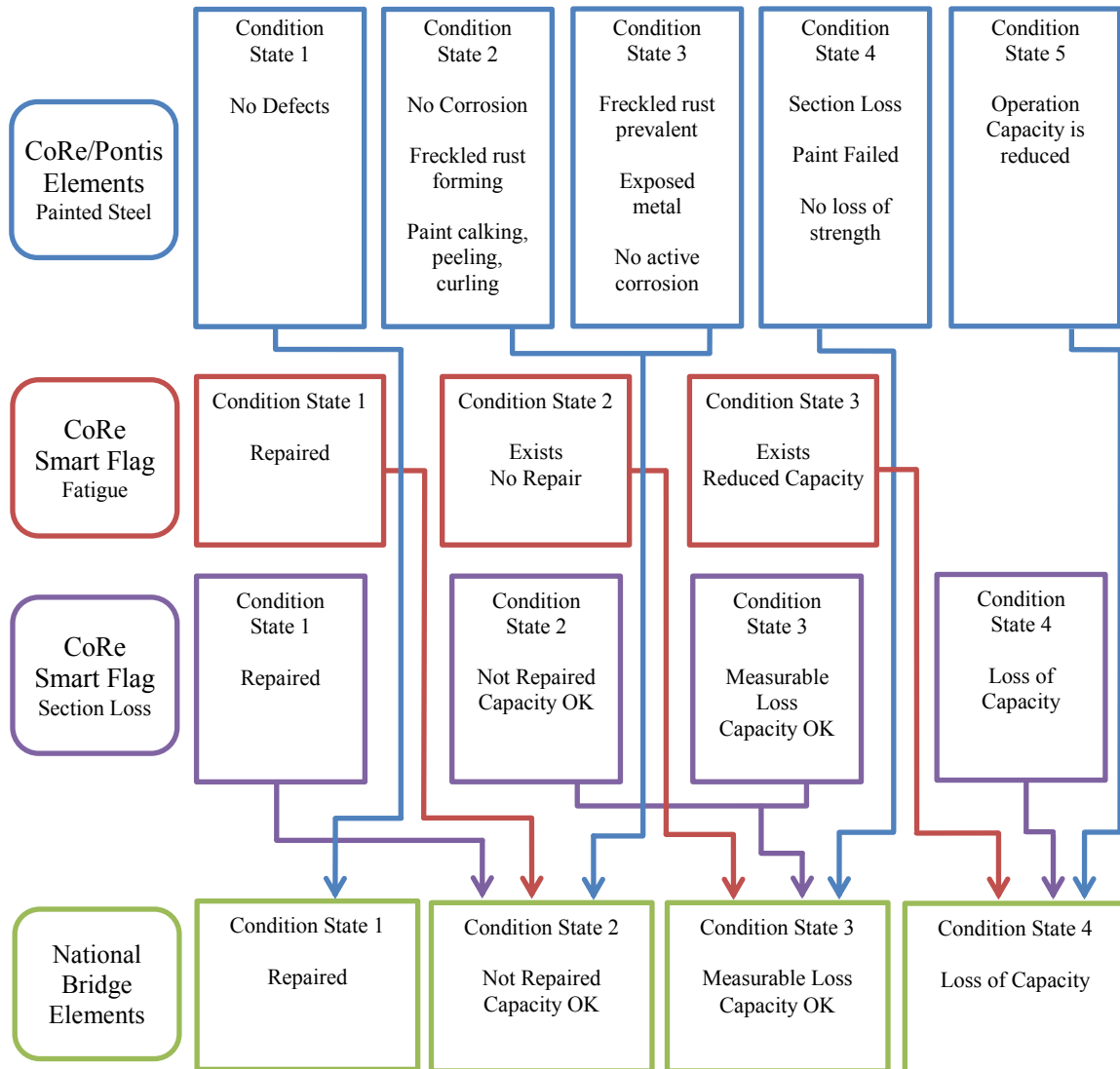


**Figure 2.5 Mapping of bridge management elements into National Bridge Elements**

Since the NBI condition ratings are assigned values on the 0-9 scale, the National Bridge Elements, which are assigned on a scale of 1-3 or 1-4, must be translated back to this 0-9 scale. In an effort to reduce the amount of time agencies spend in this translation, a computer programming tool known as the NBI translator or BMSNBI, is used to aggregate the element inspection data to the NBI scale. This tool is built into the Pontis systems, so is automatically computed for Pontis licensed states. Otherwise, state agencies should read the descriptions between element condition ratings and national

condition ratings in order to identify where the structures condition is best described and to choose the appropriate rating.

To assess fatigue deterioration of connection plates on a national scale, it is helpful to look how gusset plates are evaluated in the national bridge elements. Gusset plates are thick plates of steel used to connect beams and girders to columns or to connect truss members. Because a gusset plate and a connection plate have similarities in application, it is reasonable to assume the condition states of a gusset plate would closely resemble the condition states of a connection plate. In the hierarchy of national bridge elements (Figure 2.3), it is seen that gusset plates are an element that should be inspected as part of the bridge superstructure. The condition states for the gusset plate are summarized in Table 2.6.

**Table 2.6 Bridge element condition state definitions (AASHTO, 2010)**

<b>Defect</b>	<b>Condition State 1 (good)</b>	<b>Condition State 2 (fair)</b>	<b>Condition State 3 (poor)</b>	<b>Condition State 4 (severe)</b>
Corrosion	None	Freckled Rust	Section Loss	The condition is beyond the limits established in the condition state three (3) and/or warrants a structural review to determine the strength or serviceability of the element or bridge.
Cracking/ Fatigue	None	Arrested Cracks Exist	Moderate Cracks Exist	
Connections	Sound	Sound	Isolated Failures	
Load Capacity	No Reduction	No Reduction	No Reduction	

Cracking/Fatigue is a major consideration in the inspection and evaluation of gusset plates. Specifically, arrested cracks, cracks with arrest holes and are no longer growing, are observed to be in fair condition, while moderate cracks, cracks that have not been addressed, are observed to be in poor condition. Using Table 2.6 in parallel with Table

2.7, arrested cracks are considered condition state 2, where protective action may be required, and moderate cracks are considered condition state 3, which may require immediate repair or rehabilitation.

**Table 2.7 Actions associated with bridge element condition states (AASHTO, 2010)**

<b>Condition State 1</b>	<b>Condition State 2</b>	<b>Condition State 3</b>	<b>Condition State 4</b>
Do Nothing Protect	Do Nothing Protect	Do Nothing Protect Repair Rehab	Do Nothing Rehab Replace

## **2.2 Fatigue Failure Mechanics**

Failure mechanics describes the process a member fails at when subjected to fatigue (FHWA, 2012). In engineering terms, failure has been traditionally defined as the condition when an element exceeds or falls below a predefined limit state (Sarja, et al., 1996). This limit state defines a boundary that once surpassed; a structure would no longer fulfill its design criteria. In general, limit states may be set as three types: serviceability limit state (e.g. large deflection and exceeding a code requirement), damage limit state (e.g. excessive cracking) and ultimate limit state (e.g. collapse and fracture) (Massarelli, et al., 2001). The serviceability limit state corresponds to the boundary beyond which specified service requirements for a structure or structural element are no longer met. Thus, if a structure has not reached its serviceability limit state, the structural behavior is in compliance with standard criteria values and remains functional to withhold routine loadings. The damage limit state describes the boundary beyond which the structure has experienced an intolerable amount of damage. In many instances a crack on a structure may not have an impact on the safety or performance of a structure. These cracks may be inactive or growing at a slow rate on secondary components. The

damage limit state sets a boundary for that sets limits for crack sizes and locations. The ultimate limit state describes the boundary beyond which excessive deformation and/or collapse may occur. The damage and ultimate limit states are most relevant to the stages of degradation associated with a structure's fatigue life.

### **2.2.1 Fatigue Life**

A structure has reached the end of its fatigue life when the number of load cycles it is subjected to initiate and propagate a fatigue crack to critical size; confronting the structures limit state. Within a structure's fatigue life, a structure is considered to experience two different stages over two different periods in time:

- Crack initiation
- Crack Propagation (Fracture Mechanics)

The crack initiation stage describes the time when cracks are just beginning to initiate from points of stress concentrations in structural details. Once a fatigue crack has initiated, applied repeated stresses cause propagation, or growth, of a crack across the section of the member until the member is capable of fracture. Fracture of a member is the separation of the member into two parts. The fracture of a "fracture- critical" member may cause a total or partial bridge collapse. It is technically significant to consider the crack initiation and crack propagation stages separately because the practical conditions that have a large influence on the crack initiation period, are different from the conditions that will influence the crack propagation period (Schijve, 2009).

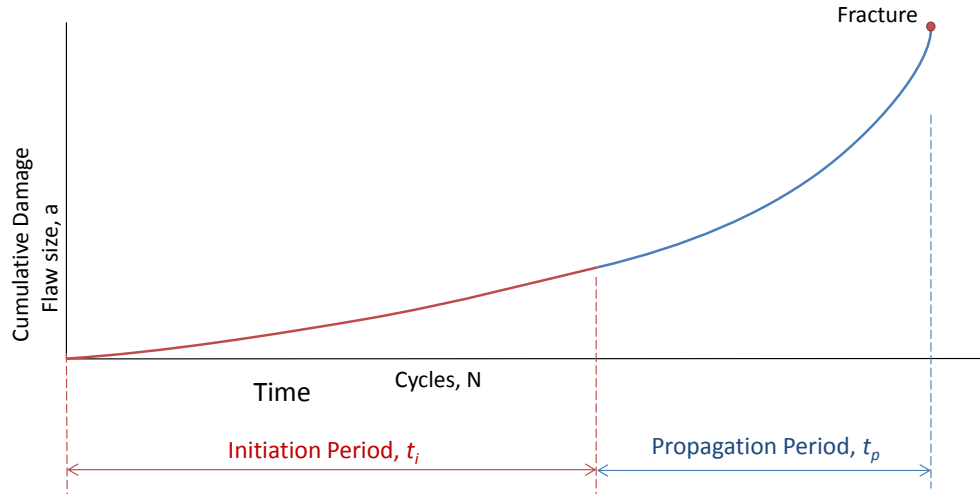


**Figure 2.6 Illustration of fatigue life concepts**

The crack initiation and propagation stages are associated with a moment in time when the structure is undergoing some form of deterioration. In the crack initiation stage, the term *failure* is used to describe a damage limit state, i.e. the moment of transition from crack initiation to crack propagation. For this stage, failure occurs when an existing crack reaches a predefined critical crack size, typically a microscopic crack that has just become visible in size. The number of cycles required to initiate a fatigue crack to this critical crack size is known as the fatigue-crack-initiation life. In the crack propagation stage, failure also describes the moment in time when a crack has reached a critical size, which is more associated with the ultimate limit state. At this stage, the number of cycles to propagate a specific initial crack size to a final crack size is called the fatigue-crack-propagation life. The final crack size can be determined from the material fracture toughness. When a structure has experienced a crack size at the end of the propagation life the structure is capable of fracture and is also considered to be at the end of its total fatigue life; the sum of the initiation and propagation lives. Bridge engineers use estimations of total fatigue life in predicting the performance of steel bridge members

(FHWA, 2012). Figure 2.6 illustrates the difference between the initiation period and propagation periods within a structures fatigue life. Details regarding the fatigue crack initiation period are discussed in Chapter Three: *Theoretical Development of Fatigue Crack Initiation Period* and the details regarding the fatigue crack propagation period and the corresponding three regions are discussed in Chapter Four: *Theoretical Development of Fatigue Crack Growth Period*.

### 2.2.2 Fatigue Life Prediction

There are two major numerical damage accumulation approaches that can be integrated together to predict the fatigue life of a structure: an empirical correlation approach, and fracture mechanics approach (Chen, et al., 2005). The empirical correlation approach uses a damage parameter that correlates with laboratory fatigue test results, and the fatigue life calculation is generally performed with respect to crack initiation. The application of fracture mechanics is best fit for crack propagation life, since it deals with crack growth.

The basis of the empirical correlation approach is to use a proposed empirical damage parameter,  $D$ , that correlates the fatigue life (number of stress cycles to failure,  $N_f$ ), with the number of stress cycles the structure has endured. The empirical correlations approach is generally divided into three categories: the stress-based method, the strain-based method, and the energy-based method, when stress, strain, or energy is used as the damage parameter, respectively (Chen, et al., 2005). For any one of these methods, the damage parameter to fatigue life functions generally takes the form of:

$$D - D_0 = F(N_f)^\alpha \quad (\text{Equation 2.1})$$

where,  $\alpha < 0$ ,  $F > 0$  and as  $N_f \rightarrow \infty$ ,  $D \rightarrow D_0$  ( $D_0$  is the corresponding value at the fatigue limit). Coefficients  $F$  and  $\alpha$  are evaluated by a best fit technique from experiment data. Figure 2.7 displays a schematic representation of the damage function in Equation 3.2. Since the mid-1800s a standard approach to fatigue analysis and design has been through the stress-based method, and is the method used for fatigue assessments of structural details in AASHTO LRFD Bridge Design Specifications 2012.

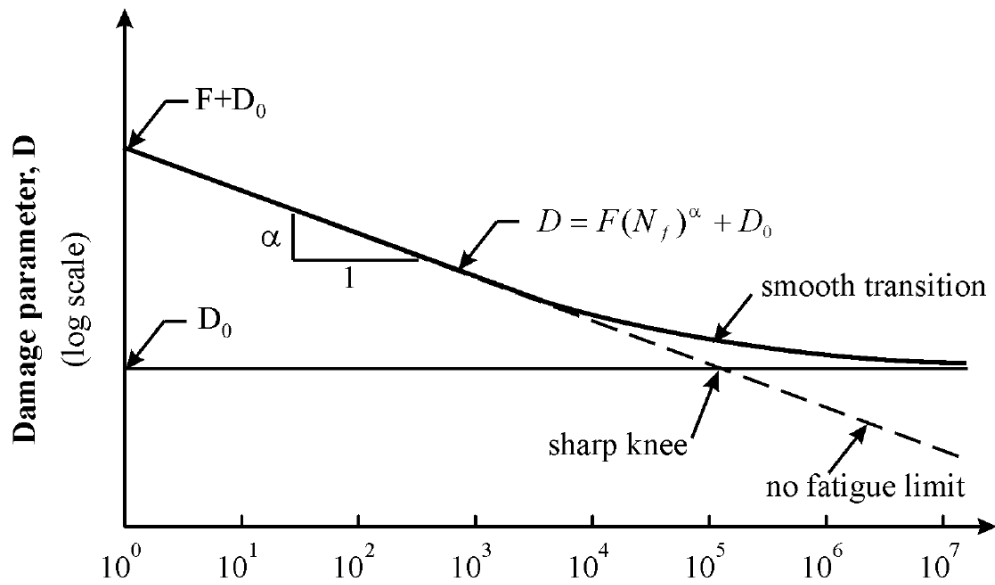


Figure 2.7 Schematic plot of damage parameter versus fatigue life curve (Chen, et al., 2005)

### 2.2.2.1 Stress-Based Method

The stress-based method currently underlies many fatigue specifications and remains to be the most widely used method in fatigue analysis (Chen, et al., 2005). Stress-based fatigue analysis is used to estimate initiation of a fatigue crack in a component under loading due to the uniaxial applied stress. The crack initiation is characterized by the S-N curve, also known as the Wöhler curve in honor of August Wöhler who was first to conclude that cyclic stress ranges are the governing parameter on

fatigue life. S-N curves are used to relate the stress range (S) vs. number of loading cycles ( $n_i$ ) and ultimately define the fatigue life of the material. S-N curves comprise the influence of material, the geometry of the local structure, and the surface condition. The stress-based method is most applicable to cases of high cycle fatigue where material response is mostly elastic.

#### **2.2.2.2 *Fracture Mechanics***

For many engineering structures, the most significant portion of its fatigue life falls within the crack propagation stage, which is governed by fracture mechanics. Fracture mechanics deals with the specific concept within solid mechanics: that a crack is present in the structure. For this reason, fracture calculations are typically not performed in design but are often used in service to assess a particular defect (Chen, et al., 2014). Analyses within fracture mechanics seek to find quantitative relations between the crack length, the crack growth rate through the material type, and the stress at which the crack propagates to cause structural failure (Roylance, 2001). The use of fracture mechanics in crack propagation life prediction has become widespread when it became obvious that the fluctuation of the stress field at the crack tip should control the rate of crack growth (Paris, 1998).

The parameter describing the stress field around the advancing crack tip is an important component in the fracture mechanics approach. This parameter is referred to as the stress intensity factor. The stress intensity factor,  $K$ , is used in linear-elastic fracture mechanics (LEFM) when the nominal stress versus strain response is essentially elastic. High-strength structural materials very often have a low ductility, but this doesn't mean they are necessarily brittle. At the microscopic level, the ductility of these

materials means a small plastic zone is created at the crack tip (Schijve, 2009). When plasticity effects are considered, crack growth parameters are conducted through an elastic-plastic fracture mechanics (EPFM) analysis, such as the energy release rate by the J-integral or the Crack Opening Displacement method. Since EPFM analyses account for plasticity and where the crack tip zone is large, then EPFM analysis may be better suited for highly ductile materials. However, for small-scale plasticity conditions, such as those found in engineering steel, LEFM analysis that is corrected for the effect of the small plastic zone effect offers the greatest advantages regarding the correlation of crack growth data (Chen, et al., 2005).

From the quick review on fatigue life prediction models, the integration of an empirical correlation approach together with a fracture mechanics approach serves as an appropriate method to predict the fatigue life of a structural detail; the former for crack initiation life and the latter for crack propagation life. Because of the small stresses generally present in fatigue problems, the plastic zone at the tip of cracks is limited and LEFM is therefore a useful tool for fatigue crack propagation life prediction (Chen, et al., 2005). By using these two methods, analyses of fatigue damage assess the onset of fatigue cracks, the amount of fatigue cracking, the crack length, and crack growth rates until the ultimate limit state is reached.

### **2.3 Role of Structural Health Monitoring in Failure Mechanics**

Various approaches for obtaining reliable information on fatigue loading have been developed through the use of structural health monitoring. Structural health monitoring (SHM) uses sensing instrumentation to observe and monitor the response of a system over a period of time using sampled dynamic measurements from a sensor or from an array of sensors. A SHM system serves the role of detecting damage in civil infrastructure and statistical analysis of these features determines the operational condition and durability. Numerous SHM methodologies, techniques, hardware and software have been developed and are utilized to achieve different bridge management goals, such as to increase safety (Alampallia, et al., 2008).

SHM technologies used in bridges provide accurate field measurements because no assumptions need to be made for uncertainties. Thus, the most accurate method for assessing the dynamic effects from traffic loads on the bridge is to use sensors to measure the stress in identified fatigue-critical members. The effects of varying vehicle weights and their sporadic combinations are reflected in the sensor data. This data is used to perform assessments of the structure's remaining useful life.

### **2.4 SHM Paired with Condition Assessments**

For accurate condition assessment, AASHTO's *Bridge Element Inspection Manual 2010* encourages non-destructive testing results to be taken into consideration in the condition assessments. Many states currently use some non-destructive evaluation (NDE) methods in their condition rating assessments. The NDE methods are limited to a short-term SHM system that is temporarily installed, records live load responses, and is then removed (BDI, 2014). The primary purpose of short-term monitoring is to obtain

quick and valuable assessments of a structure's structural integrity and load-carrying capacity. However, the methods used are not long-term structural health monitoring methods and provide only limited insight into a structure's condition. While short-term testing can be used to assess the performance of structural components under applied loading, structural damage is rarely caused by the stresses exceeding those predicted by design. Damage from fatigue occurs from the repetition of repeated loads that are far below the strength of the structure. Furthermore, the fracturing of materials before plastic deformation is visible (aka brittle fracture), due to fatigue cracking, is one of the most common causes of steel bridge components failures (Xia, et al., 2005). In order to observe continuously stressed bridges that are subject to fatigue loads, long-term monitoring should be used. Long-term monitoring refers to the installation of a SHM system that will remain in place for weeks, months, or years and automatically collects and stores data (BDI, 2014). Thus, a long-term SHM system gathers real-time and accurate measurements of a structures behavior under various environmental and loading conditions and provides a much needed insight into the cumulative damage and degradation of strength within a structure. This insight can be used with element condition evaluations.

## Chapter Three: Theoretical Development of Fatigue Crack Initiation Period

The crack initiation periods describes the time when cracks are just beginning to initiate from points of stress concentrations in structural details. The occurrence of fatigue cracks within the crack initiation period is most often described as a “material surface phenomena” (Schijve, 2009). An initial microscopic crack grows a microscopically small amount in size each time a load is applied. Starting with an inclusion in the material, the crack growth rate is slow and the initiation period may cover a significant part of the fatigue life. Crack growth occurs at the crack front and the failure point in the fatigue-crack-initiation life occurs when a fatigue crack becomes large enough in size that it is considered a macro crack; often visible to the human eye. Figure 3.1 displays an illustration of the fatigue-crack-initiation life. Ultimately, the fatigue-crack-initiation life of a steel structure is governed by three factors (Mertz, 2012):

- 1) The number of loading cycles to which the member is subjected
- 2) The type of detail under examination
- 3) The stress range at the location of the detail

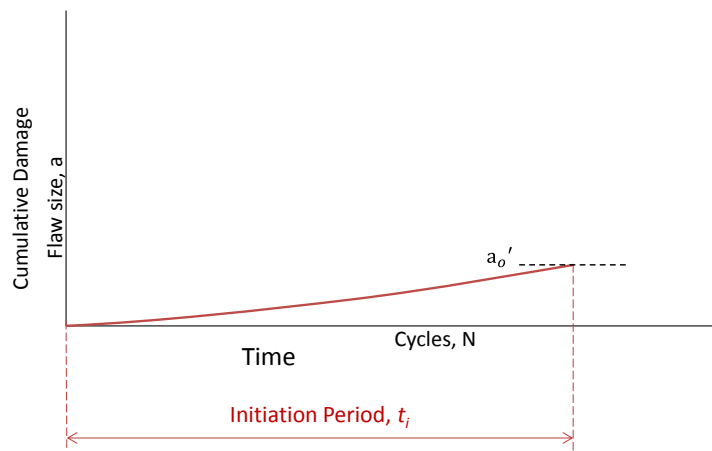
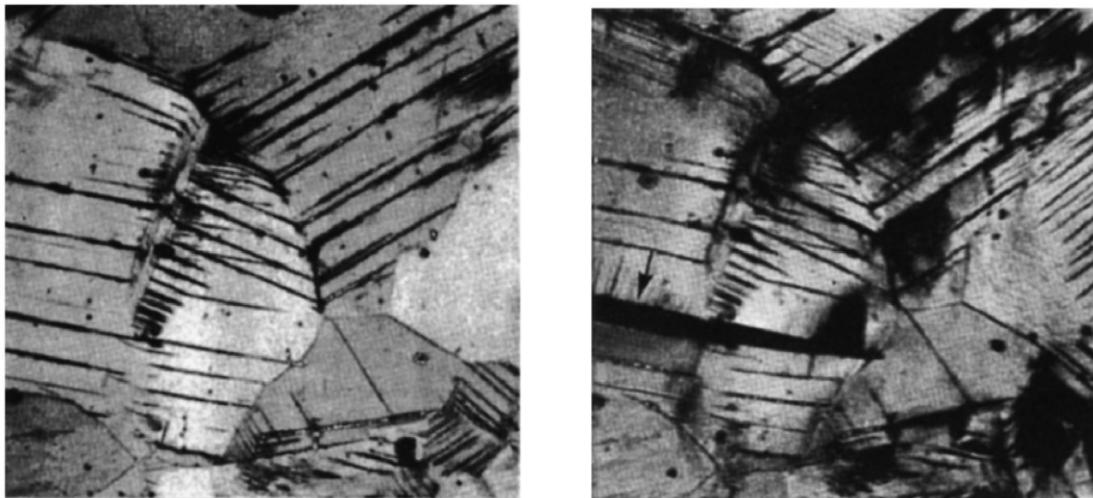


Figure 3.1 Illustration of fatigue-crack-initiation life

### 3.1 Crack Initiation

Fatigue crack initiation and crack growth are consequences of cyclic slip. Cyclic slip occurs with dislocation activities, which is a type of plastic deformation. Because material fatigue transpires at stress amplitudes below the yield stress, the cyclic slip develops at grains in the material surface. The surface is more susceptible to damage because it is exposed to the environment it is less constrained by surrounding material; as opposed to subsurface grains. Therefore, much lower stress amplitudes are needed for cyclic slip to occur at the surface than anywhere else in the material (Schijve, 2009).



**Figure 3.2 Development of cyclic slip bands and a microcrack (Schijve, 2009)**

A surface crack that is just beginning to develop as a result of cyclic slip is also known as a microcrack. A microcrack can occur from a single load cycle that creates a tiny imperfection in the material. As the material continues to experience reoccurring load cycles the crack grows; typically a crack grows perpendicular to the tensile stresses or load direction. The crack growth rate is measured as the crack length increment per loading cycle. Initially, the crack growth rate will be dictated by the surrounding grain boundary. For instance, the penetration growth rate of the crack in the material decreases

when the crack tip approaches the first grain boundary. After penetrating through the first grain boundary the crack growth rate increased throughout the next grain, but it decreased when approaching the second grain boundary (Schijve, 2009). The illustration of a crack penetrating a material is provided in Figure 3.3.

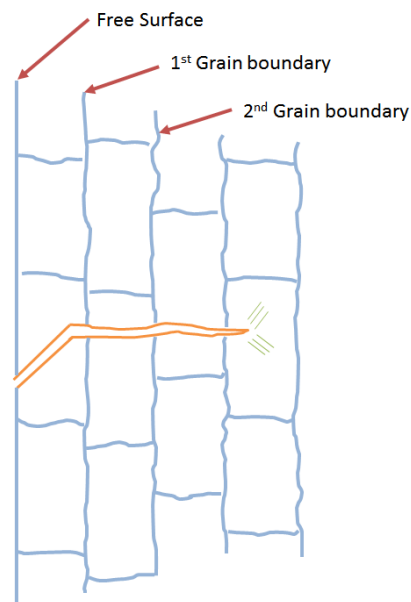


**Figure 3.3 Surface crack penetrating grain boundaries (Schijve, 2009)**

Once the crack has penetrated through a substantial number of grains, the crack growth is a different picture. The crack can no longer grow in each grain in an arbitrary direction and cannot continue to grow at any rate independent of crack growth in adjacent grains. Rather, as the number of grains becomes sufficiently large, crack growth occurs as a continuous process along the crack front. The crack growth is then approximated as a continuous line with semi-elliptical shape (illustrated in Figure 3.4). The surface aspects are no longer relevant and the crack growth rate will be dependent on the crack growth resistance of the material; the crack growth is no longer a surface phenomenon. This portion of crack growth behavior is discussed further in Chapter Four.

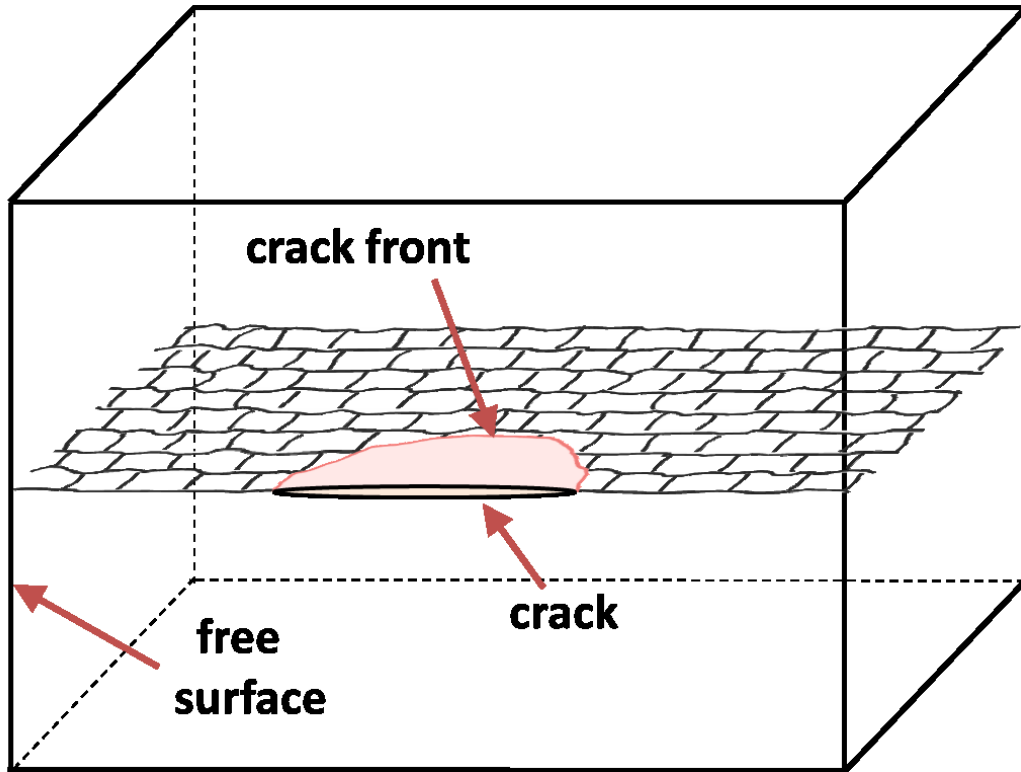
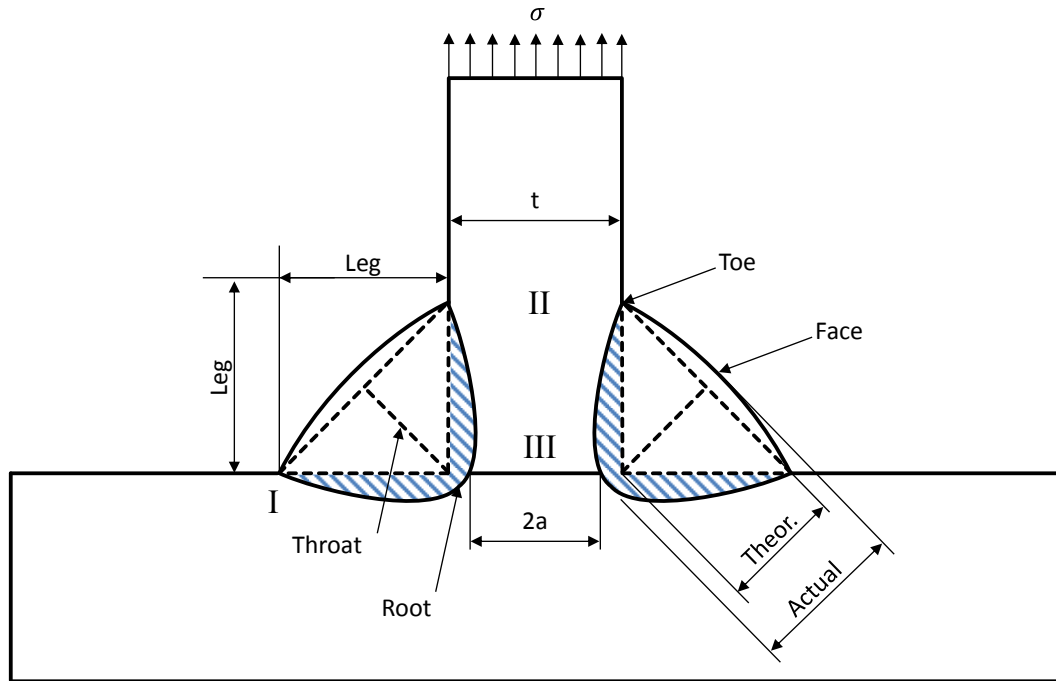


Figure 3.4 Elliptical crack front as crack passes through multiple grains

### 3.1.1 Defects in Fabricated Steel Structures

Cracks not only occur on a material surface from repeated loads, but they also develop from material defects which should not be present, such as defects in a welded joint. Figure 3.5 provides an illustration and nomenclature of a typical fillet weld, where the structure's geometry is positioned with a transverse gusset and longitudinal plate. This geometry is characteristic for connections plates, gussets, web stiffeners, and other similar elements on bridges. There are five main parts to each fillet weld, the face, root, toe, leg and throat. The face of the weld is the outer portion of the weld that you see when looking at a fillet weld. The root of the weld is the point of deepest penetration that is the opposite angle from the face. The legs are the width and height of the fillet weld. The throat is the distance from the center of the face to the root of the weld.



**Figure 3.5 Nomenclature of fillet welds**

Fillet weld sizes determine the theoretical throat of the weld, labeled “Theor.” in Figure 3.5. However, due to conservative design approaches, full penetrations at the weld root is has become typical design for fillet welded assemblies, and the actual throat is measured by the distance from the depth of penetration to the face of the weld convexity (Janosch, 1993). Penetration requirements for a fillet weld can be as high as 25 to 50 percent of the thickness of the base metal (FAA, 2008).

With a transverse gusset welded to a longitudinal plate, the toe of the weld forms a sharp angle at the weld periphery between the weld and the face of the gusset. This creates a line of elevated tension where fatigue cracking can start from the small, sharp discontinuities (Mertz, 2012). Nonetheless, the preferred crack-initiation sites are at the toe and the root of the welds, labeled as I, II, and III in Figure 3.5. More detail about the cracking with fillet welds is provided in section 4.1.2 *Cracks on Welded Structures*.

The quality of the weld is determined by the weld defects. Test data on welded details have shown that all fatigue cracks begin at the weld periphery or from some initial discontinuity in the weld. The kinds of defects that may occur in a welded joint include partial penetration, undercut or micro flaws at the weld toe, lack of fusion, porosity (gases in the unfused area expanding and getting trapped in the solidifying weld), inclusions such as slag, and start-stop locations from welding repair or arc strikes (Mertz, 2012). While fabricators attempt to minimize these defects, due to the welding process itself, it is impractical and not economically possible to eliminate them. Figure 3.6 displays an illustration the typical defects in a welded joint. The lack of penetration of a weld is the most serious weld defect, especially under tension loads. The defect can grow relatively large in size and acts similar to a surface crack. A weld undercut is another serious defect, especially if the profile is sharp at the bottom of the undercut. Since cracks begin at sharp profiles, these undercuts can be hotspots for crack initiation (Schijve, 2009). Even if an undercut is not present, the transition of the excess weld material to the base material still provides an area for stress concentration at the weld toe. Porosity and slag inclusions can also cause serious defects for crack initiation. Slag inclusions are usually more damaging than porosity, because the shape of these inclusions can create sharp profiles in the weld.

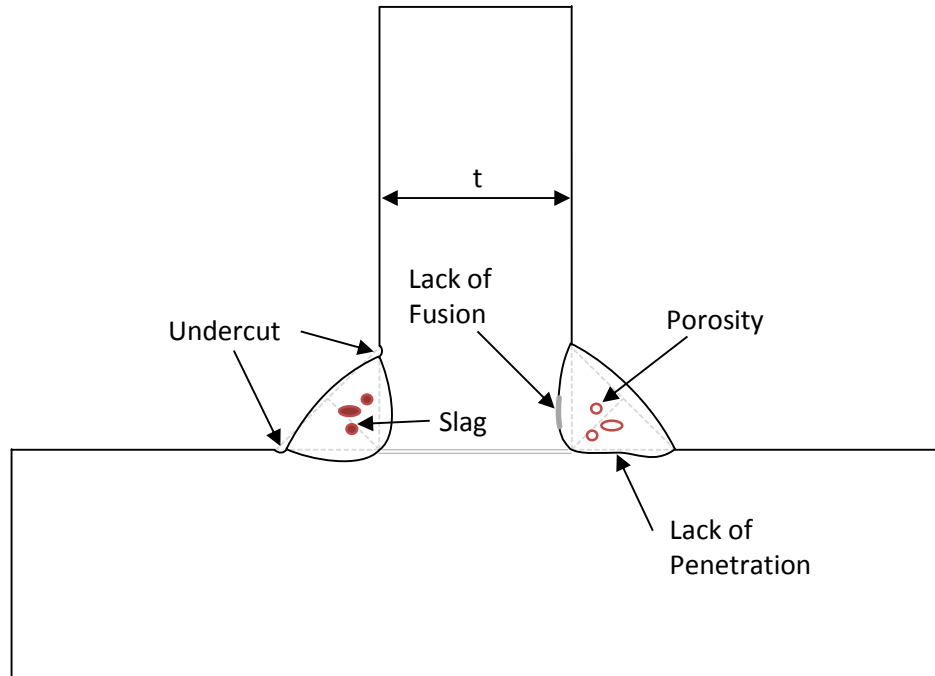


**Figure 3.6 Illustration and terms of possible weld defects**

The most critical conditions for crack initiation at structural details are those combining, high stress concentrations due to flaws, high stress concentrations due to connection details, and high stress concentrations due to out-of-plane distortions. The welding process itself introduces high stress concentrations due to thermal transformation from the melting temperature of the weld material when the weld is first applied and it cools to outside temperature. While the welding material attempts to contract, it is restrained by the steel plates, introducing residual stresses with residual tensile stresses in the weld direction. Upon loading, the residual stresses are more likely to induce fatigue crack initiation either at the ripples of the weld or related defects.

Figure 3.7 and Figure 3.8 show the establishment of fatigue cracks due to porosity in the welds. In cases with external defects, data shows that as much as 80% of the fatigue life has been consumed from crack initiation to an observable crack size at the surface (Mertz, 2012).

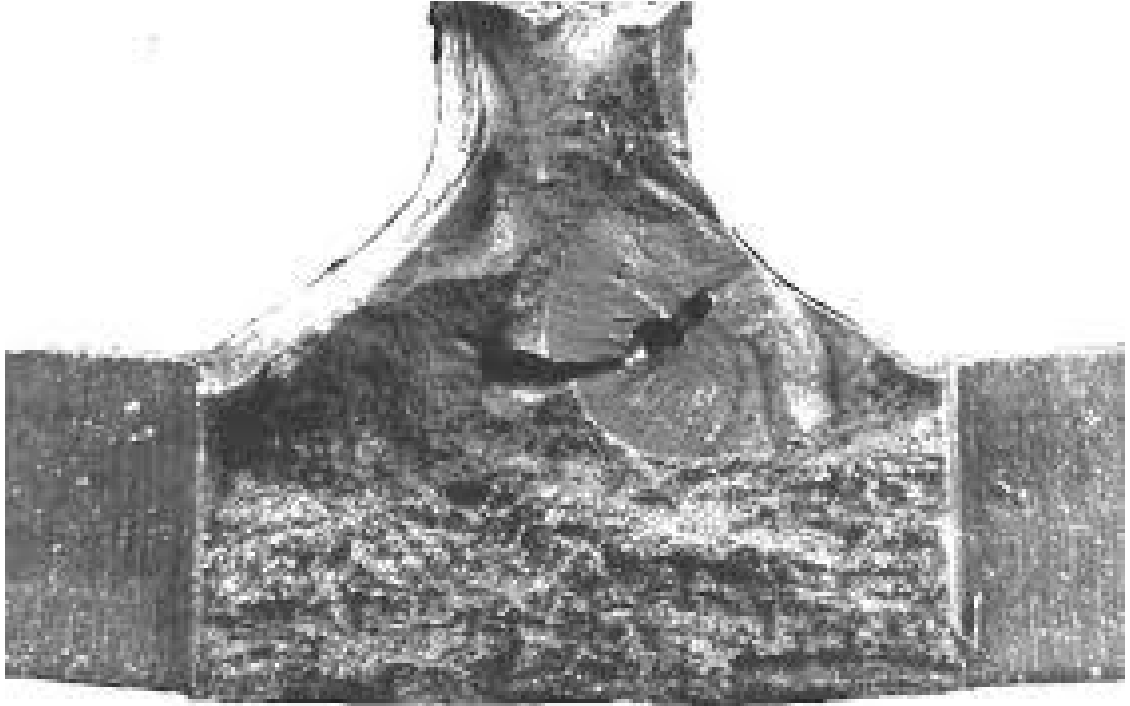


**Figure 3.7 Fatigue crack forming from internal porosity in web-flange connection (Mertz, 2012)**

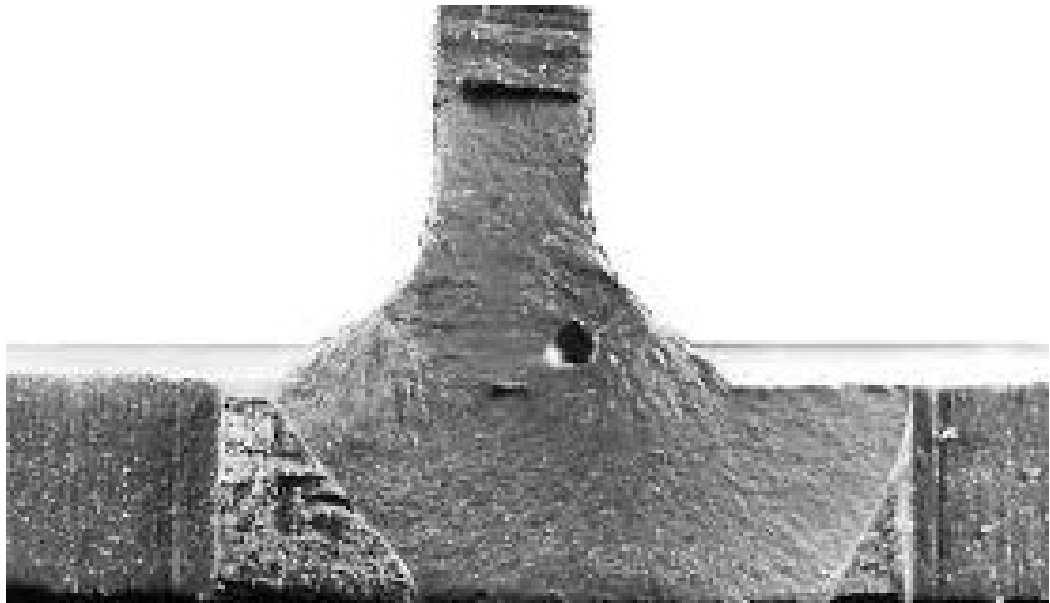


**Figure 3.8 Fatigue crack enlarged to three –ended crack from internal porosity (Mertz, 2012)**

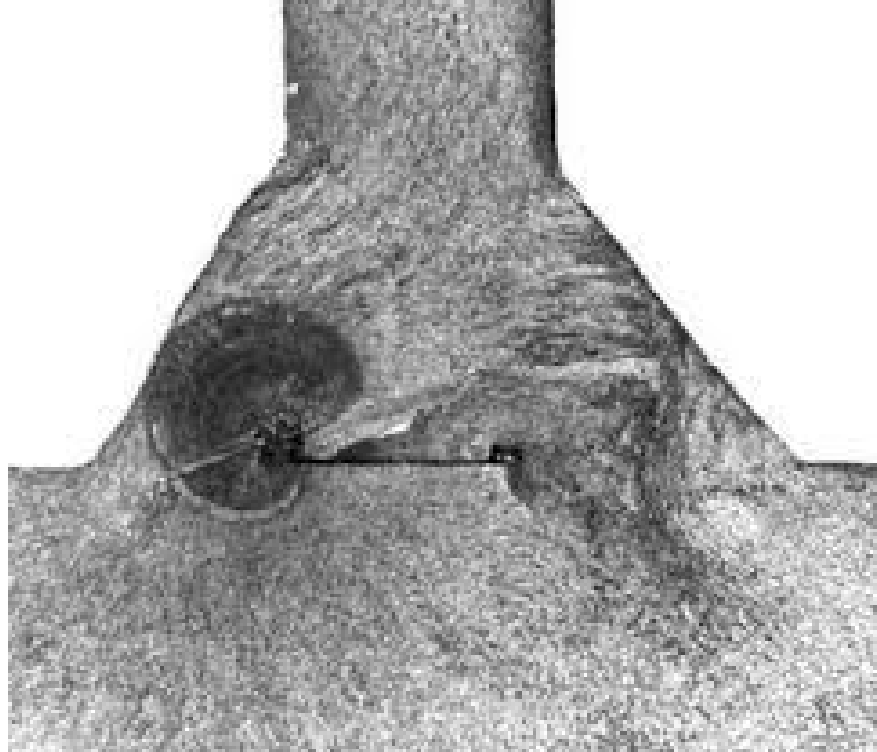


**Figure 3.9 Fracture surface of cross section (Mertz, 2012)**

Steel structures that are fabricated by welding contain "residual" or "locked-in" stresses that are a consequence of the welding process. These have considerable influence on the initiation and expansion of fatigue cracks.

### **3.2 Load-Induced Fatigue from Variable-Amplitude Loading**

When evaluating bridges for fatigue damage, the loading conditions are essential impacts on the structures service life, so it is necessary to accurately determine the effects from traffic loads. The most accurate method for assessing these effects is to directly measure the loads in identified fatigue critical members using structural health monitoring (SHM). A SHM system that is set up for long-term monitoring gathers real-time measurements of a structures behavior under various environmental and loading conditions. Compared with analytical methods for damage assessments, field strain

measurement is most accurate since no assumptions need to be made for uncertainties in load distribution such as unintended composite action between structural components, contribution of nonstructural members, stiffness of various connections, and behavior of concrete deck in tension (Zhou, 2006). Implementation of strain gauges captures the effects of varying vehicle weights and their random combinations in multiple lanes.

### 3.2.1 Strain Gage Analysis

The electrical resistance strain gage is the most frequently used sensor for acquiring strain data and conducting strain analyses (Pilkey, 2005). An electrical resistance strain gage is a strain-sensing element made of multiple metal foil loops that are calibrated to measure strain along the axis of the strain gage, i.e. axial strain. The gage operates on the principle that the electrical resistance of metal wire varies with strain. The fractional change in resistance ( $R$ ) per strain ( $\epsilon$ ), where  $\epsilon = \Delta L/L$ , is known as the sensitivity, ( $S_A$ ) of the metal that the strain gage is made from. In order for a strain gage to be used as a practical instrument, a strain gage should have the sensitivity to measure extremely small changes in the resistance of a wire with high accuracy (Kuphaldt, 2006).

The strain measurements are made by bonding the strain gage to the surface of the specimen under test and by sensing voltage changes that occur when the resistance of the metal foil loops change. The circuitry used to measure the voltage changes across the resistance gages is known as a Wheatstone bridge. The circuit of a basic Wheatstone bridge is displayed in Figure 3.10, where  $I_1$  is the current across ABC,  $I_2$  is the current across ADC, and  $R_1$ ,  $R_2$ ,  $R_3$ , and  $R_4$  are the four resistors that make up a full-bridge configuration.

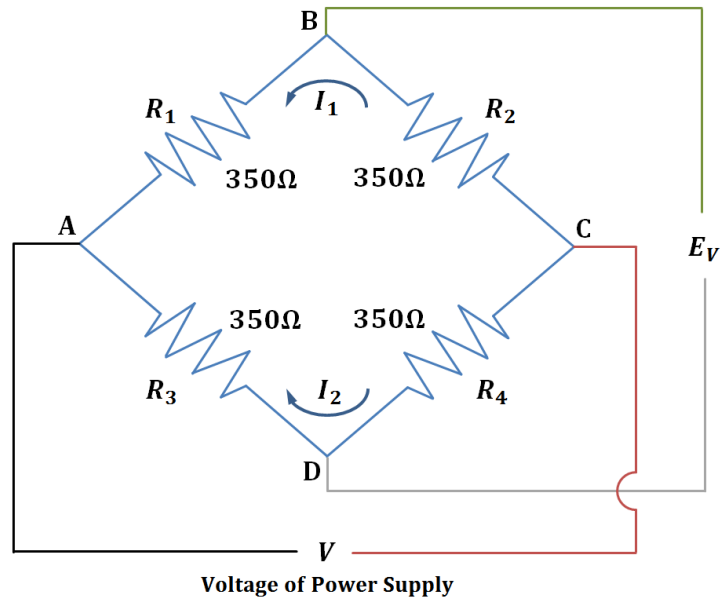


**Figure 3.10 Circuit of Wheatstone Bridge**

The changes in resistance of the sensing elements in the Wheatstone bridge result in a bridge output voltage that is proportional to the strain the material is experiencing. That is, the measured output voltage ( $\Delta E$ ) of the bridge scales with the excitation voltage. The voltage difference across the Wheatstone bridge solved from:

$$E_V = \frac{R_1 R_3 - R_2 R_4}{(R_1 + R_2)(R_3 + R_4)} \text{ Volts} \quad (\text{Equation 3.1})$$

The measured strains reflect the actual load distribution in the particular member of the structure where the strain gauge is placed.

### 3.2.2 Strain Data Acquisition

The acquired strain data on bridge elements is referred to as the load spectrum. The load spectrum gives information about the load-time history of the specific structural element that is being monitored. The load spectrum is made up of multiple stress cycles that correspond to the loading that is applied. The fatigue-crack-initiation life is defined

as the number of stress cycles ( $N$ ) within a load history to grow a crack to a specific crack size ( $a_{crit}$ ). The number of stress cycles is proportional to the number of trucks that cross the bridge during its service life. Heavier vehicles, typically trucks, create the largest stress cycles. The number of stress cycles a bridge experiences is relative to the age, location and span configuration of the structure (FHWA, 2012).

The most significant points in a stress cycle are the maximums and minimums, which are characterized by the stress range. At large stress ranges, cyclic slip occurs in the material, either at the material surface or in the crack tip plastic zone (Schijve, 2009). Thus, the accumulation of larger stress ranges at a faster rate of occurrence will result in a shorter fatigue life. Every stress cycle in a load history can be described by several parameters, including the stress amplitude ( $\sigma_a$ ), the mean stress ( $\sigma_m$ ), the maximum stress ( $\sigma_{max}$ ), the minimum stress ( $\sigma_{min}$ ), and more commonly the stress range ( $\Delta\sigma$ ). Stress range is defined as the algebraic difference between the maximum stress and the minimum stress:

$$\Delta\sigma = \sigma_{max} - \sigma_{min} \quad (\text{Equation 3.2})$$

From a fatigue mechanistic point of view,  $\sigma_{min}$  and  $\sigma_{max}$  are the more important parameters because they will describe the stress levels at which the loading is reversed; which means cyclic slip is also reversed (Schijve, 2009). These parameters are illustrated in Figure 3.11 and Figure 3.12 for two different loading types: constant amplitude loading and variable amplitude loading.

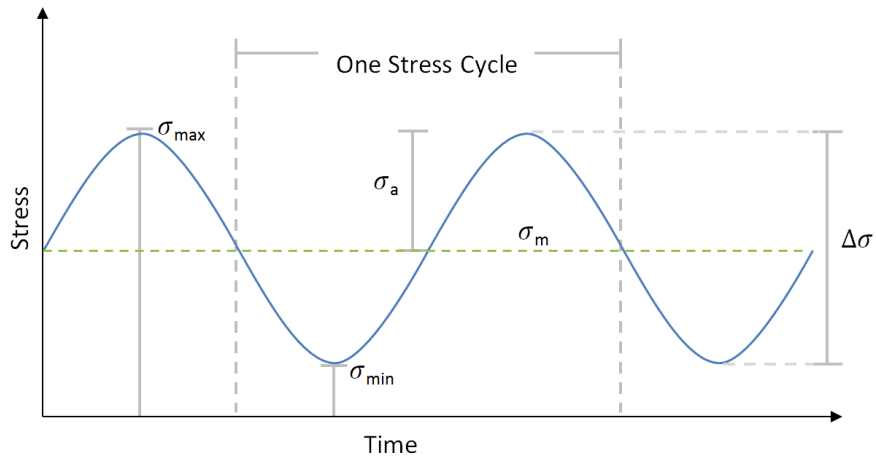


**Figure 3.11 Illustration of stress range and associated variables for CAFL**

A load spectrum for fatigue outputs two different patterns of load history: constant amplitude fatigue loading (CAFL) and variable amplitude fatigue loading (VAFL). Constant amplitude fatigue loading is associated with structures that are subjected to a cyclic loading and have a constant amplitude response and constant mean load. A sinusoidal curve, such as the one in Figure 3.11, is a typical example of a constant amplitude fatigue load. Variable amplitude fatigue loadings possess a more complicated load spectrum than constant amplitude loadings. The loading is sporadic and one stress cycle may be composed of different maximum and minimums.

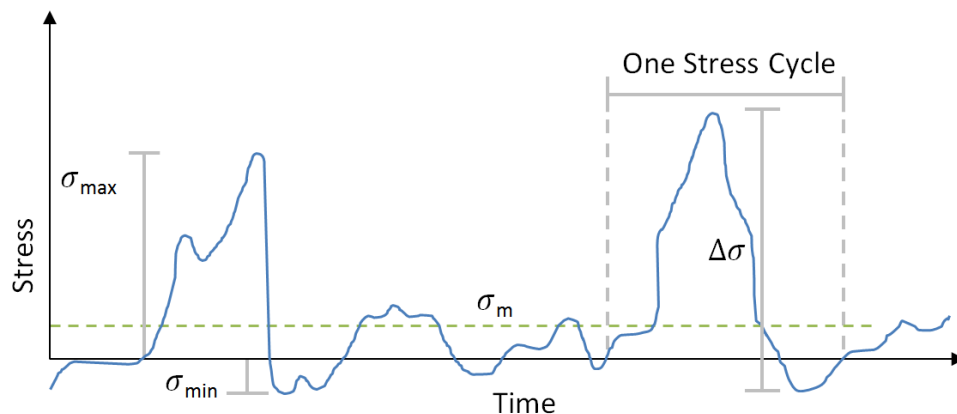


**Figure 3.12 Illustration of stress range and associated variables within VAFL**

In order to accurately characterize load histories, the content of a measured signal should be summarized and quantified in a meaningful way. Methods to help summarize the data and identify the fatigue relevant events within a complex load history are referred to as counting methods. Counting methods rely on the materials stress and strain response to applied loads. In order to illustrate the fundamental concepts behind counting methods, the stress-strain relationships for a specimen undergoing tensile and compression tests are illustrated in 3.2.3 *Stress-Strain Relationships*.

### 3.2.3 Stress-Strain Relationships

Stress-strain curves are derived from loading tests and provide insight into a specimen's mechanical properties. The stress-strain curve is found by applying an increasing uniaxial load to a specimen, while simultaneously recording the elongation. Thus, stress-strain curves display the amount of deformation (strain) at distinct intervals of loading (stress). A typical stress-strain curve for an engineering tension test is provided in Figure 3.13.

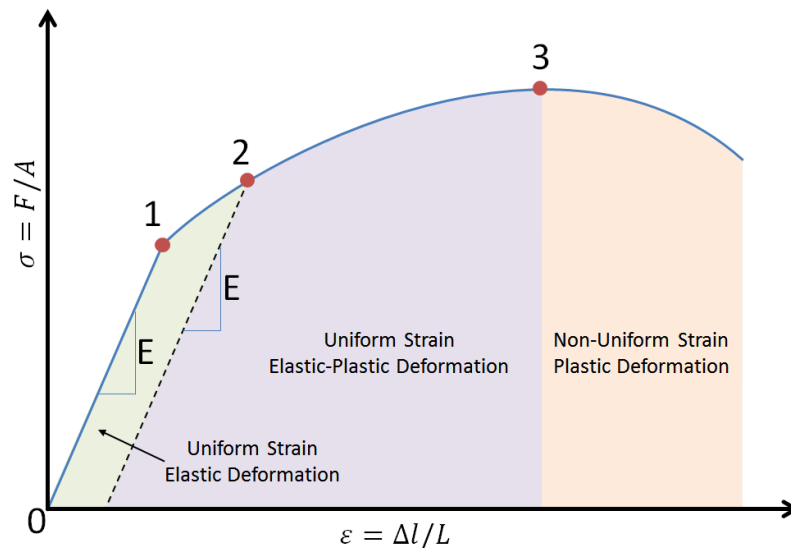


Figure 3.13 Engineering stress-strain curve

The stress-strain curve is divided into three regions, broken up by points 1, 2, and 3. Point 1 represents the proportional limit, also referred to as the elastic limit. From the origin to point 1, the specimen experiences uniform straining, where stress and strain are linearly related. This linear relation is known as Hooke's Law: a first order linear approximation of an elastic body's real response to an applied force:

$$\sigma = E\varepsilon \quad (\text{Equation 3.3})$$

Where,  $\sigma$  is stress,  $\varepsilon$  is strain and  $E$  is the modulus of elasticity. Upon reaching the elastic limit, the material will no longer go back to its original shape once a load is removed. From point 1 to point 2 the curve the material is partly elastic and partly plastic in behavior. While this is still considered uniform straining, the stress and strain are no longer linearly related. Point 2 represents the offset yield strength, the point where plastic deformation begins, i.e. permanent strain. Since it is often difficult to pinpoint the exact stress at which plastic deformation begins, the yield stress is often taken to be the stress needed to induce a specified amount of permanent strain, typically 0.2% strain (Roylance, 2001). To find the corresponding offset yield stress, a line with slope  $E$  is drawn from the strain axis (at  $\varepsilon = 0.2\%$ ) and runs parallel to the initial elastic loading line. The intersection point (Point 2) of this line and the stress-strain curve is the offset yield stress. Point 3 corresponds to the maximum tensile stress the specimen can withstand. Beyond this point, the specimen experiences non-uniform straining, i.e. plastic deformation, until it ultimately fractures; the end point of the graph.

The stress-strain curve in Figure 3.13 displays the relationship between stress and strain for a specimen under the loading of tensile stress. When the tension load is

released from the specimen and then reapplied, the specimen once again experiences elastic behavior before entering any region of plasticity; illustrated in Figure 3.14.

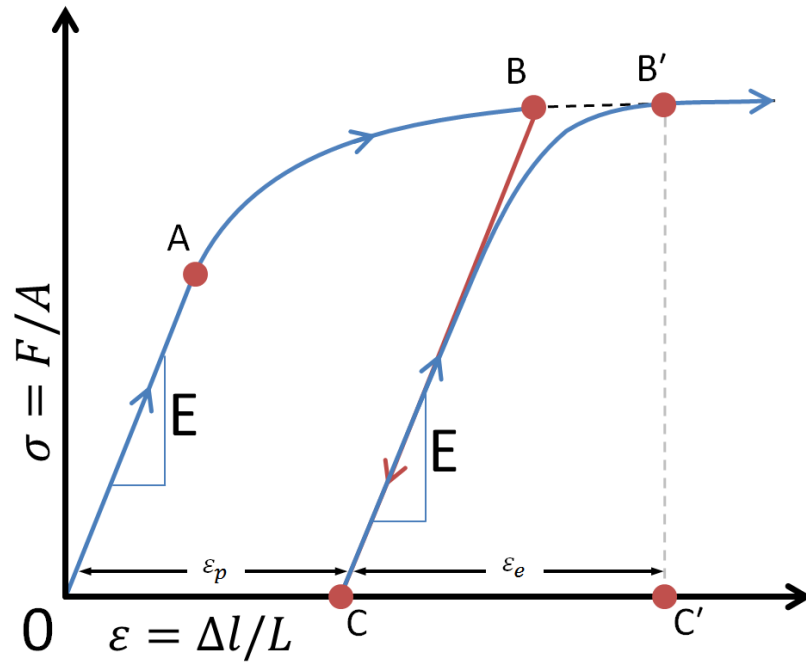
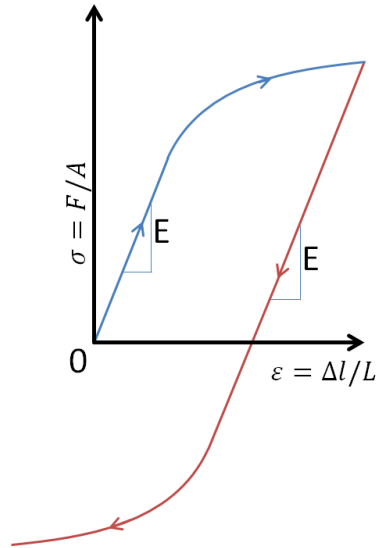
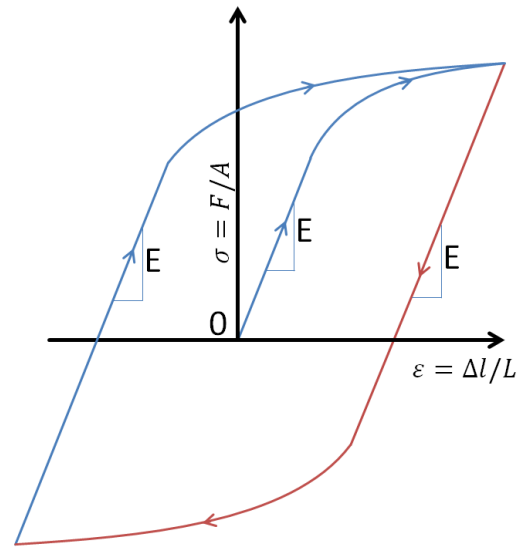


Figure 3.14 Loading and unloading on a stress strain specimen

In this figure, 0-A represents the elastic behavior of the material, the same behavior illustrated in the generic engineering stress-strain curve, Figure 3.13. The material is loaded to point B, at which point the specimen is unloaded until point C where it no longer has an applied load. The unloading from points B-C follows the same slope as 0-A, revealing that the specimen has retained its mechanical properties. The specimen is reloaded from point C, and experiences both elastic deformation and elastic-plastic deformation until it reaches point B', where it rejoins the original curve. The specimen rejoins the original curve because it had already experienced some permanent strain at point C. From B' the specimen continues to be loaded in tension until it surpasses its ultimate tensile strength and fracture occurs.



**Figure 3.15 Tension and compression loading on specimen**



**Figure 3.16 Complete stress-strain hysteresis**

Figure 3.13 and Figure 3.14 illustrate the stress-strain behavior of a specimen under tension loads. However, a specimen subjected to fatigue loads would undergo both tension and compression loadings. Figure 3.15 illustrates the stress-strain curve a specimen that was subjected to tension loads, was unloaded, and then subjected to a compression load of the same magnitude as the tension load. When the specimen is subjected to a complete cycle of loading and unloading with both tension and compression forces the result is a stress-strain hysteresis. The loading and unloading effect demonstrated through the stress-strain hysteresis is a linear problem and the relationship between stress and strain is demonstrated through Hooke's law, Equation 3.3. As seen in the hysteresis in (Figure 3.16), the material properties, i.e. Young's Modulus  $E$ , will be consistent even though some deformation is understood to have taken place. A stress-strain hysteresis is also associated with energy dissipation and fatigue damage (Lee, et al., 2012), where the enclosed area of the hysteresis corresponds to the energy dissipated in the loading cycle.

### 3.2.4 Rainflow Cycle Counting

There are various methods for counting the stress cycles within a loading history. However, the rainflow cycle counting method is recognized as the most accurate and substantial way of representing variable amplitude loading (Shantz, 2010) and is preferred for statistical analysis of load-time histories. In the rainflow counting method, each cycle in the load spectrum is associated with a closed stress-strain hysteresis. Consider the stress and strain time histories (Figure 3.17 and Figure 3.18) and the corresponding hysteresis response (Figure 3.19). In Figure 3.17 and Figure 3.18, the blue line represents the loading of the applied stress and the red line represents the unloading of the applied stress. The stress-strain hysteresis is formed by plotting the stress and strain points on the same graph.

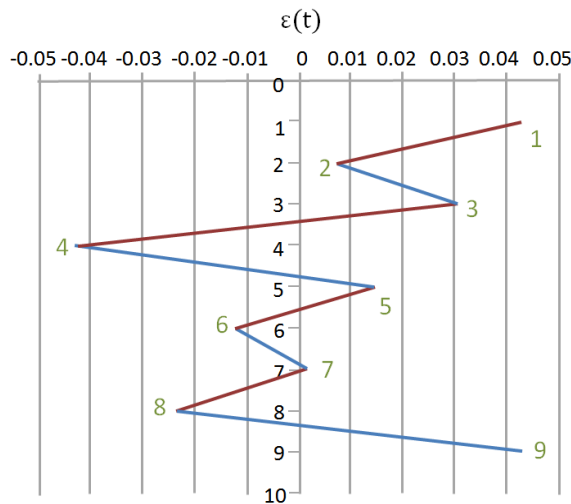


Figure 3.17 Sample of variable amplitude strain data

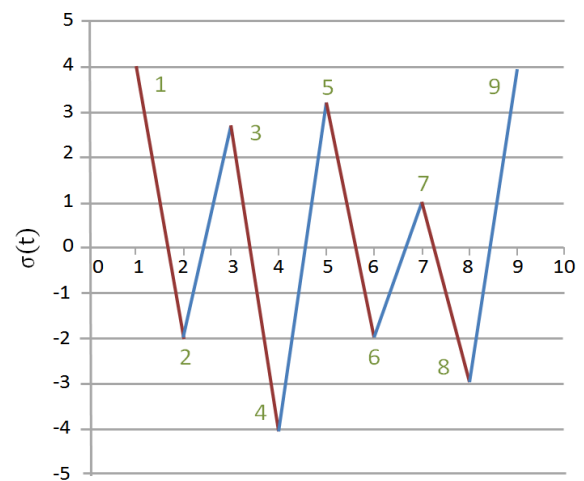
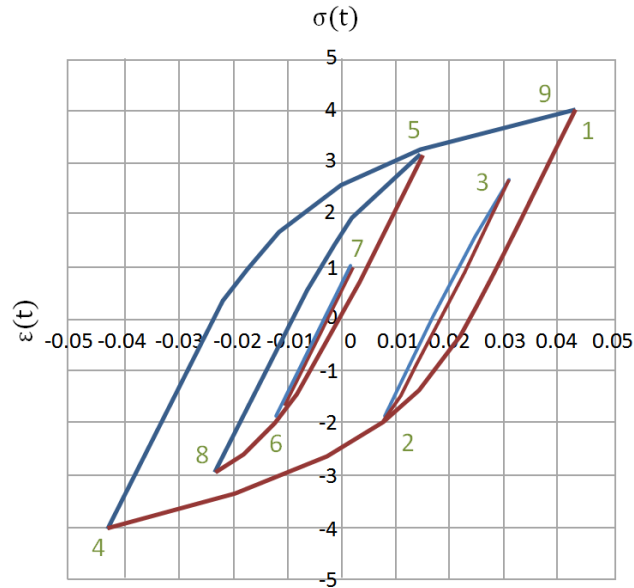


Figure 3.18 Sample of variable amplitude stress data



**Figure 3.19 Hysteresis loop to stress data (Lee, et al., 2012)**

The rainflow counting method is used to identify these hysteresis cycles within the load spectrum. The “rainflow” analogy is derived from a comparison of this method to the flow of rain falling on a pagoda and running down the edges of the roof. The analysis is started by rotating a time history of strain clockwise by  $90^\circ$  so the resulting shape is imaged to form a series of rooftops of the pagoda (Figure 3.20). Next, a raindrop will drop from one rooftop to the next, being limited by only two restrictions:

1. A raindrop must stop flowing when it passes an peak of the same sense (pointing in a different direction) unless it is of equal or greater amplitude than the peak from which the drop originated
2. A raindrop may not flow in any section of a rooftop where a previous raindrop had flowed (Manson, et al., 2006)

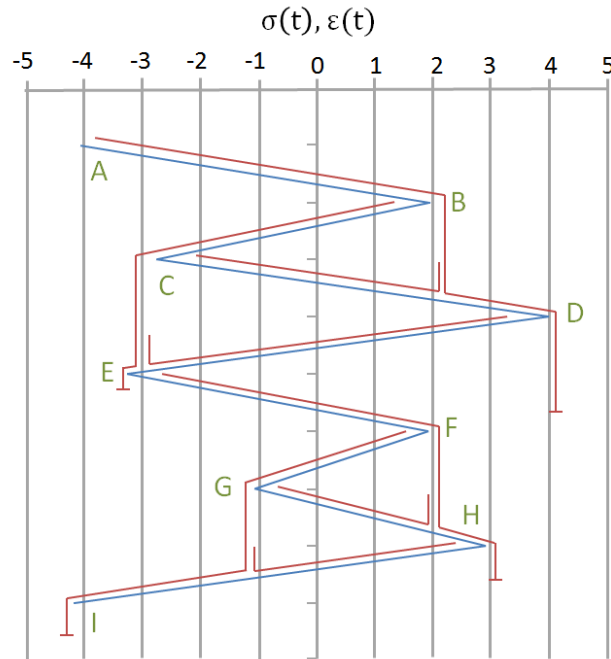


**Figure 3.20 Rainflow cycle counting on the load history**

For the example in Figure 3.20, begin by identifying the first largest reversal, AD. Starting with point A in the rain flows to B and falls along segment CD where it drops and stops (Rule #1). Next, a raindrop is started at B and flows towards C, falls onto segment DE where it drops and stops (Rule #1). Then, a raindrop is started from C and flows toward D, but is stopped because it encounters a previous flow (Rule #2). To resume, the flow begins at D and falls to E, however this is also stopped because it encounters a previous flow (Rule #2). The rain then flows from E to F where it drops onto GH and drops and stops (Rule #1). Next, the raindrop starts at F and falls to G, where it drops to segment HI and then drops and stops again (Rule #1). Finally a raindrop starting at G and falling to H encounters a previous flow; and the same with a raindrop starting at H and falling to I (Rule #2).

Rainflow counting method is advantageous to other range counting methods because it offers realistic counting results while preserving the amplitudes of the acquired

stress ranges. Since fatigue damage is related to these stress ranges, maintaining their amplitudes is significant; especially the larger ranges where there is likely to be greater fatigue damage. The rainflow counting method maintains these larger stress ranges by counting the intermediate smaller ranges separately. For instance, in Figure 3.21, a small load variation, BC, occurs within the larger range, AD. Range AD is counted as a separate cycle and then removed from the major load.

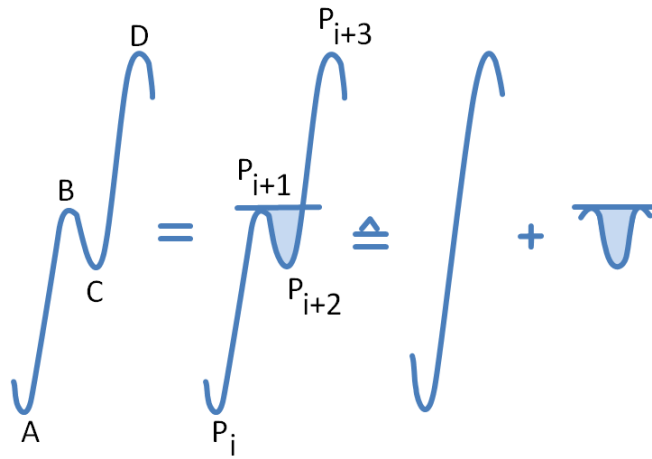


**Figure 3.21 Illustration of rainflow counting on stress cycle (Schijve, 2009)**

The rainflow counting continues to remove the smaller cycles, until only larger ranges are left. These remaining ranges are known as the “residue.” This removal of cycles is found in Figure 3.22. The successive graphs from (a) to (d) illustrate the removal of smaller load cycles in a load-time history. In each step, the cycles of a certain range are counted and then removed from the load-time history from a straight line that connects the gap. In an ascending load range, the algorithm for counting and removing a small range from a larger range is (Schijve, 2009):

$$P_{i+1} < P_{i+3} \text{ and } P_{i+2} > P_i \quad (\text{Equation 3.4})$$

Likewise, in a descending load range, the algorithm for counting and removing a small range from a larger range is (Schijve, 2009):

$$P_{i+1} > P_{i+3} \text{ and } P_{i+2} < P_i \quad (\text{Equation 3.5})$$

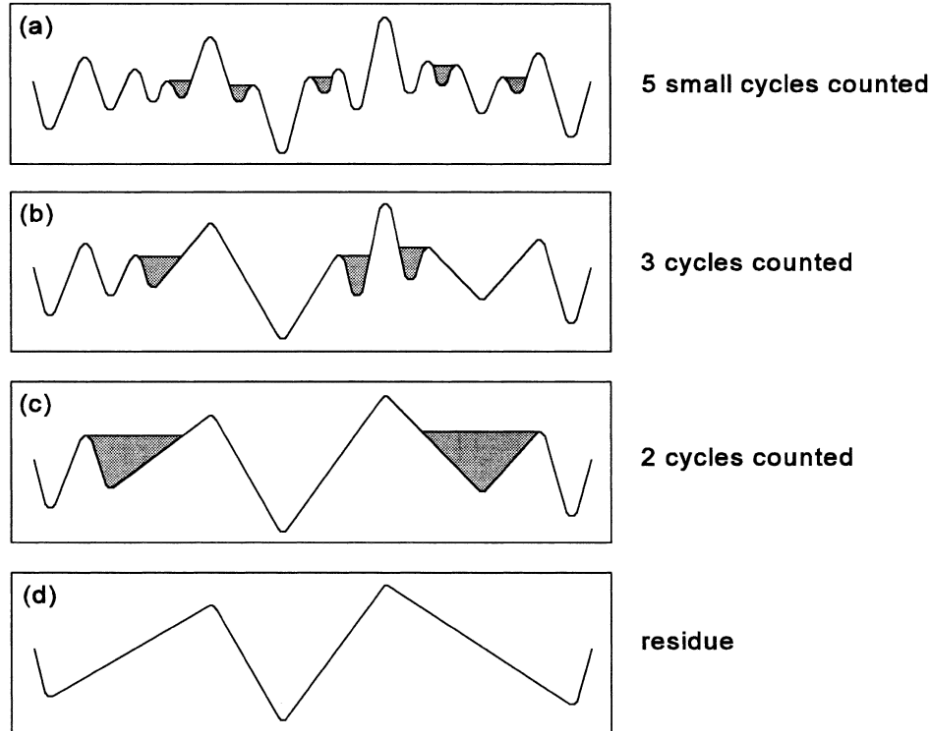
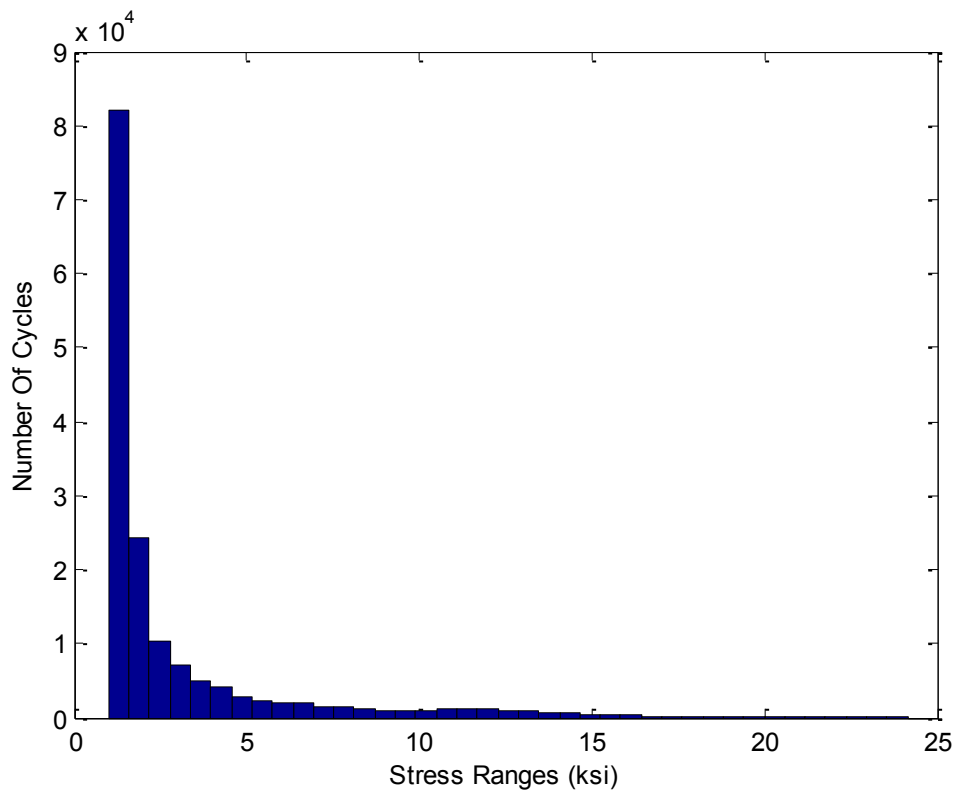


Figure 3.22 Successive rainflow counts (Schijve, 2009)

Ultimately the rainflow counts are stored into a matrix where the data is later used to make histograms and/or other statistical representations.

### 3.2.5 Stress Range Histograms

After cycle counting methods are applied, the stress range cycles are stored into a histogram, where the individual bins that reflect the number of cycles for the relative stress range. A measured histogram is shown in Figure 3.23.



**Figure 3.23 Histogram that reflects the frequency of measured stress ranges**

Histograms provide graphical representation of the distribution of data. They can be used to estimate the probability density function, i.e. the likelihood that a variable will take on a given value. Histograms are often considered to be simple kernel density estimations, and can be fit with a kernel function to smooth frequencies over the bins, as shown in Figure 3.24. Since the kernel function will smooth the frequencies over the bins, it will usually more accurately reflect the distribution.

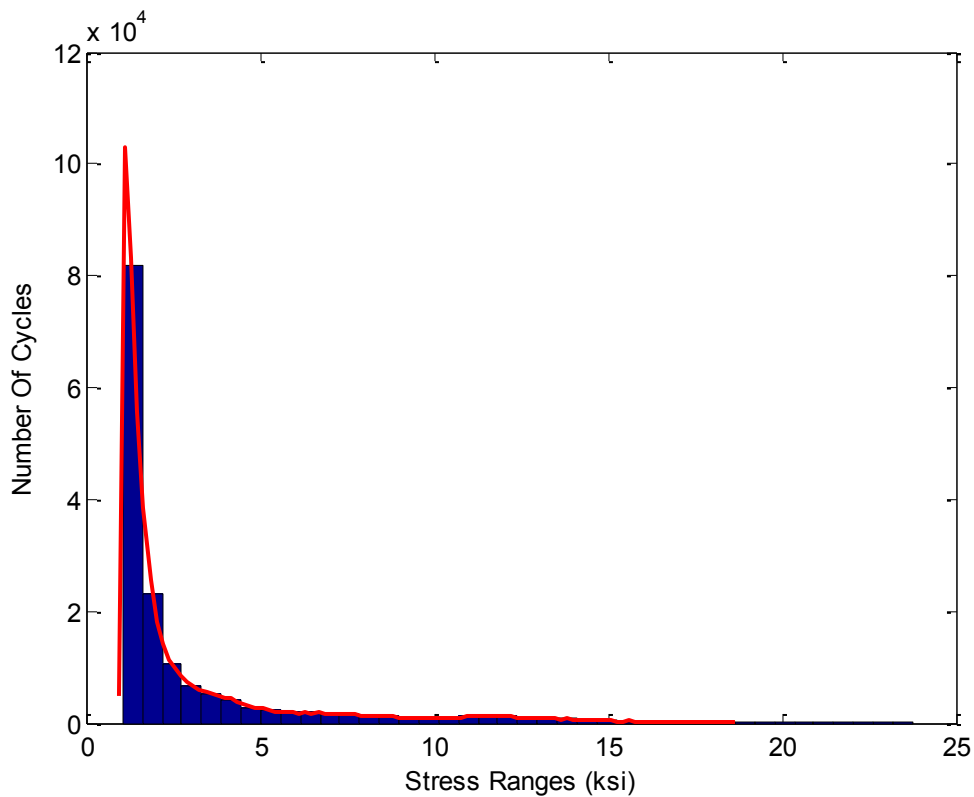


Figure 3.24 Kernel density fit to histogram

### 3.2.6 Extrapolation of Load Histories

The variable amplitude loads acquired from the traffic data are also referred to as stochastic loads or random loads. They are statistical in nature and cannot be predicted to occur within a certain magnitude at any given moment. A description of stochastic loads can be achieved using statistical distributions that assign a probability that a particular load will occur. In many cases the statistical properties of stochastic loads are not very well known, although long-term measurements provide useful data for fatigue analysis (Schijve, 2009).

The data acquired from long term monitoring is the most accurate way of obtaining information about a bridge since no assumptions need to be made for uncertainties in the load distribution. While long-term monitoring may be the optimal solution to acquiring

data that accurately reflects to bridge behavior, it remains difficult to continuously acquire accurate data. This interruption in the continuous acquisition generates uncertainties in future traffic loads. Acquisition of data may be disrupted when sensors experience temperature fluctuations causing them to operate incorrectly and data acquisition systems may require large amounts of power and would stop functioning during instances of power outages. Furthermore, the permissions from bridge owners to implement instrumentation may only be temporary and not a long enough time period to capture changes in behavior and conditions. While the service life of a structure is approximately 75 years, structural health monitoring instrumentation is not designed to “set it and forget it.” To account for these short time signals or interruptions, it has been customary in traditional methods to use a measured load history and simply repeat the load block. However, this method has the drawback that only the cycles in the measured signal will appear in the extrapolation, even though other cycles are possible (Johannesson, 2006).

Nevertheless, long-term monitoring provides a long load-time history with stationary character; resembled in the histogram of the stress ranges vs. the number of cycles. This data can be fit with exceeding probability curve that also has a stationary character. In statistical terms, the curve that fits the histogram distribution becomes an estimate of the probability function of the occurrence of peak values. Statistical methods can be used to extrapolate the measured load history and can also account for load variability by capturing more extreme cycles than the observed cycles while remaining within a reasonable range of possibly measured loads.

### ***3.2.6.1 Statistical Extreme Value Theory***

The statistical extreme value theory can be used to make statistical inferences about extreme values in a population or a random process (Davison, et al., 1990). Thus, the method can be used to randomly generate extrapolated load blocks by modifying the highest maxima and lowest minima in previously measured load blocks. Only the extreme values over previously defined max threshold and min threshold levels are modeled. By only considering the excesses over these threshold levels, then under certain conditions these excesses approximately follow an exponential distribution that is representative of the measured the data. This method of extrapolation is applicable to fatigue data and can be done in the rainflow domain. While metal fatigue analysis is sometimes characterized in the time domain since it identifies occurrences of specific “events” in a load-time sequence, (Shantz, 2010), the rainflow domain method is well adopted for really long extrapolations of the spectrum, whereas the time domain method is computationally more demanding. Both types of extrapolations have proven to give similar results for fatigue loading examples (Johannesson, 2006).

In order to calculate the number of stress cycles the structural component has experienced, the acquired strain measurements from structural health monitoring are processed and analyzed through the rainflow cycle method. These strain measurements are often discretized to a certain number of load levels, which enables well-organized storage of the density of rainflow cycles in the form of a rainflow matrix. Each bin of the rainflow matrix contains the number of cycles for that relative range.

Using the theory of statistical extreme values, the rainflow matrix is extrapolated to estimate data that was not captured in the observed data. To obtain the results for the

rainflow matrix, the equivalence between counting rainflow cycles and counting crossings of intervals is used (Johannesson, 2006). Since, the number of peaks ( $n_{peak}$ ) is equal to the number of peaks at the preceding interval ( $n_{exc,j=i-1}$ ) minus the number of positive level crossings ( $n_{exc,j}$ ) about that level (Equation 3.6), the rainflow matrix can be derived from a peak counting result (Potter, et al., 1989).

$$n_{peak,i} = n_{exc,j=i-1} - n_{exc,j=i} \quad (\text{Equation 3.6})$$

The technique used for extrapolating the rainflow matrix is the *Peak Over Threshold* (POT) technique. In this method, only the extreme excesses over a threshold level,  $u$ , are modeled. In accordance with this technique, when a high enough threshold level is set in place, then under certain conditions these excesses approximately follow an exponential distribution (Johannesson, 2005). Exponential distributions are based on the Poisson process, which describes the occurrence of some random events that occur continuously in time or space (Ayyub, 2003). The approximation of for the excess is described as  $Z = \text{Max} - u \in \text{Exp}(m)$  where  $m$  = mean excesses over  $u$ , and the cumulative distribution function for an exponential distribution:

$$F(z) = 1 - \exp\left(-\frac{z}{m}\right) \quad (\text{Equation 3.7})$$

The estimation of the parameter (mean excesses) in the exponential distribution is the mean of the excesses in the measured data:

$$m = \frac{1}{N} \sum_{i=1}^N z_i \quad (\text{Equation 3.8})$$

The mean of each hour,  $m$ , across the measured weekdays was used for the exponential probability density. where  $N$  = Number of cycles in that specific hour,  $z$  = corresponding stress range affiliated with the each stress cycle.

### ***3.2.6.2 Analytical procedure for extrapolation***

The algorithm for extrapolating the rainflow matrix is described below, with additional details in the subsequent sections.

#### **Algorithm**

The generation of the extrapolated data was performed using the following steps:

- 1) Start with a time signal of raw data acquired from strain gauge
- 2) Convert data to stress and detrend the data if necessary
- 3) Extract the turning points of the time signal
- 4) Count the number of stress cycles using rainflow counting method, and remove small (considered negligible) cycles with rainflow filter. As discussed earlier, a value of 1ksi is used.
- 5) Choose threshold levels  $u_{\min}$  and  $u_{\max}$  for the extrapolation. These choice are defined later.
- 6) Choose interval values for splitting exponential distribution. This is discussed later.
- 7) Count the number of measured stress cycles within each interval.
- 8) Average the number of stress ranges across each hour of the day for the measured data. Do this for each interval.
- 9) Estimate the mean excesses  $m_{\min}$  and  $m_{\max}$  under and over the thresholds  $u_{\min}$  and  $u_{\max}$ , respectively. Can also be considered as estimating the mean stress ranges.
- 10) Generate the extrapolated load block by simulating stress ranges as exponential random numbers. Replace each measured stress range with a simulated stress range for each load block.
- 11) Repeat step 9 for the computed average number of stress ranges for each hour of the day (Step 7) until the number of load blocks desired is extrapolated.
- 12) Repeat steps 9 and 10 for each defined interval

The completed extrapolated signal is obtained by concatenating the rainflow cycles and creating a rainflow matrix. These cycles are then used with the AASHTO S-N diagrams.

### **Threshold Levels**

It is customary to remove small oscillations that do not contribute to fatigue damage. Further, the stress ranges caused from smaller vehicles are often considered negligible compared to trucks. This is not only established in AASHTO design guideline (AASHTO, 2002), but the NCHRP Report, *Fatigue Evaluation of Steel Bridges*, also pays distinct attention to truck loads when estimating fatigue life, mentioning that, “the effective stress range shall be estimated as either the measured stress range or a calculated stress range value determined by using a fatigue truck as specified in the AASHTO LRFD Bridge Design Specification 2012 (NCHRP, 2012).” Because of the significance of truck loads compared with smaller vehicular passages, it has been the rationale for neglecting stress cycles below 1 ksi (Massarelli, et al., 2001). This rationale has also been adopted for this analysis and the minimum threshold level is set to 1 ksi.

The maximum stress range of the measured data is useful for determining the max threshold level. This value is not taken verbatim as the max threshold value because it is believed that other stress ranges may occur on the structure and the monitoring was only done for a finite time period of the structures life. Therefore, a default choice is to set the threshold range to 5% of the total range of the signal (Johannesson, 2006)

$$u_{max} = 1.05(S_{r(max)}) \quad (\text{Equation 3.9})$$

This range is observed to be reasonable after empirical investigation shows it agrees well with the measured load spectrums.

## Interval Values

Interval values are chosen in order to separate the disparity between the stress cycles caused by smaller traffic loads (e.g. vehicular passage) and the stress cycles caused between the medium and large truck loads. Figure 3.25 illustrates how the stress cycles are allocated to different interval levels. Each interval of stress ranges approximately follows an exponential distribution.

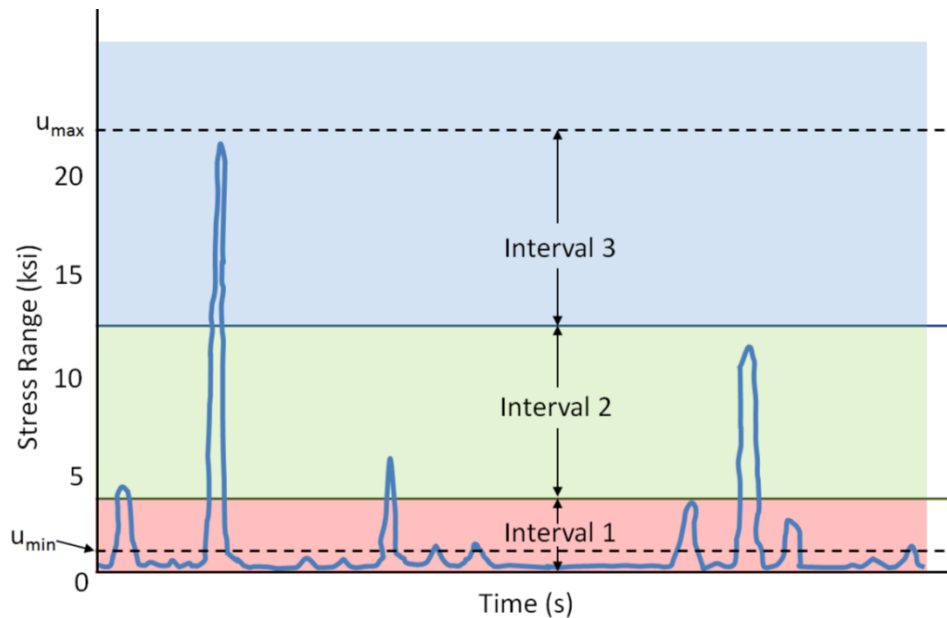


**Figure 3.25 Allocation of stress ranges into specific intervals**

It is important to verify the exponential assumptions are fulfilled for the interval levels. At the beginning of the extrapolation process, careful consideration is given to determining where the extrapolation of exponential random numbers will begin for each interval level. These levels should be chosen to account for relative stress ranges of measured data and should be visually inspected with histograms in order to assure the statistical extreme value theory provides reasonable results. As seen in Figure 3.26, the interval levels are cut off where there is large disparity in the exponential plots. The

intervals chosen from the measured data were configured to stress ranges starting at 3ksi and stress ranges starting at 10.4 ksi.

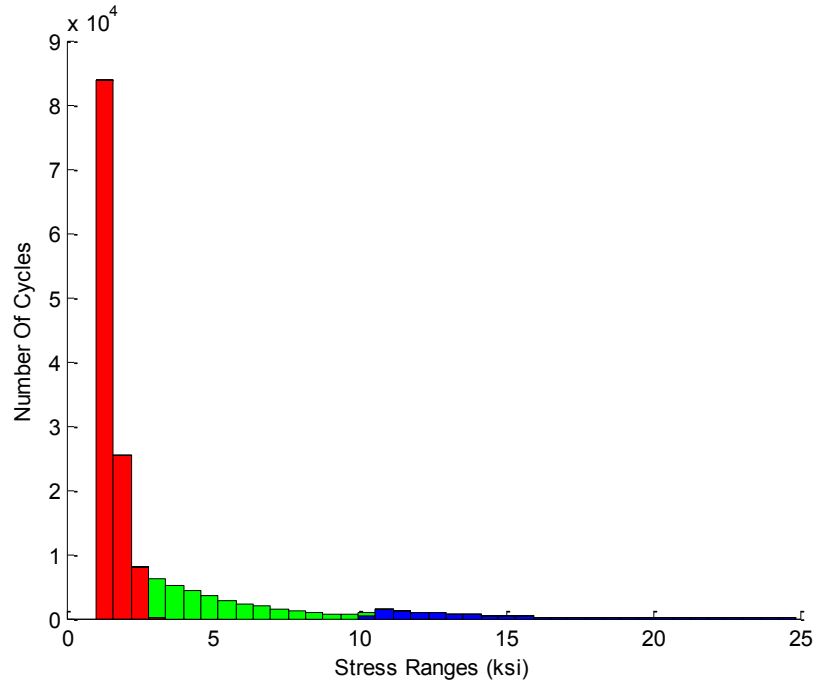


**Figure 3.26 Traffic load distribution as histogram**

The measured rainflow histogram is fitted by three probability density functions. Each density function is assigned to a vehicle type. Density function 1 describes the probability of occurrence of cars, function 2 of light or empty trucks and function 3 represents ordinary and heavy trucks (Peil, 2005). Figure 3.27 illustrates how the exponential distribution functions are fit to the histograms.

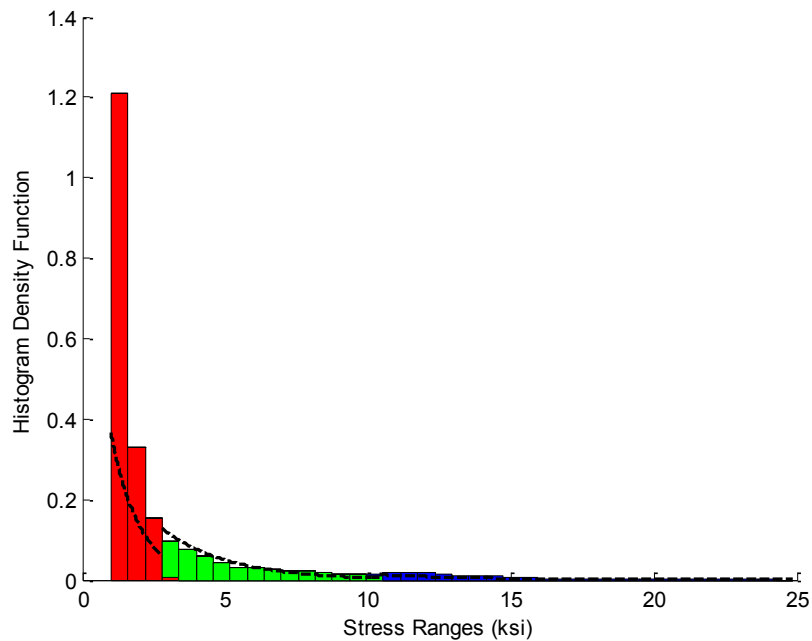


**Figure 3.27 Exponential distribution fit to histogram**

### **3.3 Crack-Initiation Life Prediction**

The S-N curve is typically generated in the laboratory on test specimens, where a testing machine applies a constant sinusoidal stress (constant amplitude),  $S$ , and counts the number of cycles,  $n_i$ , until failure,  $N_f$ . As discussed in Chapter Two, failure is defined at the initiation of a crack that is of a critical size. Until the onset of this fatigue crack, the specimen can be characterized by the amount of current fatigue damage in terms of its fatigue life. So the specimen may be at  $x\%$  of its fatigue life, or the specimen can be classified to have  $(100-x)\%$  remaining useful life. This damage may not be visible upon inspection, but is definitely still present in the material.

### 3.3.1 Linear Cumulative Damage Rule

A specimen's fatigue life is based on the laboratory test specimens that are used to develop the S-N curves. Thus, the fatigue damage is defined as the cycle ratio,  $n/N_f$ , seen in Equation 3.10:

$$\sum \frac{n}{N_f} = 1 \quad (\text{Equation 3.10})$$

The simplicity of this linear cumulative damage model, which is more generally known as the Miner rule, works best under constant amplitude loading, since it was derived from test specimens exposed to constant amplitude loads. For variable amplitude loadings, the Miner rule is still applied, but is modified to account for the variance in stress amplitudes and the number of cycles corresponding to these amplitudes. Consider the simple variable amplitude load made up of two load blocks, presented in Figure 3.28. This load block is commonly referred to as a “HiLo” load sequence since it transitions from a higher stress range to a smaller one.

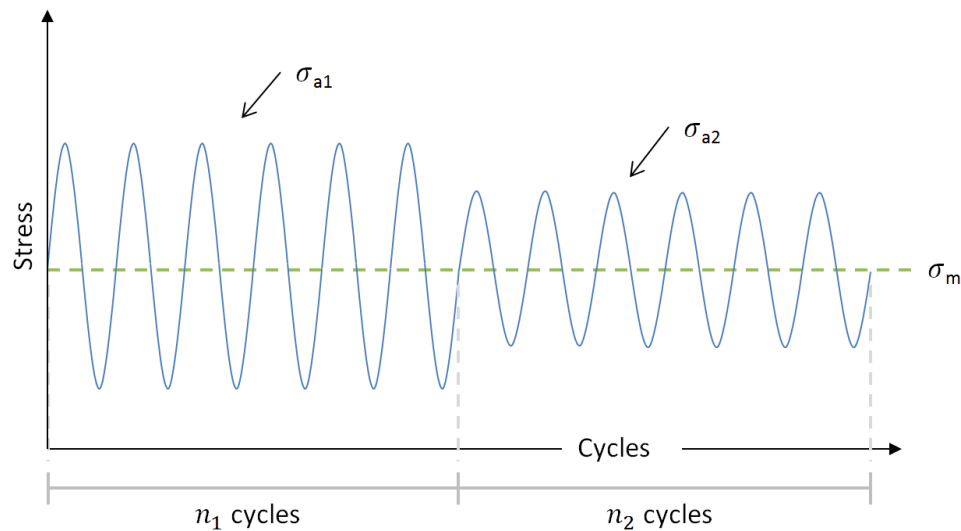


**Figure 3.28 Variable amplitude loading with two blocks of load cycles (Schijve, 2009)**

From the two load blocks, the Miner rule implies crack initiation failure occurs at,

$$\frac{n_1}{N_1} + \frac{n_2}{N_2} = 100\% \quad (\text{Equation 3.11})$$

Where  $n_1$  is the number of cycles at  $\sigma_{a1}$  and  $n_2$  is the number of cycles at  $\sigma_{a2}$ .  $N_1$  and  $N_2$  represent the fatigue lifes at the correspond stress amplitudes. For multiple load blocks (i), the equation is written as,

$$\sum \frac{n_i}{N_i} = 1 \quad (\text{Equation 3.12})$$

Since the hypothesis that the Miner rule can be applied to variable amplitude (VA) loads, numerous VA fatigue tests were carried out to check the hypothesis. In many cases, significant discrepancies were found and new theories and hypotheses were published. However, these proceeding hypotheses were found to have their own discrepancies as well and lacked sufficient credibility. Miner did his own VA load tests and found cycle ratio values ( $\sum n/N$ ) varying from 0.61 to 1.45; reasonably close to an average of 1.0 (Schijve, 2009). Thus, the Miner rule has remained the most widely used tool for fatigue life estimates with variable amplitude loads. Nonetheless, due to the inconsistencies and variation of results from variable amplitude tests, the shortcomings of the rule should be understood in order to arrive at a reasonable fatigue life estimates.

### ***3.3.1.1 Shortcomings of the Miner Rule***

When fatigue life predictions are made using a variable amplitude load spectrum with the Miner rule, it should be realized that the results have inherent assumptions and only provide a rough estimate of a structures fatigue life. The fundamental shortcoming of the Miner rule is that fatigue damage is indicated by a single parameter only, i.e.  $n/N$ , which accumulates from zero (pristine specimen) to 1 (failure) (Schijve, 2009). The

Miner rule can be broken into three different topics that are not recognized in the Miner rule and are the largest deficiencies of the model:

- Small cycles (with an amplitude below the fatigue limit) are not damaging
- Sequencing of stress cycles is not accounted for
- The crack length at failure

### **The Miner rule does not account for cycles below the fatigue limit**

This first assumption of the Miner rule is inconsistent with the definition of fatigue, i.e. the initiation and propagation of microscopic cracks into macro cracks by the repeated application of loading (Fisher, et al., 1998). The inconsistency relies in the fact that the S-N curves were not developed based on the existence of crack. These curves were developed to understand the number of cycles a structure can withstand before a crack of critical size will develop in the material; focusing on what has become known as just the fatigue-crack-initiation life.

Consider the load spectrum in Figure 3.28. In accordance with the miner rule, if  $\sigma_{a2}$  is below the fatigue limit, then  $N_2$  is infinite and ( $n_2/N_2 = 0$ ). The specimen will never fail because the condition  $\sum n/N = 1$  (Equation 3.1) cannot be satisfied. The inherent assumption of the rule is that the cycles with an amplitude of  $\sigma_{a2}$  cannot propagate a growing crack. This assumption was first made when the Miner rule was developed for constant amplitude loading. With CA loads, the small load cycles below the fatigue limit will not be enough to create a crack, which means there won't be a crack to grow. However, due to the sporadic nature of variable amplitude loads, a structure may have a much different response. For variable amplitude loads, once a crack exists, any loading or stress ranges will have an impact on the damage, even if they are below a predefined

fatigue limit. This leads into the next shortcoming of the Miner rule, which is the effect the sequence of loads will have on a structure.

**Miner rule does not account for the sequence effect**

The significance of the fatigue damage contribution is highly dependent on the type of load spectrum. Consider the scenario where a microcrack does not initially exist in a structure. For the first load spectrum, the structure experiences a LoHi VA load sequence illustrated in Figure 3.29a. If the first load block of smaller stress loads falls below the fatigue limit, then these cycles will not create a crack, nonetheless contribute to the crack growth at the microcrack level.

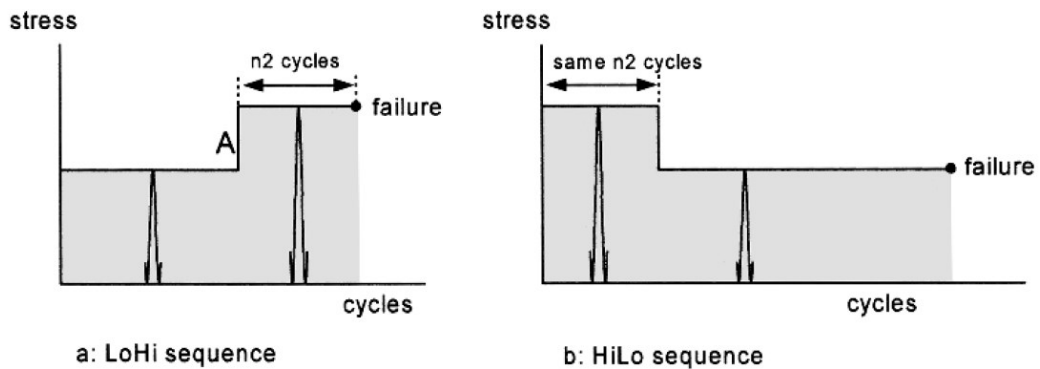


**Figure 3.29** Sequence in loadings, each with two different size load blocks (Schijve, 2009)

However, if the large loads are then followed by smaller loads, (consider the HiLo VA load sequence in Figure 3.29b) then the small loads may also affect the structure, even if they are still below the fatigue limit. The initial large loads may be large enough in size to introduce residual stresses, introduce plasticity into the structure or may even create an initial crack. Therefore, the subsequent smaller loads will contribute to the stress field at the crack tip, and will consequently affect the crack growth (Schijve, 2009). For this scenario, the LoHi sequence will lead to a larger fatigue life than the HiLo

sequence, which will experience residual stresses from the initial loading. The next scenario with an initial crack size leads to the next shortcoming of the Miner rule.

### **Miner rule does not account for the length of the crack at failure**

Consider the scenario where a microcrack exists in a structure with an initial crack size of .5 mm ( $a = .5\text{mm}$ ). Using the LoHi sequence in Figure 3.29a, assume that the lower stress amplitude no longer falls below the fatigue limit. At the load stress amplitude, the microcrack may have the capability to grow until  $a = 10\text{mm}$ , which could be the point of failure. However, if this small load block is interrupted by a larger load block, as Figure 3.29a suggests, then the high-amplitude block could lead to immediate failure because a small crack is more fragile at higher stress level (Schijve, 2009). For this half of the scenario, a load sequence of  $\frac{\sum n}{N} < 1$  should be expected. In the reversed sequence, Figure 3.29b, the structure experiences a larger load first. The end of the first load block may leave a crack in the structure that would be considered near failure, i.e.  $n/N$  is close to 1. After the transition to the smaller load block, substantial crack growth is still possible, but the structure is capable of withstanding more cycles. For this half of the scenario, a load sequence of  $\frac{\sum n}{N} > 1$  should be expected. Opposite to scenario of no existing microcrack, in this scenario, the LoHi sequence will lead to a shorter fatigue life than the HiLo sequence.

#### **3.3.1.2 Nonlinear Damage Accumulation**

Along with the linear damage accumulation model, non-linear models for damage estimations are also proposed in literature. Non-linear models were initially comprised from the assumption that fatigue damage should be quantified by the size of the crack. However, the non-linear models do not omit the crack initiation period but are intended

to account for the crack initiation and crack growth periods. Since the rate of crack growth is an exponential function, the corresponding amount of fatigue damage would also follow an exponential curve, Figure 3.31b. Fatigue damage as a non-linear, exponential function can be written as:

$$D = \sum_{j=1}^k \left( \frac{n_i}{N_i} \right)^{C_j} \quad \text{(Equation 3.13)}$$

Where  $C_j$  is a material parameter related to the  $i$ th loading level, a value that should be experimentally obtained (Manson, et al., 2006).

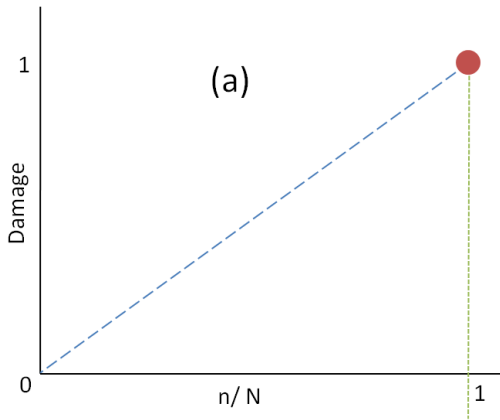


**Figure 3.30 Illustration of linear damage accumulation (Modified from (Schijve, 2009))**

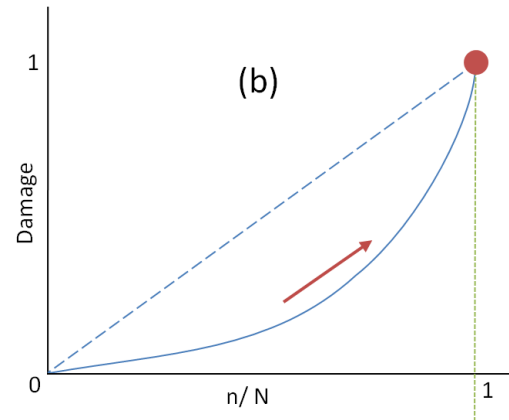


**Figure 3.31 Illustration of non-linear damage accumulation (Modified from (Schijve, 2009))**

The accumulation of damage as a non-linear function poses some difficulties. Consider the load block in Figure 3.28 or Figure 3.29b (both illustrate a HiLo VA sequence). As discussed previously, the sequence effects in VA loadings are a significant shortcoming of linear damage models and continue to be shortcomings of the non-linear damage accumulations. This is shown in Figure 3.33. As the figure shows, the damage will accumulate along the first curve for the first set of cycles with stress amplitude,  $\sigma_{a1}$ , and then transition to the second curve for the second set of cycles with stress amplitude,

$\sigma_{a2}$ , until failure at  $D=1$ . The problem with this assumption is that the sum of  $n_1/N_1$  and  $n_2/N_2$  will be smaller than 1.0 because  $N_1$  and  $N_2$  will represent two different curves. The reversed sequence, with LoHi stress amplitudes, will lead to a similar dilemma, i.e. the value “1.0” will not accurately describe the failure point. For a LoHi sequence, the non-linear damage analysis will conclude  $n_1/N_1 + n_2/N_2 > 1$ . The results of non-linear damage models showed that damage does not need to be defined to any particular physical manifestation. Any family of damage curves would obtain the same answers, as long as they are in proper relations with each other (Manson, et al., 2006). Lastly, it should be stated that like linear damage models, the non-linear models also ignore interaction effects, acquiring some of the similar assumptions that are made in the Miner rule.

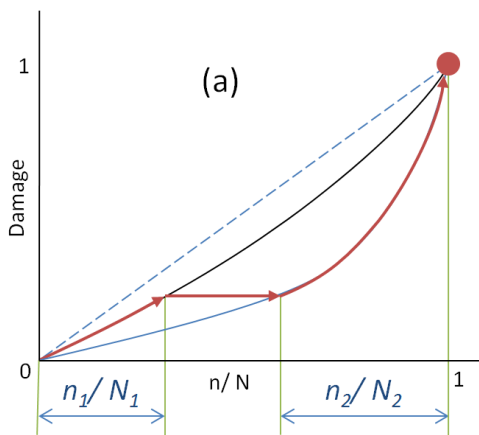


**Figure 3.32 Non-linear damage curve from HiLo VA sequence (Modified from (Schijve, 2009))**

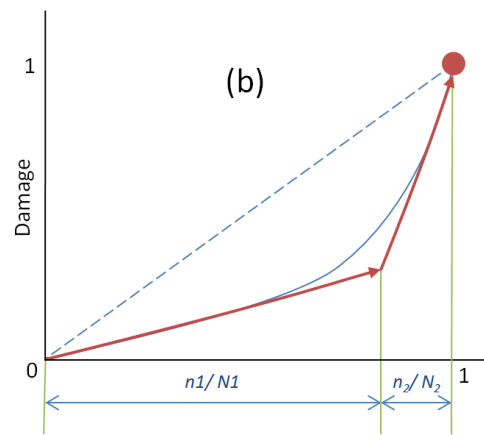


**Figure 3.33 Non-linear damage curve approximated by double linear functions (Modified from (Schijve, 2009))**

It is worth mentioning that non-linear damage accumulation models can be approximated by double linear functions, Figure 3.33, with the linear damage accumulation rule applied (Zhang, et al., 2013). The importance with the double linear

models is the “kneepoint” or “breakpoint” from the transition of one linear segment into the next. This value depends only on the fraction of life from the first load segment. For two-block loading problems, these values should be experimentally determined. Nonetheless, these simplifications have been successfully applied to two-block loading problems, but the parameters are too complicated for the multi-block loading or complex VA loading, such as traffic loads.

### ***3.3.1.3 Linear vs. Nonlinear Damage Accumulation***

There is a variance in the calculated damage results between the double linear damage rule and the linear damage rule. The DLDR is useful when attempting to understand the fatigue life of a specimen subjected to known loading-order effects, where “breakpoint” values are predetermined. Due to the need to derive values experimentally, the DLDR is not a good fit for the analysis on steel bridges. Each variable load the bridge will experience is highly dependent on the large erraticism of traffic loads (i.e. frequency and size) the bridge will experience. This is especially true at the location of welded joints, where the Miner rule is generally considered to be the only calculation rule available (Schijve, 2009). Because both models have shortcomings and provide rough estimates, results show that a preponderant number of cases require no more than the Miner rule to get satisfactory results (Manson, et al., 2006). While the limitations of the Miner rule still exist, the Miner rule continues to be the preferred method, provided it is used cautiously.

### **3.3.2 Application of S-N Curve**

The purpose of the S-N curve is to illustrate the stress and life relationship by plotting the cyclic stress (S) against the number of cycles to failure ( $N_f$ ). An S-N curve is

typically constructed as a piecewise-continuous curve consisting of two distinct linear regimes when plotted on log-log coordinates, as seen in Figure 3.34. For steel specimens, fatigue strength values are typically,  $N_2 = 10^3$ , and  $N_1 = 10^6$  define an S-N curve. The corresponding fatigue stress values are referred to as,  $S_2$  and  $S_1$ , respectively.

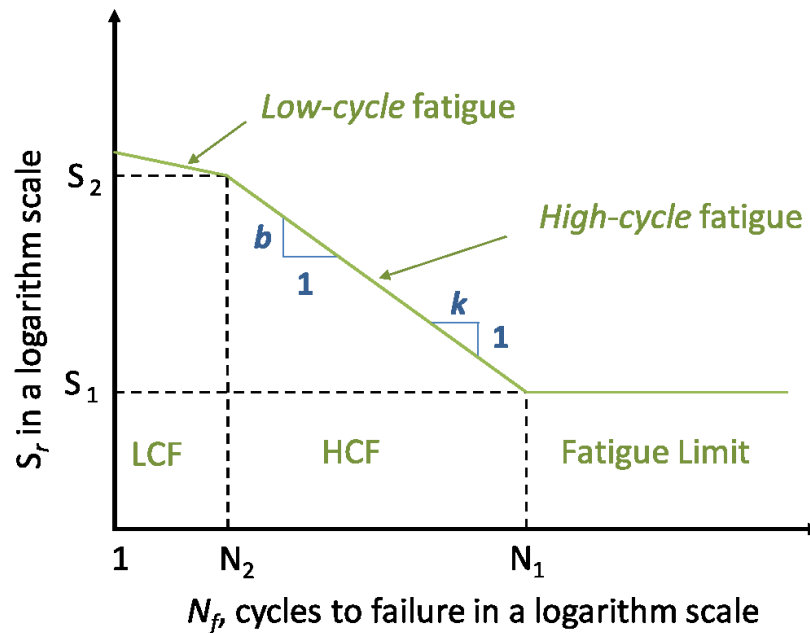


Figure 3.34 Schematic constant amplitude S-N curve of a steel component (Lee, et al., 2005)

In the curve, the two sloped linear segments represent the low-cycle fatigue (LCF) and high-cycle fatigue (HCF) regions, and the horizontal segment represents the bending fatigue limit. LCF applies to structures that experience high amplitudes, low amount of cycles, and have a short fatigue life. HCF accounts for structures that are exposed to a large number of cycles. The more relevant difference between the two conditions is that low-cycle fatigue is associated with macro plastic deformation in every cycle and high-cycle fatigue is more related to an elastic behavior of the material. In summary, cases with high cycle fatigue conditions endure:

- High number of cycles to failure
- Little plastic deformation due to cyclic loading

Thus, high-cycle fatigue is more common in applications and low-cycle fatigue is associated with a more specific load spectrum.

Due to the cyclic operating stresses from constant amplitude loading, a microcrack will develop and nucleate within a grain of the material. The microcrack will grow to the size of about the order of a grain width until the grain boundary barrier impedes its growth. The grain barrier is a much stronger part of the steel, causing crack growth to slow and may become arrested. The minimum stress amplitude to overcome the crack growth barrier for further crack propagation is referred to as the fatigue limit. Upon reaching and/or surpassing the fatigue limit the microcrack will eventually propagate to a macro crack and lead to failure, i.e. the end of the fatigue-crack-initiation life.

The S-N curves displayed in Figure 3.34 are used for estimating fatigue life of a specimen for applied constant amplitude stresses. However, when the specimen is exposed to variable amplitude loading, some of the subsequent stress amplitudes could exceed the fatigue limit and influence the crack to propagate. Thus, under variable amplitude loadings, the fatigue limit should be modified. As discussed in section 3.3.1, the Miner Rule is a proposed method to include the effect of these variable amplitude overloads with low stress amplitudes.

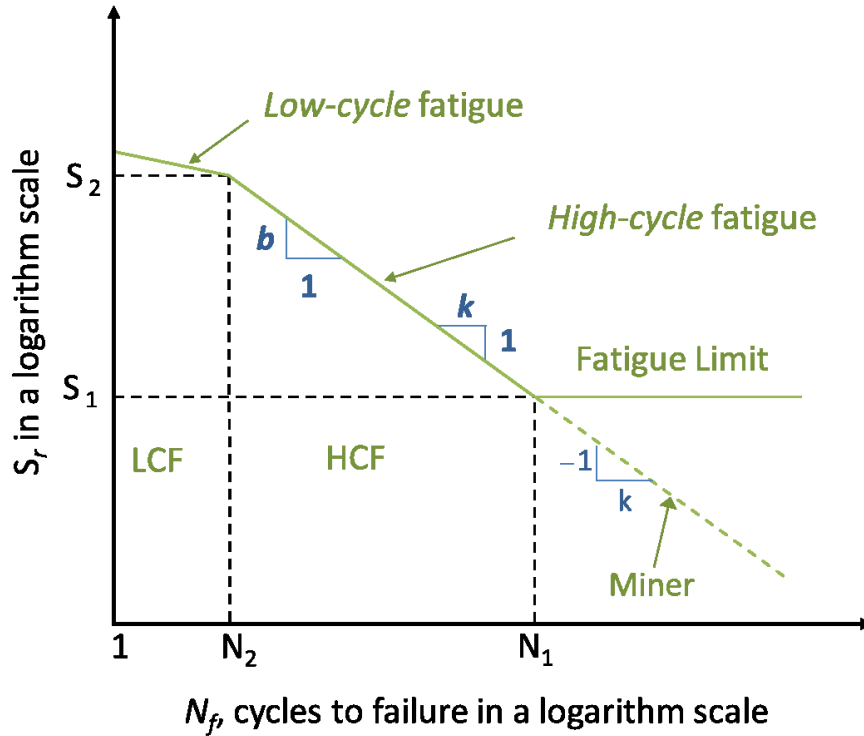


Figure 3.35 CA S-N curve for a steel component subjected to VA loads

As illustrated in Figure 3.35, the Miner rule extends the HCF region of the S-N curve with the same slope factor,  $k$ , to approach zero stress amplitude. The slope of the S-N curve in the HCF regime is denoted as,  $b$  (the height-to-base ratio) or as,  $k$  (the negative base-to-height ratio). The slopes are related through the following expression:

$$k = -\frac{1}{b} \quad (\text{Equation 3.14})$$

where the parameter  $k$  is nothing more than a slope factor. In general, if fatigue behavior is dominated by the crack propagation mechanism, e.g. welded joints, the S-N curve often has a steep slope ( $b \approx -0.3$ ;  $k \approx 3$ ) (Lee, et al., 2005). Any two S-N data points in the HCF regime are related by the slope or the slope factor in the following equation.

$$\frac{N_2}{N_1} = \left(\frac{S_1}{S_2}\right)^k \quad \text{also written as} \quad N_2 = \left(\frac{N_1}{S_2^k}\right) S_1^k \quad (\text{Equation 3.15})$$

Therefore, any point between  $(S_2, N_2)$  and  $(S_1, N_2)$  can be obtained by a known slope and a known reference point, such as  $(S_2, N_2)$  or  $(S_1, N_2)$ . The HCF region of the S-N curve is commonly expressed as:

$$N = AS_F^k \quad (\text{Equation 3.16})$$

### ***3.3.2.1 Fatigue Prone Details***

The fatigue strength of bridge components are based on the same experimental data that correlate the magnitudes of stress ranges with the number of cycles to fatigue failure for various types of details (Zhou, 2006). Fatigue damage often occurs at the element level of bridge components and more specifically occurs at welded, riveted, or bolted locations with large stress concentrations and construction defects; essentially where the rigidity of the structural member changes. Fatigue resistance at an element location depends on the direction and variation of the live loads, the member sizes, fastener and weld characteristics, and quality assurance processes (Sobanjo, et al., 2013). Laboratory experiments were conducted on the following types of structural details in order to characterize their susceptibility to fatigue damage,

- 1) Plain Material away from Any Welding
- 2) Connected Material in Mechanically Fastened Joints
- 3) Welded Joints Joining Components of Built-Up Members
- 4) Welded Stiffener Connections
- 5) Welded Joints Transverse to the Direction of Primary Stress
- 6) Transversely Loaded Welded Attachments
- 7) Longitudinally Loaded Welded Attachments
- 8) Miscellaneous

These laboratory experiments were conducted by placing the structural details under fatigue loads in order to correlate the magnitudes of stress ranges with the number of cycles to fatigue failure (Zhou, 2006). The geometry of the details and location of the applied load on these details have had the greatest impact on their susceptibility to fatigue damage. *AASHTO LRFD Bridge Design Specifications 2012*, describes the fatigue categories in full detail for load induced fatigue details. The details are grouped into eight categories, called detail categories, based on their ability to withstand fatigue loads. Bridge details (welded, bolted and riveted) are categorized as A, B, B', C, C', D, E, or E' based on their fatigue strengths. Category A is for the base material steel and has the highest fatigue strength. Category E' represents the poorest welded details that have the lowest fatigue strength. Experience and past data both indicate that in the design process the fatigue considerations for Detail categories A through B' will rarely govern; they are included in LRFD Bridge Design Specifications 2012 for completeness (AASHTO, 2012). All federal and state agencies are encouraged to teach their bridge inspectors to locate and identify the category E and E' details. While failure of these structural details is not always significant to the whole structure, their failure is extremely significant in structural members that are lacking redundancy. Table 3.1 shows category E and E' details, which are more prone to fatigue.

Table 3.1 Sample of details that are considered fatigue prone (Oregon DOT, 1996)

Fatigue Prone Details Category Definitions	
<p>Termination of Welded Coverplates in tension zone</p> <ul style="list-style-type: none"> <li>▪ Coverplate wider than flange without weld across end (E')</li> <li>▪ Coverplate narrower than flange and flange thickness ≤ 0.8 inches (E)</li> <li>▪ Coverplate narrower than flange and flange thickness &gt; 0.8 inches (E')</li> </ul>	
<p>Plates welded longitudinally to tension members where weld is 12x the plate thickness or greater than 4 inches (e.g. lateral bracing gusset plate attached to girder web or edge of flange)</p> <ul style="list-style-type: none"> <li>▪ Plate is &lt; 1 inch (E)</li> <li>▪ Plate is ≥ 1 inch (E')</li> </ul>	
<p>Plates welded longitudinally to tension members with:</p> <ul style="list-style-type: none"> <li>▪ A transition radius &lt; 2 inches or the end welds are not ground smooth (E) No plate thickness or detail length restrictions apply.</li> <li>▪ Plate and flange are not of equal thickness and reinforcement is not removed (E).</li> </ul>	
<p>Intermittent fillet welds (E)</p> <p>Shear stress on throat of fillet welds where the ends of the weld are developed abruptly (e.g. welded splice plates on a tension member) (F)</p>	
<p>Section through head of eyebar or pin plate (E)</p>	
<p>Source – Standard Specifications for Highway Bridges, American Association of State Highway and Transportation Officials, 2002.</p>	

The number of cycles to failure for bridge details in the S-N curve is expressed as:

$$N_f = AS_r^{-3} \quad (\text{Equation 3.17})$$

where  $N_f$  is the number of stress cycles to fatigue failure,  $S_r$  is the nominal stress range at a fatigue detail and  $A$ =detail category constant, varying with the type of detail. The AASHTO S-N curve is shown in Figure 3.36. The S-N curve shows high cycle linear regime that bends into the constant amplitude allowable fatigue stress range, or constant amplitude fatigue limit (CAFL), represented by a horizontal dashed line.

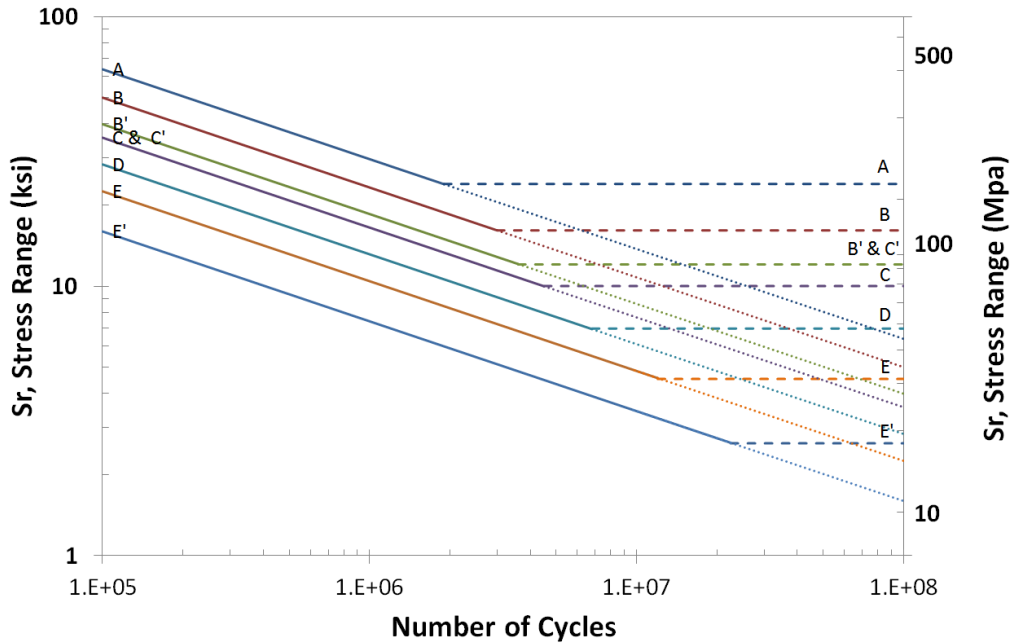


Figure 3.36 AASHTO fatigue strength S-N curves

The CAFL varies for the fatigue prone categories depending on the number of stress cycles a component is exposed to. Table 3.2 displays the variance in the CAFL for the fatigue categories based on the number of cycles (AASHTO, 2002). However, a bridge experiences millions of cycles per year and the more relevant CAFL for most bridge structures applies to categories over 2,000,000 cycles.

Table 3.2 Allowable Fatigue Stress Range for CAFL

Category	CAFL Allowable Range of Stress, $F_{sr}$ (ksi) <sup>b</sup>			
	For 100,000 Cycles	For 500,000 Cycles	For 2,000,000 Cycles	For over 2,000,000 Cycles
A	63.0	37.0	24.0	24.0
B	49.0	29.0	18.0	16.0
B'	39.0	23.0	14.5	12.0
C	35.5	21.0	13.0	10.0
D	28.0	16.0	10.0	7.0
E	22.0	13.0	8.0	4.5
E'	16.0	9.2	5.8	2.6
F	15.0	12.0	9.0	8.0

The CAFL category constants for all fatigue categories are summarized in Table 3.3. These values represent the constant amplitude fatigue limits on the AASHTO S-N curve. The values for this table are found in the *AASHTO LRFD Bridge Design Specifications 2012* (AASHTO, 2012) and are used alongside the AASHTO S-N curve Figure 3.36.

**Table 3.3 Constant A and CAFL of AASHTO Fatigue Categories**

Category	Constant A		CAFL	
	$\times 10^8 \text{ ksi}^3$	$\times 10^{11} \text{ MPa}^3$	ksi	MPa
A	250.0	(82.0)	24.0	(165.5)
B	120.0	(39.3)	16.0	(110.3)
B'	61.0	(20.0)	12.0	(82.7)
C	44.0	(14.4)	10.0	(68.9)
C'	44.0	(14.4)	12.0	(82.7)
D	22.0	(7.21)	7.0	(48.3)
E	11.0	(3.61)	4.5	(31.0)
E'	3.9	(1.28)	2.6	(17.9)

### 3.3.2.2 *Effective Stress Range*

Since the data in S-N curves were developed under constant-amplitude cyclic loading, an effective stress range should be calculated to equivalently represent the variable-amplitude cyclic loading on bridge structures. The effective stress range for a variable-amplitude spectrum is defined as the constant-amplitude stress range that would result in the same fatigue life as the variable-amplitude spectrum. Variable amplitude load spectrum can be defined by the Rayleigh distribution, with most cycles occurring below the constant amplitude fatigue limit. Rayleigh distribution is schematically represented in Figure 3.37.

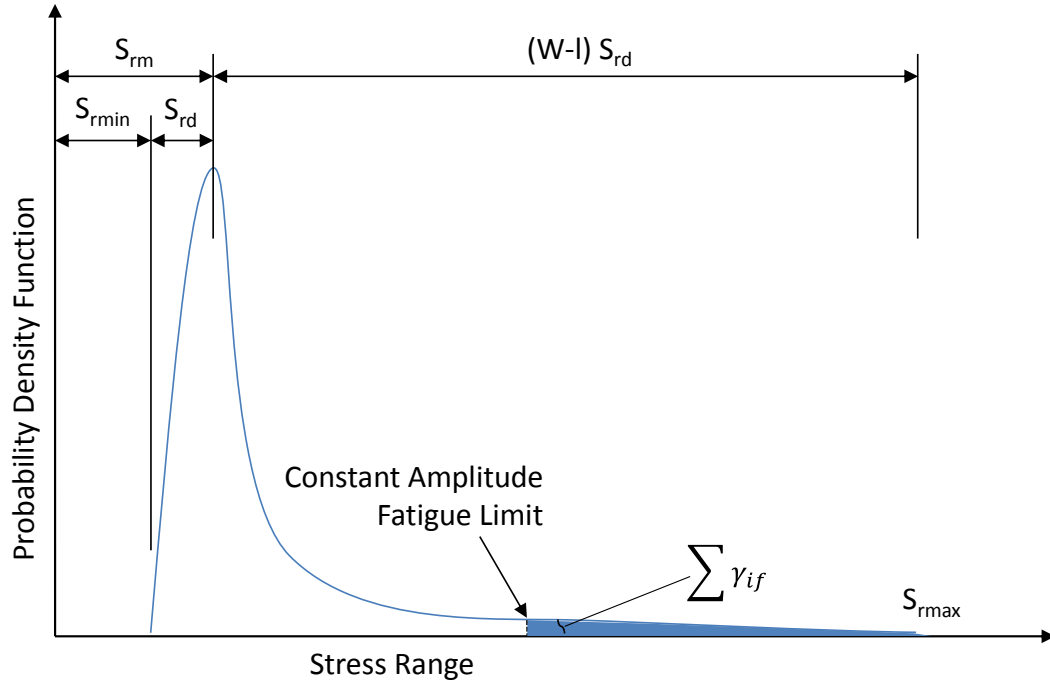


**Figure 3.37 Rayleigh-type stress range histogram** (Fisher, et al., 1983)

For steel structures, the root-mean cube stress range (Equation 3.18) calculated from a variable amplitude stress range histogram and is used with the constant amplitude S-N curves for fatigue life analyses (Zhou, 2006). The summation of stress ranges in the histogram is an acceptable way of approximating the area under the Rayleigh distribution.

$$S_{re} = \left( \sum \gamma_i S_{ri}^3 \right)^{1/3} \quad \text{(Equation 3.18)}$$

where  $S_{ri}$  is the mid-width of the  $i$ th bar, or interval, in the frequency-of-occurrence histogram, 3 is the reciprocal of the slope in the constant S-N curve, and  $\gamma_i$  is the fraction of stress ranges in that same interval (Keating, et al., 1986).

### ***3.3.2.3 Truncation Stress Range for Fatigue Details***

A fatigue detail is most affected by the largest stress ranges that exceed the constant amplitude fatigue limit (CAFL). For most bridge components, only a small fraction of the stress range histogram is greater than the CAFL while the majority of the measured stress cycles will fall below the fatigue limit. Thus, calculations for the effective stress range are distorted by the large amount of smaller cycles which lowers the effective stress range value. It has been proposed that a lower truncation stress range, or cutoff, be established, which would calculate an effective stress range that emphasizes the effects of the large cycles (Zhou, 2006). The higher the truncated stress range, the higher the calculated effective stress range.

Based on research results of variable amplitude fatigue in the United States and Europe, the magnitude of the truncation stress range was decided as a fraction of the CAFL of the detail. A truncation value of  $0.5\text{CAFL}$  was found to be reasonable yet conservative (Zhou, 2006). Therefore, all stress ranges lower than  $0.5\text{CAFL}$  are excluded in the effective stress range calculation. While the  $0.5\text{CAFL}$  value provides reasonable results for most cases, case-specific factors should also be considered in the determination of the truncation stress range. These factors include: (1) the level of ambient noise if signals from sensing equipment are not filtered, (2) stress cycles due to light vehicles based on results of a calibration test, which correlates the strain response with a control vehicle of known weight, and (3) traffic information such as the average daily truck traffic (ADTT).

### 3.4 Remaining Useful Life – Crack Initiation Period

Finally, the damage prognosis is calculated for the fatigue-crack-initiation period. The remaining useful life is calculated by comparing the current life of a specimen to the predefined laboratory values of specimens. Figure 3.38 illustrates how the effective stress range can fit into the AASHTO S-N curves. As shown, the hypothetical data is extended below the fatigue limit to accommodate VA loading with the Miner rule.

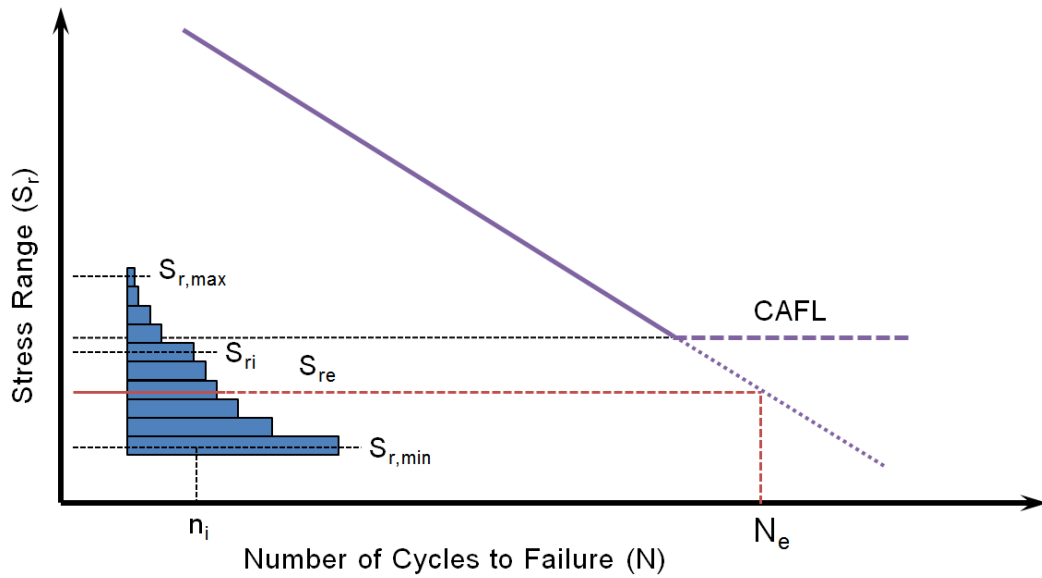


Figure 3.38 Effective stress range fits into S-N curves

The number of stress cycles to fatigue failure is found from the S-N curve that corresponds with the effective stress range. Thus the cumulative damage from the fatigue crack initiation life is written as a percentage of the fatigue life by dividing the number of current cycles at the effective stress range,  $N_e$ , by the number of stress cycles to fatigue failure,  $N_f$ .

$$d_{initiaion} = \frac{N_e}{N_f} \quad \% \text{ damage} \quad (\text{Equation 3.19})$$

Further, subtracting the current number of cycles at the effective stress range from the number of cycles that defines the fatigue life, provides the remaining useful life of the crack initiation period in terms of *cycles*,

$$RUL_i = N_f - N_e \quad \text{cycles} \quad (\text{Equation 3.20})$$

Or the remaining useful life of the crack initiation period in terms of *years* as,

$$RUL_i = N_f / N_e \quad \text{years} \quad (\text{Equation 3.21})$$

### 3.5 Uncertainties in Crack-Initiation Life Modeling

There is a diverse number of factors that contribute to the fatigue performance of a structure and uncertainties have proved impossible to capture through accurate quantitative methods or rational arguments (Schijve, 2009). This is especially difficult from structures in service, since fatigue properties largely come from laboratory tests that don't represent the real life statistical distributions. Rather than attempting to quantify the uncertainties in fatigue assessments, it is conventional to use safety factors or other similar methods. The choice of safety factors is a matter of experience and engineering judgment (Schijve, 2009).

The most common reasons for uncertainties involved with fatigue performance are:

- Uncertainties within the load spectrum or the extrapolation
- Uncertainties about the fatigue properties of the structure
- Uncertainties about the reliability of predictions

Variations in the load spectrum were discussed in detail in section 3.2 *Load-Induced Fatigue from Variable-Amplitude Loading*. The essence of this section described the

stochastic nature of variable amplitude loads, which results in large variation between the stochastic loads and deterministic loads applied in the laboratory. Even if a bridge was built with the same design and construction at a different location, the bridge will not experience the same traffic loadings. For instance, if a bridge is built in a location that is not traveled by a lot of trucks, the bridge will not experience as high of stress ranges than the bridge in a high truck volume location. Further, a bridge in a different location may even be subjected to different weather conditions. A bridge in a marine environment is more susceptible to corrosion damage, which would accelerate the fatigue effects on a bridge.

The next reason for uncertainties is associated with the fatigue properties of the structure. Since cracking will almost always begin at a material imperfection or defect, the time to initiate a crack will vary across the structure. While material properties for a standardized composition may be obtained from data banks, it cannot be guaranteed that these properties are always the same; statistical variations are related with material properties and production quality. Further, fatigue damage more often occurs on the connections between steel members, because the welded, riveted, or bolted details are often associated with high stress concentrations and construction defects (Sobanjo, et al., 2013).

The last reason often associated with uncertainties is the reliability and accuracy of fatigue-crack initiation prediction model. The remaining useful life is obtained from S-N curves and corresponding fatigue limits that were derived from constant amplitude loads. However, for high-cycle fatigue regimes, scatter of fatigue lives is not the most important issue. The scatter is more concerned around the fatigue limit. The section, 3.3.1.1

*Shortcomings of the Miner Rule*, provided insight into the drawbacks of using the linear-damage accumulation model (which are well suited for constant amplitude loads) with variable amplitude loadings. This section provided the necessary insight that with variable amplitude loads, stress ranges below the fatigue limit may also contribute to the fatigue failure.

### 3.6 Summary

Figure 3.39 presents the flowchart that summarizes the method to fatigue-crack-initiation life analysis. The flowchart begins with the measured strain-time history and ends in the damage prognosis for the bridge detail in question. The flowchart presents the method of fatigue analysis presented here, in 0.

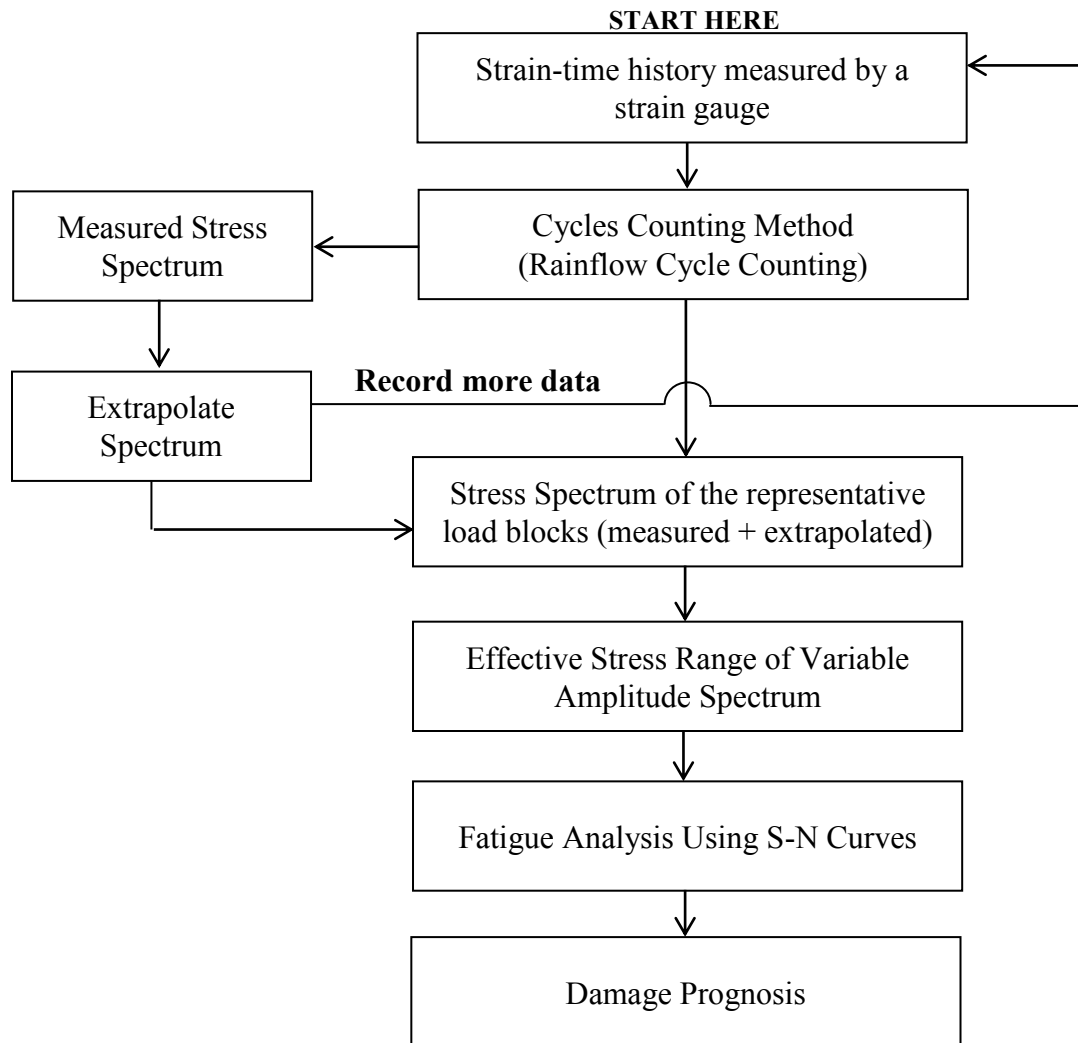


Figure 3.39 Approach to fatigue crack-initiation life analysis

## Chapter Four: Theoretical Development of Fatigue Crack Growth Period

Once a fatigue crack has initiated, applied repeated stresses cause propagation of a crack across the section of the member until the crack grows to a size where the member is capable of fracture. This period of crack growth is known as the propagation period. The crack initiation period (0) dealt mostly with microcrack development and trivial crack growth at the material surface. Microcracks usually have negligible effect on the ultimate strength of a structure. However, once the crack becomes larger in size, i.e. a macrocrack, the static strength of the structure is substantially reduced. In the crack propagation period, the crack is considered to be a macrocrack and is now growing through the material. Thus, the crack propagation period is based around the rate of crack growth. As illustrated in Figure 4.1, crack growth transitions from the end of the crack initiation period and ends once the structure has fractured: the separation of the member into two parts. The crack propagation period can be separated by three regions of crack growth, further discussed in section 4.2.1 *Crack Growth Behavior*.

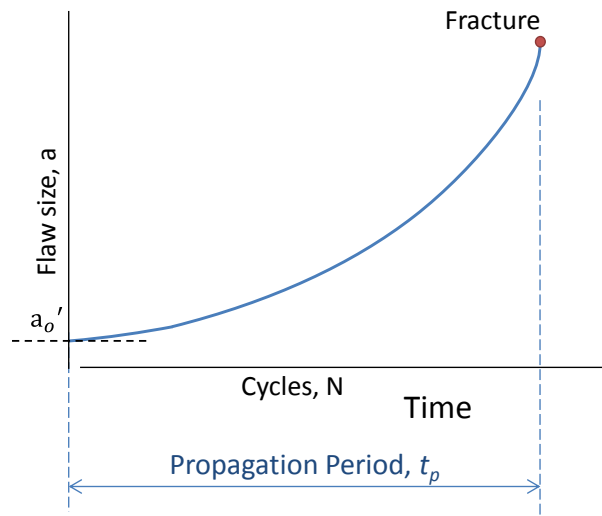


Figure 4.1 Illustration of fatigue-crack-propagation life

## 4.1 Crack Types

Since a structure contains a crack throughout the entire propagation period, then it is clear that some macrocrack sizes are deemed acceptable. Cracks may be acceptable for different reasons, for instance the crack may have negligible effect on the function of the structure. Depending on the size of the crack and the rate of crack growth, cracks may not have significant safety or economic consequences.

Two well-known examples of crack types where the crack growth is important include:

- I. A crack in sheet metal, where the crack is growing through the full thickness of the material. These cracks are more often referred to as through thickness cracks. An example where these cracks occur often is within the skin of an aircraft structure.
- II. Part through cracks, where a corner crack or a surface crack starts at a hole in the structure. These cracks may also occur as surface cracks in welded structures at the toe of the weld. A surface crack with a curved crack front has 3D character, as seen in Figure 4.2.

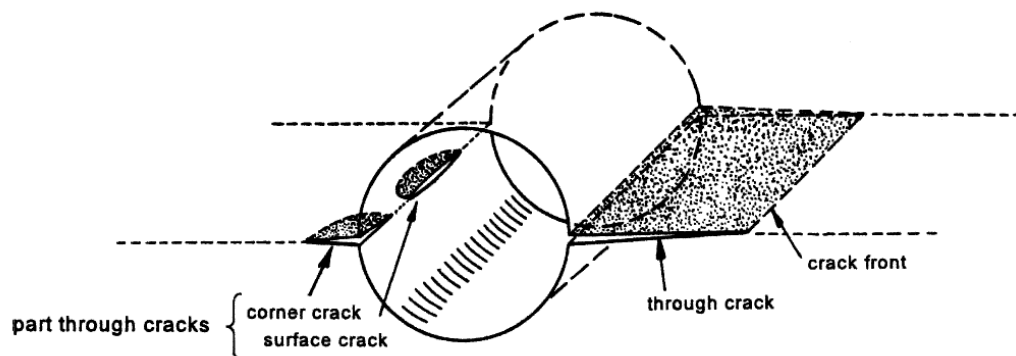
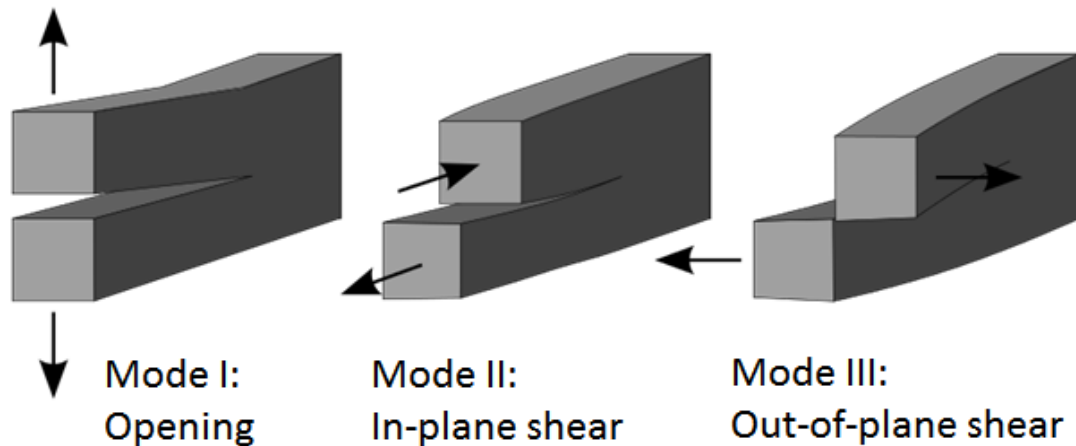


Figure 4.2 Different types of cracking starting from a hole (Schijve, 2009)

Fatigue cracks are distinguished by three modes of loading, illustrated in Figure 4.3. The first mode describes tensile loading where the crack surfaces move directly apart and

a fatigue cracks grows in a direction that is perpendicular to the main principle stress. This mode is the cause of most fatigue cracks for structures in service. The second mode describes in-plane shear where crack surfaces slide over one another in a direction perpendicular to the leading edge of the crack. The third mode is a tearing mode where the crack surfaces move relative to one another and parallel to the leading edge of the crack. Modes II and III will occur under cyclic shear stress. While experience shows that small cracks may nucleate under pure shear loading, these cracks will quickly exhibit a transition to fatigue crack growth in the tensile mode, i.e. mode I. Mode I is the dominant mode and mode of interest for fatigue cracks. Tensile stresses that open the crack will influence the conversion of cyclic plastic deformation into crack extension.



**Figure 4.3 Three modes of loading used in fracture mechanics**

The crack-tip stress equations (Equation 4.1, Equation 4.2, Equation 4.3) are very similar for each of the modes. Consequently, the fracture and crack growth analysis procedures for each of the modes turn out to be identical. Therefore, if analysis can be completed for mode I, then analysis can be performed for the additional modes as well.

$$K_I = \lim_{r \rightarrow 0} \sqrt{2\pi r} \sigma_{yy}(r, 0) \quad \text{(Equation 4.1)}$$

$$K_{II} = \lim_{r \rightarrow 0} \sqrt{2\pi r} \sigma_{yx}(r, 0) \quad (\text{Equation 4.2})$$

$$K_{III} = \lim_{r \rightarrow 0} \sqrt{2\pi r} \sigma_{yz}(r, 0) \quad (\text{Equation 4.3})$$

In practice, most cracking occurs from mode I loading. The other two modes do not occur individually, but they may occur in combination with mode I. However, if the loading of these modes is in phase, cracks will rapidly choose a direction of growth and mode I will dictate (Broek, 1989). Thus, due to the nature of crack growth, the majority of apparent combined mode cases are reduced to mode I. There are also instances where material strength or properties may dictate the mode path, and should not be simplified to a mode I. These occur in mode I and mode II combinations where the crack may be directed to a different part of the material that is less resistant to cracking and fracture (Broek, 1989).

#### 4.1.1 Crack Detection

Since fatigue cracks initiate on a microscopic scale then there is no specific crack size that occurs and is titled to be a fatigue crack. Instead, micro cracks begin at the microstructure scale in the slip planes and progress at different rates through the fatigue life of the crack. The term “initial crack size” is reserved for crack sizes that are detectable. Various methods have been used for the detection of cracks: visual, dye penetrant, magnetic particles, x-ray, ultrasonic, eddy current, acoustic emission. Each of these methods is capable of detecting crack sizes at different lengths. Table 4.1 lists these inspection methods, a brief overview of the method, and approximate crack sizes these methods have been able to detect.

**Table 4.1 Compilation of non-destructive testing methods and the detectable crack size**

<b>Inspection Method</b>	<b>Principle (Broek, 1989)</b>	<b>Detectable Crack Size (Miki, 2004)</b>
Visual	Naked eye, assisted by magnifying glass, lamps and mirrors.	1-5mm
Penetrant	Colored liquid is brushed on to penetrate into crack, then washed off. Quickly-drying suspension of chalk is applied (developer). Penetrant in crack is extracted by developer to give colored line.	10mm 6mm (after paint removal)
Magnetic Particles	Liquid containing iron powder. Part placed in magnetic field and observed under ultra-violet light. Magnetic field lines indicate cracks.	~ 5mm 2mm (after paint removal)
X-ray	X-rays pass through structure are caught on film. Cracks are delineated by black line on film.	unknown
Ultrasonic	Probe (piezo-electric crystal) transmits high frequency wave into material. The wave is reflected by crack. Time between pulse and reflection indicates position of crack.	5mm 6mm (after paint removal)
Eddy Current	Coil induces eddy current in the metal. In turn this induces a current in the coil. Under the presence of a crack the induction changes.	5mm 5mm (after paint removal)
Acoustic Emission	Measurement of the intensity of waves emitted in the material due to plastic deformation at crack tip.	unknown

Visual inspection is the only inspection method that is required by the FHWA. Visual inspection would only be supplemented by these other inspection methods. Currently, the approximate value of the initial crack size is normally taken as an engineering size crack that is easily visible with the naked eye, approximately 1-5mm (Chen, et al., 2005). Most steel bridges are coated with paint in order to protect them from weathering corrosion. Discontinuities of paint films, which are easy to detect, are the sign that cracks are present (Miki, 2004).

### 4.1.2 Cracks on Welded Structures

Once a crack is visible and detected, the type of crack can provide more information about the structure, i.e. the direction of internal forces, or the bending of the member. As mentioned in Chapter 3, welded joints may be especially prone to cracking because defects in the material create a vulnerable spot for crack initiation when subjected to bending and tension loads.

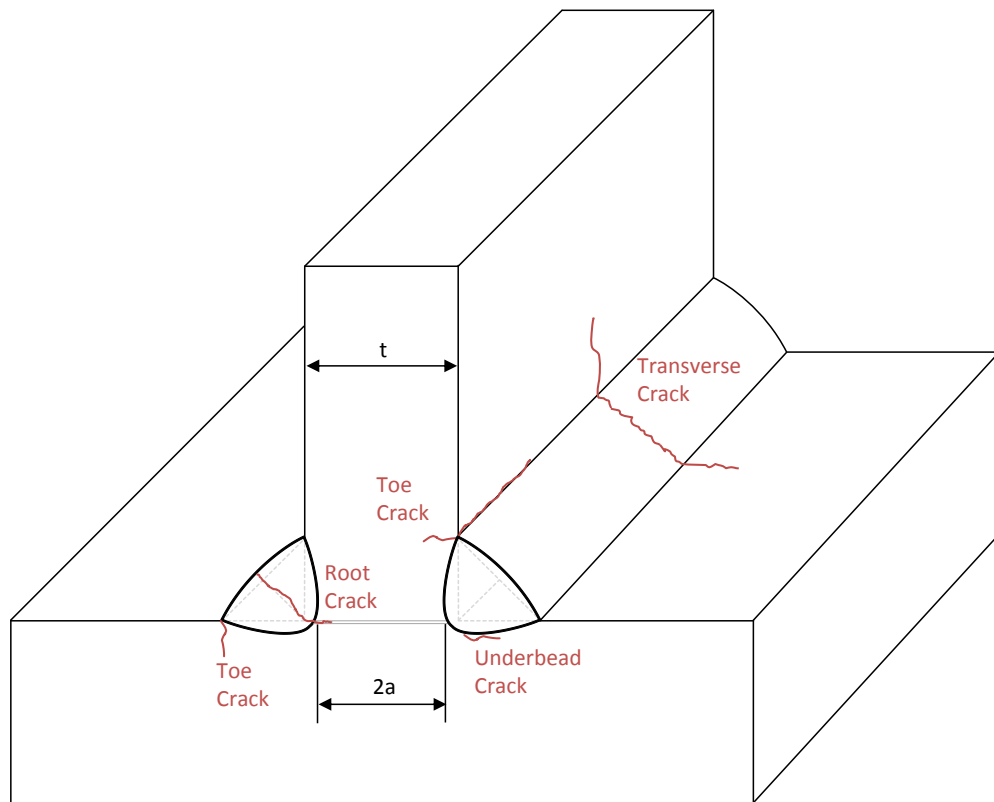
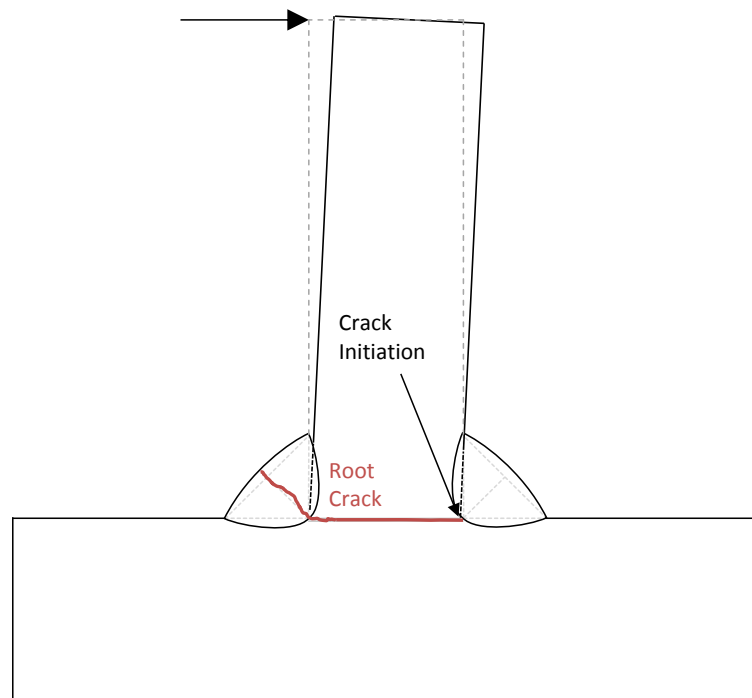


Figure 4.4 Transverse gusset on a plate - types of crack in a weld

Figure 4.4 displays typical types of cracks that may occur on a welded structure, where the structure's geometry is positioned with a transverse and longitudinal plate; a typical geometry found on bridge elements such as cover plates, gussets, or stiffeners. Transverse cracks are perpendicular to the direction of the weld. These are generally the result of longitudinal stresses acting on weld metal of low ductility. An underbead crack,

also known as an undercut crack, is often the result of internal stresses that arise in the welding process from unequal contraction between the base metal and the weld metal. While transverse cracks and underbead cracks have occurred on welded structures, they can be alleviated through proper design and welding processes. However, a root crack and a toe crack are more likely to develop from applied tension loads on the transverse connection plate, illustrated in Figure 4.9. Thus, a crack that forms at the root or toe are the more common types of cracks found on bridge elements. A root crack forms at the root of the weld and between the joint of the steel plates and usually occurs from a horizontal applied load, as shown in Figure 4.5 (AISC, 2005).



**Figure 4.5 Initiation of root crack**

A toe crack begins at the toe of the weld and the steel plate, and forms perpendicular to the applied load. With a transverse gusset welded to a longitudinal plate, the toe of the weld forms a sharp angle at the weld periphery between the weld and the face of the gusset. This creates a line of elevated tension where fatigue cracking can start from the

small, sharp discontinuities (Mertz, 2012). An illustration of a toe crack and a root crack is shown in Figure 4.6.

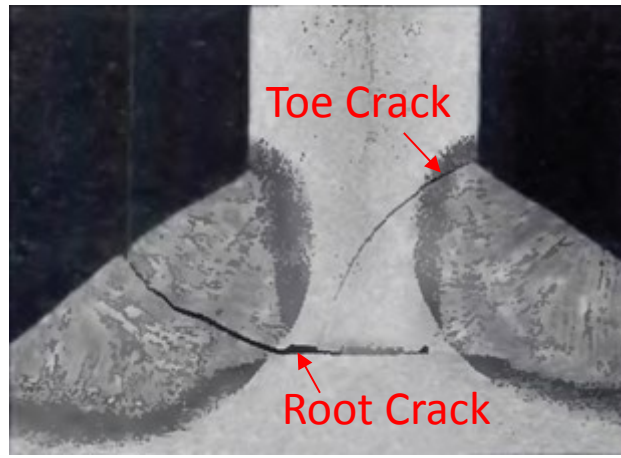


Figure 4.6 Simultaneous propagation of cracks from toe and root of weld (Janosch, 1993)

## 4.2 Linear Elastic Fracture Mechanics

A crack in a structure can grow under repeated applications of stress that are large enough in range. The rate of this crack growth is high dependent on the material type. While the nature of the material cracking is a non-elastic deformation, the region beyond the crack (at the crack tip) experiences a linear elastic stress field under load.

Because the stresses at the crack tip are so small in fatigue problems, the plastic zone is limited and linear elastic fracture mechanics (LEFM) is therefore a useful tool for fatigue crack propagation life prediction. Paris model is most widely used model in linear elastic fracture mechanics for the prediction of crack growth. In this model, the range of the stress intensity factor ( $\Delta K$ ) is the main factor driving the crack growth with two parameters  $C$  and  $m$  that reflect the material properties.

$$\frac{da}{dN} = C(\Delta K)^m \quad (\text{Equation 4.4})$$

Where  $a$  is the initial crack size,  $N$  is the number of fatigue loading cycles,  $C$  and  $m$  are material properties, and  $\Delta K$  is the stress intensification factor. For a given initial crack size, once the crack growth rate is determined, then the existing crack size can be easily calculated through a summation over crack size increments starting from the known size.

#### 4.2.1 Stress Intensity Factors

The stress in the local crack tip is described as a function of the applied stress in the form of stress intensity factors. Stress intensity factors are used to describe the severity of a stress distribution around a crack tip, the rate of crack growth and the onset of fracture (Zafosnik, et al., 2002). Even at relatively low loads, there will be a high concentration of stress at the crack tip, and plastic deformation can occur (Mertz, 2012). The simplest form to describe the “intensity” of a stress distribution around a crack tip can be written as,

$$K = \beta S \sqrt{\pi a} \quad (\text{Equation 4.5})$$

Where,  $S$  is the remote loading stress,  $a$  is the crack length, and  $\beta$  is a dimensionless factor depending on the geometry of the specimen or structural component. One important feature this equation illustrates is that the stress distribution around the crack tip can be described as a linear function.

#### 4.2.2 Stress Intensity Factor and Similarity Factor

From Equation 4.5 it is shown that the stress intensity factor,  $K$ , and the remote loading stress are linearly proportional. Therefore, if the cyclic stress varies between  $S_{\min}$  and  $S_{\max}$  then the corresponding stress intensity factor will vary between  $K_{\min}$  and  $K_{\max}$ .

The stress ratio is the same for the cyclic stress and the cyclic K-value, shown in Equation 4.5 and illustrated in Figure 4.7.

$$R = \frac{S_{min}}{S_{max}} = \frac{K_{min}}{K_{max}} \quad (\text{Equation 4.6})$$

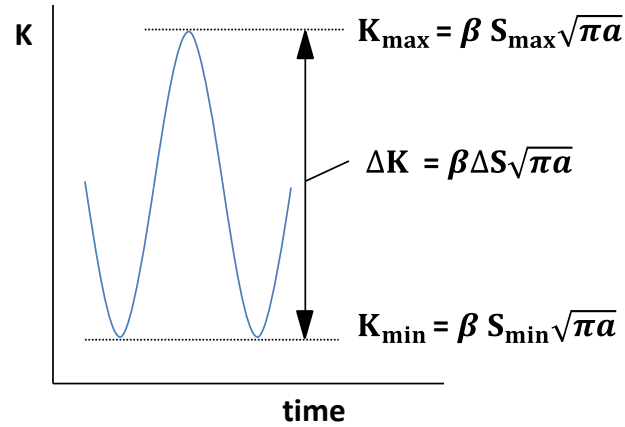


**Figure 4.7** Variation of stress intensity factor related to the variation in stress cycle (Schijve, 2009)

To exemplify the similarity principle, two specimens with different size cracks and loadings are compared against each other, seen in Figure 4.8. The one specimen with a large crack is loaded by a low cyclic stress. The other specimen has a small crack and is loaded by a high cyclic stress. Each of these specimens should experience the same stress intensity factor, and in accordance with the similarity principle, the amount of damage, or propagation in the crack, should also be the same in each specimen. The results are that the crack growth rate must be a function of  $\Delta K$ , which is a function of the stress ratio, seen in Equation 4.7,

$$\frac{da}{dN} = f(\Delta K, R) \quad (\text{Equation 4.7})$$

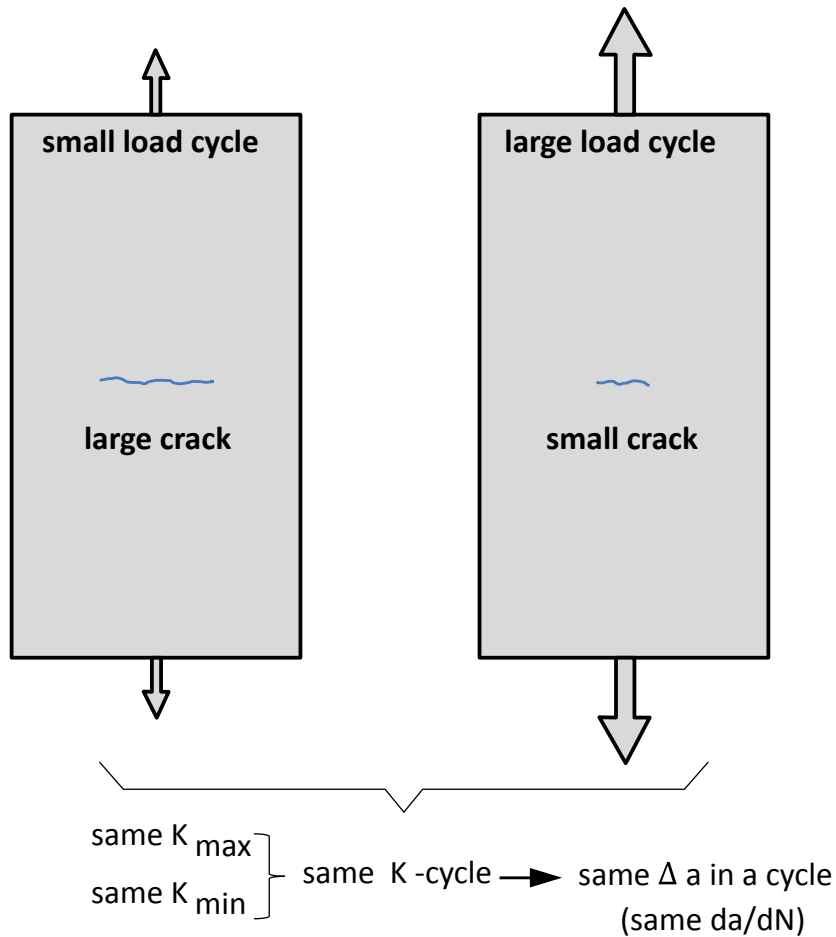


Figure 4.8 Example of similarity principle (Schijve, 2009)

### 4.2.3 Crack Growth Behavior

The stress intensity factor is the driving force for fatigue crack growth ( $da/dN$ ) results. The relationship between the stress intensity factor and the crack growth curve is a sigmoidal curve, illustrated in Figure 4.9. When  $da/dN$  is plotted as a function of  $\Delta K$  on a double log scale, the function  $da/dN = f_r(\Delta K)$  can be divided into three regions that describe the behavior of crack growth. The corresponding regions are referred to as the threshold region, the Paris region, and the stable tearing crack growth region.

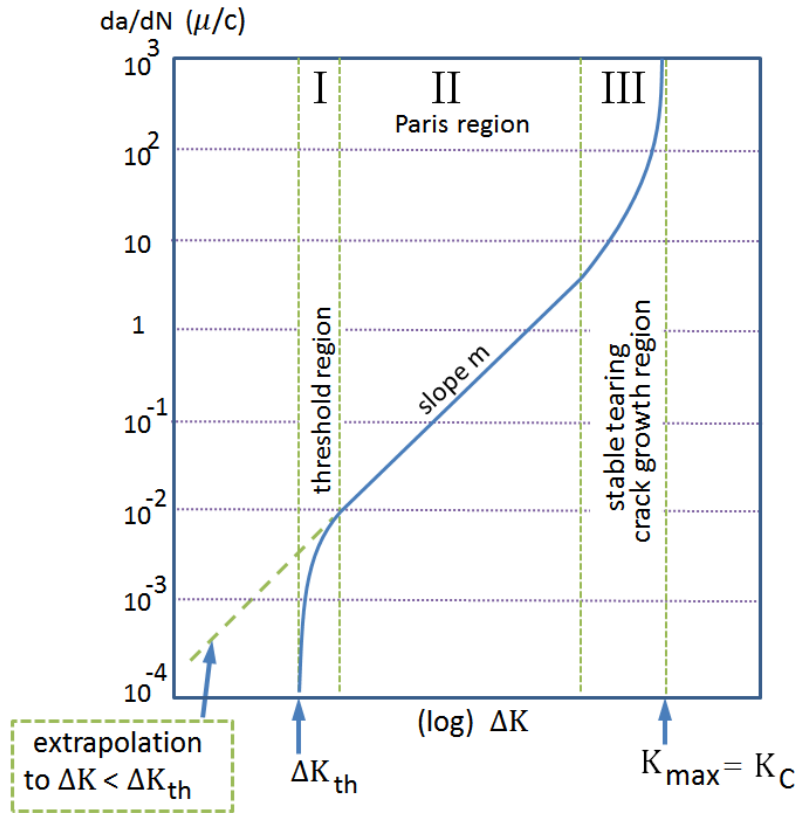


Figure 4.9 Schematic of crack growth curve showing crack growth regions (Schijve, 2009)

In the first region, the threshold region, the cracking behavior is associated with threshold effects, i.e. the transition from microcrack to macrocracks. Thus, the threshold value,  $\Delta K_{th}$ , is concerned with fatigue cracks that have grown to a macroscopic size at a  $\Delta K$  level above  $\Delta K_{th}$ . If  $\Delta K$  is then decreased below  $\Delta K_{th}$ , then crack growth slows down to a point where it is assumed that no further growth occurs (Schijve, 2009). However, the determination of the  $\Delta K_{th}$ -value has a problematic character. This value is obtained in experiments with a decreasing crack growth rate until the crack driving force can no longer surpasses the crack growth resistance. However, these threshold conditions are not a true representative for crack growth under variable amplitude loading; cycles in VA loads may be preceded by some erratic crack growth mechanism that is not captured in threshold experiments. As described earlier in 3.3.1.1

*Shortcomings of the Miner Rule*, stress ranges that occur below the fatigue limit may actually influence fatigue damage. Then in accordance with the similarity principle, it should be expected that cycles with  $\Delta K < \Delta K_{th}$  can still contribute to crack growth. In the same way that the high cycle fatigue slope is extended on the S-N curves, it is recommended to extrapolate the  $da/dN - \Delta K$  data in the Paris region to lower  $\Delta K$ -values in the threshold region.

The second region of the crack growth curve shows a log-linear relationship between  $da/dN$  and  $\Delta K$ . Most current crack growth models are fit to this region and utilize linear elastic fracture mechanics to describe the crack growth behavior. While many “curve fits” in this region have been suggested, the Paris equation, Equation 4.4, is the most widely accepted.

In the third and last region of crack growth, crack growth rates are extremely high and little fatigue life is involved. This region is often referred to as the stable-tearing crack growth region. Much like the threshold region, the crack growth life spent in this region is short, which implies that its engineering significance is limited. As seen in Figure 4.9, the asymptote that ends this region also completes the sigmoidal curve that describes crack growth. The asymptote describes a  $\Delta K$  cycle that has reached a critical value,  $K_c$ , which describes complete failure of the specimen, i.e.  $K_{max} = K_c$ .

Figure 4.10 illustrates how the crack growth curve fits into the fatigue life curve. The crack growth curve is superimposed onto the fatigue life curve, so the vertical and horizontal axes of the crack growth curve are still scaled logarithmically, while the axis of the fatigue life curve is a linear scale. The first region is part of the initiation period since it deals with remedial crack growth that is not yet visible for inspection. The crack

becomes of macroscopic size at the end of the initiation period where the propagation period begins. The stable (linear) crack growth region governs the crack growth sigmoid curve, which is how linear elastic fracture mechanics is used to model the growth rate in the propagation period.

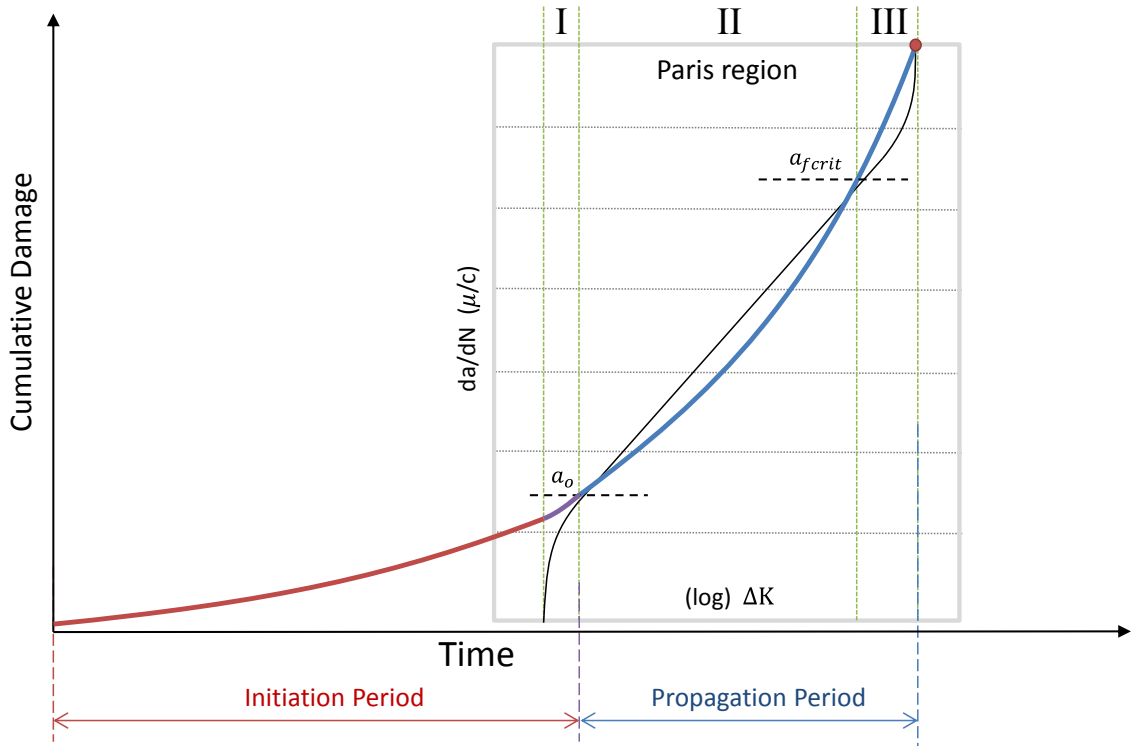


Figure 4.10 Crack growth curve fits into fatigue life curve

### 4.3 Fracture Toughness

When the value of the stress intensification factor surpasses  $K_{max}$  and is no longer in a stable region of cracking, the stresses at the crack tip are too high for the material to endure and fracture takes place. This critical stress intensity value is more often referred to as the fracture toughness,  $K_{Ic}$ , where  $I$  denotes opening mode, and  $c$  represents critical. Fracture toughness is a measured material property, just like Poisons ratio or Young's Modulus, and is usually measured through standard compact specimens. The fracture

toughness is used to describe the ability of an already cracked material to resist fracture. The fracture toughness can also be used to indicate the sensitivity of the material and the materials susceptibility to experiencing cracks under loading (Schijve, 2009). Thus, stress intensity factors can be compared with the fracture toughness variables to determine if the crack will propagate (CAE Associates, 2013). The relationship between the stress intensity factors and the fracture toughness is similar to that between tensile stress and tensile strength:

$$K \leq K_{IC} \quad (\text{Equation 4.8})$$

When the applied stress intensity equals or exceeds the material fracture resistance,  $K_{IC}$ , fracture is predicted.

#### **4.3.1 Charpy V-Notch Test**

The Charpy V-Notch (CVN) test is commonly utilized to measure the fracture toughness for structural steel (Wright, 2012). In the CVN test a small 10x10x55mm rectangular bar with a broached notch on one face is mounted on a fixture. A weighted pendulum or hammer, strikes the test specimen and the energy required to initiate fracture is measured. This provides a relative measure of material toughness.

The CVN test was not enough by itself to give accurate predictions of the fracture toughness. It was also found in the CVN tests that the amount of energy absorbed by a particular steel specimen varies as a function of the material temperature and loading rate. The consideration of these factors has led to a two-step transition-temperature approach to prevent fracture. This two-step procedure correlates the CVN tests and temperature was developed in order to more accurately predict the fracture toughness. The first step is to calculate the toughness of the material as if it had just underwent the CVN test:

$$K_{IC} = \sqrt{5(CVN)E} \quad (\text{Equation 4.9})$$

Where CVN is the Charpy V-notch energy (ft-lb) and E is modulus of elasticity (psi) and  $K_{IC}$  is  $psi\sqrt{in}$ . Since, the CVN test is performed at dynamic impact loading rates that are much higher than the loading rate experienced by bridges due to live load. The next step is to calculate a temperature shift between the static and CVN test curve.

$$T_{shift} = 215 - 1.5\sigma_{YS} \quad (\text{Equation 4.10})$$

Figure 4.11 displays the relationship between the dynamic impact loading and the fracture toughness at bridge loading rates.

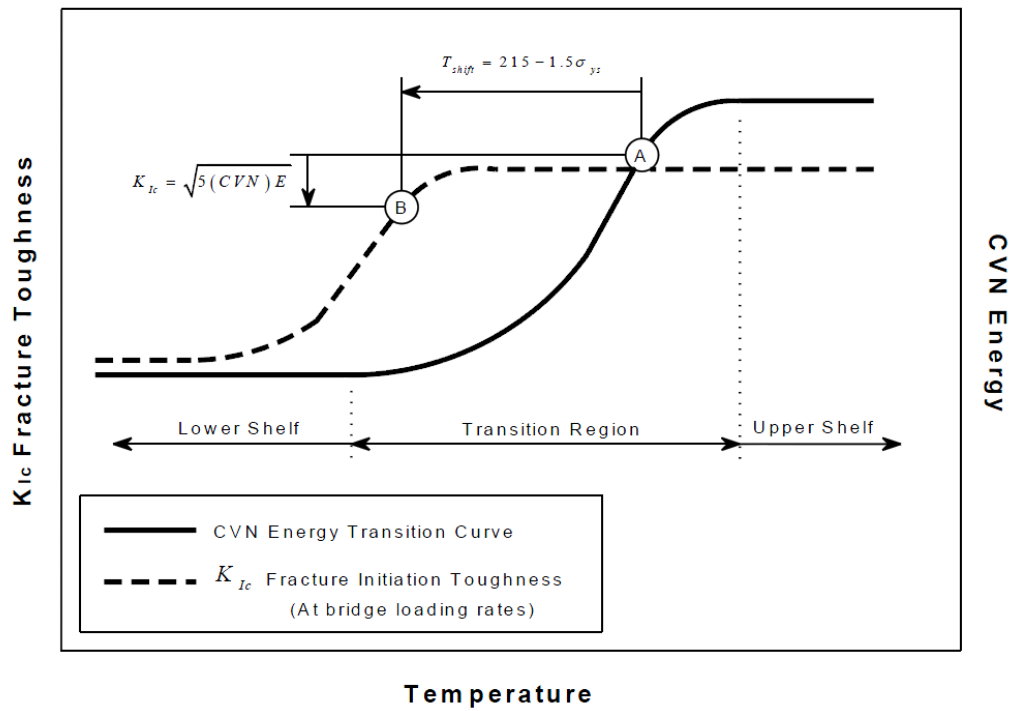


Figure 4.11 CVN transition curve relating temperature with fracture toughness (White, November 2012)

### **4.3.2 Computations of Stress Intensity Factors**

For many ordinary cases of cracking, the calculations of stress intensification factors for various crack geometries and loading cases have already been computed and can be obtained from previously published literature, e.g. elliptical cracks embedded in very large bodies (Schijve, 2009). These results to these configurations are often referred to as  $K$  solutions. The  $K$  solutions are presented as a function of the geometric correction factor  $\beta$  and are displayed in graphs that show how  $\beta$  depends on geometric ratios. The graphs can then be used to estimate unknown stress intensification factors by evaluating the available data for “similar” geometries. While there is extensive literature on  $K$ -values, these pre-computed solutions are limited to a special few configurations and many practical cases for  $K$  solutions for cracks are not available (Schijve, 2009). To compensate for this, sometimes the values are approximated by available solutions for less complicated geometries. Furthermore, for cases with more complex geometries, more accurate  $K$  values should be independently calculated. Finite element modeling has proven to offer satisfactory results for the stress intensification factors (Schijve, 2009).

### **4.3.3 Modeling Stress Intensification Factors**

Finite element (FE) modeling offers a variety of techniques and efficient computation to the derivation of stress intensity factors (SIF). In finite element models, the crack is treated as an integral part of the structure, and can be modeled in as much detail as necessary to accurately reflect the structural load paths, both near and far from the crack tip. Thus, finite element models have been shown to provide acceptable accuracy, which has made the finite element method the most popular tool in computing SIF (Jia, et al., 2004). Further, finite element models offer large enough computation

capacity to capture multiple load effects (Figure 4.3). The most common FE methods for determining stress intensity factors include, the energy release rate by using the complex J integral and the displacement extrapolation method (Zafosnik, et al., 2002).

Accurate modeling of the crack proves to be a difficult challenge. Even if it is known where the crack location is, modeling the crack in a FEM is not trivial, especially in cases of modeling crack propagation. Under crack propagation, the crack geometry will affect how the load is redistributed around the crack, and multiple models will be needed to implement the new crack geometry, crack direction or change the meshing around the crack tip (CAE Associates, 2013).

#### ***4.3.3.1 Displacement extrapolation method***

The stress intensity factors can be determined using displacement correlation near the crack tip. The displacement extrapolation method uses the nodal displacements around the crack tip to determine the stress intensity factor. Within the FE model, a very fine mesh is required around the crack tip in order to account for the large gradients of stress and strain. The formula for the stress intensification relating to tensile stress (mode I),  $K_I$ , can be written as:

$$K_I = \Delta v \frac{E \sqrt{2\pi/r}}{8(1 - \nu^2)} \quad (\text{Equation 4.11})$$

The formula for the stress intensification relating to in-plane shear stress (mode II),  $K_{II}$ , can be written as:

$$K_{II} = \Delta u \frac{E \sqrt{2\pi/r}}{8(1 - \nu^2)} \quad (\text{Equation 4.12})$$

Where,  $\nu$  = Poisson's ratio,  $\Delta v$  = displacements in the y-direction of a local coordinate system,  $\Delta u$  and  $\Delta v$  = displacements in the x-direction and y-direction of a local coordinate system, respectively,  $r$  is the distance of a node on the crack surface in a local polar-coordinate system, and  $E$  is Young's Modulus. The displacement correlation method is computed in ANSYS using the KCALC command. The displacement extrapolation method is a more traditional analysis method and is a post processing activity, only valid for linear elastic problems. The employment of the displacement extrapolation method is described in the following section, Validating FEM Models with a simple LEFM model.

#### 4.4 Validating FEM Models with a simple LEFM model

When a through thickness crack is subjected to fatigue loads in cyclic tension only, the crack front is perpendicular to the material surface. A through crack with a straight crack front is usually treated as a two-dimensional problem. A two-dimensional problem is the easiest to model and to calculate results. Under the assumptions of this being a plain strain problem where linear elastic fracture mechanics is applicable, then an analytical solution can be determined through the following equation:

$$K = \beta \sigma \sqrt{\pi a} \quad (\text{Equation 4.13})$$

Where the equation for this specific geometry (Pilkey, 2005):

$$\beta = \left[ 1 - 0.1 \left( \frac{a}{b} \right)^2 + .96 \left( \frac{a}{b} \right)^4 \right] \sqrt{\sec \frac{\pi a}{b}} \quad (\text{Equation 4.14})$$

Modeling of structures takes place in a global Cartesian coordinate system. Because cracks are such a small geometry as opposed to the entire system, the crack is modeled with its own coordinate system that is defined at the crack tip, shown in Figure 4.12. This coordinate system is useful for expressing the displacements at the crack tip in terms of crack tip movement.

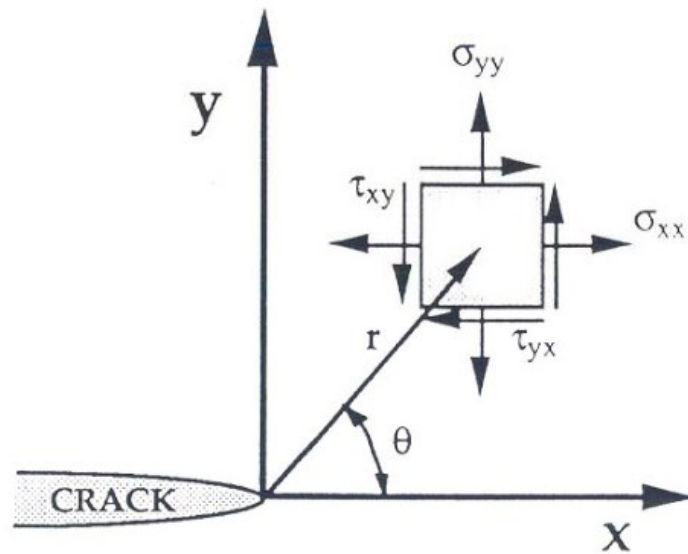


Figure 4.12 Stress field at the crack tip

#### 4.4.1 Stress Intensity Factor with 2D Geometry in ANSYS

An example of a 2D problem was adopted from Dr. Anh-Vu Phan at the University of Alabama (Phan, 2005). A steel plate with dimensions:  $b = 0.2$  m,  $a = 0.02$  m,  $\sigma = 100$  MPa and properties: Young's modulus  $E = 200$  GPa and Poisson's ratio  $\nu = 0.3$ . From Equation 4.14, the analytical solution yields,  $K_I^{Calc} = 25.680 \text{ MPa} \sqrt{\text{m}}$ .

To demonstrate the accuracy of the KCALC command in ANSYS, the stress intensity factor was computed for a finite plate in tension, with a mode I through thickness crack. Firstly, the equation for a mode I stress intensification factor, Equation

4.11, was rearranged in a different form and is described by the shear modulus; for reasons that will become clear in the following section. The relationship between the shear modulus and elasticity modulus is:

$$G = \frac{E}{2(1 + \nu)} \quad (\text{Equation 4.15})$$

The equation for a mode I stress intensity factor becomes:

$$K_I = \sqrt{2\pi} \frac{G}{4(1 - \nu)} \frac{\Delta v}{\sqrt{r}} \quad (\text{Equation 4.16})$$

Where  $\Delta v$  is the motion of one crack face with respect to another and  $r$  is some location on the crack face defined by the local coordinate system. In Equation 4.16,  $\Delta v/\sqrt{r}$  is the only term that doesn't remain constant and is evaluated based on the nodal displacements and their location in the local coordinate system. There is an approximate linear relationship between the variables  $\Delta v$  and  $\sqrt{r}$ .

$$\frac{\Delta v}{\sqrt{r}} = A + Br \quad (\text{Equation 4.17})$$

By using the displacements at known nodal locations along the crack path, constants A and B can be solved for with a simple linear regression model.

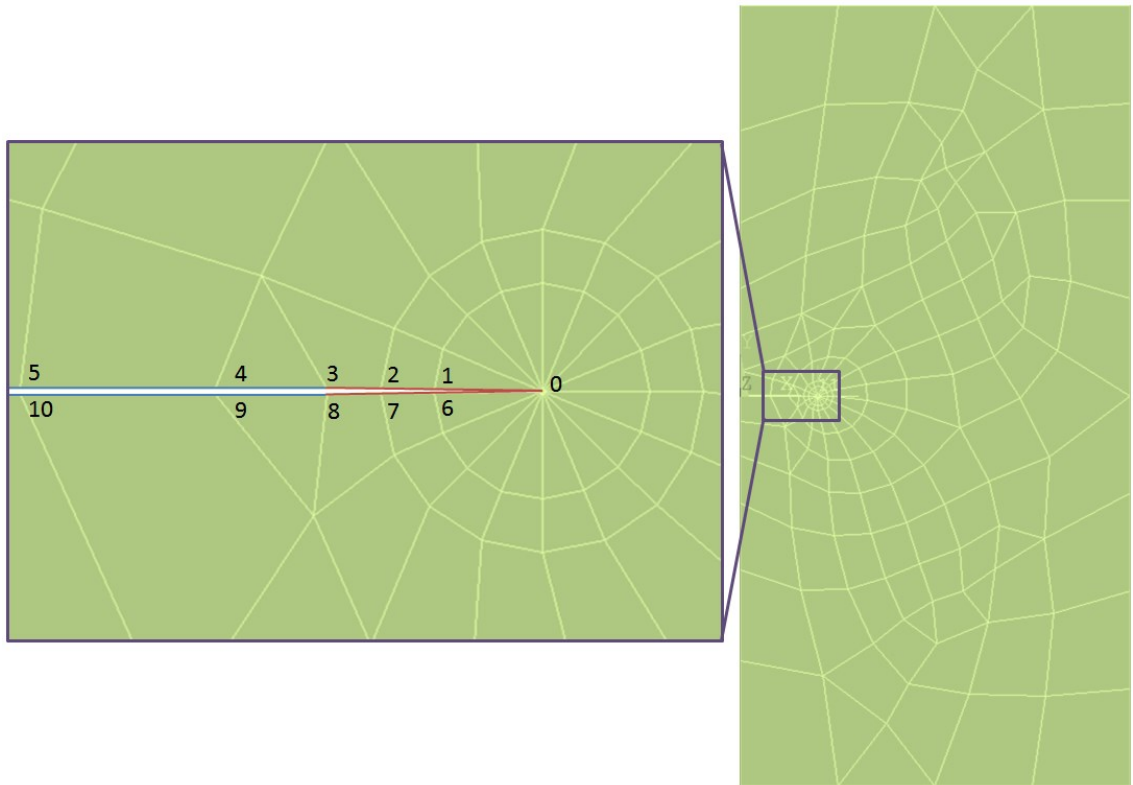


**Figure 4.13 Elements and nodes of 2D full crack model**

For a full crack model, the selected crack path in ANSYS requires at least five nodes to be evaluated on the crack face; two nodes on the top of the crack face, two nodes on the bottom of the crack face, and the node at the crack tip. Figure 4.13 displays the elements and numbering along the crack face and crack tip. In accordance with Figure 4.13, the selected crack path would consist of some combination between nodes 5, 4, 3, 10, 9 and 8 along with the node at the crack tip, node 0. The solved displacements and coordinates of these nodes are outlined in Table 4.2.

**Table 4.2 Coordinates and displacements of nodes on crack face**

	Undeformed Coordinates		Nodal Displacements		Deformed Coordinates	
	u	v	$\Delta u$	$\Delta v$	$u_{def} = u + \Delta u$	$v_{def} = v + \Delta v$
<b>Node 5</b>	-1.21E-02	5.00E-05	-3.84E-06	1.77E-05	-1.22E-02	6.77E-05
<b>Node 4</b>	-7.62E-03	5.00E-05	-6.05E-06	1.51E-05	-7.62E-03	6.51E-05
<b>Node 3</b>	-5.00E-03	5.00E-05	-7.32E-06	1.28E-05	-5.01E-03	6.28E-05
<b>Node 2</b>	-3.75E-03	3.75E-05	-7.97E-06	1.12E-05	-3.76E-03	4.87E-05
<b>Node 1</b>	-2.50E-03	2.50E-05	-8.59E-06	9.33E-06	-2.51E-03	3.43E-05
<b>Node 0 Crack Tip</b>	0.00E+00	0.00E+00	-4.93E-10	-4.93E-10	-4.93E-10	-4.93E-10
<b>Node 6</b>	-2.50E-03	-2.50E-05	8.59E-06	-9.33E-06	-2.49E-03	-3.43E-05
<b>Node 7</b>	-3.75E-03	-3.75E-05	7.97E-06	-1.12E-05	-3.74E-03	-4.87E-05
<b>Node 8</b>	-5.00E-03	-5.00E-05	7.32E-06	-1.28E-05	-4.99E-03	-6.28E-05
<b>Node 9</b>	-7.62E-03	-5.00E-05	6.05E-06	-1.51E-05	-7.61E-03	-6.51E-05
<b>Node 10</b>	-1.21E-02	-5.00E-05	3.84E-06	-1.77E-05	-1.21E-02	-6.77E-05

Figure 4.14 illustrates how the nodal variables and terms are defined within the deformed and undeformed shapes on the crack face. The values associated with the motion of one crack face with respect to another,  $\Delta v$ , are outlined in Table 4.3.

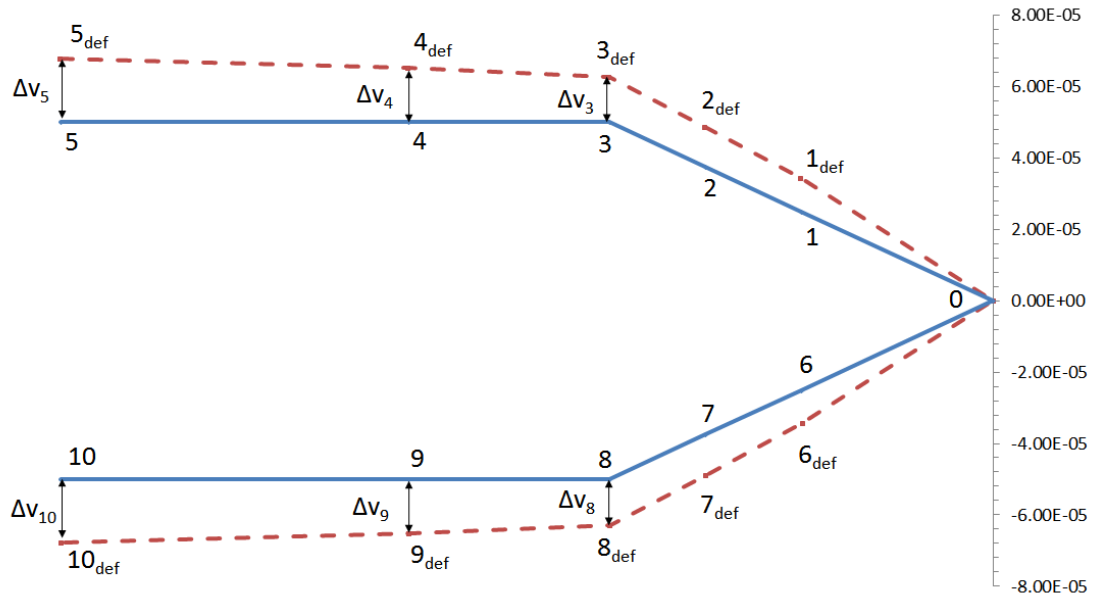


**Figure 4.14 Deformed and undeformed shape of crack tip**

**Table 4.3 Motion of one crack face with respect to another,  $\Delta v$**

Total Displacements, $\Delta v$	
$\Delta v_5 + \Delta v_{10}$	3.55E-05
$\Delta v_4 + \Delta v_9$	3.03E-05
$\Delta v_3 + \Delta v_8$	2.55E-05

**Table 4.4 Local coordinates and final factor,  $\Delta v / \sqrt{r}$**

	$r = \sqrt{u_{\text{def}}^2 + v_{\text{def}}^2}$	$\Delta v / \sqrt{r}$
<b>Node 5</b>	0.01215352912	0.00032193
<b>Node 4</b>	0.00762333257	0.00034667
<b>Node 3</b>	0.00500771480	0.00036063

For the nodal coordinates and nodal displacements on the crack face, the values for  $\Delta v / \sqrt{r}$  can be solved, displayed in Table 4.4. Linear regression between these three values yields the following linear relationship:

$$\frac{\Delta v}{\sqrt{r}} = A + Br \cong 0.0003878617 - 0.0054213125r \quad (\text{Equation 4.18})$$

Since  $r$  is some location on the crack face in the local coordinate system, then as  $r$  approaches 0 (the crack tip), then the linear relationship in Equation 4.18 can be used to solve for the stress intensification factor. Therefore, when moving closer to the crack tip, the displacements get smaller, and the stress intensification factor converges to a known value, as seen in Figure 4.15.

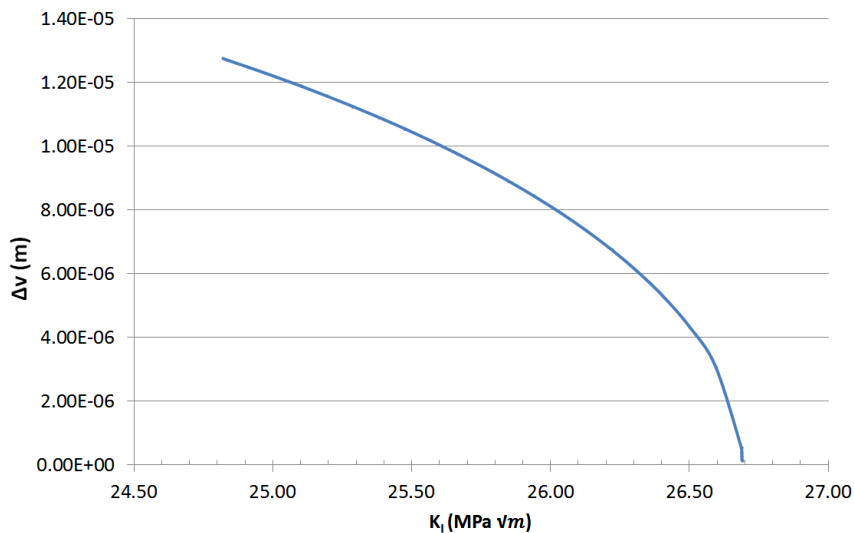


**Figure 4.15 Relationship between crack face displacements and stress intensity factor**

```

**** CALCULATE MIXED-MODE STRESS INTENSITY FACTORS ****
ASSUME PLANE STRAIN CONDITIONS|
ASSUME A FULL-CRACK MODEL <USE 5 NODES>
EXTRAPOLATION PATH IS DEFINED BY NODES:      20      18      16      36      34
WITH NODE      20 AS THE CRACK-TIP NODE
USE MATERIAL PROPERTIES FOR MATERIAL NUMBER      1
EX =      0.20000E+06  NUXY =      0.30000  AT TEMP =      0.0000
**** KI =      26.686      ,  KII =      0.13902      ,  KIII =      0.0000      ****

```

Figure 4.16 SIF results of the FEM analysis on full crack model with 2D geometry

After the FEM analysis, the stress intensity factor for mode I is computed to be  $K_I^{ANSYS} = 26.686 \text{ MPa} \sqrt{m}$ . Figure 4.16 displays the ANSYS dialogue box. This result is compared to the analytical solution for verification. The error between the two methods can be computed as:

$$\epsilon = \frac{K_I^{ANSYS} - K_I^{Calc}}{K_I^{Calc}} = \frac{26.686 - 25.680}{25.680} = 3.917\% \quad (\text{Equation 4.19})$$

Conclusively, the displacement extrapolation method used with finite elements can effectively compute the stress intensity factor at the crack tip with minimal error.

#### 4.4.2 Stress Intensity Factor with 3D Geometry in ANSYS

The example of solving for the stress intensity factor on a 2D plate (4.4.1 Stress Intensity Factor with 2D Geometry in ANSYS) is expanded upon for a plate with 3D geometry. The 3D plate is configured with the same material properties and loading, i.e. Young's modulus  $E = 200 \text{ GPa}$ , Poisson's ratio  $\nu = 0.3$  and  $\sigma = 100 \text{ MPa}$ . The same geometry is used, with dimensions:  $b = 0.2 \text{ m}$ ,  $a = 0.02 \text{ m}$  and additional thickness of  $t = 0.02 \text{ m}$  is applied.

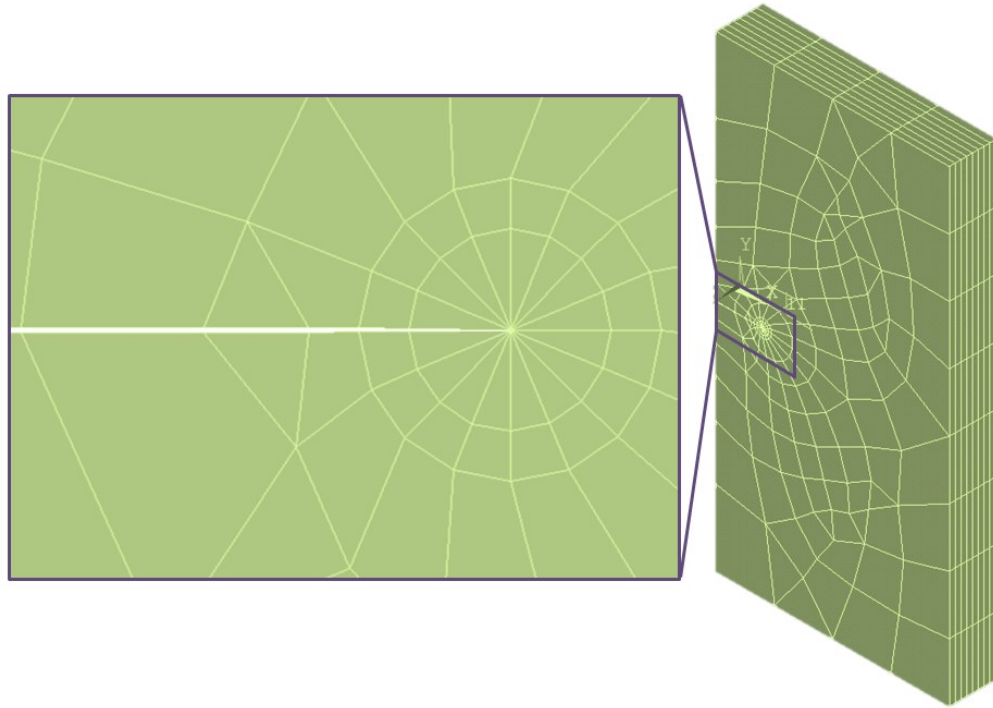


**Figure 4.17 Elements of 3D full crack model**

The 3D model was created by extruding the geometry and meshed area from the 2D plate. For areas that are pre-meshed in 2D, the ANSYS command *VOFFST* allows the volume and mesh to be extruded; provided the default number of divisions in the along the thickness of the shape is predefined; done through the *ESIZE* command. For a 3D solid, it is best to use a 20 node brick element for the element type. As seen in Figure 4.17, the 3D plate was set to be divided into eight divisions. The displacement extrapolation method was used to solve for the stress intensity factor. Calculations were proceeded in the same way as a 2-dimensional plate, and the crack path is chosen by selecting 5 nodes along the crack face.

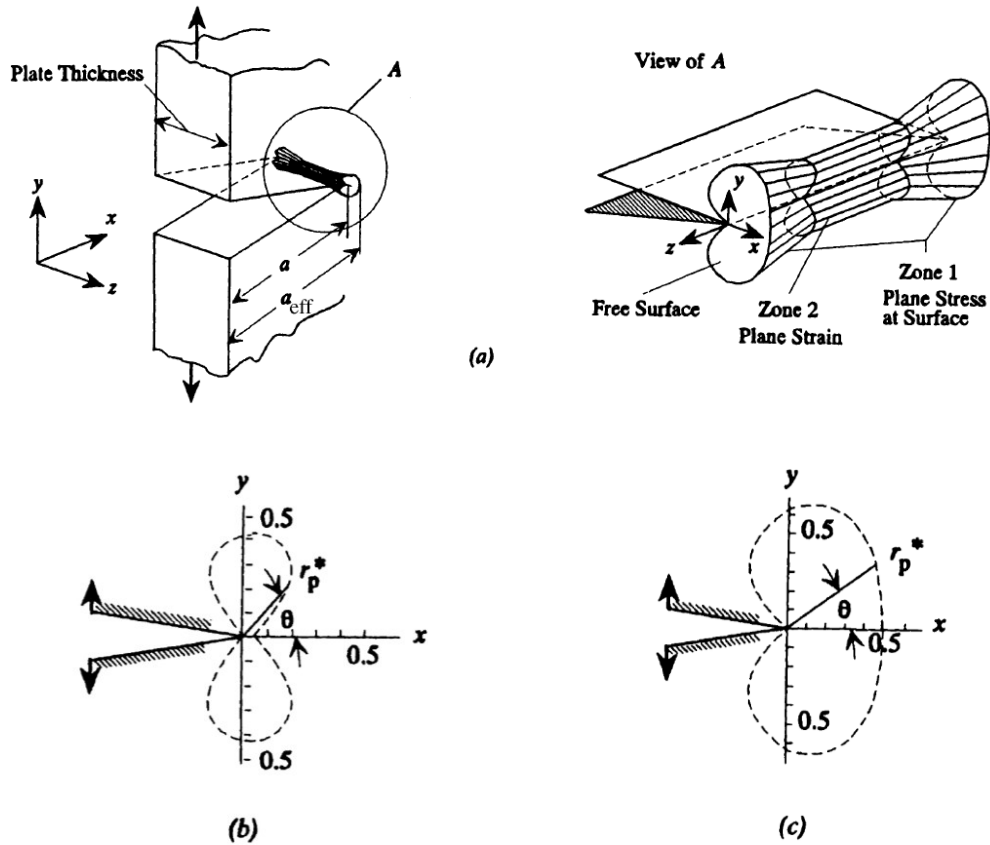
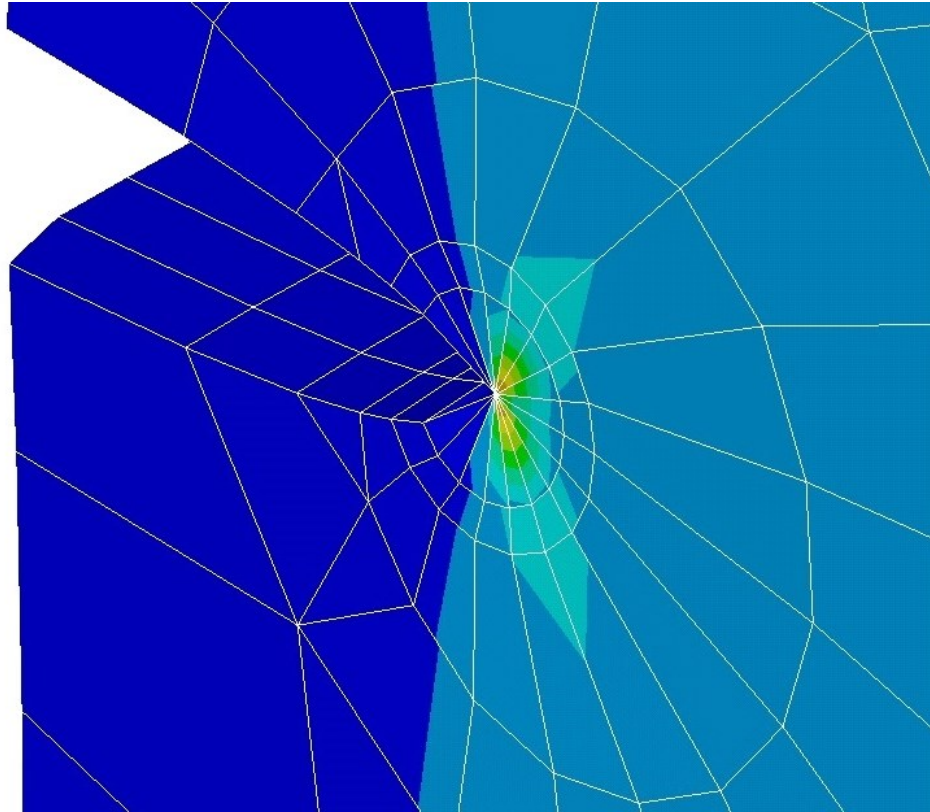


Figure 4.18 Crack zone for mode I loading (Pilkey, 2005)  
 (a) plastic zone at crack tip; (b) plane strain state; (c) plane stress state

When considering the plate thickness, the crack zone can be identified as two different zones along the plate thickness. The first zone is at the free surface,  $\sigma_z = 0$ , where the plane stress state exists. The second zone occurs midway through the plate thickness, where the strain is constrained and plane strain exists.

Figure 4.18 displays the plastic zone at the crack tip for a through thickness crack, where  $a$  represents the original crack length and  $a_{eff}$  is the effective crack length, i.e. accounts for the plasticity zone beyond the actual crack tip. If the size of the plastic zone (in  $x$  and  $y$  direction) is large, or within the magnitude of the plate thickness, then the crack can be modeled as plane stress. If the size of the plastic zone is much smaller than the plate thickness, the inner zone will dominate and the crack

can be considered in plane strain (Pilkey, 2005). For most cases, the plastic zone will be smaller than the plate thickness and plain strain will govern. Figure 4.19 displays the plane strain results around the crack tip for the geometry modeled in Figure 4.17.



**Figure 4.19 Elastic strain in the Y-direction at the crack tip**

After the FEM analysis, the stress intensity factor for mode I is computed to be  $K_I^{ANSYS} = 26.195 \text{ MPa} \sqrt{m}$ . Figure 4.20 displays the ANSYS dialogue box for the computed stress intensity factors. This result is compared to the analytical solution for verification. The error between the two methods can be computed as:

$$\epsilon = \frac{K_I^{ANSYS} - K_I^{Calc}}{K_I^{Calc}} = \frac{26.195 - 25.680}{25.680} = 2.005\% \quad (\text{Equation 4.20})$$

The stress intensity factor for a mode I crack once again is close to the actual value with only 2.005% error.

```

**** CALCULATE MIXED-MODE STRESS INTENSITY FACTORS ****
ASSUME PLANE STRAIN CONDITIONS
ASSUME A FULL-CRACK MODEL <USE 5 NODES>
EXTRAPOLATION PATH IS DEFINED BY NODES:      20      18      16      36      34
WITH NODE      20 AS THE CRACK-TIP NODE
USE MATERIAL PROPERTIES FOR MATERIAL NUMBER      1
EX =      0.20000E+06      NUXY =      0.30000      AT TEMP =      0.0000
**** KI =      26.195      ,      KII =      0.13678      ,      KIII =      0.34617E-14 ****

```

Figure 4.20 SIF results of the FEM analysis on full crack model with 3D geometry

#### 4.5 Crack Growth Models and AE sensors

Fatigue cracks typically grow intermittently and the ability to track this change using non-destructive evaluation (NDE) technologies can be a practical piece of information for structural engineers (Haldipur, et al., 2010). Acoustic emission (AE) sensors, which are a type of NDE technology, have been used to monitor fatigue crack propagation; a well-known source of acoustic emission. AE sensors are used for real time monitoring of defect formations and failures of structural materials. Under loading conditions, materials experience internal stress distributions within their internal structure and emit energy in the form of elastic waves (Huang, et al., 1998). These waves, which can be thought of as a “naturally generated ultrasound” are picked up by AE sensors attached to the surface of the material (NDT Resource Center, 2012). Mainstream AE sensors are designed implemented only on flat surfaces of the material. In order to determine the location AE event source, simple geometry can be used with the difference in the arrival times from the recorded AE events. However, it

has more recently been shown that piezoelectric film sensors (a type of AE sensor) offer the benefit of adaptability to eccentrically shaped surfaces, including being applied directly onto a weld (Zhou, 2013).

The frequency of acoustic emission waves may range from tens of kHz to tens of MHz, depending on their source. Within this broad spectrum of frequencies lies the captured waveform that represents the internal stress distributions from crack growth or other spurious sources of acoustic emission, e.g. friction between crack surfaces. Nonetheless, when crack-related AE signals are isolated from other sources of acoustic emission, then the information extracted from the signals can be used to monitor crack growth (Rabiei, 2011).

In order to capture only the relevant signals related to crack growth, data acquisition systems are set to only record AE amplitudes that rise above a predefined threshold value. Figure 4.21 shows a burst AE signal and the commonly used parameters of AE techniques. When the AE sensor receives a signal above the threshold limit than an AE event is captured and stored. The number of times the AE signal passes the established threshold is the count of the AE event, known as the AE count.

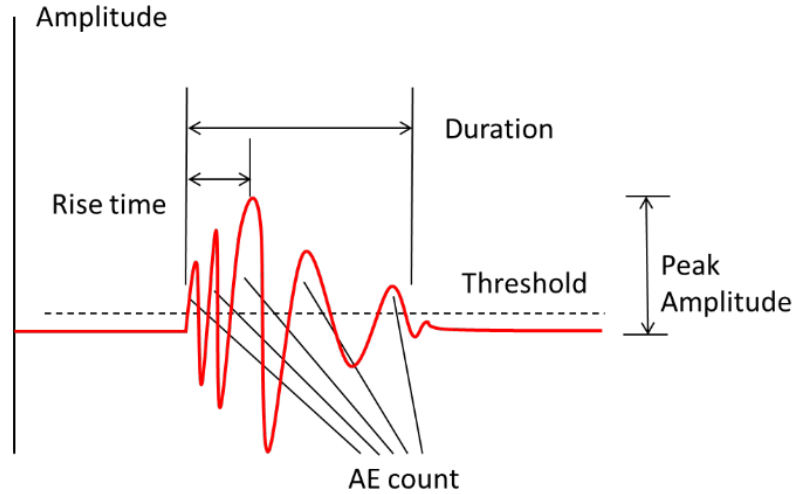


**Figure 4.21 AE signal with labeled parameters (Zhou, 2013)**

Certain features of acoustic emission signals are stochastically correlated with crack growth model variables, such as stress intensity factor,  $\Delta K$ , and crack growth rate  $da/dN$ . Two of the more commonly used AE parameters that are associated with crack growth are the AE count,  $c$ , and its derivative, count rate,  $dc/dN$  (Rabiei, 2011). The following formulation is proposed for the relationship between the AE count rate,  $dc/dN$  and the stress intensity factor,  $\Delta K$  (Bassim, et al., 1994):

$$\frac{dc}{dN} = A_1(\Delta K)^{A_2} \quad (\text{Equation 4.21})$$

Where  $c$  is defined as the number of times that a signal amplitude exceeds a predefined threshold value, and  $A_1$  and  $A_2$  are the model parameters and mainly depend on material properties. Rearranging this equation and solving for  $\Delta K$ :

$$\Delta K = \frac{dc}{dN}^{1/A_2} A_1^{-1/A_2} \quad (\text{Equation 4.22})$$

Taking the log of both sides to yield a linear relationship between variables:

$$\log \Delta K = \alpha_1 \log \left( \frac{dc}{dN} \right) + \alpha_2 \quad (\text{Equation 4.23})$$

Where  $\alpha_1 = A_1^{-1/A_2}$  and  $\alpha_2 = 1/A_2$  are the new model constants to be determined experimentally from data. Thus, Equation 4.23 uses data from AE sensors to estimate and solve for the stress intensity factor, the driving force in crack growth modeling.

The stress intensity factor displays the same log-linear behavior with the AE count rate,  $dc/dN$ , as it does with the crack growth,  $da/dN$ . Therefore, substituting Equation 4.23 into the Paris equation (Equation 4.4), gives the following relationship:

$$\log \frac{da}{dN} = \beta_1 \log \left( \frac{dc}{dN} \right) + \beta_2 \quad (\text{Equation 4.24})$$

Where  $\beta_1$  and  $\beta_2$  are the model parameters that describe the log-linear relationship between AE count rate and crack growth.

The estimation of  $\Delta K$  through the use of acoustic emission signals removes the need for complex modeling that is typically used in fracture mechanics to calculate stress intensity factors. These computations become especially difficult for 3-dimensional cases with curved crack fronts. While calculations are possible, extensive computer capacity and experience is often required. Nonetheless, the relationship between the AE events and crack growth rate means that the rate of crack growth can be estimated solely on features of the AE signals.

## 4.7 Crack Propagation Period Cumulative Damage

Prediction models are often used to obtain information about the crack growth. Models that predict fatigue crack growth propagation emphasize that crack growth is largely dependent on the cycle-by-cycle process. Thus, the accumulation of damage for fatigue crack growth models is consequent of the change in crack size,  $a$ , shown in Equation 4.25, where  $a_0$  is the initial crack size,  $\Delta a_i$  is the change in crack size per cycle, and  $a_n$  is the updated crack size (Schijve, 2009).

$$a_n = a_0 + \sum_{i=1}^{i=n} \Delta a_i \quad (\text{Equation 4.25})$$

Prediction models are referred to as interaction models and non-interaction models. Interaction effects imply that the crack growth rate in a particular cycle is also dependent on the load history of the preceding cycles, rather than an independent effect from one cycle. An interaction prediction model is more often used for assessment of fatigue crack growth under variable amplitude loads, where the cyclic load history may result in growth retardations and accelerations. Types of interaction effects include the sequence effects of loading cycles, the thickness effect of the material, and the effect of overload cycles. Fatigue testing that analyzes the consequences from interaction prediction models have shown that interaction effects more often result in crack growth retardations, as opposed to crack growth accelerations (Schijve, 2009).

A non-interaction prediction model is used if the interaction effects in the variable amplitude history are assumed to be absent. Since the type of material and the thickness of the material will be constant under regardless of the loading type, then

the basic crack growth data under constant amplitude load should still be representative for the conditions of the structure. Thus, a non-interaction crack growth prediction will then give a first indication about the possible duration of the crack growth period before complete failure. In a non-interaction model, crack growth in each cycle is assumed to be dependent on the severity of the current cycle only and not on the load history in the preceding cycles. It is expected that a non-interaction model will lead to a more conservative life prediction than models that account for interaction effects, considering interaction effects account for retardation in crack growth (Schijve, 2009). A non-interaction model can be used to provide quick and useful information about fatigue crack growth behavior, particularly crack growth rates.

The non-interaction prediction model leads to a simple numerical summation with Equation 4.25 and values  $\Delta a = da/dN$ , where stress ranges are obtained from variable amplitude tests and the stress intensity factor from finite element models. Thus, crack growth data is a function of  $K$  and the stress ratio effect  $R$  from the similarity principle.

$$\Delta a_i = f(\Delta K_i, R) \quad (\text{Equation 4.26})$$

where  $a_n$  is the crack length after  $n$  cycles,  $a_0$  is the initial crack length, and  $\Delta a_i$  is the crack extension  $\Delta a$  in cycle number  $i$ . The crack size at any given time is a function of the stress intensity factor, as portrayed in Equation 4.27,

$$a = \frac{K}{\pi\beta^2\sigma^2} \quad (\text{Equation 4.27})$$

## 4.8 Remaining Useful Life – Crack Propagation Period

The remaining useful life is calculated by comparing the current crack size of a specimen to the critical crack size that defines failure of the crack propagation period. The critical crack size can be solved for using the value of the stress intensity factor at failure. This was found from the Charpy V-Notch Test, detailed in section 4.3.1 *Charpy V-Notch Test*. Therefore, the critical crack size results in,

$$a_{crit} = \frac{K_{IC}}{\pi\beta^2\sigma^2} \quad (\text{Equation 4.28})$$

The estimate for the fatigue-crack-propagation life is significantly influenced by the initial crack size and is less sensitive to the critical crack size. Assume  $a_{crit} = a_f$ , since the definition of the critical crack size is the crack size at failure. As shown in Figure 4.22, large changes in values  $a_f$  will result in small changes of  $N_f$  (Total Materia, 2015).

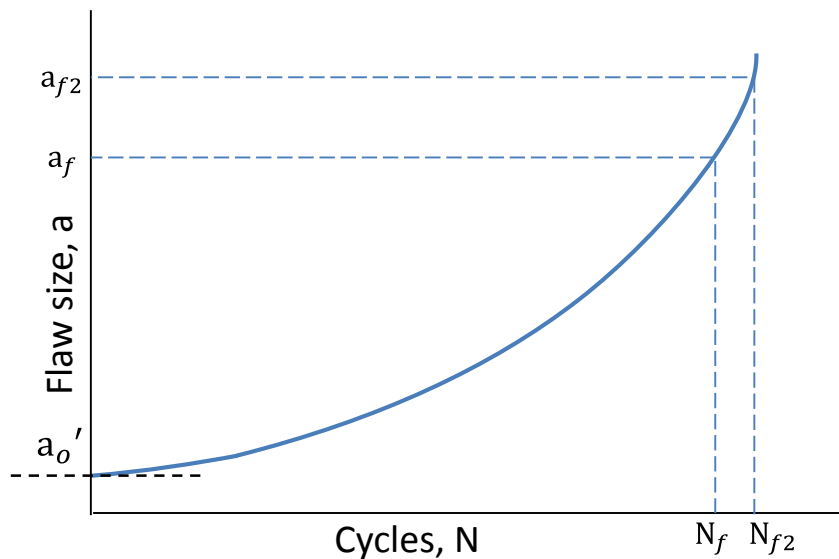


Figure 4.22 Propagation-life curve with final crack sizes

Using the initial crack size and the critical crack size, the crack growth equation, Equation 4.4, can be rearranged to solve for the number of cycles to failure  $N_f$ .

$$N_f = \int_{a_0}^{a_{crit}} \frac{da}{C(S_{reff}\beta\sqrt{\pi a})^m} \quad (\text{Equation 4.29})$$

Equation 4.29 after integration yields,

$$N_f = \frac{a_{crit}^{1-\frac{m}{2}} - a_0^{1-\frac{m}{2}}}{C \left(1 - \frac{m}{2}\right) (S_{reff}\beta\sqrt{\pi})^m} \quad (\text{Equation 4.30})$$

The crack size, after any amount of stress cycles,  $N$ , can be solved for with the following,

$$a_n = \left( NC \left(1 - \frac{m}{2}\right) \left(\sigma\beta\sqrt{\frac{\pi}{2}}\right)^m + a_0^{1-\frac{m}{2}} \right)^{\frac{2}{2-m}} \quad (\text{Equation 4.31})$$

Thus the cumulative damage from the fatigue crack propagation life is written as a percentage of the fatigue life by dividing the current crack size,  $a_n$ , by the critical crack size at failure,  $a_{crit}$ .

$$d_{propagation} = a_n/a_{crit} \quad (\text{Equation 4.32})$$

The remaining useful life is calculated by subtracting the initial crack size,  $a$ , from the critical crack size at failure that corresponds to the critical crack size at failure. Dividing by the change in crack size using an effective stress range and the number of cycles,  $N_e$ , solves the remaining useful life of the structure in terms of *years*,

$$RUL_{propagation} = \frac{a_{crit} - a}{a_i} \text{ years} \quad (\text{Equation 4.33})$$

## **Chapter Five: System Failure due to Fatigue**

The design of a steel bridge can potentially increase the susceptibility to fatigue damage and ultimately affect an inspector's assessment of the damage. Specifically, aspects of the bridge design that influence damage include: the bridge geometry and the configuration of the bridge components. The configuration of bridge components is crucial to properly distributing the applied loads throughout the structure in order to maintain its durability. Along with the configuration of these components, special scrutiny should be given to transverse members, i.e. the vertical steel plates that are welded to the longitudinal members and are used to either stiffen the longitudinal members or used as connection plates to cross braces. Further, the structural details that are used to combine structural members are considered hot spots for fatigue damage. Using the damage estimations for fatigue prone details in Chapter 3 and the fracture mechanics analyses in Chapter 4, these quantitative fatigue assessments can be structured into bridge management systems.

### **5.1 Geometry of the Bridge**

Due to geometric constraints caused by intersecting roadways or the terrain of the construction site, a bridge may be built to accommodate these constraints. In some cases, the substructure supports are often set at a skew angle, seen in Figure 5.1. The skew angle is the angle between the centerline of a support and a line normal to the roadway centerline (AASHTO, 2012).

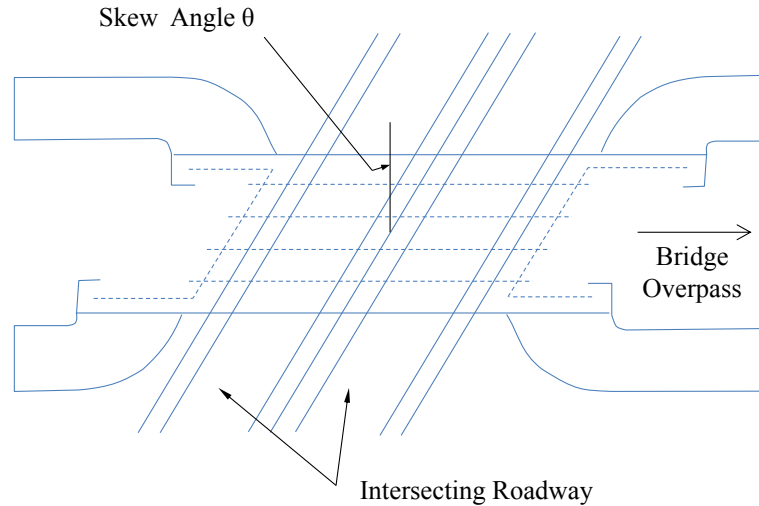


**Figure 5.1 Plan view of bridge with skewed supports (Helwig, et al., 2012)**

The cross braces on the bridge can be built to be parallel to the skewed abutment or built perpendicular to the girder lines. For skew angles greater than 20 degrees, AASHTO LRFD Bridge Design Specifications 2012 require the cross bracing to be built perpendicular to the girder line. Otherwise, for skew angles less than 20 degrees, cross braces can be built parallel to the skewed abutment. Actually, if the skewed cross frame is properly sized for the stiffness and strength requirements for the expected loading, then there is no technical reason why a cross frame cannot be oriented parallel to the skew for angles for angles larger than 20 degrees (Helwig, et al., 2012). Under these circumstances, the most important factor to consider is the length of the cross brace. As the skew angles become larger in size, the cross brace becomes longer in length, so the stiffness of the cross frame is affected by the skew.

Due to the geometry, the behavior of a bridge with skewed supports is more complicated than one with normal supports, because the skew angles increase the interaction between the steel girders and the braces. This interaction often results in large live load forces in the cross-frames or diaphragms, which can lead to fatigue

problems around the brace locations (Helwig, et al., 2012). Although, the skewed bracing creates a more susceptible location for fatigue damage, the severity of the fatigue damage is dependent on the details and connections that are used for the bracing.

## 5.2 Bridge Configuration

A bridge is designed to withstand an applied load over a certain period of time. The configuration of a bridge allows the transfer and distribution of applied loads from the superstructure components to the substructure components. For bridge inspectors the redundancy of bridge components plays an important role in evaluating the bridge condition, while nonredundant bridge configurations contain fracture-critical members.

### 5.2.1 Redundancy of Bridges

Redundancy in a bridge provides additional load paths or elements of support in order to maintain stability. The *FHWA Bridge Design Handbook 2012* puts together three types of redundancies that may exist on a bridge structure (Mertz, 2012). These classifications are found in Table 5.1.

**Table 5.1 Redundancy classifications (Fu, et al., 2014)**

<p><b>Load Path Redundancy</b></p>	<p>A member is considered load path redundant if an alternative and sufficient load path is determined to exist. Load path redundancy is the type of redundancy that designers consider when they count parallel girders or load paths. However, merely determining that alternate load paths exist is not enough. The alternative load paths must have sufficient capacity to carry the load redistributed to them from an adjacent failed member. If the additional redistributed load fails the alternative load path, progressive failure occurs, and the members could in fact, be fracture-critical. In determining the sufficiency of alternative load paths, all elements present (primary</p>
------------------------------------	--

	and secondary members) should be considered.
<b>Structural Redundancy</b>	A member is considered structurally redundant if its boundary conditions or supports are such that failure of the member merely changes the boundary or support conditions but does not result in the collapse of the superstructure. Again, the member with modified support conditions must be sufficient to carry loads in its new configuration. For example, the failure of the negative-moment region of a two span continuous girder is not critical to the survival of the superstructure if the positive-moment region is sufficient to carry the load as a simply supported girder.
<b>Internal Redundancy</b>	A member is considered internally redundant if alternative and sufficient load paths exist within the member itself such as the strands in a wire cable.

When fatigue cracks occurs in a known location a determination can be made about the consequences of the crack in terms of any of the three types of redundancy. However, the location of future cracks is unknown so it is impossible to be certain whether a future crack would be protected by a structural or internal redundancy (Sobanjo, et al., 2013). Bridge inspectors are concerned primarily with load path redundancy and can neglect structural and internal redundancy when identifying fracture-critical members.

### **5.2.1.1 Fracture-critical structures**

A fracture-critical structure is a structure that lacks alternative load paths, meaning the failure of a single primary load carrying member would interrupt the load flow causing other members to carry more load than which they were designed to withstand; resulting in the failure of the entire structure (Fu, et al., 2014). Of all bridge construction materials, only steel bridge members are designated as fracture-critical. A bridge is considered fracture-critical if it contains at least one fracture-critical member in tension or if portions of the flexural member are subject to tension

stress. A member is fracture-critical if its failure (brittle fracture) would cause a collapse of a bridge, i.e. at a minimum the bridge geometry would be rendered as unfit for use due to partial collapse or total bridge collapse (Sobanjo, et al., 2013). While most modern bridges are built with additional load paths to transfer loads in the event of bridge element failures (Sobanjo, et al., 2013), nearly 20,000 bridges currently in service in the United States are fracture-critical (Transportation for America, 2013). Of these 20,000 fracture-critical bridges, an Associated Press analysis found 7,800 have been ranked as structural deficient; a bridge in need of repair or replacement due to poor conditions (Lowy, et al., 2013). Most fracture-critical bridges were built around World War II and are nearing the end of their design life; if not having already surpassed it. Fracture-critical bridges often raise public concern because some of the worst bridge collapses in U.S. history happened on them, e.g. the collapse of the I-35W Bridge over the Mississippi River in 2007 and the collapse of the I-5 Skagit River Bridge in 2013. Due to the collapse of these bridges, further inspection requirements have been added to state agencies to assist with more stringent inspection. The primary difference between a fracture-critical member and a member that contains a fatigue prone detail is redundancy.

#### ***5.2.1.2 Determination of fracture-critical members***

Bridge plans and shop drawings for bridges designed after about 1980 are to have FCMs clearly identified (FHWA, 2012). For bridges built before 1980, it has been the responsibility of the inspector to determine which components are fracture-critical members. Thus, inspection reports from previous inspections are particularly useful in identifying specific locations that require special attention during an inspection. These

reports have chronological inspection records that include the date and type of inspection. The records should indicate the critical inspection findings relevant, but not limited, to: earthquake data, fracture-critical member information, deck evaluations, and corrosion studies when available (FHWA, 2012). In cases where a crack has been detected in previous inspections on a fracture-critical member, the location of the crack and fracture-critical members are clearly outlined in previous inspection reports to receive special attention (FHWA, 2012). Information from earlier inspections can be compared against current conditions to estimate rates of deterioration and to help determine the seriousness of the degradation and the anticipated remaining life of the structure.

In the event that fracture-critical members are not clearly identified then finite element methods can also be used to determine redundancy. A three-dimensional finite element structural analysis for fracture-criticality can be used to determine the exact consequences to the bridge if member fails (FHWA, 2012).

### ***5.2.1.3 Fracture-critical members in failure mechanics***

The primary members of a bridge are those necessary for the bridge to efficiently operate under normal operating conditions. Secondary members are additional components that may not be part of the main structural system. All primary bridge members are now required by *AASHTO Bridge Design Specifications 2012* to have a minimum level of fracture toughness. The Charpy V-notch test, discussed in chapter 4, provides an acceptable measure of fracture toughness. Charpy V-notch testing is required for all primary longitudinal superstructure components and connections sustaining tensile stress (AASHTO, 2012). These primary components are classified

as either fracture-critical or non-fracture-critical. Due to the sensitivity of fracture-critical members, they are required to have higher levels of fracture toughness compared to the non-fracture-critical members. Table 5.2 and Table 5.3 display the Charpy V-notch requirements for the appropriate temperature zones.

**Table 5.2 AASHTO CVN impact energy requirements for fracture-critical members**

Grade (Y.P./Y.S.)	Thickness (in.)	Fracture-Critical			
		Min. Test Value Energy (ft-lbs.)	Zone 1 (ft-lbs. @ °F)	Zone 2 (ft-lbs. @ °F)	Zone 3 (ft-lbs. @ °F)
36	$t \leq 4$	20	25 @ 70	25 @ 40	25 @ 10
50/50S/50W	$t \leq 2$	20	25 @ 70	25 @ 40	25 @ 10
	$2 < t \leq 4$	24	30 @ 70	30 @ 40	30 @ 10
HPS 50W	$t \leq 4$	24	30 @ 10	30 @ 10	30 @ 10
HPS 70W	$t \leq 4$	28	35 @ -10	35 @ -10	35 @ -10
HPS 100W	$t \leq 2-1/2$	28	35 @ -30	35 @ -30	35 @ -30
	$2-1/2 < t \leq 4$	36	not permitted	not permitted	not permitted

**Table 5.3 AASHTO CVN impact energy requirements for nonfracture-critical members**

Grade (Y.P./Y.S.)	Thickness (in.)	Nonfracture-Critical		
		Zone 1 (ft-lbs. @ °F)	Zone 2 (ft-lbs. @ °F)	Zone 3 (ft-lbs. @ °F)
36	$t \leq 4$	15 @ 70	15 @ 40	15 @ 10
50/50S/50W	$t \leq 2$	15 @ 70	15 @ 40	15 @ 10
	$2 < t \leq 4$	20 @ 70	20 @ 40	20 @ 10
HPS 50W	$t \leq 4$	20 @ 10	20 @ 10	20 @ 10
HPS 70W	$t \leq 4$	25 @ -10	25 @ -10	25 @ -10
HPS 100W	$t \leq 2-1/2$	25 @ -30	25 @ -30	25 @ -30
	$2-1/2 < t \leq 4$	35 @ -30	35 @ -30	35 @ -30

#### **5.2.1.4 Evaluating Fracture-critical Members and Fatigue Prone Details**

Fatigue prone details can be located on fracture-critical members, but not all members that have fatigue prone details are fracture-critical. If a redundant steel

member is in tension and contains at least one of the accepted fatigue sensitive details, it can be classified as Fatigue Prone (Oregon DOT, 1996). If a steel member is a non-redundant tension member, it is classified as a fracture-critical member.

### **5.2.2 Distortion-Induced Fatigue**

There are two types of fatigue cases in steel bridges: load-induced fatigue and distortion-induced fatigue. Until this section, the fatigue assessments described in chapter three have been for the case of load-induced fatigue. Load-induced fatigue is the fatigue damage on a bridge detail caused from the directly repeated cyclic live load stress ranges. Normally, load-induced fatigue occurs in main members of the steel bridge because of relatively high stress ranges, or fatigue-prone details with large weld defects. Load-induced fatigue is normally caused by global and in-plane stress ranges and prevention against fatigue is controlled by the stress ranges at the specific detail (Chen, et al., 2014).

Distortion-induced fatigue, also known as secondary-stress-induced fatigue is caused from local relative distortion between bridge members and attached elements. Distortion-induced fatigue often occurs at the gap between a girder top flange and the connection plate for a cross-frame where a continuous load path is interrupted and cannot properly transmit forces from the connection plate to the flange. Figure 5.2 provides an illustration of a connection plate that is welded to the web of the girder and not connected to the top flange. A floor beam is attached to the connection plate with a bolted connection. For this illustration, distortion-induced fatigue will occur under the passage of traffic when the floor beam begins to rotate as shown. Under this rotation, the bottom flange of the floor beam lengthens under tension and the top

flange shortens under compression. Lengthening of the bottom flange will not be restrained because it is pushing into the web of the girder, which is ductile enough withstand some flexibility. Since the top flange of the girder is restrained by the deck slab, the shortening of the top flange can only be accommodated by deformation within the gap at the top of the connection plate. This deformation is also shown in Figure 5.2, with the label, “Detail at gap.” For this situation, studies have shown that fatigue cracks could develop either at the weld at the top of the connection plate or at the web-to-flange fillet weld at the girder, or both (Mertz, 2012). Cracks caused by out of plane distortion are not covered in AASHTO fatigue categories A – E’ (FHWA, 2012).

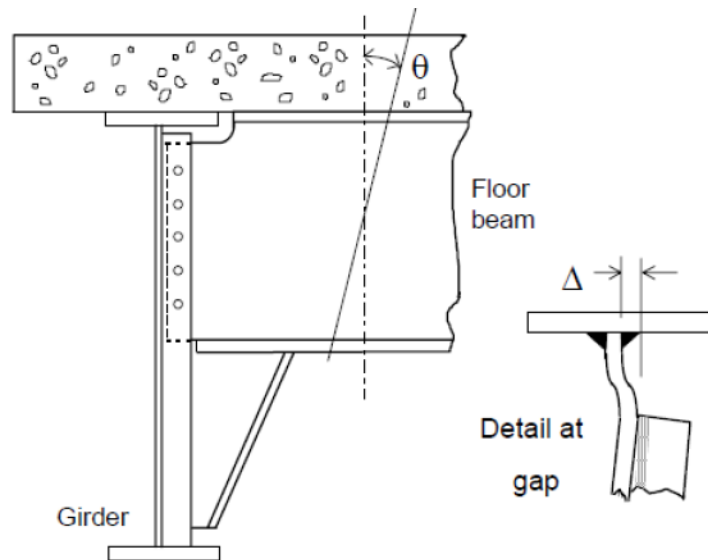


**Figure 5.2 Distortion induced fatigue at floor beam-to-girder connection (Mertz, 2012)**

Cutting the transverse stiffeners short of the flange was standard practice for many years. The purpose was to eliminate welds on the flange that would be perpendicular to the direction of the stress; a hotspot for fatigue damage. However, data in the last 20 years has shown that the fatigue life of the detail is independent on

whether the stiffener terminates in the web or is extended down to the flange. According to *AASHTO LRFD Bridge Design Specifications 2012*, connection plates should be welded or bolted to both the compression and tension flanges of the cross-section where “connection diaphragms or cross-frames are attached to transverse connection plates or to transverse stiffeners function as connection plates” (AASHTO, 2012). While distortion-induced fatigue will be eliminated by design in modern bridges, it should be on the radar for inspectors who are looking for fatigue damage on steel bridges.

### **5.3 Damage Prognosis of Fatigue Life**

Damage prognosis is the estimate of a system’s remaining useful life. Chapter 3 and Chapter 4 presented the damage accumulation models that result in the damage prognoses for the fatigue-crack initiation life and fatigue-crack propagation life, respectively. For structures with existing cracks, these damage accumulation models are not exclusive to each other, but actually link together to form a complete fatigue life-damage prognosis. Thus, for structural elements in question, a fatigue-damage prognosis can be computed for its entire fatigue life. Figure 5.3 displays the various aspects of fatigue analyses that are considered in the derivation of a fatigue-damage prognosis.

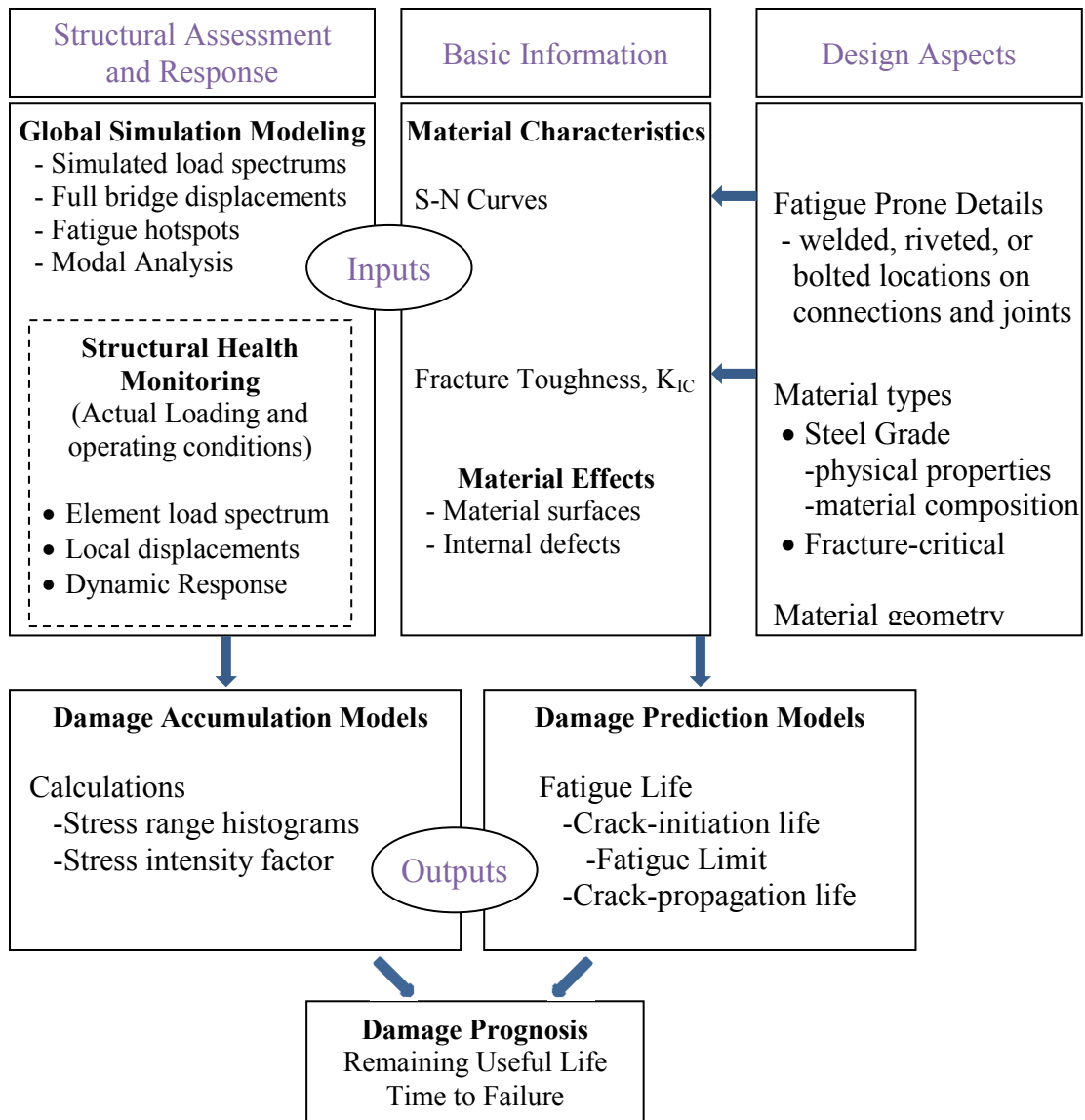


**Figure 5.3 Fatigue damage prognosis with structural health monitoring**

The damage prognosis is based on the output of damage accumulation models, which are compared with the outputs from damage prediction models. Damage accumulation models are created by coupling information from simulation modeling and structural health monitoring. Likewise, damage prediction models are created by coupling material property information with the construction and design of the structural element. Therefore, a complete damage prognosis attempts to forecast system performance by measuring the current state of the system, estimating future

loads for that system and ultimately determining the remaining useful life of the system (Farrar, et al., 2003).

#### 5.4 Integration of Damage Prognosis with Condition States

State Departments of Transportation (DOTs) report their bridge inspection findings using AASHTO Pontis software, which poses the guidelines for capturing damage of bridge elements. As discussed heavily in Chapter Two, the conditions of bridge elements are categorized into element condition states to reflect these damages. The AASHTO Pontis software is most useful for state DOTs, since it provides an internal tool for mapping the element condition states back into the national condition ratings; federal law requires all states are required to report the condition of their bridges in terms of the national bridge condition ratings. The AASHTO Pontis system considers fatigue damage as a Commonly Recognized Elements (CoRe). Fatigue damage as an AASHTO CoRe is translated into the national bridge management element (NBE), as displayed in Figure 5.4

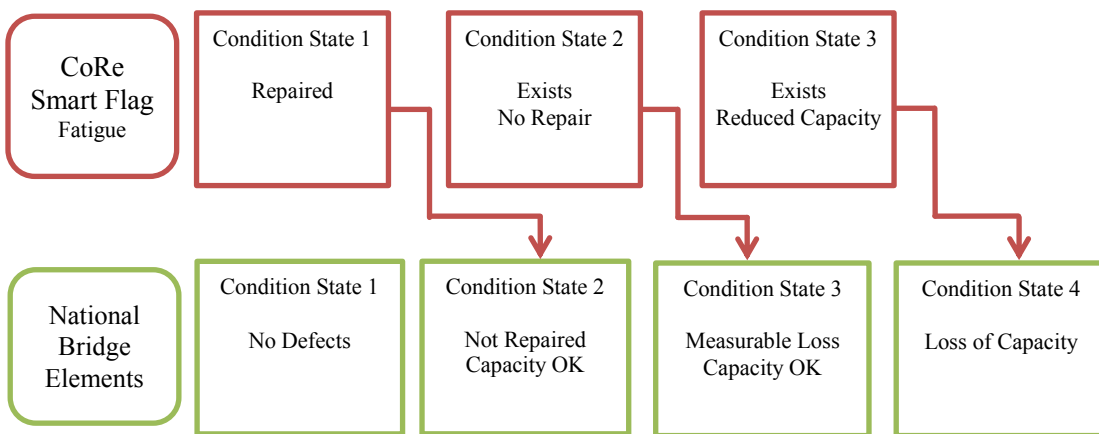


Figure 5.4 CoRe fatigue elements mapped into national bridge elements

After the translation of the fatigue smart flags into the national bridge element condition states, a more intricate description fatigue damage at each condition state is established, as seen in Table 5.4.

**Table 5.4 Fatigue condition states translated into national bridge element (MDSHA, 2003)**

<b>Defect</b>	<b>Condition State 1 (good)</b>	<b>Condition State 2 (fair)</b>	<b>Condition State 3 (poor)</b>	<b>Condition State 4 (severe)</b>
Cracking/ Fatigue	None	<b>Fatigue Damage</b>	<b>Analysis Warranted</b>	<b>Severe Fatigue Damage</b>
		Fatigue damage exists but has been repaired or arrested. The element may still be fatigue prone.	Fatigue damage exists which is not arrested. Condition State used for first time element is identified with crack	Fatigue damage exists which warrants analysis of the element to ascertain the serviceability of the element or bridge

The condition states in Table 5.4 can be used with the fatigue life curve in order to gather quantitative information of the fatigue life. An element in condition state one (CS1) is considered a new element or in “like new” condition; it has no fatigue damage present. This element falls within the early stages of the crack life-initiation period. Condition state two (CS2) recognizes fatigue damage. This damage could be found from a stress-cycle analysis that showed the structure was nearing the end of the crack initiation life or could be the result of a visual inspection from of a small crack that is considered by inspectors to not be in immediate need of repair. An element in condition state two will be approaching the critical crack size of the crack initiation period and is merging into the crack propagation period. Thus fatigue damage in condition state three (CS3) is midway through the propagation life. Condition state three explicitly calls for additional analyses. In many state DOT’s, it is suggested that

deterioration modeling be used for fatigue damage in order to assess the damage and evaluate the probability of transitioning from condition states (MDSHA, 2003). A stress-cycle history can be used to obtain information about the daily or yearly cycle count and stress ranges on the structure. In the even there is enough information about the crack, crack growth models can be used to obtain information about the crack growth rate. This is particularly important information to obtain if the fatigue damage is on a primary component of the structure. Finally, an element in condition state four (CS4) is in need of immediate rehabilitation or replacement. Analysis should still be used to understand the problem with this section of the bridge in order to make appropriate changes and to increase the bridge life.

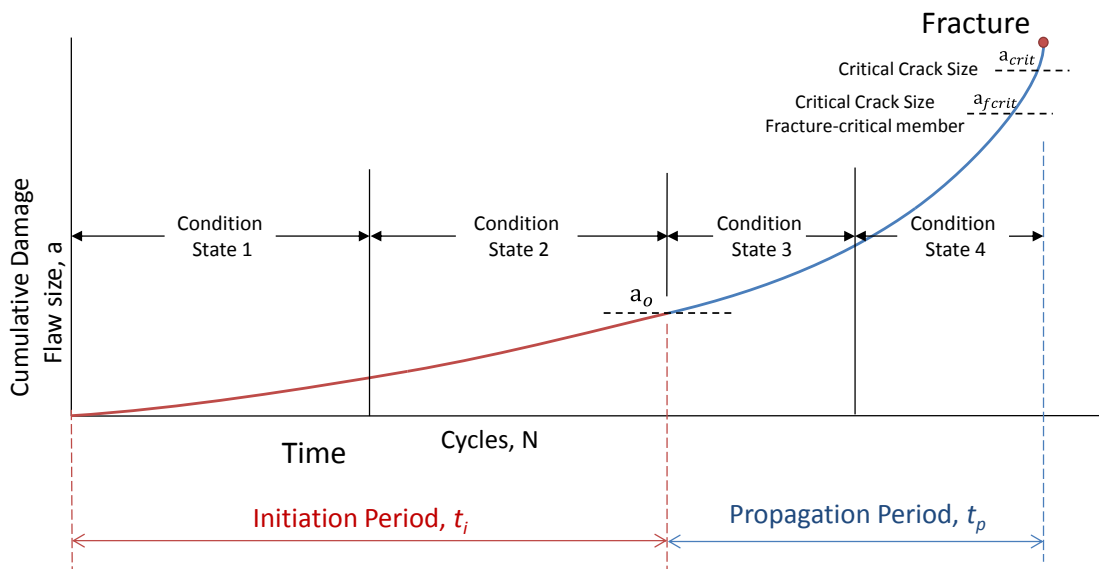


**Figure 5.5 BME condition states integrated into fatigue life curve**

A description of the national bridge element condition states are described in Table 5.4 and is used in parallel with Table 5.5, which hosts the commonly employed feasible actions that inspectors and state DOT's should take, given the condition state of their bridge. These feasible actions were put together by the FHWA Bridge

Preservation Guide, which provides a framework for a preventive maintenance program for bridge owners or agencies.

**Table 5.5 Actions associated with bridge element condition states (FHWA, 2011)**

Condition State 1	Condition State 2	Condition State 3	Condition State 4
Do Nothing	Preventive Maintenance	Rehabilitation	Rehabilitation or Replacement

#### 5.4.1 Calculation of Total Damage from Stress Cycles and Fracture

Recall from Equation 3.19, now rewritten in Equation 5.1, the cumulative damage for the crack initiation period,  $d_i$ , was assessed using Miner's rule with an effective stress range.

$$d_i = N_e / N_f \quad (\text{Equation 5.1})$$

From Equation 4.32, now rewritten in Equation 5.2, the cumulative damage for the crack propagation period,  $d_p$ , was assessed using Paris Law based on the stress intensity factor.

$$d_p = a / a_f \quad (\text{Equation 5.2})$$

The damage in the initiation period and the damage in the propagation period can be combined to assess the total cumulative fatigue damage on a specific component:

$$D_{Total} = \begin{cases} d_i, & N_e \leq N_f \\ d_i + d_p, & N_e > N_f \end{cases} \quad (\text{Equation 5.3})$$

where  $d_i$  is obtained from Equation 5.1 and  $d_p$  is obtained from Equation 5.2. However, each period does not occur over equal lengths of time. In order to more appropriately characterize the cumulative damage with the rate of damage, coefficients

$\alpha_I$  and  $\alpha_P$  can be used to represent the relative impact of the stress-cycle damage and crack growth damage, respectively.

$$D_{Total} = \begin{cases} \alpha_I d_i, & N_e \leq N_f \\ \alpha_I d_i + \alpha_P d_p, & N_e > N_f \end{cases} \quad (\text{Equation 5.4})$$

Testing data has shown that the fatigue life spends the majority of time in the crack initiation period. For instance, since  $d_i$  and  $d_p$  represent the amount of fatigue damage (% damage) at certain stages, a value of 0.70 for  $\alpha_I$  and a value of 0.30 for  $\alpha_P$  may approximate the proportion of  $d_i$  and  $d_p$ . These coefficients can be altered from the results of additional testing, in order to reflect the rate of damage. Altering these coefficients should not alter the condition state. Instead, altering the coefficient would mean altering the percentages for  $D_{Total}$ , shown in Table 5.6.

**Table 5.6 Mapping of damage calculations into condition states**

Condition State	$D_{Total}$	$D_{Total}, \%$
CS1	$0 \rightarrow \frac{1}{2} \alpha_i$	0→35%
CS2	$\frac{1}{2} \alpha_i \rightarrow \alpha_i$	35→70%
CS3	$\alpha_i \rightarrow \frac{1}{2} \alpha_p$	70→85%
CS4	$\frac{1}{2} \alpha_p \rightarrow (\alpha_i + \alpha_p)$	85→100%

## 5.5 Integration of Damage Prognosis into Federal Condition Ratings

In the paper, *Effect of Local Damage Caused by Overweight Trucks on the Durability of Steel Bridges*, that studied the durability of deteriorating steel bridge components, a finite element model was used to quantify the damage on bridge elements from traffic loads and environmental factors (Cha, et al., 2015). The total cumulative damage of the bridge was taken to be an average of the damage of each bridge element. To map the total cumulative damage with the condition ratings in the National Bridge Inventory, the following linear relationships was used:

$$D_{Average} = \frac{1}{N_{el}} \sum_{i=1}^{N_{el}} D_{total_i} = \kappa \left( \frac{9 - CR}{9 - 2} \right) \quad (\text{Equation 5.5})$$

where  $N_{el}$  is the total number of elements in the FE model and  $D_{total_i}$  is the total damage (loading and environmental) for the particular element and  $D_{Average}$  is the total cumulative damage index for the entire bridge. This relationship maps the NBI condition ratings, CR (9 for excellent down to 2 for extremely critical), into the scale for the damage index (0 for no damage to 1 for complete damage) with an appropriate factor of proportionality,  $\kappa$ . In accordance with the study, the proportionality factor was assigned a value of 0.7. This value was assigned after careful deliberation over what factor would constitute a realistic match between the observed damage in the FE model and the one reported by a bridge inspector (Cha, et al., 2015).

In a similar fashion, the damage accumulation from fatigue, Equation 5.3, can be mapped into the NBI condition ratings. A good way to see how the damage accumulation models should fit into the federal condition ratings is to look at the

“commonly employed feasible actions” put forth in the Bridge Preservation Guide. The feasible actions for the condition ratings are the same feasible actions for the condition states (Table 5.5). Therefore, it is useful to use the actions from the Bridge Preservation Guide to correlate the condition states with the condition ratings. A description of the condition ratings is provided in Table 2.2.

**Table 5.7 Actions associated with NBI condition ratings (FHWA, 2011)**

<b>Condition Ratings</b>	Condition Ratings 9,8,7	Condition Ratings 6,5	Condition Ratings 4,3,2,1
<b>Commonly Employed Feasible Actions</b>	Do Nothing Preventive Maintenance	Preventive Maintenance; and/or repairs	Rehabilitation or Replacement
<b>Condition States</b>	Condition State 1 & 2	Condition State 3	Condition State 4

## **Chapter Six: Validation of Fatigue-Damage Accumulation Model by Field Test and Data Processing**

The fatigue analysis in this paper was conducted as part of the University of Maryland project to design and implement an integrated structural health monitoring system that is particularly suited for fatigue detection on highway bridges. Data for the analyses was acquired from a highway bridge carrying traffic from interstate 270 (I-270) over Middlebrook Road in Germantown, MD, seen in Figure 6.1. This bridge is referred to as the Middlebrook Bridge.



**Figure 6.1 Maryland bridge carrying I-270 over Middlebrook Road**

The Middlebrook Road Bridge was built in 1980 and at the time of testing the bridge was 32 years old. With help from Maryland bridge inspectors, this bridge was selected as a good candidate for fatigue monitoring due to the average daily truck traffic, the bridge's maintenance history, the geometric configuration, and the identification of existing fatigue cracks on the connection plates.

The Middlebrook Bridge is a composite steel I-girder bridge consisting of 17 welded steel plate girders with a span length of 140 ft. The bridge has three traffic lanes in the southbound roadway and five traffic lanes in the northbound; i.e. a high occupancy vehicle lane, an exit lane, and three travel lanes. Five fatigue cracks were reported in the Maryland State Highway June 2011 Bridge Inspection Report. These five cracks were all found in the welded connections between the lower end of the cross brace connection plate and the girder bottom flange. The framing plan in Figure 6.2 shows the five identified crack locations. All are in the Southbound Roadway and are near the center of the simple span; where the largest deflection will take place.

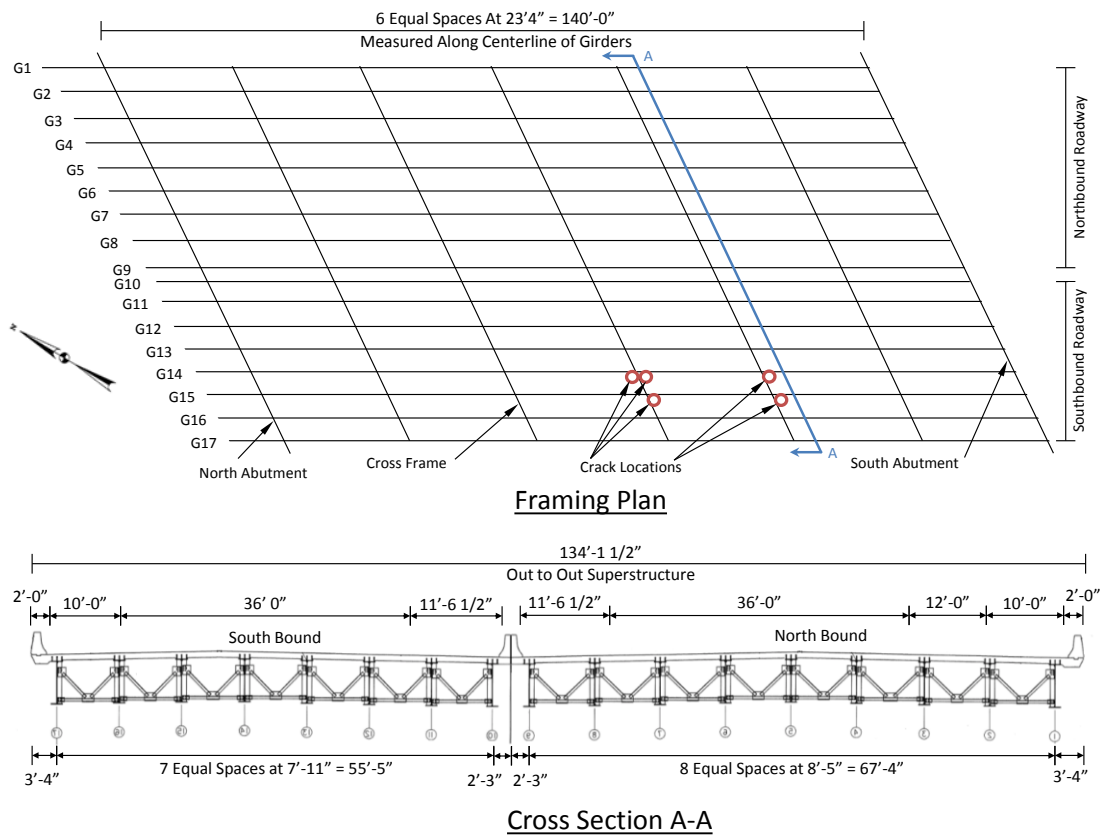


**Figure 6.2 I-270 Bridge framing plan and cross section**

The I-270 Bridge is built with skewed supports, in order to accommodate the intersecting roadway, Middlebrook Road, below the bridge. Due to the skewed

supports, the corresponding cross frames are also built with skewed angles. The Middlebrook Bridge was built with K-brace cross frame, seen in Figure 6.3.



**Figure 6.3 K-type cross brace on Middlebrook Bridge**

The skew angle of the cross frames are built to code and are in accordance with AASHTO LRFD Bridge Design Specifications 2012; so long as the skew angle is less than 20 degrees. As previously mentioned in section *5.1 Geometry of the Bridge*, a bridge with skewed cross braces is more prone to fatigue damages because its geometric configuration enhances the live load effects. The connections of the skewed cross braces are bent at an angle in order to connect with the transverse stiffeners of the bridge girders. When the bridge girders deflect, this angle introduces a bending effect into the transverse stiffeners. The load direction on the connection plates is illustrated in Figure 6.4.

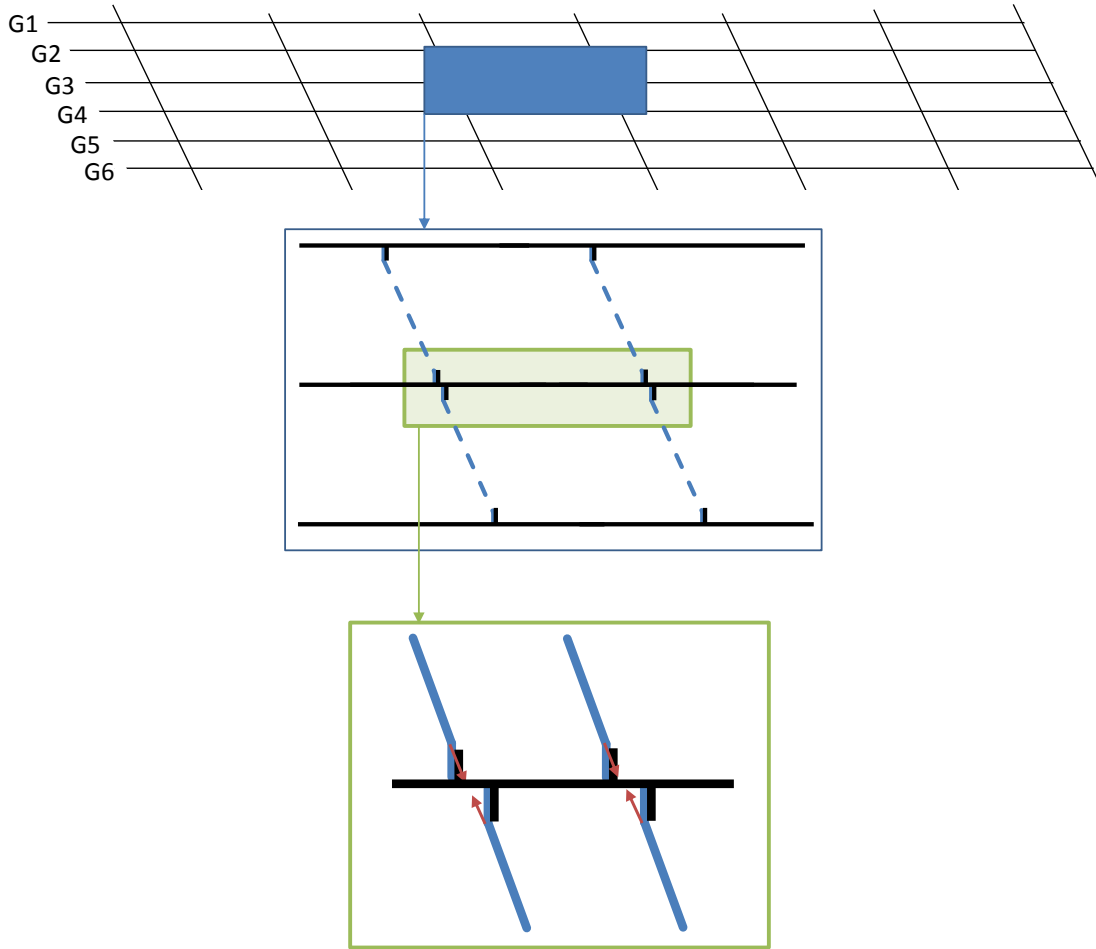


**Figure 6.4 Magnified plan view of cross frame and angle of attachment**

## **6.1 Structural Health Monitoring**

The monitoring and testing for this project was done in part of a larger project: to develop an integrated structural health monitoring system (ISHM) to monitor the health of steel highway bridges. For this project, the goal of an ISHM system was to specifically integrate various technologies and sensing instrumentation that are used for fatigue monitoring, i.e. crack detection and crack growth. This instrumentation provides condition-based feedback of a structures response to various loadings, which can ultimately reduce uncertainties in bridge health conditions. An ISHM requires proper selection of sensor types, the correct number of sensors, sensor locations, and a

suitable data acquisition (DAQ) system that meets the data management demands. Pilot testing as performed using acoustic emission (AE) sensors, accelerometers, displacement sensors and strain sensors for bridge information collection.

## **6.2 Data Acquisition Selection**

The selected DAQ system was configured to meet the requirements of the ISHM system; to read and record data from strain gauges as well as acoustic emission sensors. The selection of the data acquisition system was primarily based on the hardware requirements of the AE sensors, which require a high sampling rate. To meet this requirement, National Instruments (NI) PXI-5105 Digitizer/Oscilloscope module was selected because of its high sampling rate of 60 MS/s and has the capability of recording eight simultaneously sampled channels (NI, 2010). The DAQ system was also composed of National Instruments PXIe-4330-bridge input module, which takes signals from bridge-based sensors or bridge circuits (strain gauges and string potentiometers) and converts the signals into a form the instrumentation can process. National Instrument's bridge input module has the capability of working with 8 channels, provides signal conditioning, contains internal analog-to-digital conversion and internal filters to remove noise (NI, 2011). To complete the DAQ, the PXI system functions from an embedded controller, which cuts out the need for an external PC. The embedded controller features the functionality of a typical PC, such as an integrated CPU, hard drive, memory, Ethernet, USB, video, serial (NI, 2012). The PXI system was a good fit for our application because during field testing it was necessary to have durable equipment and NI's PXI systems have previously undergone shockwave testing and have the ability to function in high temperatures.

### 6.2.1 Preliminary Monitoring

Short-term testing was done with the sensors to first gather some fundamental understanding of the structures local behavior. Axial strain gages were placed in the vertical direction on both sides of the connection plates, where cracks were previously detected by bridge inspectors. Figure 6.5 displays the relative location of the sensors in the plan view along with a cross section of the sensor locations, which defined by a circle. The circles with a bold (red) outline are the crack locations.

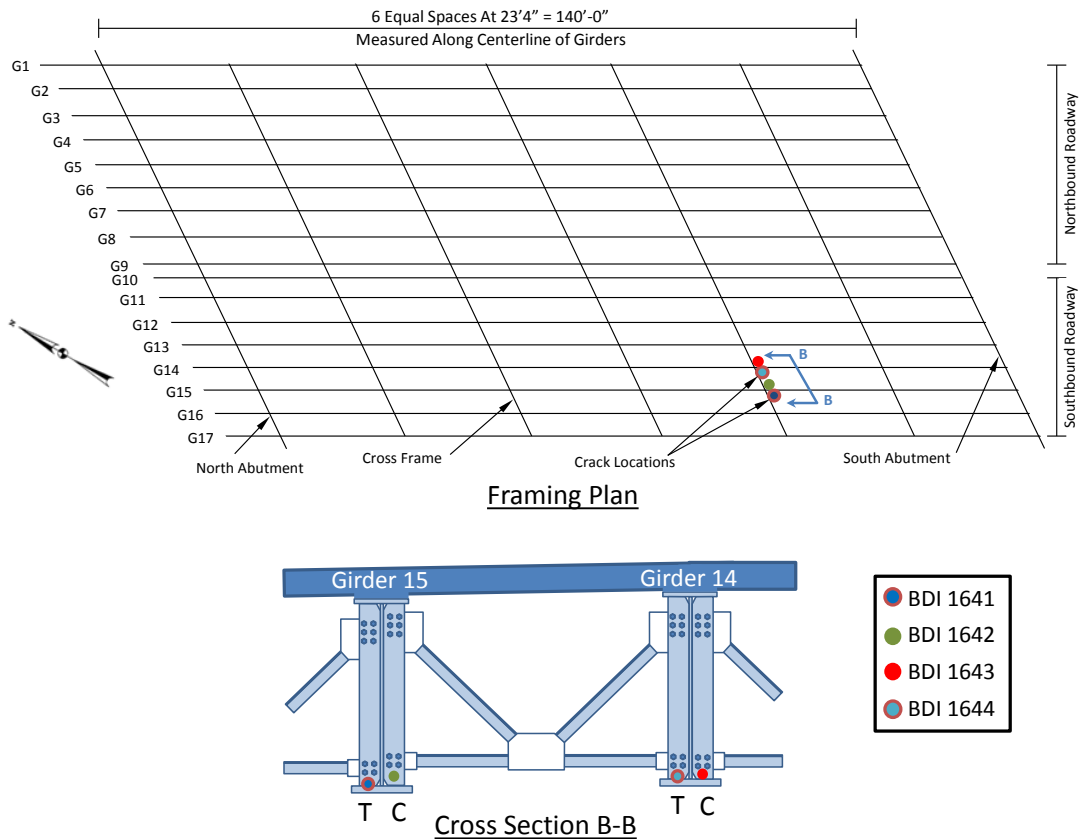


**Figure 6.5 Location of sensors for preliminary testing**

Figure 6.6 shows the recorded stresses corresponding to the crack locations. The color of the circle corresponds with the color of the recorded data. The data showed the maximum measured stress in the connection plates to be 16.1 ksi in tension for BDI 1641 on Girder 15 and 16.1 ksi in tension for Girder 14. In comparison, the

maximum stress measured on the connection plates on the opposite side measured -4.4 ksi in compression for Girder 15 and -3.9 ksi in compression for Girder 14. It is clear the cause of the crack is due to the high tension force that is experienced by the connection plate.

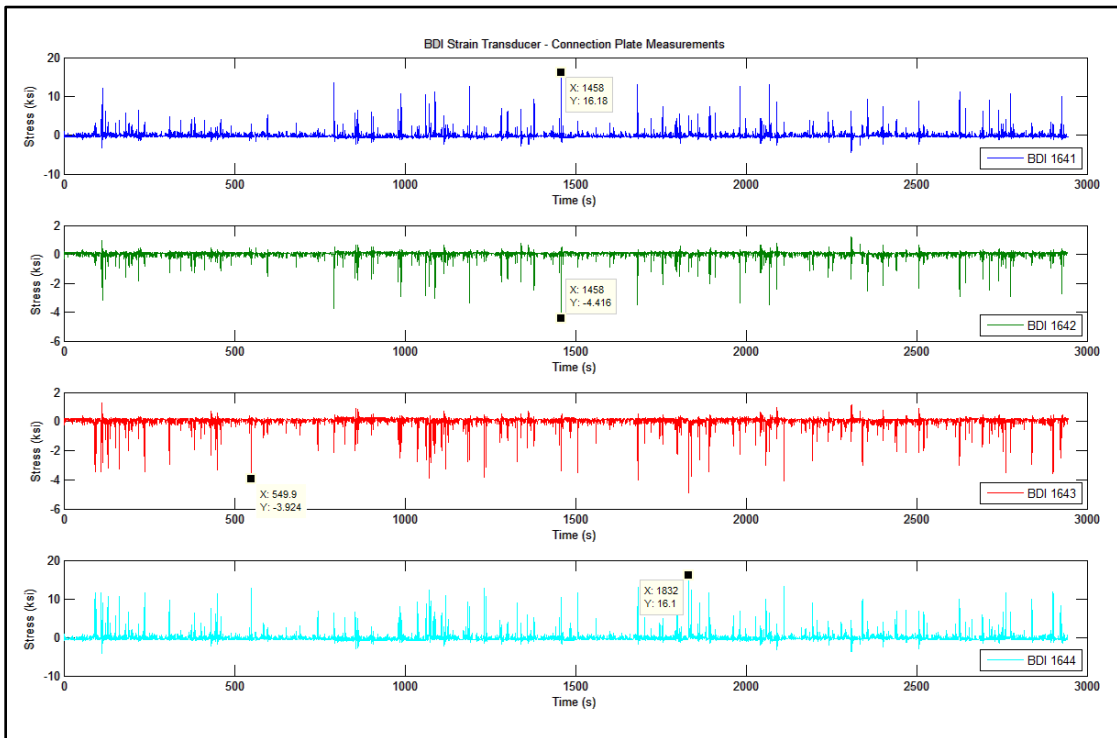


**Figure 6.6 Stress data on web stiffeners to illustrate compression and tension**

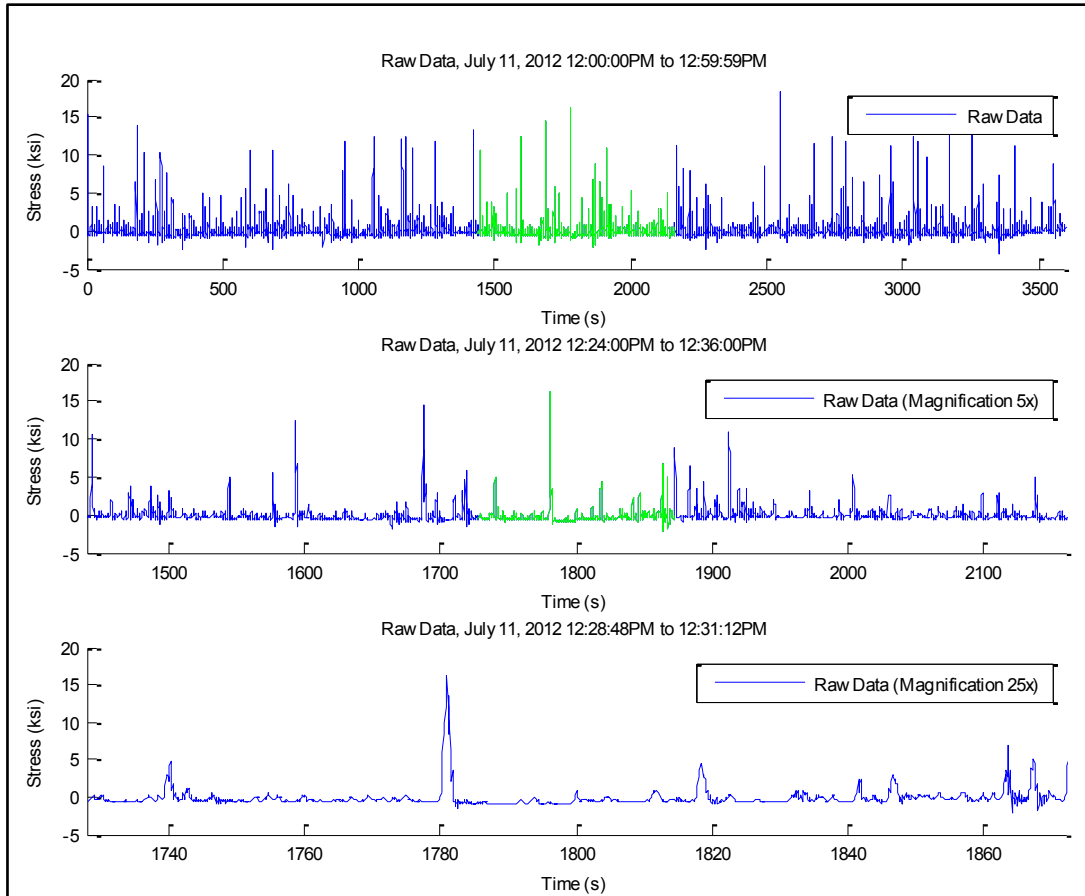
### 6.3 Long-Term Monitoring and Data Processing



**Figure 6.7 Connection plate with known crack Girder 15**

A connection plate of a steel girder highway bridge is considered for long-term monitoring, shown in Figure 6.7. This connection plate was identified from Maryland State Bridge inspectors to have an existing active crack, i.e. a crack that is growing in size. The crack was found in the weld that connects the connection plate to the top of the lower flange and was described in inspection reports as, "...very fine, crack in the top of the south side weld" (MDSHA, 2013).

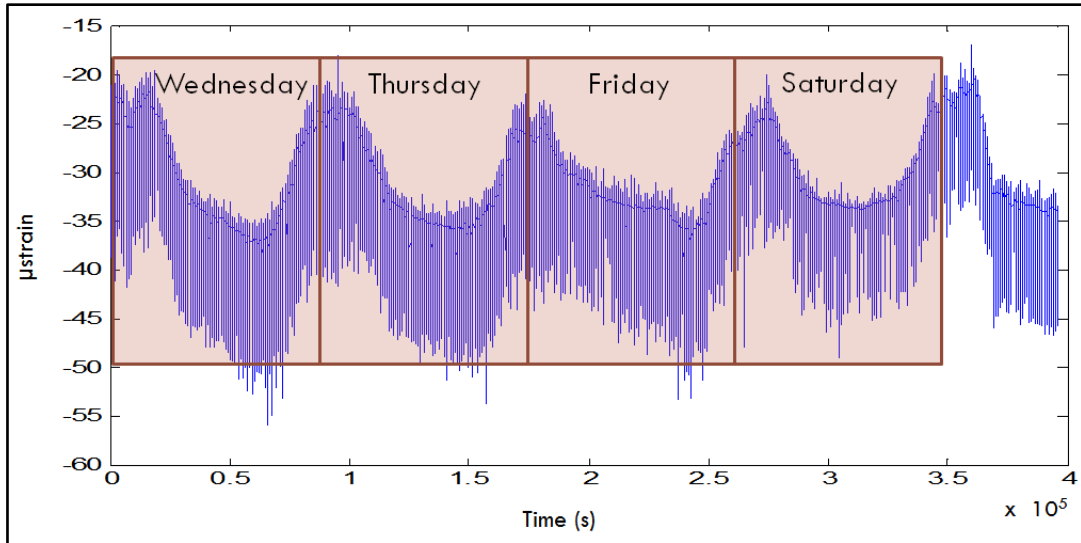




**Figure 6.9 Illustration of variable amplitude loading**

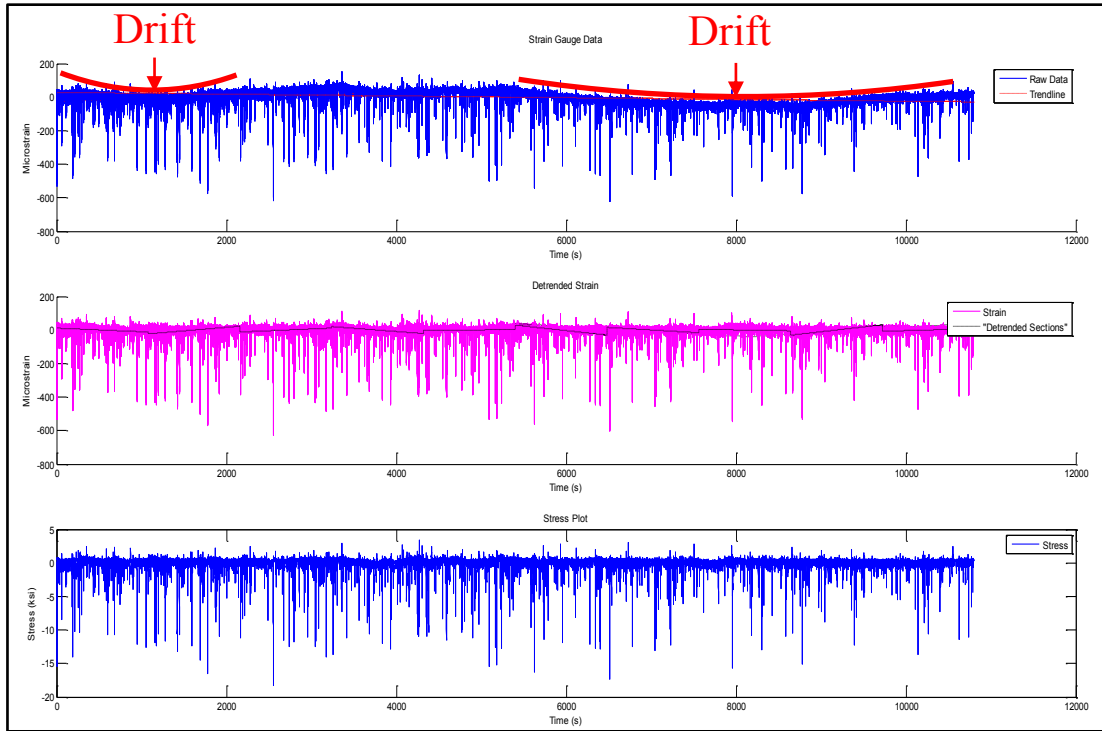
### 6.3.1 Data Detrending

Figure 6.10 shows 4.5 days of collected data where drift occurred in the data. Because the drift behaves the same way over the course of 24 hours, it is conceivable that it is the result of daily temperature fluctuation. This data can be detrended to remove the drift from the data. The process of detrending removes the linear best-fit line from the data. By removing the drift from the analysis, the fatigue analysis can concentrate on the variable amplitude fluctuations, which would otherwise be skewed from the drift.



**Figure 6.10 Illustration of drift that occurred in acquired data**

The process of data detrending is shown in Figure 6.11. The first plot displays raw strain data where there is a downward drift in the data that is visible at about 3000 seconds. This plot also displays the multiple linear trendlines where the acquired data is broken up into sections that are to be detrended. The second plot displays the strain data after it has been detrended. As the plot displays the drift is removed and the strain data more accurately represents the strain values the connection is experiencing. The last plot shows a conversion from strain to stress measurements. It is often helpful to convert strain measurements to stress; this is convenient for comparative purposes since units of stress are a more common way of representing fatigue data.



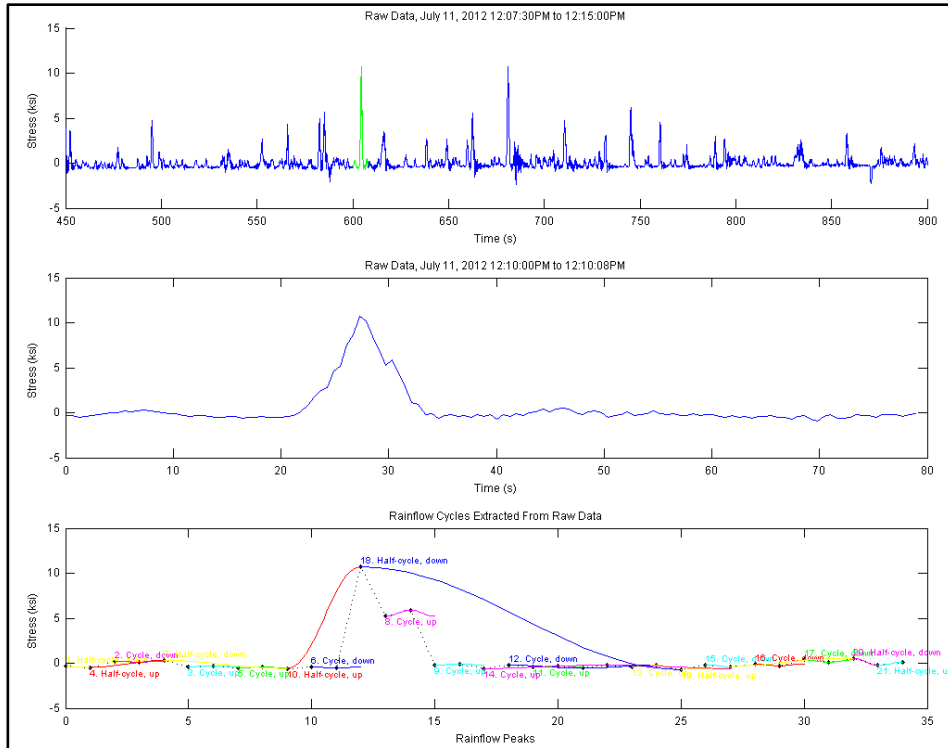
**Figure 6.11 Detrending on a segment of strain data**

## 6.4 Fatigue Analysis

After detrending, the strain data is converted to stress for linear damage accumulation models, where stress ranges are the main contribution to fatigue damage.

### 6.4.1 Rainflow Counting

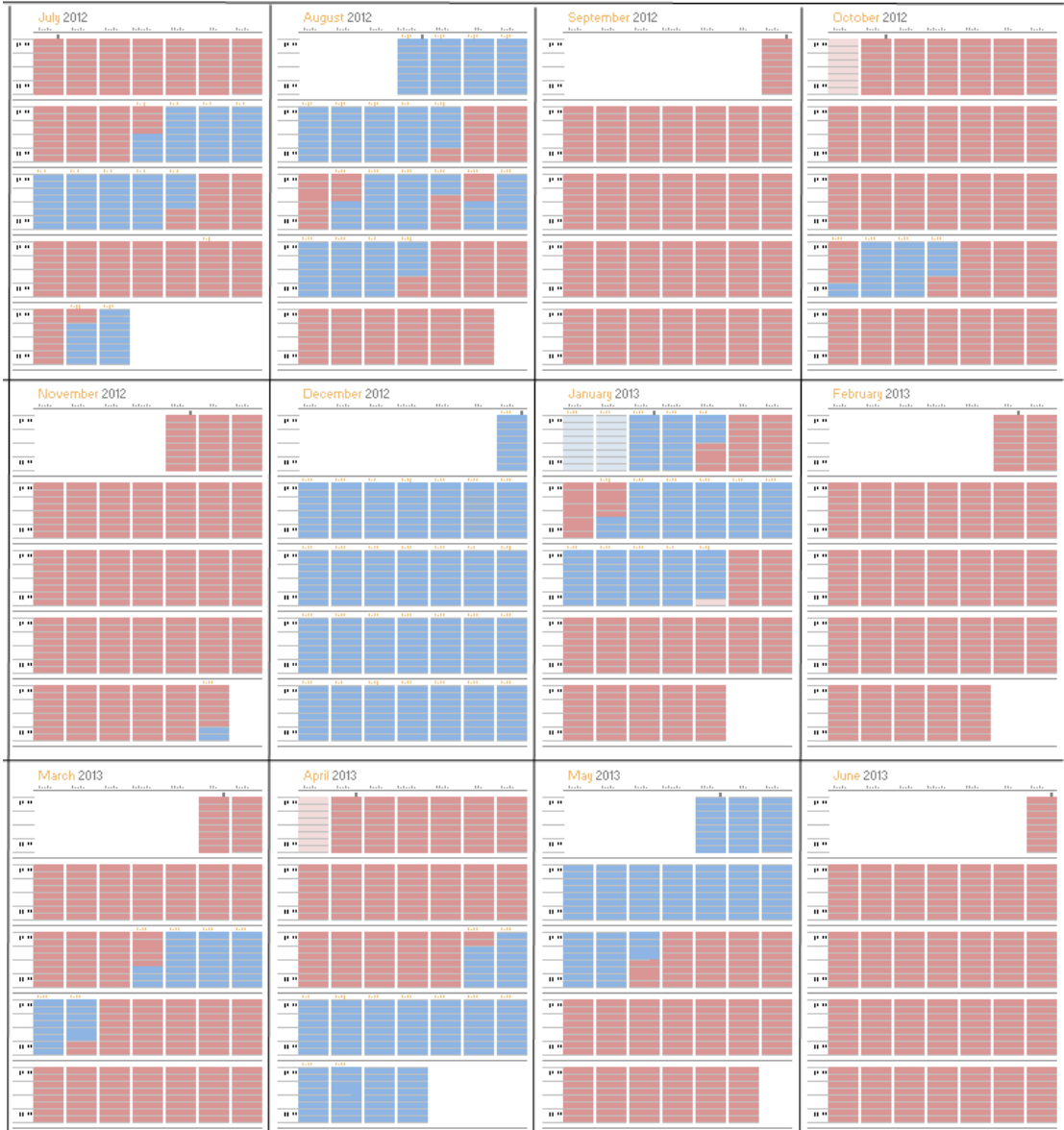
With variable amplitude stress history, there is a need to associate the variable stress cycles within a particular stress range. Rainflow method is the most popular and considered the best method of cycle counting and is described in the standard of the American Society for Testing and Materials.



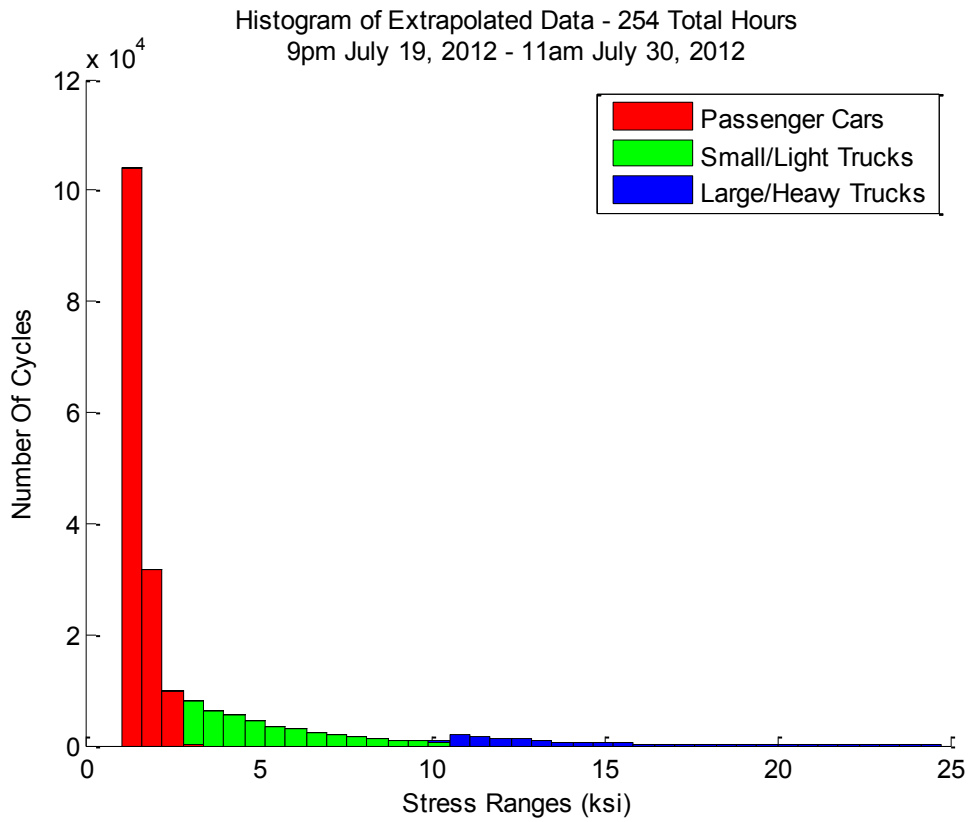
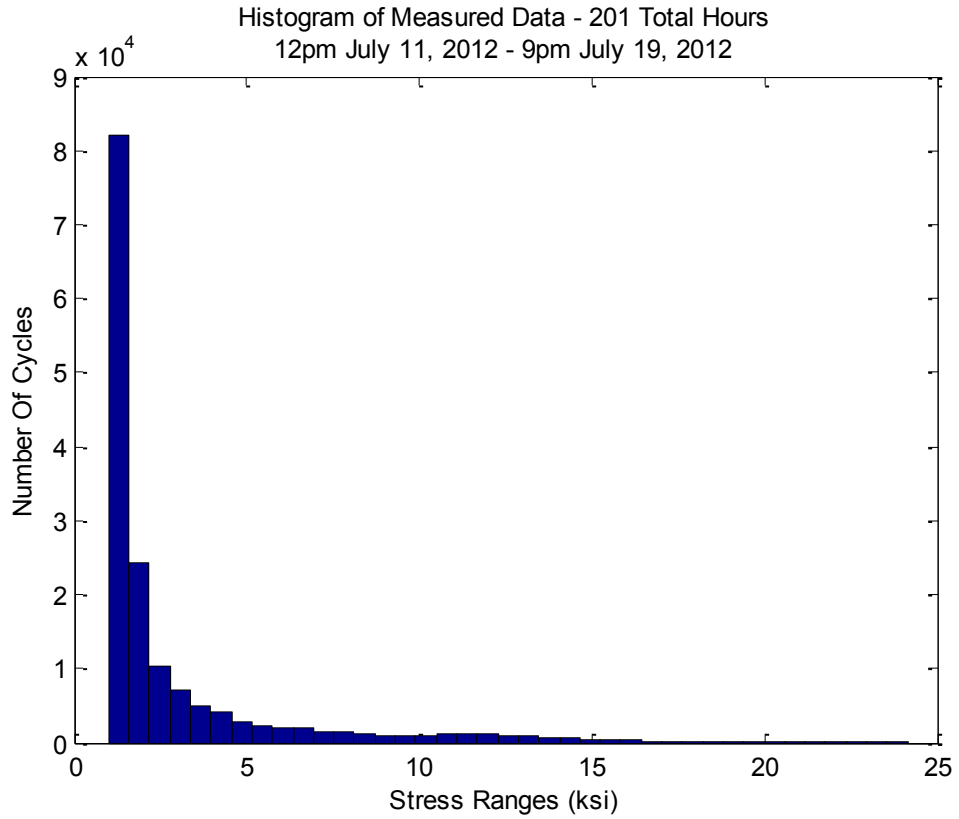
**Figure 6.12 Rainflow cycle counting implemented on variable amplitude stress**

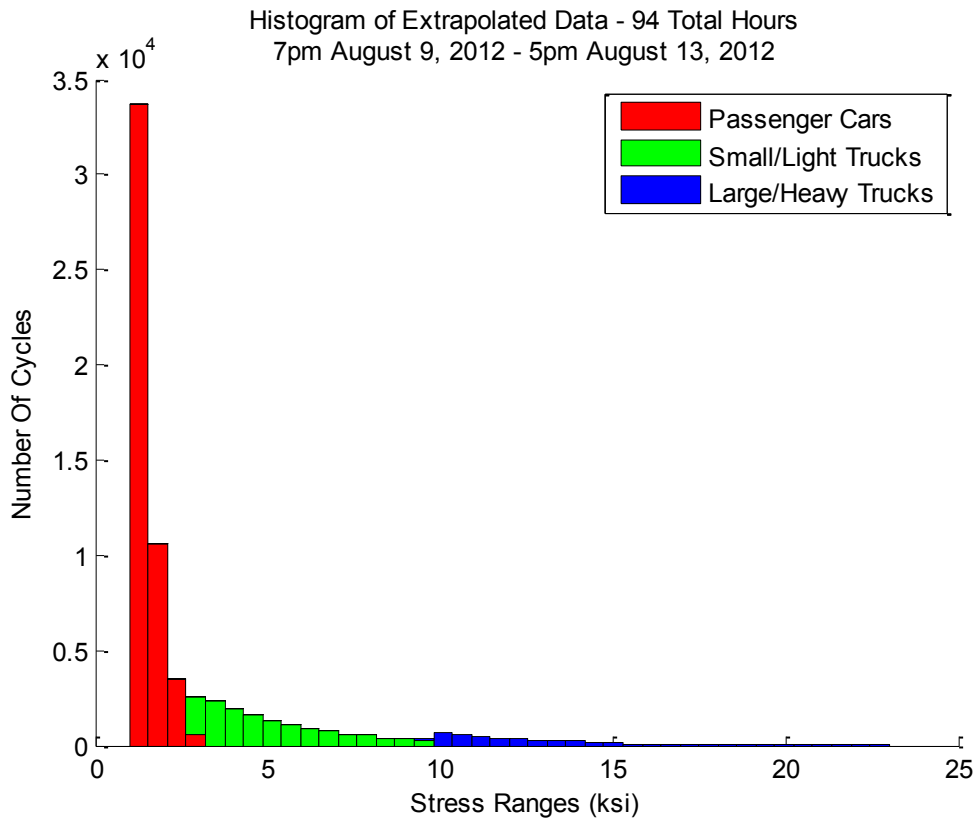
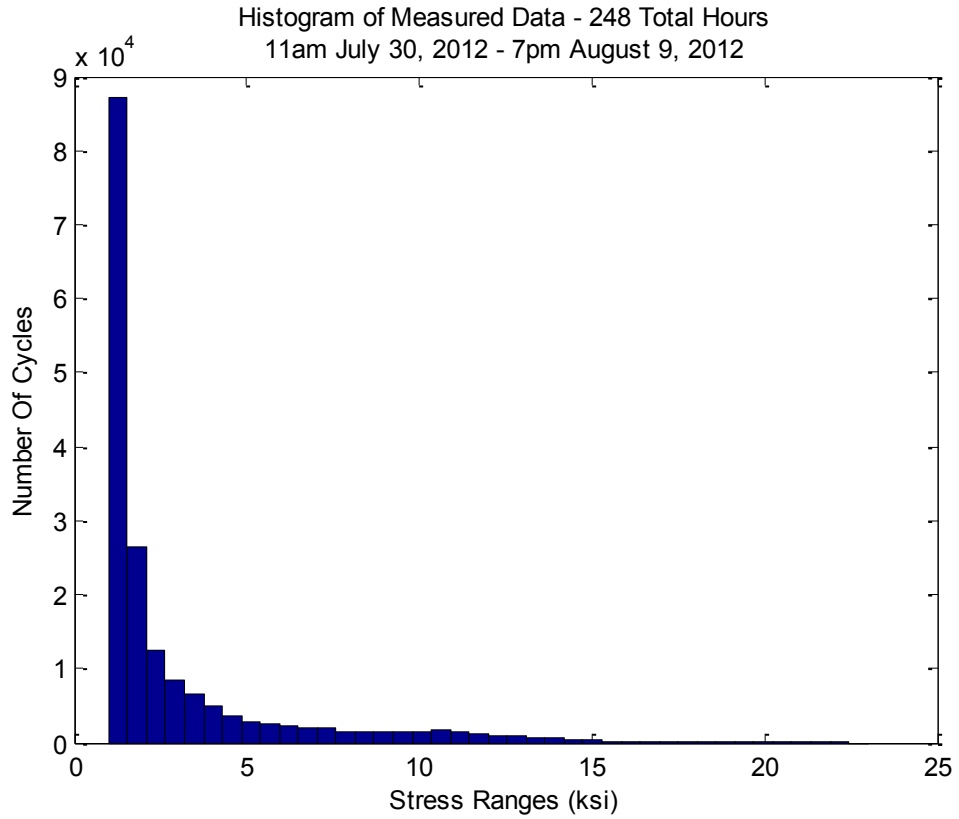
### 6.4.2 Extrapolation Results

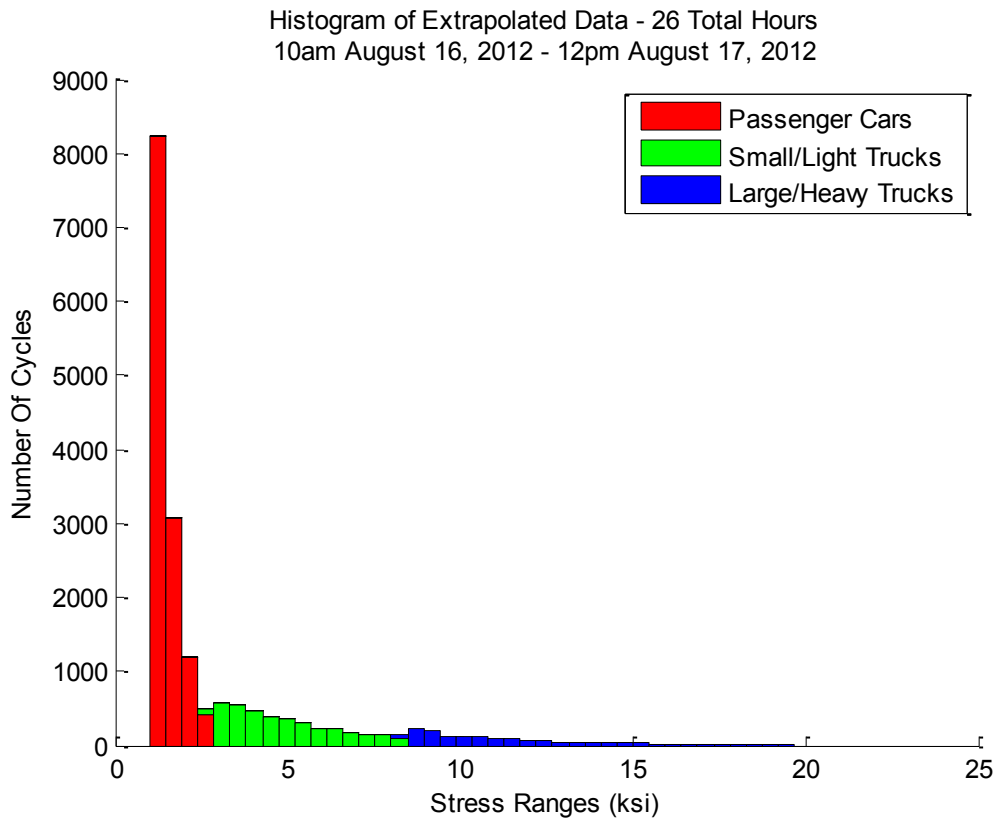
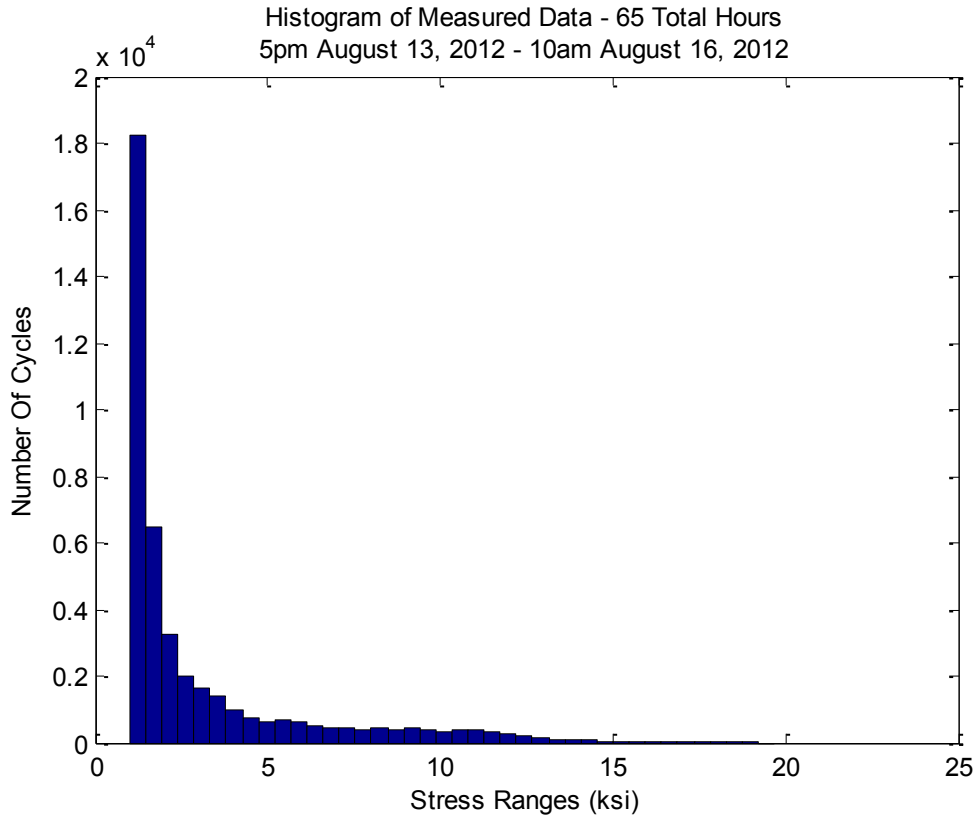
The purpose of the extrapolation was to fill in the missing days of acquired data, which are represented in Figure 6.13. The extrapolation was done using the algorithm put forth in section, 3.2.6 *Extrapolation of Load Histories*. The method of extrapolation that has been applied to the fatigue data is done in the rainflow domain. The results of the extrapolated rainflow matrix were modeled from a measured rainflow history, where the density of rainflow cycles was calculated. The calculation of this density provided the number of stress cycles and stress ranges that were to be estimated for certain hours of the day.

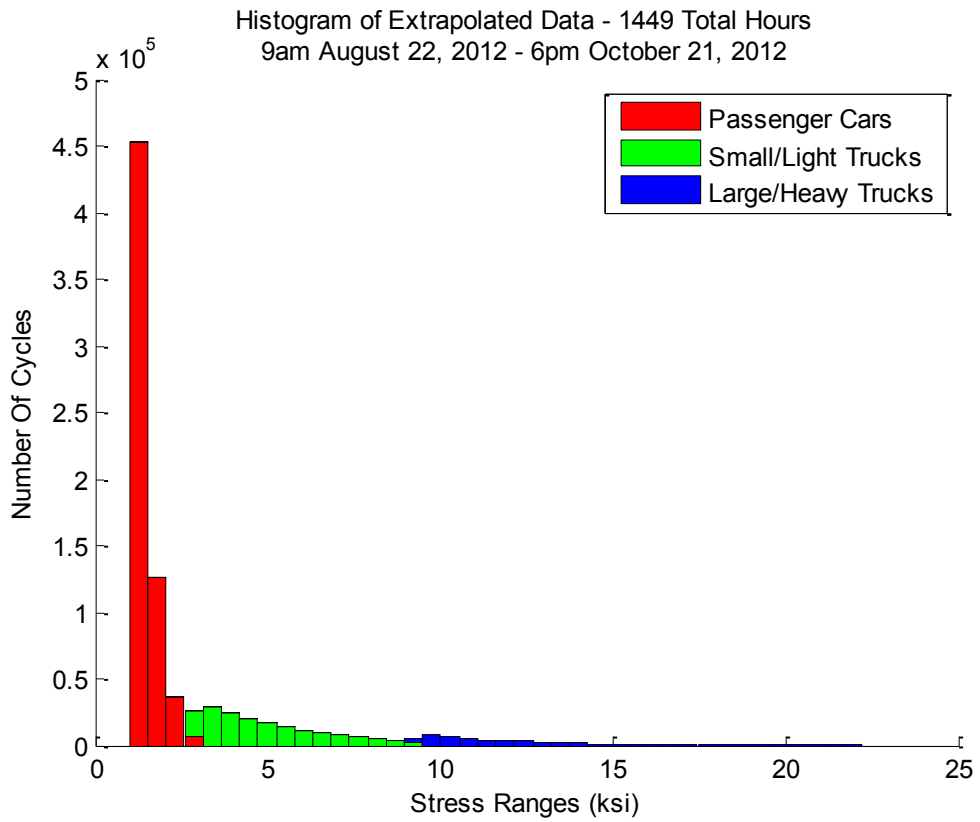
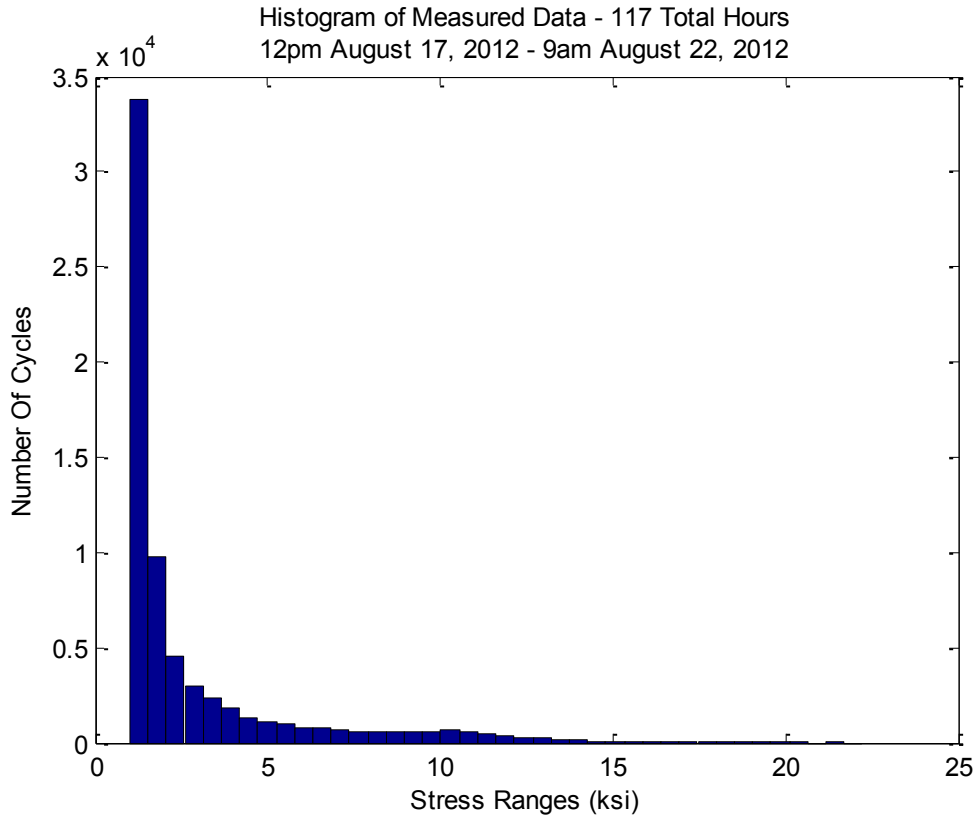


**Figure 6.13 Days of captured data (blue) and extrapolated data (red)**









### 6.4.3 Effective Stress Range

Using the histogram for one-year of measured and extrapolated data points, the effective stress range was calculated:

$$S_{re} = \left( \sum \gamma_i S_{ri}^3 \right)^{1/3} \quad (\text{Equation 6.1})$$

The fatigue prone details that fit the loading and geometry of the bridge component are listed in Table 6.1. The table displays the constant amplitude and threshold for Category C details; welded joints that are transverse to the direction of primary stress.

**Table 6.1 Selected detail categories for load-induced fatigue (AASHTO, 2012)**

Description	Category	Constant A (ksi <sup>3</sup> )	Threshold ( $\Delta f$ ) <sub>TH</sub> ksi	Potential Crack Initiation Point	Illustrative Examples
Base metal and weld metal in or adjacent to the toe of complete joint penetration groove welded T or corner joints, or in complete joint penetration groove welded butt splices, with or without transitions in thickness having slopes no greater than 1:2.5 when weld reinforcement is not removed. (Note: cracking in the flange of the "T" may occur due to out-of-plane bending stresses induced by the stem).	C	44 x 10 <sup>8</sup>	10	From the surface discontinuity at the toe of the weld extending into the base metal or along the fusion boundary	
Base metal and weld metal at details where loaded discontinuous plate elements are connected with a pair of fillet welds or partial joint penetration groove welds on opposite sides of the plate normal to the direction of primary stress.	C	44 x 10 <sup>8</sup>	10	Initiating from the geometrical discontinuity at the toe of the weld extending into the base metal or initiating at the weld root subject to tension extending up and then out through the weld	

The number of cycles to failure for a category C detail in the S-N curve is was calculated:

$$N_f = 44 \times 10^8 S_{re}^{-3} \quad (\text{Equation 6.2})$$

The number of cycles to failure is based on the effective stress range. The histograms show that an un-proportionally large amount of cycles occurs at smaller stress ranges. Therefore the stress ranges are truncated and an effective stress range is solved for. For this case study, a truncation stress of .5CAFL was used, which amounted to the effective stress range of  $S_{re} = 7.228$  ksi. At different levels of truncation stresses the effective stress range will be different, where the relationship is shown in Figure 6.14.

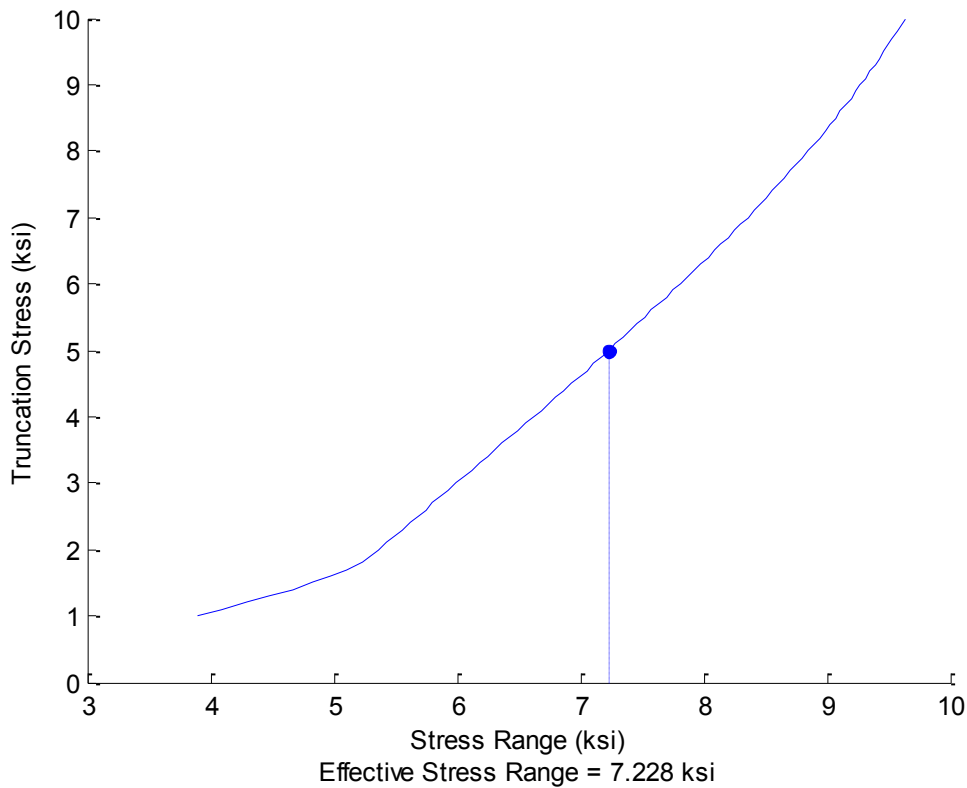


**Figure 6.14 Relationship between the truncation stress and the effective stress range**

Section 3.3.2.3 *Truncation Stress Range for Fatigue Details* provides a description of the optional truncation stress. Nevertheless, fatigue theory tells us that a larger stress range will mean a fewer number of cycles to failure, illustrated in Figure 6.15.

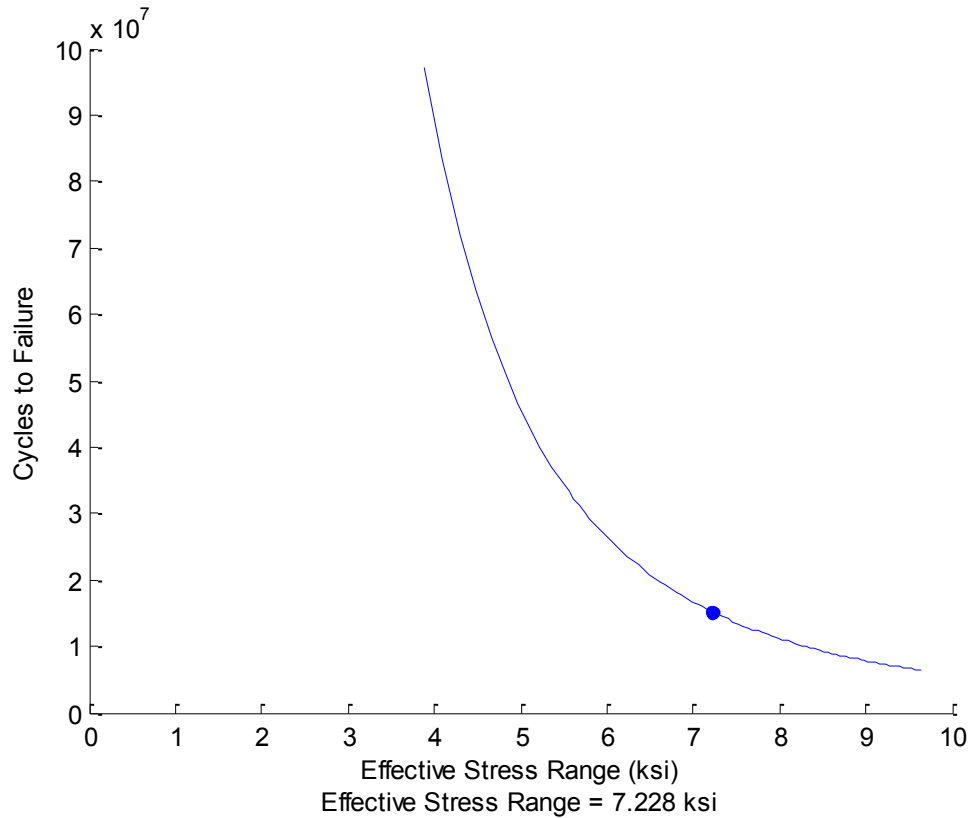


**Figure 6.15** Number of cycles to failure based on effective stress range

#### 6.4.4 Remaining Useful Life for Crack Initiation

The S-N curve is used to make predictions of the fatigue life based on the fatigue prone categories, described in 3.3.2 *Application of S-N Curve*. The AASHTO S-N curve is provided in Figure 6.16. An additional point is plotted on this curve to display the amount of fatigue damage after one year.

The length (years) of the crack initiation period is defined by Equation 3.21, rewritten here as Equation 6.4.

$$RUL_i = \frac{N_f}{N_e} \text{ years} \quad (\text{Equation 6.3})$$

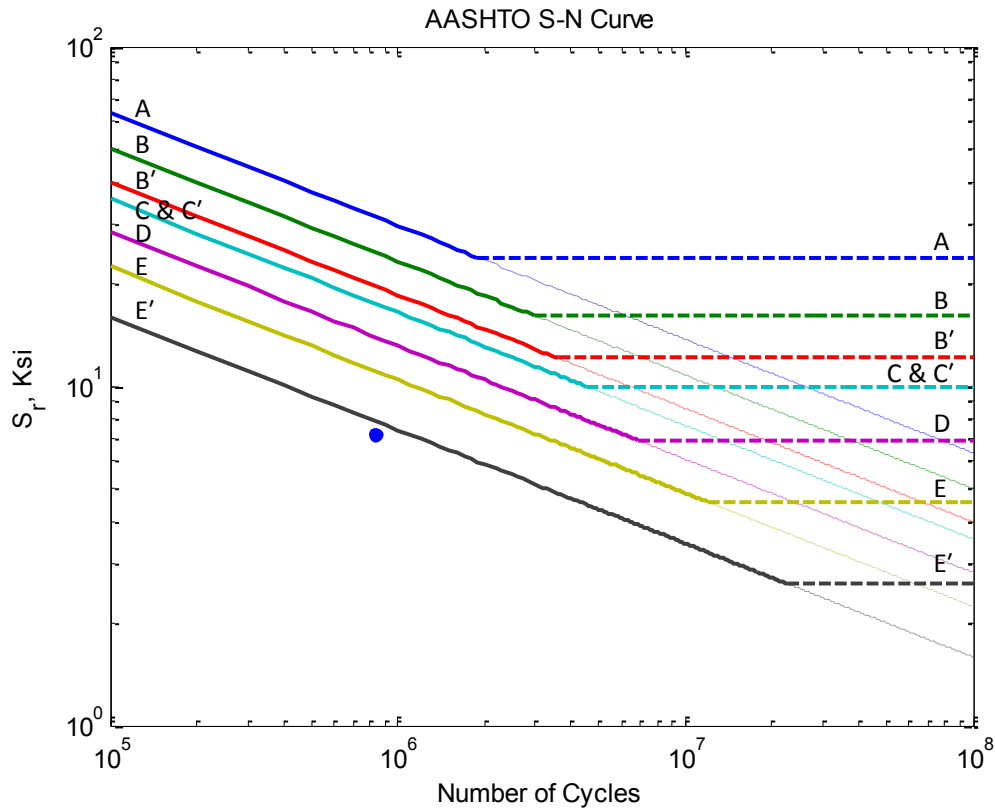


**Figure 6.16 AASHTO S-N curve with point of 1-year damage plotted**

In accordance with the histograms for this case study, as the effective stress range increases, the number of stress cycles decreases dramatically. For this reason, the fatigue life of the specimen actually increases with the effective stress range, displayed in Figure 6.17. Without including an increase in traffic volumes, the effective stress range and number of cycles are assumed consistent for each year. From Equation 6.3, the estimated fatigue live for the crack initiation period was 18.0 years. Figure 6.18 displays the yearly accumulation until failure is reached on the S-N curve.

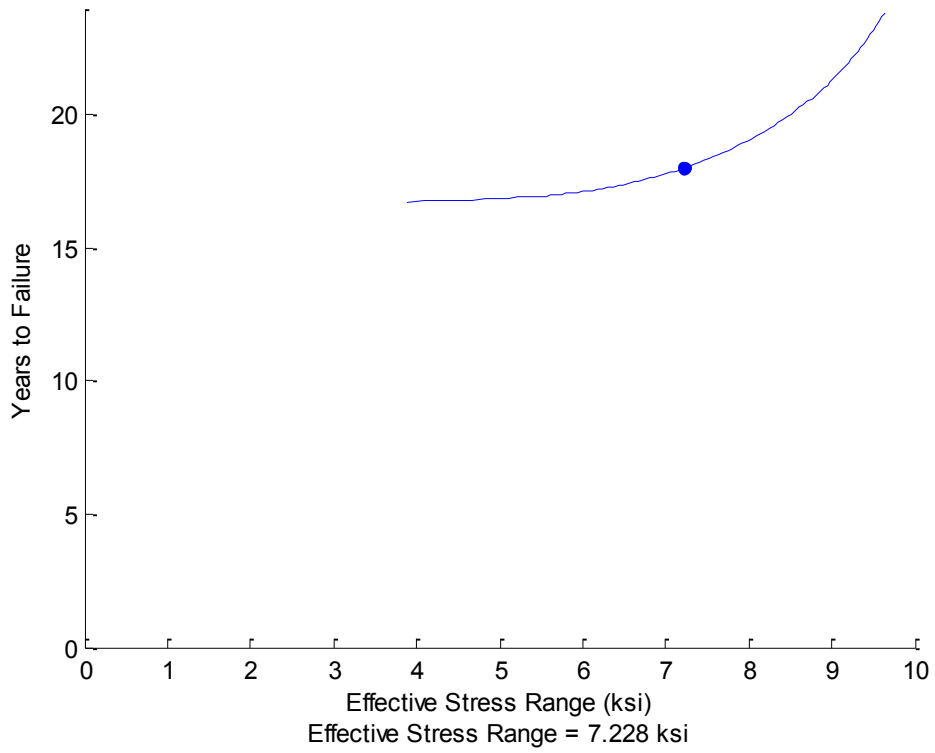


Figure 6.17 Years to failure based on effective stress range

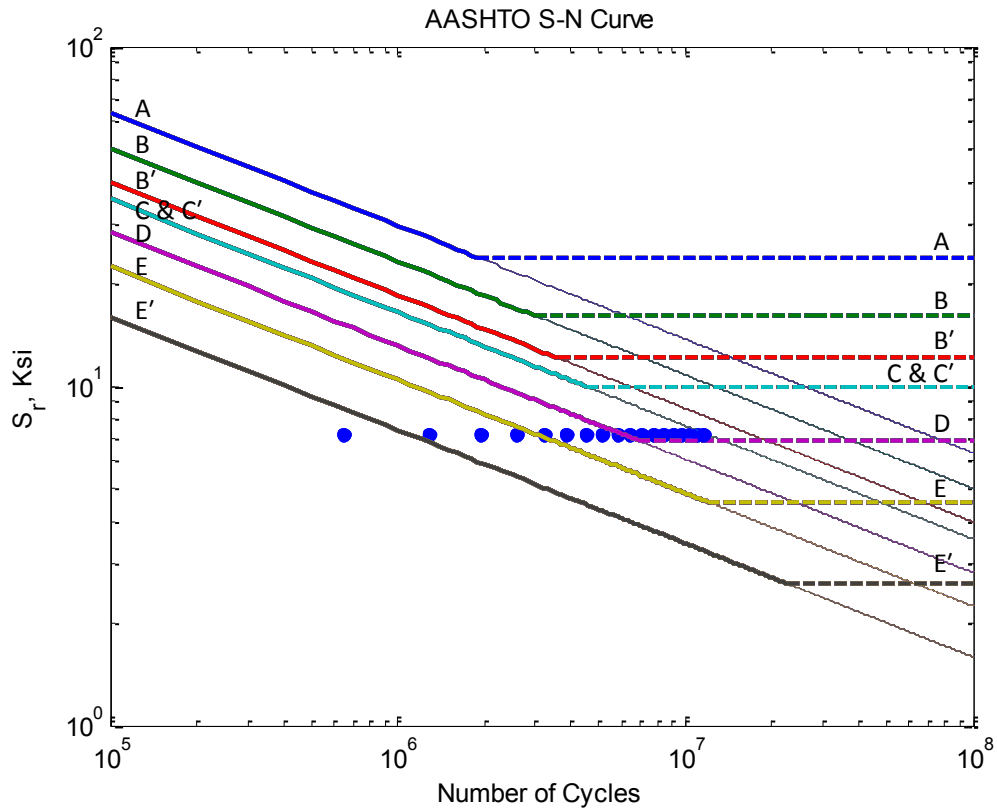
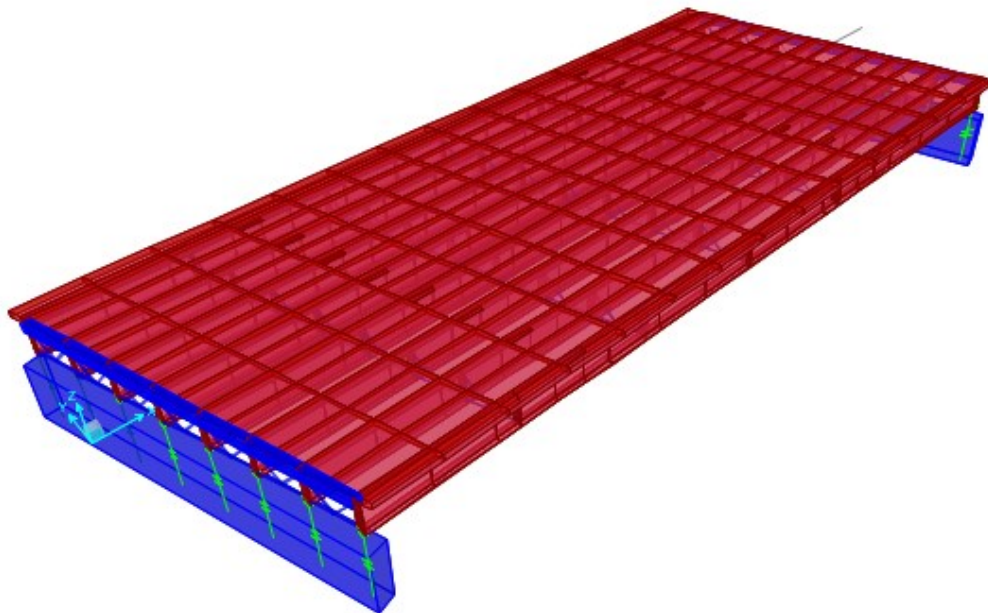


Figure 6.18 AASHTO S-N curve with cumulative points plotted until failure

## 6.5 Fracture Analysis

### 6.5.1 Finite Element Modeling

As discussed in Chapter Four, the finite element method is the most accurate method for determining the stress intensity factor. The ability of finite element models to create a very fine mesh at the crack tip provides a much needed insight into the localized stress field. In order to investigate stresses in these smaller bridge components or structural details, a smaller sub-model, i.e. a local model, should be extracted from a larger global model.



**Figure 6.19 Global model of Middlebrook Bridge (Fu, et al., 2014)**

A three-dimensional global model of the southbound direction, seen in Figure 6.1, was created in CSiBridge; an analysis and design software tool used to evaluate a bridge's response. The concrete deck, eight I-girders, and connection plates were

modeled by shell elements, whereas all the diaphragms were modeled by truss elements. The global model contains only the main components of the bridge and is mainly used for modal analysis, finding the displacement output of the whole bridge, and critical fatigue location determination known as hotspots, i.e. the locations of known high tensile strength. For the purpose of analysis, the global model used a refined mesh around the fatigue hot spots (Fu, et al., 2014). The refined mesh is depicted in the bottom of the connection plates in Figure 6.20. However, since the interest is to obtain a stress intensity factor; the global model cannot be any more refined and a local model of this critical region was created for the purpose of understanding the stress field around the crack.

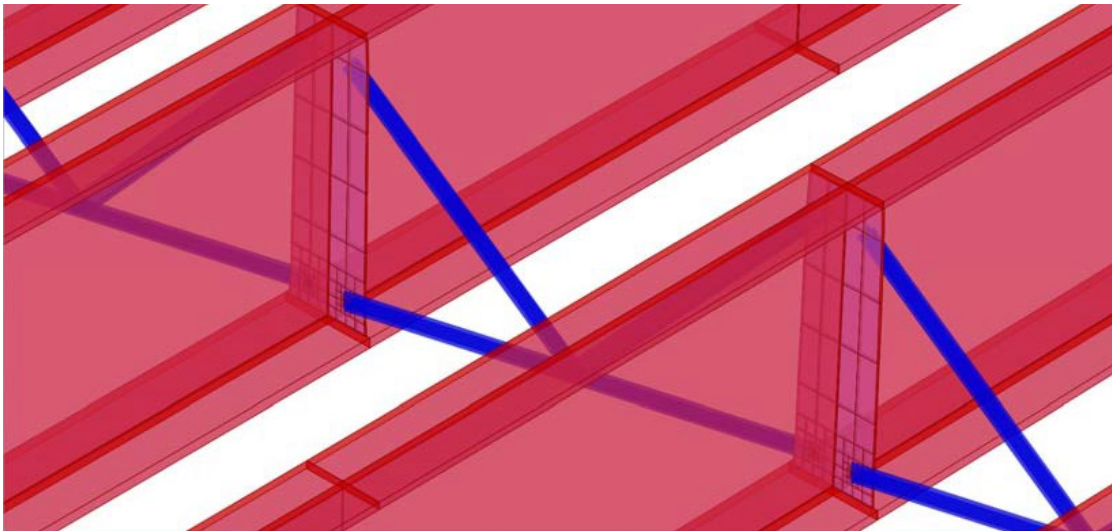
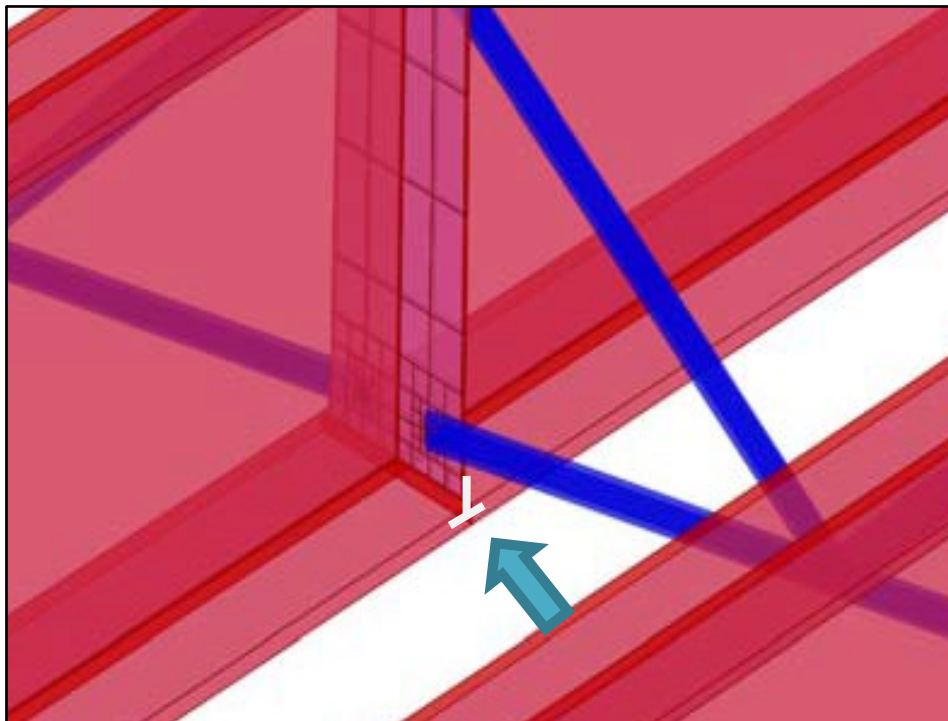


**Figure 6.20 K-brace, connection plate and girder on global model (Fu, et al., 2014)**

It is crucial when modeling a local refined model to ensure the boundary conditions are set up to correctly reflect its mechanical connections to the global model. The following guidelines are typically followed when going from a global to local model (Fu, et al., 2014):

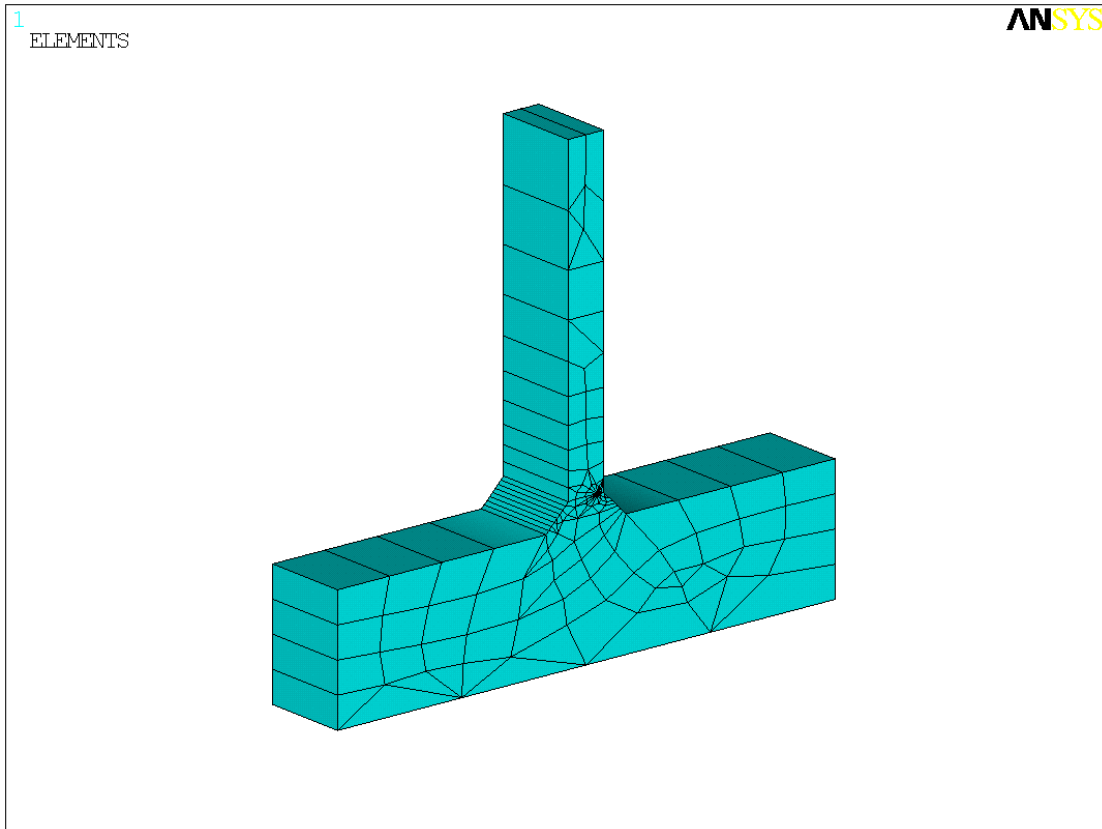
- The boundary nodes should apply the same displacements obtained from the global model.
- The boundary nodes should apply the same external forces obtained from the global model as internal forces.

In accordance with the guidelines, the resulting deflections (displacements) of the global model were applied to the perimeter of the local model as enforced displacements. Since the deflections are a result of the loading, applying the deflections simulates the loads transferred across a free-body section of the global model where the local model resides. Further the stress loads at the location of the strain gage were applied to the local model at the corresponding perimeter location. Figure 6.21 displays the location of the local model on the global structure. This location is described with white lines that outline the local model geometry.



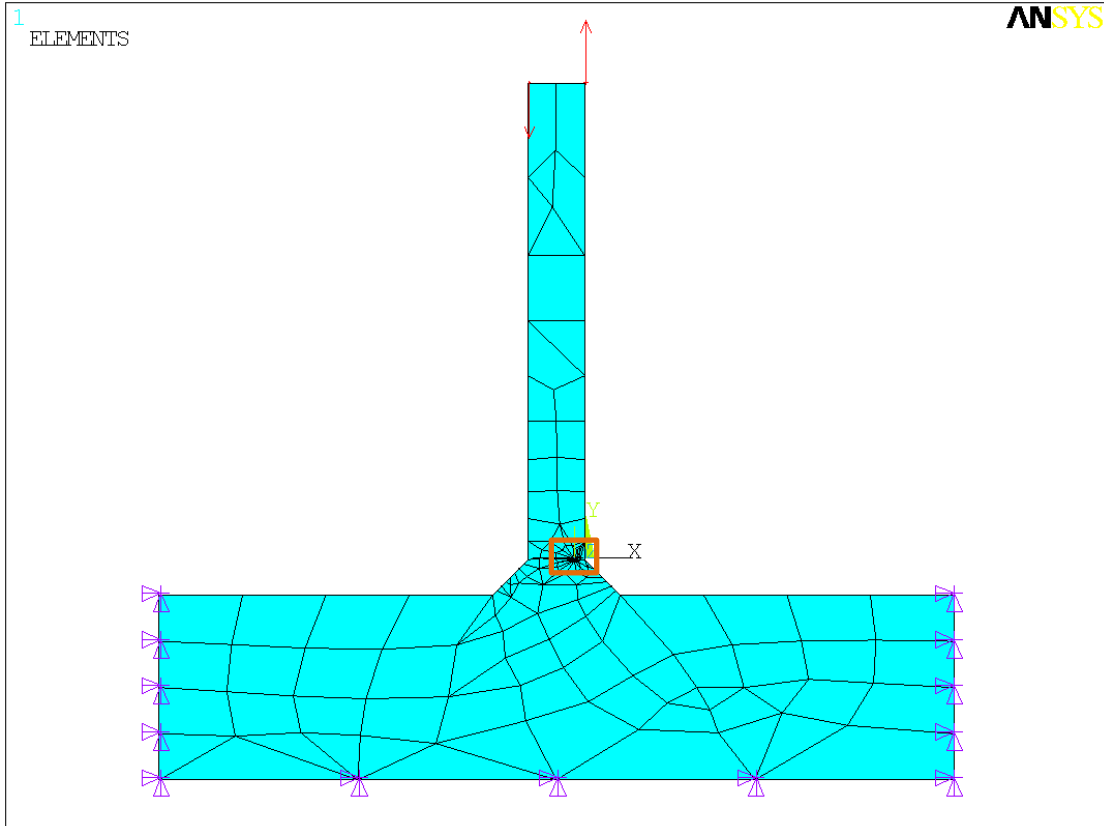
**Figure 6.21 Location of local model within the global model**

Figure 6.22 displays the three dimensional local finite element model that has been meshed. This model shows how the elements were defined and broken down across the local geometry.



**Figure 6.22 Three Dimensional local finite element model meshed into elements**

Since the purpose of the local model is to find the stress intensity factor, the problem can be treated in two-dimensions, as discussed in *4.4 Validating FEM Models with a simple LEFM model*. Figure 6.23 displays the two-dimensional local model with applied displacements and forces. An orange rectangle outlines the location of the existing crack, which is magnified in Figure 6.24.



**Figure 6.23 Finite element local model with applied displacements and forces**

As seen in Figure 6.24, a fine mesh is created around the previously-identified existing crack. The crack was modeled with an assumed depth of 1/10 inch; which is approximately the length of the penetration of the fusion in a fillet weld. So the crack was assumed to occur at the depth of penetration.

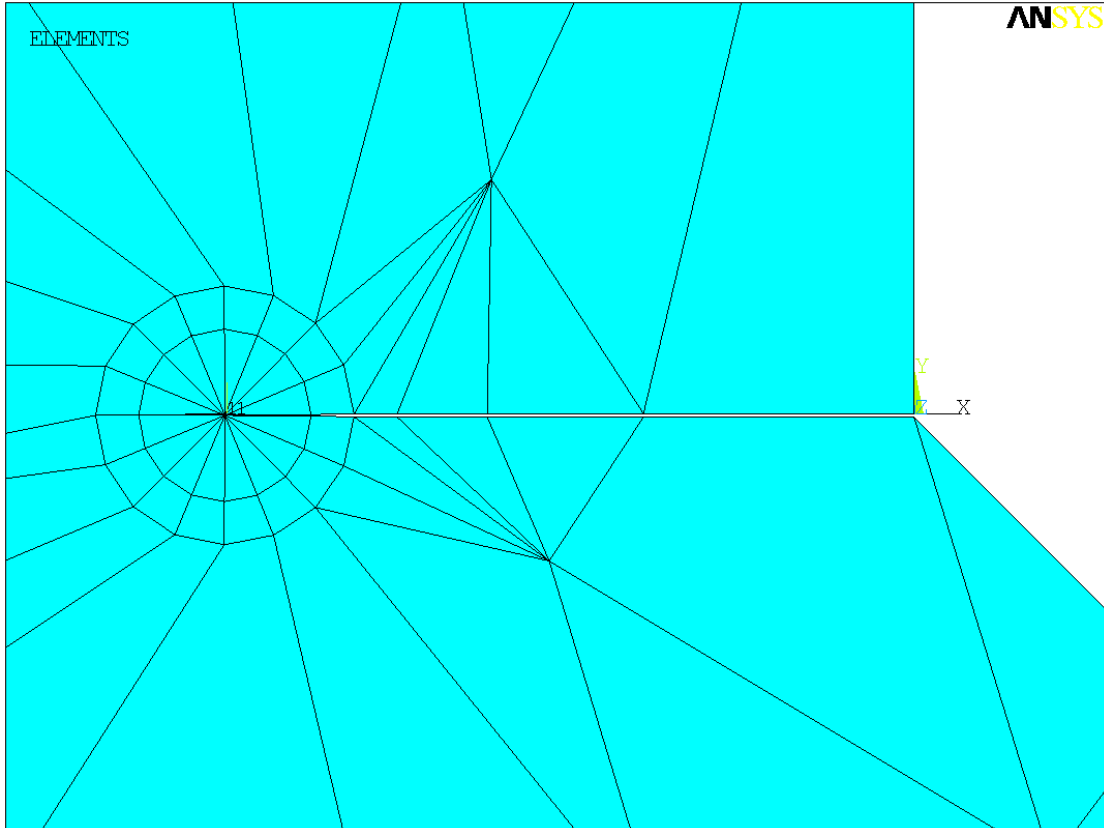


**Figure 6.24 Radial elements at the crack tip**

Figure 6.25 and Figure 6.26 display the stress contour of the y-component of the cross section. Figure 6.25 shows the front of the local model. The contour legend at the bottom represents the stress in units of psi. The deformed shape shows the bending in the connection plate, which is from the load of the bottom diagonal. The bending in the illustration is magnified by about 2.5% of the actual bending experienced. Figure 6.26 shows a magnified view of Figure 6.25 at the location of the crack. The plastic zone at the crack tip is more apparent in this graphic. Since the stress field at the crack tip is smaller than the connection plate thickness, then plane strain governs. The displacement extrapolation for solving the stress intensity factor was also based on plane strain conditions.

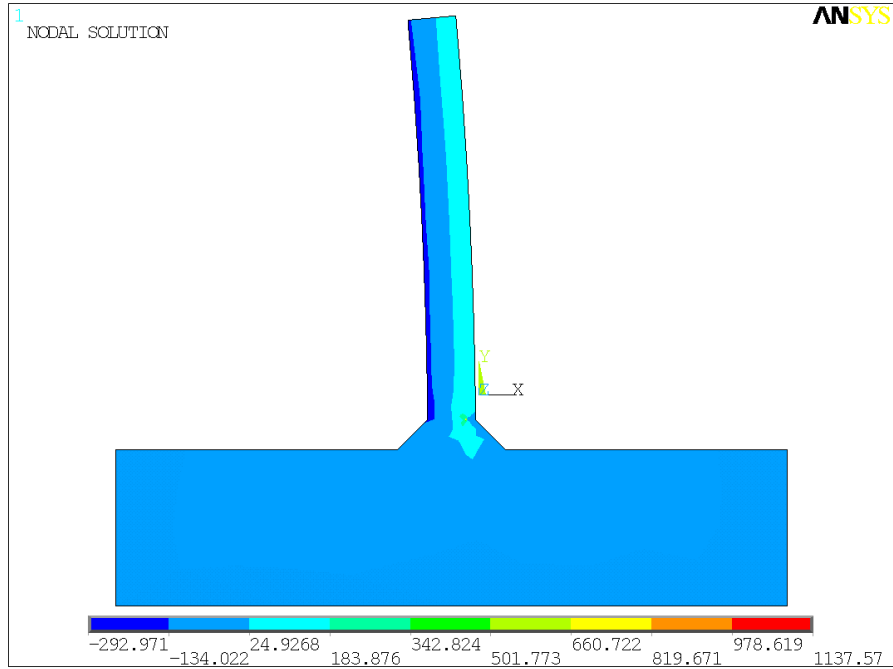


Figure 6.25 Stress contour (Y-Component) of connection between stiffener and flange

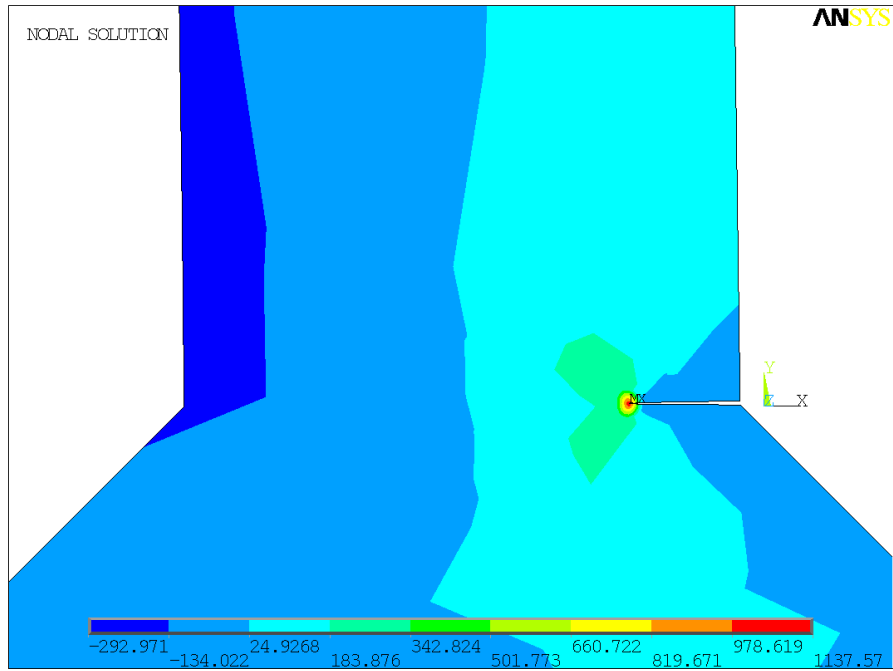


Figure 6.26 Stress contour (Y-Component) of crack between stiffener and flange

### 6.5.1.1 Stress Intensity Factor

The crack path was defined using four nodes along the crack face and one node at the crack tip, where the radial elements were configured.

```

KCALC Command
File
**** CALCULATE MIXED-MODE STRESS INTENSITY FACTORS ****
ASSUME PLANE STRAIN CONDITIONS
ASSUME A FULL-CRACK MODEL <USE 5 NODES>
EXTRAPOLATION PATH IS DEFINED BY NODES:      76      72      50      88      92
WITH NODE      76 AS THE CRACK-TIP NODE
USE MATERIAL PROPERTIES FOR MATERIAL NUMBER      1
EX =      29000.      NUXY =      0.30000      AT TEMP =      0.0000
**** KI =      36.061      ,      KII =      1.8637      ,      KIII =      0.0000      ****

```

Figure 6.27 SIF for two-dimensional crack modeled at toe of weld

Rearranging the equation for the stress intensity factor, the shape factor is solved for with the known input values.

$$\beta = \frac{K}{S_{ref} \sqrt{\pi a_0}} \quad (\text{Equation 6.4})$$

Under the parameters,  $K = 36.061 \text{ ksi} \sqrt{\text{in}}$ ,  $a_0 = .1 \text{ in}$ , and  $S_{ref} = 5.50 \text{ ksi}$ , then the geometric shape factor is solved to be:

$$\beta = .9999 \quad (\text{Equation 6.5})$$

### 6.5.2 Damage Tolerance and Fracture Toughness

The specifications of the American Society for Testing and Materials (ASTM) for A572 Grade 50 steel requires a minimum yield strength value of 50 ksi. The fracture toughness equation, as discussed in section 4.3 *Fracture Toughness*.

$$K_{IC} = \sqrt{5(CVN)E} \quad (\text{Equation 6.6})$$

For zone 2 temperature, i.e. (-1°F to -30°F), the fracture toughness of a non-fracture-critical Grade 50 steel is 20 ft-lb @ °F. Therefore, the fracture toughness for this steel is computed to be,  $K_{IC} = 1.475 \text{ ksi} \sqrt{\text{in}}$ . The critical crack length that corresponds to the fracture toughness comes from the fracture mechanics equation for critical stress intensity factor. Under the parameters that fit the Middlebrook Bridge,  $K_{IC} = 1.475 \text{ ksi} \sqrt{\text{in}}$ ,  $\beta = .999$ , and  $S_{reff} = 5.50 \text{ ksi}$ , then the geometric factor is solved to be:

$$a_{crit} = \frac{K_{IC}}{\pi\beta^2\sigma^2} = .223 \text{ in} \quad (\text{Equation 6.7})$$

The relationship between the critical crack size and the change in effective stress range is shown in Figure 6.28.

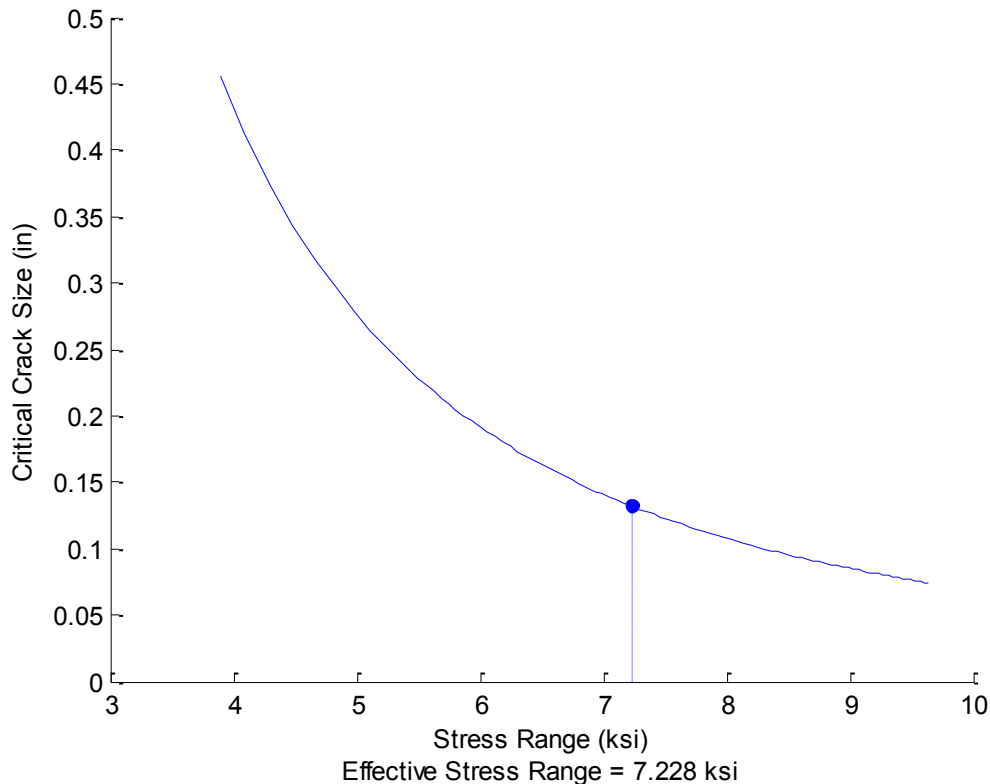


**Figure 6.28 Change in critical crack size based on effective stress range**

### 6.5.3 Crack Growth Rate

The crack growth rate, seen in Equation 4.4 and rewritten in Equation 6.8 is dependent on the range of the stress intensity factor.  $C$  and  $m$  are parameters that depend on the material, environment, frequency, temperature and stress ratio.

$$\frac{da}{dN} = C(\Delta K)^m \quad (\text{Equation 6.8})$$

Since the interest here is a steel material, the values are chosen as  $m = 3$  and  $C = 10^{-11}$ . Using a week of measured data from the bridge, the stress intensity factor varies with the stress ranges due to the similarity principle, described in *4.2.2 Stress Intensity Factor and Similarity Factor*. The relationship between the crack growth rate and the stress intensity factor is portrayed in Figure 6.29.

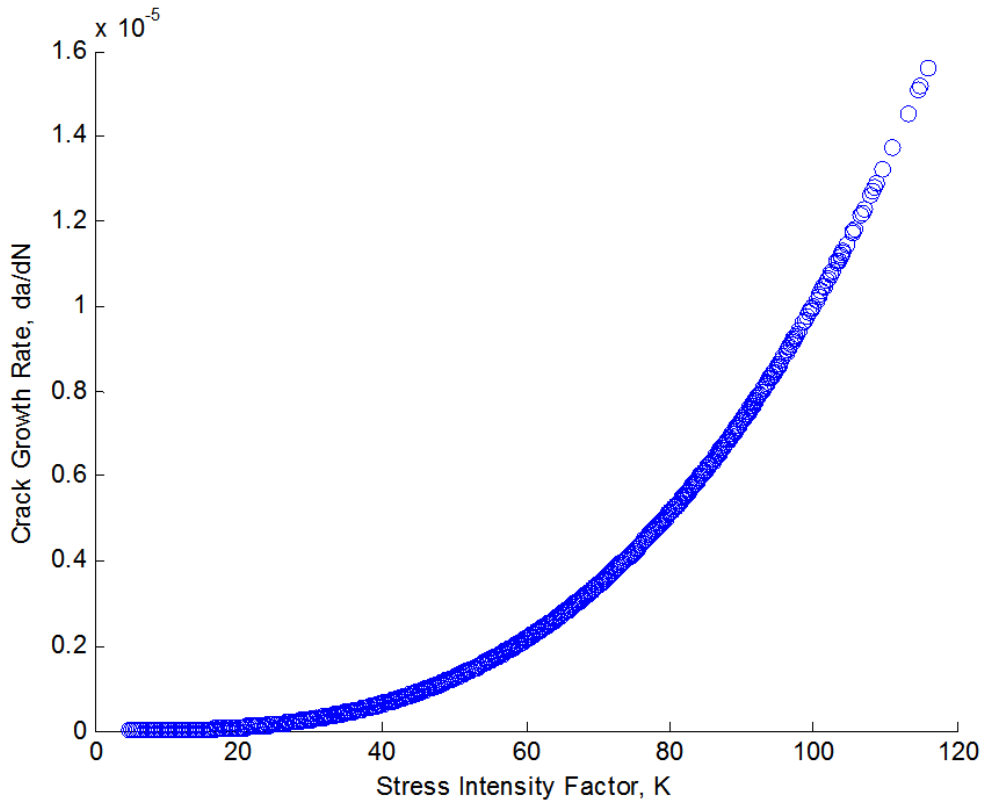


Figure 6.29 Paris Law for fatigue crack growth rates

Paris law is more often plotted on a logarithmic scale, to show a linear relationship between the stress intensity factor and the crack growth rate. This plot is shown in Figure 6.30.

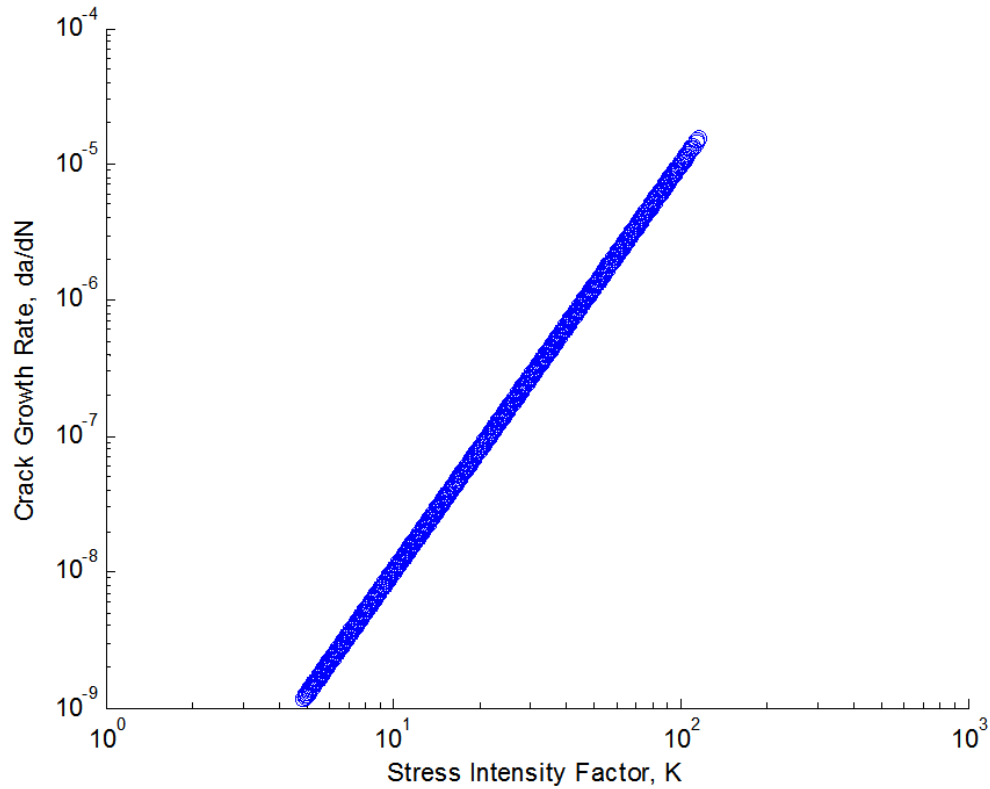


Figure 6.30 Paris Law for fatigue crack growth rates, log-log

### 6.5.1 Remaining Useful Life for Crack Propagation

The accumulation of damage for fatigue crack growth models is consequent of the change in crack size,  $a$ , shown in Equation 4.25, where  $a_0$  is the initial crack size,  $\Delta a_i$  is the change in crack size per cycle, and  $a_n$  is the updated crack size (Schijve, 2009).

$$a_n = a_0 + \sum_{i=1}^{i=n} \Delta a_i \quad (\text{Equation 6.9})$$

The crack size at any given time is a function of the stress intensity factor, as portrayed in Equation 4.27,

$$a = \frac{K}{\pi\beta^2\sigma^2} \quad (\text{Equation 6.10})$$

The relationship between the crack size and the change in effective stress range is shown in Figure 6.31.

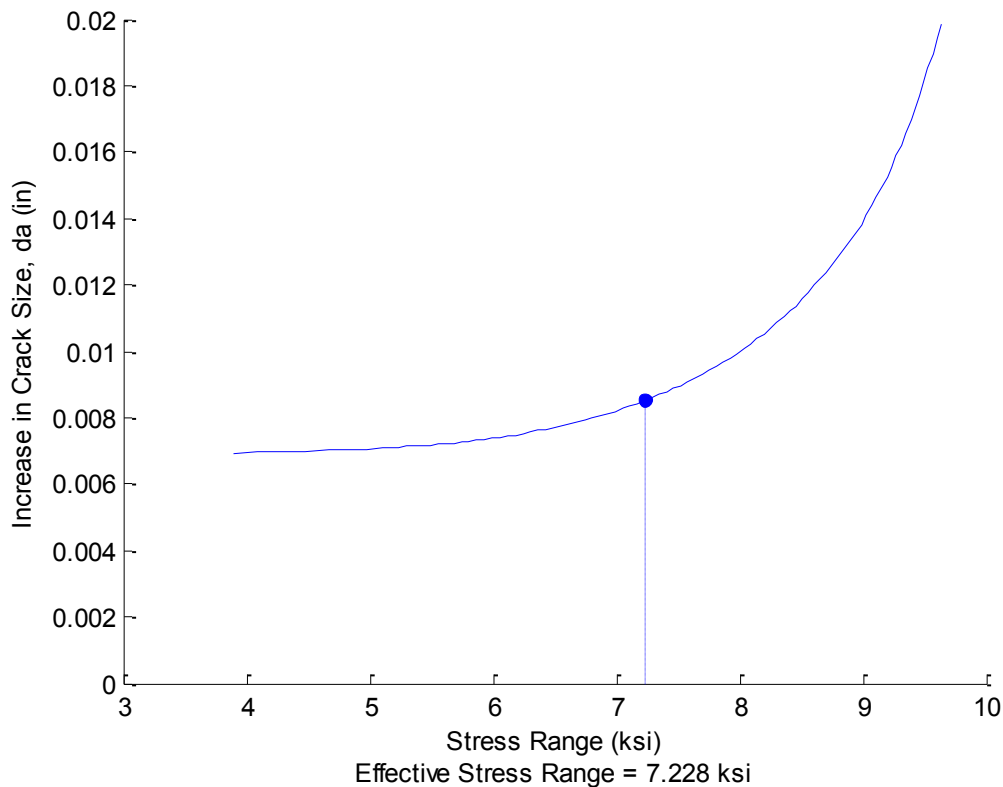


**Figure 6.31** Variation in crack size changes with the effective stress range

Using the critical crack size in Figure 6.28 and the incremental crack size in Figure 6.31, the two plots can be plotted on the same graph to show the relationships with each other; Figure 6.32. This figure also plots the critical crack size for the case where a fracture critical member exists.

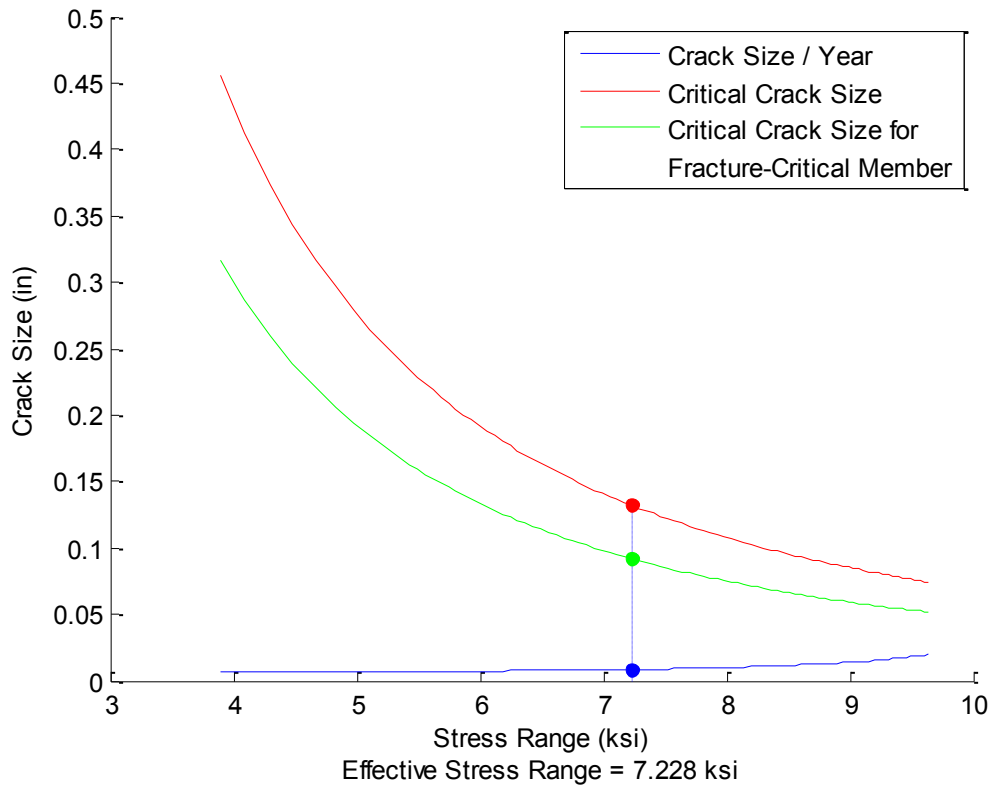


**Figure 6.32 Relationship of crack size to critical crack size**

The remaining useful life is calculated by subtracting the initial crack size,  $a$ , from the critical crack size at failure that corresponds to the critical crack size at failure. Dividing by the change in crack size using an effective stress range and the number of cycles,  $N_e$ , solves the remaining useful life of the structure in terms of *years*,

$$RUL_p = \frac{a_{crit} - a}{a_n} \text{ years} \quad (\text{Equation 6.11})$$

Figure 6.33 shows the relationship between the number of years to failure and the effective stress range, based on the crack properties. Accordingly, under the effective stress range for the Middlebrook Bridge, the number of years until a critical crack size is reached in the propagation period is 9.6 years.

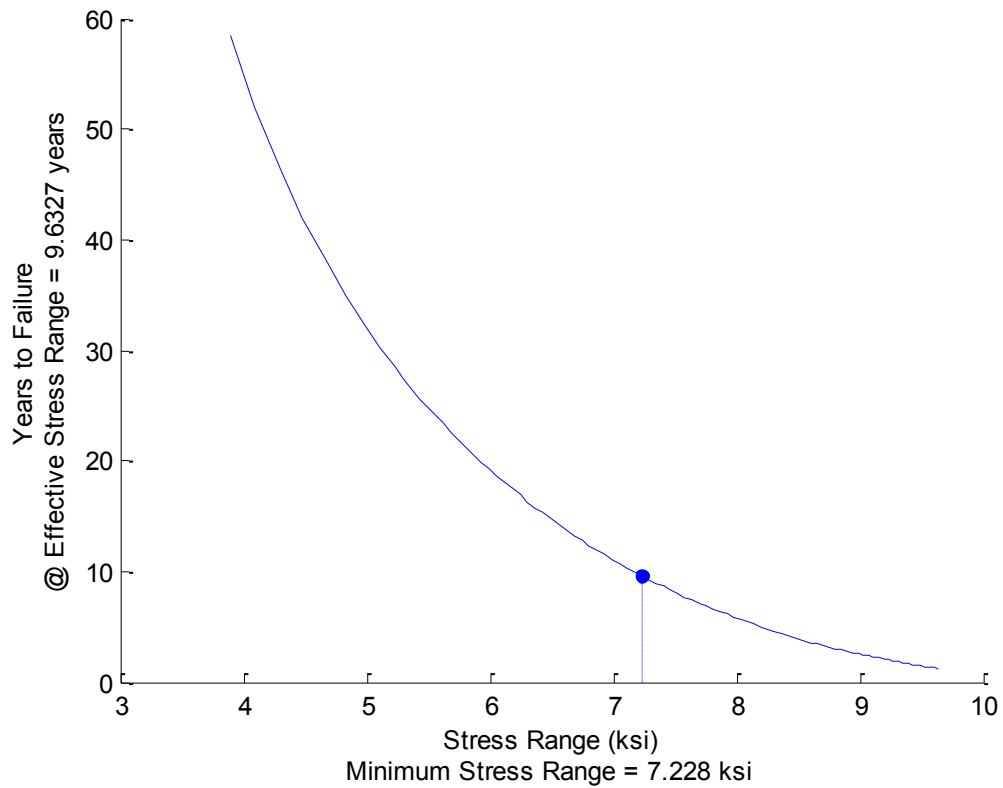


**Figure 6.33 Number of Years to failure based on the crack growth rate**

Since the bridge inspectors first noticed the bridge cracking in 2011, at the time of testing, (2012-2013), the crack had been present for 1-2 years. In 2014, when the crack was repaired, the remaining useful life for this bridge element was calculated to be 6.6 years to failure.

## 6.6 Total Cumulative Damage

The damage in the initiation period and the damage in the propagation period can be combined to assess the total cumulative fatigue damage on a specific component:

$$D_{Total} = \begin{cases} \alpha_I d_i, & N_e \leq N_f \\ \alpha_I d_i + \alpha_p d_p, & N_e > N_f \end{cases} \quad (\text{Equation 6.12})$$

Since  $d_i$  and  $d_p$  represent the amount of fatigue damage (% damage) at certain stages, for this case study, a value of 0.70 for  $\alpha_I$  and a value of 0.30 for  $\alpha_p$  would approximate the proportion of  $d_i$ , which was estimated to be approximately 18.0 years and  $d_p$  which was approximated to be 9.6 years.

**Table 6.2 Mapping of damage calculations into condition states**

Condition State	$D_{Total}$	$D_{Total}, \%$
CS1	$0 \rightarrow \frac{1}{2} \alpha_i$	0→35%
CS2	$\frac{1}{2} \alpha_i \rightarrow \alpha_i$	35→70%
CS3	$\alpha_i \rightarrow \frac{1}{2} \alpha_p$	70→85%
CS4	$\frac{1}{2} \alpha_p \rightarrow (\alpha_i + \alpha_p)$	85→100%

During the 2011 bridge inspection report, the crack was first visible. With an initial crack size of 0.05 inches, the calculated percent damage was approximately 83.3%. This would define the bridge element as condition state 3, which corresponds to a condition state description, “*fatigue damage exists which is not arrested.*” In 2014, when the crack was repaired, the calculated percent damage was 87.2%, correlating to condition state 4, “*Fatigue damage exists which warrants analysis of the element to ascertain the serviceability of the element or bridge.*” These condition

state descriptions are outlines in Table 5.4, which is also below in Table 6.3 for reference.

**Table 6.3 Fatigue condition states translated into national bridge element (MDSHA, 2003)**

<b>Defect</b>	<b>Condition State 1 (good)</b>	<b>Condition State 2 (fair)</b>	<b>Condition State 3 (poor)</b>	<b>Condition State 4 (severe)</b>
Cracking/ Fatigue	None	<b>Fatigue Damage</b>	<b>Analysis Warranted</b>	<b>Severe Fatigue Damage</b>
		Fatigue damage exists but has been repaired or arrested. The element may still be fatigue prone.	Fatigue damage exists which is not arrested. Condition State used for first time element is identified with crack	Fatigue damage exists which warrants analysis of the element to ascertain the serviceability of the element or bridge

## **Chapter Seven: Conclusions and Future Research**

### **7.1 Conclusions**

As aging steel bridges continue to experience increasing traffic volumes and are progressively more vulnerable to fatigue deterioration, there is increasing demand to assure their long term health. Due to the dynamic nature of the loads, fatigue-induced damage remains to be a primary failure mechanism. The ability to assess the cumulative fatigue damage is critical to ensuring the structural integrity of these aging-steel bridges.

This dissertation research aims to establish a damage accumulation model used for the damage prognoses of steel highway bridges through the use of existing fatigue analyses methods and fracture mechanics. The proposed damage accumulation model goes beyond the current fatigue assessments put forth in AASHTO LRFD Bridge Design Specifications. Further, this dissertation provides a means for mapping the fatigue damage prognoses into the condition states assessments within bridge management systems. To verify the damage accumulation model, fatigue damage was collected on an existing highway bridge and the data was processed to determine a damage prognoses. Specifically the major findings of this research are summarized as follows,

- Fatigue life can be more accurately characterized with two different methods of analysis that define the exponential form of a fatigue life curve; using the empirical correlation approach and fracture mechanics approach.
- The fatigue damage assessments put forth in AASHTO LRFD Bridge Design Specifications can be supplemented with a fracture mechanics analysis.

Currently, there is no defined method for fracture mechanics in AASHTO specifications.

- Structural health monitoring has a significant contribution in damage prognosis. Sensing instrumentation can be used to acquire information about a bridge's response to loads. This information can be used in linear damage accumulation models and also used in fracture mechanics to understand crack growth.
- Utility programs for data collection and analysis need to be used alongside structural health monitoring instrumentation in order to acquire the pertinent information relative to fatigue-damage. These utility programs include: data-detrending, rainflow-cycle counting, extrapolation, and damage estimations.
- Extrapolation of data can be achieved in the rainflow domain, which outputs an extrapolated rainflow matrix. Extrapolation in the rainflow domain offers the most computationally friendly approach and can estimate the rainflow matrix for an infinite number of cycles. Extrapolation converts short-term monitoring into long-term monitoring, with the capability to account for even higher loads than what was measured.
- The linear-damage accumulation rule, aka the Miner Rule, should only be used for fatigue-crack-initiation life assessments, rather than for total fatigue life estimates. The multiple shortcomings of the Miner Rule, described in 3.3.1.1 *Shortcomings of the Miner Rule*, should be realized. There are currently no fatigue analysis methods used by bridge inspectors that account for these shortcomings.

- The displacement extrapolation used in finite element modeling, is capable of providing accurate information about fatigue cracks on stressed bridge elements with complex geometries. Specifically, the displacement extrapolation method computes the stress intensity factor for a crack of a known size.
- The initial crack size will dictate the accuracy and effectiveness of finite element modeling. Since the main purpose of the finite element modeling is to solve for the stress intensity factor, having an accurate crack size is the most important parameter; assuming the remote loading stress was measured and acquired from sensors.
- Damage accumulation models can be used for the evaluation of bridge elements. The damage accumulation models are useful for estimating both the cumulative number of cycles and the damage prognosis, i.e. remaining useful life.
- Bridge management systems can be supported with damage accumulation models. These models, which are highly influenced from the feedback of structural health monitoring technologies, can be mapped into AASHTO condition states with a linear translator tool. In the event that all bridge elements are being monitored then their cumulative damage prognosis can be integrated in to the federal highway condition ratings.

### 7.3 Recommendation of Future Research

This dissertation provided a lengthy review of bridge management systems and how the condition assessments are translated into condition ratings. This section, not only contains the suggestions for next steps to be taken on this research topic, but also provides recommendations on how to fulfill a more organized federal bridge management system. Furthermore, an additional section is provided that discusses the impact of structural health monitoring on the future of bridge management systems.

The following research topics are recommended for future work:

- Verification of crack growth prediction models is limited in literature; it was previously assumed the crack growth period was relatively short and could be disregarded. Additional testing should be conducted to obtain empirical information on crack growth lives. This information would be particularly useful on structures with an existing and active crack.
- Damage accumulation models contain high levels of uncertainty and variability. Uncertainty exists as physical uncertainty or model uncertainty. In order to account for the uncertainties, stochastic damage accumulation models should be used alongside deterministic models. Probabilistic models can be used to account for the inherent scatter in fatigue data.
- Reliability models can also be used for determination of failure probabilities and estimating the fatigue life. It may be particularly useful to describe the initial crack size using a probability density function.
- Further experimental validation is needed for use of damage accumulation models with condition states.

### 7.3.1 Condition Ratings Modifications

Bridge element condition assessments should be modified to one uniform assessment process and should be used by the National Bridge Inventory. This is a feasible task since vast majority of agencies are already doing element inspections, based on the Pontis system criteria, and have adopted the condition assessments for CoRe elements. Furthermore, using element condition assessments as the National Bridge Ratings would also eliminate the need for the NBI translation tool, which has been found to have many shortcomings and should be modified. For instance, some bridge engineers have reported concerns regarding the efficiency of the Translator. Under analyses to measure the fit between the NBI generated ratings and real bridge ratings, the coefficient of determination was found to be 25%; indicating a poor fit between them (Aldemir-Bektas, et al., 2007). Furthermore, it has also been shown that the NBI translator consistently estimates lower ratings than should be designated (Aldemir-Bektas, et al., 2007). These results have also been reinforced by the National Cooperative Highway Research Program (NCHRP), which has stated (NCHRP, 2007),

*“[The NBI Translator]...is not able to make effective distinctions in the highest (6 to 9) and lowest (0 to 3) NBI condition ranges. While this might not seriously jeopardize federal funding eligibility of deteriorated bridges, it seriously impacts the accuracy of condition prediction for bridges in very good condition, which most state bridge inventories have.”*

The NCHRP also criticizes the NBI translator as overly sensitive to a small fraction of elements in poor condition states. Meaning, once deterioration has been

recognized on a component, the deterioration rate is expedited to the worse condition state in as little as 4 years (NCHRP, 2007). This is usually not a true reflection of the realistically slower deterioration process. Nonetheless, a modified NBI that captures ratings at the bridge element level would provide better data at the national level that more descriptively detail bridge conditions across the nation.

### **7.3.2 Future Role of Technology in Bridge Management Systems**

Current bridge management systems can be supplemented with structural health monitoring technologies in order to gather real-time results of a structures condition. As technology exponentially advances in the 21<sup>st</sup> century, sensing technologies will revolutionize the way we design, analyze, and maintain structures. Currently, these sensing technologies are already being implemented on bridges and infrastructure in post-construction analyses. It is foreseeable in the near future that bridges will be constructed with sensor networks that will continuously gather information about car movements, bridge vibrations, and structural integrity. The information and data gathered from these technologies are not very meaningful unless it can be paired with inspection processes and condition ratings. Since many SHM technologies are currently within research and development stages, it is more beneficial if these technologies are implemented at the state level through inspectors and agencies that are knowledgeable of the technologies.

## References

- AASHTO. AASHTO Bridge Element Inspection Manual. Vol. 1st Edition. American Association of State Highway and Transportation Officials, 2010.
- . AASHTO LRFD Bridge Design Specifications. AASHTO Standard Specifications. Washington, D.C.: American Association of State Highway and Transportation Officials, 2012.
- . Standard Specifications for Highway Bridges. AASHTO Standard Specifications. Washington, D.C.: American Association of State Highway and Transportation Officials, 2002.
- AISC. Steel Construction Manual. Vol. 13. American Institute of Steel Construction, 2005.
- Alampallia, Sreenivas and Mohammed Ettouney. "Role of Structural Health Monitoring in Bridge Security." Bridge Structures 4.3-4 (2008): 143-154.
- Aldemir-Bektas, Basak and Omar Smadi. "A Discussion on the Efficiency of NBI translator Algorithm." Mid-Continent Transportation Research Symposium. Ames, Iowa, 2007.
- Ayyub, Bilal M. Risk Analysis in Engineering and Economics. Washington DC: Chapman & Hall, 2003.
- Bassim, M.N., S. St. Lawrence and C.D. Liu. "Detection of the Onset of Fatigue Crack Growth in Rail Steels Using Acoustic Emission." 47.2 (1994): 207-214.
- BDI, Bridge Diagnostics Inc. Testing & Monitoring: What's the Difference? 2014. 21 08 2014 <<http://bridgetest.com/support/testing-monitoring-whats-the-difference/>>.
- Broek, David. The Practical Use of Fracture Mechanics. Norwell, MA: Kluwer Academic Publishers Group, 1989.
- CAE Associates. Fracture Mechanics in Workbench v14.5 ANSYS e-Learning Session. Presentation/e-Learning Session. CAE Associates. Middlebury, July 2013.
- Cha, Hun, et al. "Effect of Local Damage Caused by Overweight Trucks on the Durability of Steel Bridges." (2015).
- Chamberlin, William P. Historic Highway Bridge Preservation Practices. Washington, D.C.: Transportation Research Board, 1999.
- Chen, Huating, Gilbert Y Grondin and Robert G Driver. Fatigue Resistance of High Performance Steel. Edmonton, Alberta, Canada: University of Alberta, 2005.
- Chen, Wai-Fah and Eric M. Lui. Handbook of Structural Engineering. 2nd. Boca Raton, FL: Taylor & Francis Group, LLC, 2005.
- Chen, Wai-Fah and Lian Duan. Bridge Engineering Handbook: Construction and Maintenance. Vol. Second Edition. Boca Raton, FL: CRC Press, Taylor and Francis Group, 2014.

- Davison, A.C and R.L. Smith. "Models for Exceedances over High Thresholds." Journal of the Royal Statistical Society 52.3 (1990): 393-442.
- DelDOT. "Element Data Collection Manual." Pontis Bridge Management. Dover: Delaware Department of Transportation, 2008.
- FAA. Aviation Maintenance Handbook. FAA-H-8083-30. Washington, D.C.: Federal Aviation Administration, 2008.
- Farrar, Charles R., et al. "Damage Prognosis: Current Status and Future Needs." LA-14051-MS. 2003.
- FHWA. 2010 Status of the Nation's Highways, Bridges, and Transit: Conditions and Performance. Washington, D.C.: United States Department of Transportation, 2010.
- . "Bridge Inspector's Reference Manual." FHWA Bridge Inspector's Reference Manual. Vol. 2. Washington DC: FHWA NHI Publication No. 12-050, December 2012.
- . "Bridge Preservation Guide." FHWA-HIF-11042. 2011.
- . "Focus Accelerating Infrastructure Innovations." Federal Highway Administration Launches Steel Bridge Testing Program 27 5 2011.
- . More about AASHTO Bridge Management. 19 06 2013. US DOT FHWA. 07 10 2014 <<http://www.fhwa.dot.gov/infrastructure/asstmgt/pontmore.cfm>>.
- Fisher, John W., Dennis R. Mertz and An Zhong. Steel Bridge Members Under Variable Amplitude Long Life Fatigue Loading. Bethlehem, PA: National Cooperative Highway Research Program and Fritz Engineering Laboratory, 1983.
- Fisher, John W., Geoffrey L. Kulak and Ian F.C. Smith. "A Fatigue Primer for Structural Engineers." 1998.
- Folić, Radomir. "Durability Design of Concrete Structures Part 1: Analysis and Fundamentals." Facta Universitatis Architecture and Civil Engineering 7.1 (2009): 1-18.
- Fu, Chung C. and Shuqing Wang. Computational Analysis and Design of Bridge Structures. CRC Press Taylor and Francis Group, 2014.
- Haldipur, Pranaam and Frank Jalinoos. "Detection and Characterization of Fatigue Cracks in Steel Bridges." International Congress and Exhibition Forum. 2010.
- Helwig, Todd and Joseph Yura. Steel Bridge Design Handbook. Washington, D.C.: FHWA-IF-12-052 - Vol. 13, 2012.
- Hu, Y. and Amin. Hammad. "Location-based Mobile Bridge Inspection Support System." CSCE Specialty Conference on Infrastructure Technologies, Management and Policy. Toronto, Ontario, Canada: Canadian Society for Civil Engineering, 2005.
- Huang, Miinshiou, et al. "Using Acoustic Emission in Fatigue and Fracture Materials Research." JOM Journal of Metals 50.11 (1998).

- James, R.J., et al. "Finite Element Modeling for Reliability Evaluation of Fatigue Cracking at Welded Connections." 11 2011. Anatech Corporation. Anatech Corporation. 10 2014 <<http://anatech.com/work/publications/structural-engineering-publications/>>.
- Janosch, J.J. "Investigation into the Fatigue Strength of Fillet Welded Assemblies of E-36-4 Steel As a Function of the Penetration of the Weld Subjected to Tensile and Bending Loads." (1993).
- Jia, X.M., F. Dai and Q.Z. Wang. "Three-Dimensional Static and Dynamic Stress Intensity Factor Computations Using ANSYS." International ANSYS Conference. Pittsburgh, PA: ANSYS, Inc., 2004.
- Johannesson, Pär. "Extrapolation of Fatigue Loads." 4th Conference on Extreme Value Analysis. Gothenburg: 4th Conference on Extreme Value Analysis, 2005.
- . "Extrapolation of load histories and spectra." Fatigue & Fracture of Engineering Materials & Structures 29 (2006): 201-207.
- Keating, Peter B. and John W. Fisher. Fatigue Tests and Design Criteria. Bethlehem, PA: National Cooperative Highway Research Program and Fritz Engineering Laboratory, 1986.
- Kuphaldt, Tony R. Lessons In Electric Circuits, Volume I – DC. Vol. Fifth Edition. Open Book Project, 2006.
- Lee, Yung-Li, et al. Fatigue Testing and Analysis Theory and Practice. Burlington, MA: Elsevier Inc., 2005.
- Lee, Yung-Li, Mark E Barkey and Hong-Tae Kang. Metal Fatigue Analysis Handbook, Practical Problem-Solving Techniques for Computer-Aided Engineering. Waltham, MA: Elsevier, 2012.
- Lowy, Joan and Mike Baker. AP IMPACT: Many US bridges old, risky and rundown. Seattle, Washington: Associated Press, 2013.
- Manson, S.S. and Gary R. Halford. Fatigue and Durability of Structural Materials. Materials Park, OH: ASM International, 2006.
- Massarelli, Peter J. and Thomas T. Baber. Fatigue Reliability of Steel Highway Bridge Details. Charlottesville, Virginia: Virginia Transportation Research Council; Virginia DOT; US DOT FHWA, 2001.
- MDSHA. "Maryland State Highway Administration Bridge Inspection Report." Inspection Report 1504200. 2013.
- . Pontis Element Data Collection Manual. Maryland State Highway Administration. Baltimore, MD: Bridge Inspection and Remedial Engineering Division, Office of Bridge Development, 2003.
- Mertz, Dennis. Steel Bridge Design Handbook: Design for Fatigue. Washington, D.C.: FHWA-IF-12-052-Vol.12, 2012.
- . Steel Bridge Design Handbook: Redundancy. Washington, D.C.: FHWA-IF-12-052 - Vol. 9, 2012.

- Miki, Chitoshi. "Non-Destructive Evaluation (NDE)." Vers. [www.ocw.titech.ac.jp/index.php?module=General&action=Download&file=2004-61059-20041202-7,8.pdf&type=cal](http://www.ocw.titech.ac.jp/index.php?module=General&action=Download&file=2004-61059-20041202-7,8.pdf&type=cal). 02 12 2004. Tokyo Tech OpenCourseWare. Tokyo Institute of Technology Department of Civil Engineering. 09 2014 <<http://www.ocw.titech.ac.jp/>>.
- NBIS, FHWA National Bridge Inspection Standards. "U.S. Department of Transportation FHWA." 5 4 2011. Revisions to the National Bridge Inspection Standards (NBIS). 28 8 2012 <<http://www.fhwa.dot.gov/bridge/nbis/t514021.cfm>>.
- NCHRP. Fatigue Evaluation of Steel Bridges. National Cooperative Highway Research Program Report 721. Washington, D.C.: National Academy of Sciences, Transportation Research Board, 2012.
- . Multi-Objective Optimization for Bridge Management Systems. Washington, DC: Transportation Research Board, 2007.
- NDT Resource Center. NDT Course Material - Acoustic Emission. 03 June 2012. 2014 <[https://www.nde-ed.org/EducationResources/CommunityCollege/Other%20Methods/AE/AE\\_Theory-Sources.htm](https://www.nde-ed.org/EducationResources/CommunityCollege/Other%20Methods/AE/AE_Theory-Sources.htm)>.
- NI, National Instruments. NI PXI-5105. 9 6 2010. 27 8 2012 <<http://sine.ni.com/ds/app/doc/p/id/ds-239/lang/en>>.
- . NI PXIe-4330. 8 3 2011. 27 8 2012 <<http://sine.ni.com/ds/app/doc/p/id/ds-208/lang/en>>.
- . "What is PXI?" 2012. National Instruments. 27 8 2012 <<http://www.ni.com/pxi/whatis/#tab2>>.
- ODOT. 2013 Bridge Inspection Report. Salem: Oregon Department of Transportation, 2013.
- Oregon DOT. "Fatigue Prone Detail Bridge Inspection Program Policy." 1996.
- Paris, P.C. "Fracture Mechanics and Fatigue: A Historical Perspective." 21.5 (1998).
- Peil, Udo. "Assessment of Bridges via Monitoring." Structre and Infrastructuer Engineering 1.2 (2005): 101-117.
- Phan, Anh-Vu. ANSYS Tutorial - 2D Fracture Analysis. ANSYS Tutorial. University of Alabama. Mobile: University of Alabama, 2005.
- Pilkey, Walter D. Formulas for Stress, Strain, and Structural Matrices. Vol. 2. Hoboken: John Wiley & Sons, Inc., 2005.
- Potter, John M. and Roy T. Watanabe. Development of Fatigue Loading Spectra. Philadelphia, PA: American Society for Testing and Materials (ASTM), 1989.
- Rabiei, Masoud. A Bayesian Framework for Structural Health Management using Acoustic Emission Monitoring and Periodic Inspections. PhD Thesis. College Park, MD: University of Maryland, 2011.
- Roylance, David. Introduction to Fracture Mechanics. Cambridge, MA: Department of Materials Science and Engineering, MIT, 2001.

- . Stress-Strain Curves. Cambridge, MA: Department of Materials Science and Engineering, MIT, 2001.
- Ryan P.E., Thomas W., et al. Bridge Inspector's Reference Manual (BIRM). Arlington, Virginia: Federal Highway Administration, 2012.
- Sarja, A. and E. Vesikari. Durability Design of Concrete Structures, Report of RILEM Technical Committee 130-CSL. London, UK: Chapman & Hall, 1996.
- Schijve, Jaap. Fatigue of Structures and Materials. Vol. Second Edition. Netherlands: Springer Science+Business Media B.V., 2009.
- Shantz, Christopher R. Uncertainty Quantification in Crack Growth Modeling Under Multi-Axial Variable Amplitude Loading. PhD Thesis. Nashville, Tennessee: Graduate School of Vanderbilt University, 2010.
- Sobanjo, John O. and Paul D. Thompson. Development of Risk Models for Florida's Bridge Management Systems. Tallahassee, FL: Florida Department of Transportation, 2013.
- Svirsky, Alexander. The National Bridge Inventory Database. 2014. Alexander Svirsky. 20 09 2014 <<http://nationalbridges.com/nbi>>.
- Total Materia. 2015. Key To Metals. Total Materia. 03 2015 <<http://www.keytometals.com/page.aspx?ID=CheckArticle&site=kts&NM=49>>.
- Transportation for America. The Fix We're In For: The State of Our Nations Bridges 2013. Washington, D.C.: Transportation for America, 2013.
- VDOT. "BMS Element Level Data Collection Manual." Pontis Bridge Management. Richmond: Virginia Department of Transportation, 2007.
- White, Don. "Structural Behavior of Steel." FHWA-IF-12-052 - Vol. 4 (November 2012).
- Wright, William J. Steel Bridge Design Handbook: Bridge Steels and Their Mechanical Properties. Washington, D.C.: FHWA-IF-12-052 - Vol. 1, 2012.
- Xia, Yong, et al. "Short-term and Long-term Monitoring Experience of a Short Highway Bridge: Case Study." Bridge Structures 1.1 (2005): 43-53.
- Zafosnik, B., et al. "Evaluation of Stress Intensity Factors Using Finite Elements." 12 September 2002. Durability and Life Extension (DLE): Finite Element Simulation of Fracture and Crack Growth. FENet: A NAFEMS Project. 05 09 2014 <[http://www.fe-net.org/downloads/FENet\\_Meetings/Trieste\\_Italy\\_Sep\\_2002/FENET\\_Trieste\\_Sept2002\\_DLE\\_Zafosnik.pdf](http://www.fe-net.org/downloads/FENet_Meetings/Trieste_Italy_Sep_2002/FENET_Trieste_Sept2002_DLE_Zafosnik.pdf)>.
- Zhang, Wei, C.S. Cai and Fang Pan. "Nonlinear Fatigue Damage Assessment of Existing Bridges Considering Progressively Deteriorated Road Conditions." 56 (2013).
- Zhou, Changjiang. Fatigue Crack Monitoring with Coupled Piezoelectric Film Acoustic Emission Sensor. PhD Thesis. College Park: University of Maryland, 2013.

Zhou, Y. Edward. "Assessment of Bridge Remaining Fatigue Life Through Field Strain Measurement." Journal of Bridge Engineering (2006): 737-744.